

COALESCENCE BEHAVIOUR OF LIQUID DROPS  
AT SOLID SURFACES

by

Asher Inayatullah Najmi

A thesis submitted to the University  
of Aston in Birmingham for the  
degree of Doctor of Philosophy

Department of Chemical Engineering  
The University of Aston in  
Birmingham  
September, 1979.

## SUMMARY

A. I. Najmi

Ph. D.

1979

### Coalescence Behaviour of Liquid Drops at Solid Surfaces

The literature on droplet hydrodynamics and coalescence mechanisms in packed beds has been reviewed. The fundamentals of liquid-liquid and solid-liquid coalescence, and characterisation of 'wetting' or 'non-wetting' behaviour in liquid-vapour-solid systems by contact angles are summarised.

Contact angle measurements have been extended to liquid-liquid-solid systems. Five organic liquids and water were investigated using both high and low surface energy solid surfaces. The contact angle varied with the size of the drop and with surface characteristics of the solid. The mechanisms by which a contact angle is subtended are explained with respect to the nature of a surface. The true contact angle was that measured with a 'wetted' surface; with a 'non-wetted' surface the drop actually 'rested' on adsorbed immiscible liquid.

Single drop coalescence studies were performed to characterise drop behaviour in packings used as coalescing aids. The coalescence, but not the droplet retention and passage, mechanisms depended upon the wetting characteristics of the packing material since, irrespective of the nature of the packing material, drops larger than the packing size were retained whilst drops of equivalent aperture size passed through the void.

The enhanced coalescence at a composite surface, incorporating a junction between a 'wetted' and 'non-wetted' solid, was investigated and a mechanism proposed for it. The studies were extended to the coalescence of swarms of drops in beds packed with composite packings. Coalescence mechanisms in the packed section, and at the inlet and outlet, are explained. A correlation is proposed to predict exit drop size.

Proposals are made for the design of a coalescer. The magnitude of forces of attraction between solid-liquid molecules must be predicted for design and a model is proposed for these for any liquid-solid-liquid-solid system.

Key words:

Droplet Coalescence, Junctions, Contact Angles.

## ACKNOWLEDGEMENTS

The author is deeply indebted and wishes to record his sincere thanks to all members of staff and postgraduates of the Department of Chemical Engineering, particularly:-

Professor G. V. Jeffreys

for providing the facilities for this research and  
for his helpful guidance in this project.

Dr. C. J. Mumford

for his constant advice, continual help, constructive  
criticism and encouragement.

Professor A. B. Ponter

for his interest in part of this work.

Mr. & Mrs. Malik Rehmat Ali

his parents for their financial and moral assistance.

Finally, the author is especially grateful to his wife, Mrs. Shemin Najmi, for her patience and co-operation during the period of this research and for typing this thesis.

## LIST OF CONTENTS

	Page
<b>INTRODUCTION</b>	
<b><u>CHAPTER 1.</u></b>	
1) Liquid-Liquid Coalescence	1
1.1) Drop-interface coalescence	1
1.1.1) Rest-time distributions	10
1.1.2) Factors affecting coalescence	12
1.2) Stepwise coalescence	22
1.2.1) Factors affecting stepwise coalescence	27
1.3) Drop-drop coalescence	31
1.4) Coalescence of swarms of drops	34
1.4.1) Monolayers	34
1.4.2) Multilayers	36
 <b><u>CHAPTER 2.</u></b>	
2) Behaviour of Liquid Drops at a Vapour- Solid Interface	42
2.1) The contact angle	42
2.2) Work of 'cohesion' and 'adhesion'	44
2.3) Young's Equation	45
2.4) Surface free energy	48
2.5) High and low energy solid surfaces	49
2.5.1) Wetting of high surface energy solid materials	50
2.5.2) Wetting of low surface energy solid materials	50
2.6) Factors affecting contact angle	52
2.6.1) Surface roughness	52

LIST OF CONTENTS(contd. )

	Page
2. 6. 2) Interfacial velocity	53
2. 6. 3) Temperature	54
2. 6. 4) Time	54
2. 6. 5) Hysteresis	55
2. 6. 6) Experimental techniques	56
 <u>CHAPTER 3.</u>	
3) Droplet Hydrodynamics in Extraction Equipment	57
3. 1) Coalescence in extraction equipment	58
3. 2) Flow phenomena in packed columns	62
3. 3) Formation of liquid drops in an immiscible liquid	63
3. 3. 1) Variables governing drop formation	63
3. 3. 2) Mathematical modelling of drop formation	66
 <u>CHAPTER 4.</u>	
4) Coalescence of Liquid Dispersions	73
4. 1) Primary dispersions	73
4. 1. 1) Coalescence in packed beds	75
4. 1. 2) Break-up in packings	83
4. 1. 3) Coalescence in 'Universal' packings	86
4. 2) Secondary dispersions	90
4. 3) Coalescing aids	96

LIST OF CONTENTS (contd. )

	Page
<u>CHAPTER 5.</u>	
5) Experimental Investigation	100
5.1) Single drop studies	100
5.1.1.) Selection and preparation of solid surfaces	101
5.1.2.) Experimental apparatus	107
5.1.3.) Cleaning technique	115
5.1.4.) Experimental technique	115
5.1.5.) Measurement of size of single drops and voids	117
5.2) Drop swarm studies	118
5.2.1.) Experimental apparatus	118
5.2.2.) Construction of junction coalescer	123
5.2.3.) Experimental technique	124
5.3) Photographic technique	128
<u>CHAPTER 6.</u>	
6) Results and Discussion	130
6.1) Single drop studies	132
6.1.1.) Behaviour of liquid drops at flat solid plates	132
6.1.1. a) Solid surfaces wetted by dispersed phase	139
6.1.1. b) Solid surfaces wetted by continuous phase	159
6.1.2.) Behaviour of a liquid drop at a packing	176

LIST OF CONTENTS (contd. )

	Page
6.1.2.a) Effect on coalescence of a thin film of dispersed phase liquid on the packing	177
6.1.3.) Behaviour at flat composite surfaces	181
6.1.3.a) Horizontal junctions	181
6.1.3.b) Vertical junctions	192
6.1.3.c) Parallel junctions	192
6.1.3.d) Interdrop coalescence at a junction	196
6.1.3.e) Rest-time distribution at a junction	206
6.1.4) Coalescence behaviour at composite packings	215
6.1.4.a) Nozzle with a junction	216
6.1.4.b) Other geometrical arrangements	224
6.2.) Coalescence of Swarms of Drops	228
6.2.1) Prediction of exit drop size	229
6.2.2) Coalescence mechanisms	231
6.2.2.a) Inlet mechanisms	231
6.2.2.b) Exit mechanisms	235
 <u>CHAPTER 7.</u>	
7) General Conclusions	243
7.1.) Main Conclusions	243
7.2.) Applications to the Design of a Coalescer	246
7.3.) Recommendations for further work	249

## LIST OF CONTENTS (contd. )

### APPENDICES

Physical properties of liquid-liquid systems	A
Matching the densities of liquids	B
Volumes and surface areas of liquid drops	C
Liquid-liquid-solid-solid interfacial tensions	D
Effect of liquid-liquid interfacial tensions on contact angles	E
Exponential factors 'f'	F
Maximum drop diameters	G
Coalescence mechanisms	H
Effect of density difference on contact angles	I
Factors affecting coalescence of swarms of drops	J
Prediction of exit drop size	K
Air-liquid contact angles	L

### NOMENCLATURE

### REFERENCES

## INTRODUCTION

Liquid-liquid dispersions play an important role in many chemical engineering operations and it is generally necessary at some stage to separate the two phases. There are two types of dispersion. A primary dispersion is characterised by a drop size of the order of  $>100\mu\text{m}$  and will separate by gravity settling: a secondary dispersion is cloudy in appearance and consists of microscopic droplets of diameter generally  $<100\mu\text{m}$  which do not settle readily under gravity.

The separation of immiscible, or partially miscible, liquid phases is a common problem in liquid-liquid extraction, the treatment of liquid effluents, and the separation of oils from aqueous streams or water from oil. Many techniques ranging from gravity settlers to fibrous bed packings, may be used to achieve separation. The packings generally improve the rate of coalescence and the efficiency of a packing is demonstrated by the ratio of mean outlet drop size to that at the inlet. Within the packings, however, the phenomena involved depends primarily upon the nature of the dispersion to be treated; the mechanisms of collection and coalescence of primary dispersions differ greatly from those for secondary dispersions.

With primary dispersions two distinct mechanisms of coalescence can be observed in a packing depending upon the nature of the material of construction. On the surface of a packing wetted by the dispersed phase liquid, coalescence of drops arriving at the surface forms a film of dispersed phase liquid. The drainage of this film occurs across the bed and the droplets are detached from the packing at the outlet by a 'drip-point' mechanism. The other mechanism of coalescence

of primary dispersions is the process of interdrop coalescence; this occurs, for example, in the interstices of packing which is not wetted by the dispersed phase liquid. In this case, the packing serves simply as a mechanical structure to hold the drops in close contact. Whilst the former is a drop-interface mechanism, the latter is a drop-drop mechanism. The efficiency of separation is highly dependent on the mechanism of coalescence.

The efficiency is greater if the dispersed phase liquid wets the packing. Therefore, the mechanism of coalescence in a packing wetted by the dispersed phase liquid has been further investigated in the present work and a mechanism is proposed for it.

An optimum design of packing must specify both the material of the packing, the shape, the surface area/volume ratio and the voidage. The choice of the material of the packing governs the wetting conditions in a particular liquid-liquid system. This can be quantitatively described by the contact angle. At present, however, there is little published data on contact angles in liquid-liquid-solid systems. Therefore, part of this work involved measurement of a range of liquid-liquid contact angles at solid surfaces of both high and low surface energy materials.

An enhanced coalescence effect has also been reported with a packing of mixed components but no previous attempts have been made to explain the coalescence process which occurs in such packings. In this work, the junction mechanism has been investigated with the aid of high speed cine photography and the results obtained with single drops at flat plates and packings were extended to characterise the behaviour of liquid

dispersions in a column packed with an ideal coalescer constructed from mixed components of solid materials.

The natural phenomena of coalescence is not fully understood and an attempt has been made in the present work to explain the processes which occur at wetted, non-wetted and composite solid surfaces in liquid-liquid-solid and liquid-liquid-solid-solid systems. It was first essential to review the literature on the various coalescence processes and on solid surface characteristics.

Although the major objective was to extend basic knowledge regarding droplet behaviour on solid surfaces of different geometries and materials, the results are applicable to the design and selection of coalescers.

## CHAPTER ONE

### LIQUID-LIQUID COALESCENCE

The coalescence of liquid drops at a plane solid surface is fundamentally a liquid-liquid process with the solid acting as a rigid boundary. With a primary dispersion, two distinct mechanisms of coalescence can occur in packings. In the first case, a film is formed on the packing surface and the coalescence of subsequent drops occurs at this dispersed phase film in a stepwise manner. In the second case, the mechanism is one of inter-drop coalescence in the interstices of the packing, with the packing serving simply to hold the drops in intimate contact.

To improve coalescence performance requires an understanding of the fundamentals involved in the coalescence of single drops or dispersions at solid surfaces. The complex phenomena involved in drop coalescence is therefore reviewed below.

#### 1.1 Drop-Interface Coalescence

Much of the research effort in coalescence has concentrated on the coalescence of drops at an interface rather than coalescence between adjacent drops. Both processes are involved in industrial liquid-liquid separation operations.

The coalescence of a single drop at a plane liquid-liquid interface has been described as following five stages (70)

- (a) Arrival of the drop at the interface,
- (b) Mutual deformation of the drop and the interface,
- (c) Rupture of the film,
- (d) Drainage of the continuous phase film trapped between the drop and the interface,

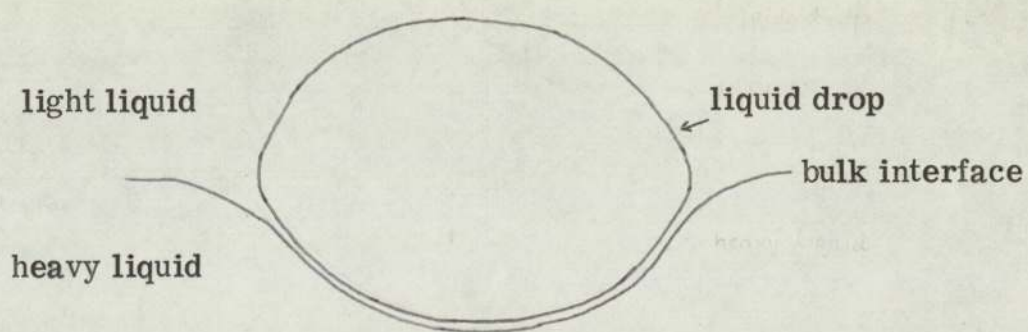
- (e) Deposition of the contents of the droplet into the bulk of the drop phase.

When a liquid drop arrives at a liquid-liquid interface, both the drop and the interface deform mutually as shown in Figure 1.0. Efforts have been made to simulate the deformed profiles mathematically. The shape of a fluid drop at an interface has been tabulated by Princen (114) for different values of interfacial tension, density difference and drop size. The theory was experimentally verified by Princen and Mason (115) for stabilised air bubbles at an air-water interface. Jeffreys and Hawksley (69) photographed the profile of a drop of water at a benzene-water interface and obtained the variation in pressure outside the drop from measurements of the principal radii of curvature. The shape of the free drop is given by the Bashforth and Adams Tables II. Referring to Figure 1.1, B. A. T. 1 gives  $r_a/z_a$  for different values of  $B = \Delta\rho g \cdot b^2/\gamma$  so the value of  $B$  may be obtained from  $r_a'/z_a'$ . B. A. T. II and V give  $r_a/b$  and  $z_a/b$  for different values of  $B$  and so the value of  $b'$  may be obtained knowing the value of  $r_a'$  or  $z_a'$ . The value of  $V_t/b^3$  may be obtained from B. A. T. III knowing the values of  $B$  and  $\omega_c$  and this gives  $V_t'$ , as  $b'$  is known. Now  $(V_t' + V_c') f^3 = V$  and this gives the linear scale factor,  $f$ , and hence the actual dimensions of the drop. The superscripts refer to the dimensions of magnified image of the drop.

In research studies the drop must remain at the interface long enough for photography. This may be achieved by using a fairly viscous light liquid as this decreases the rate of film drainage and hence increases the rest time of the drops at the interface.

Figure 1.0.

Liquid drop at a liquid-liquid interface



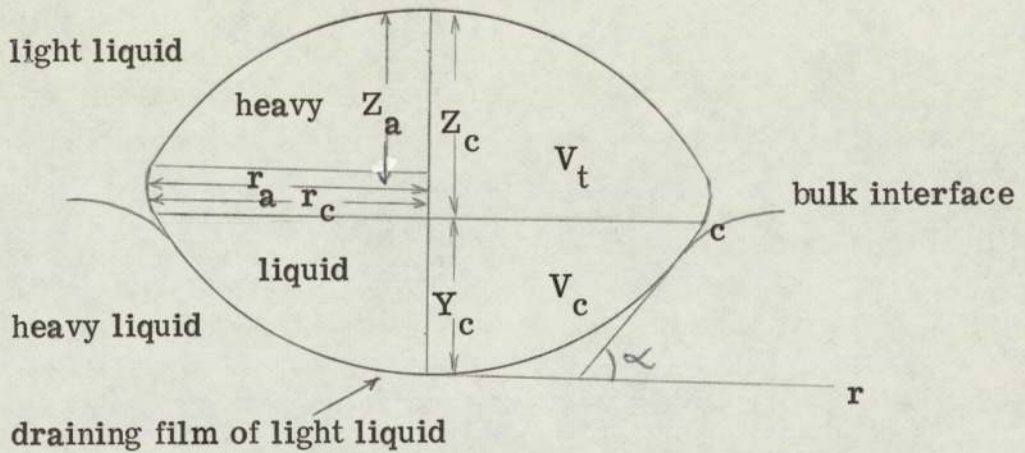
Initial stage in drop-interface coalescence; mutual deformation of the drop and the interface.

Thus Hartland (54) photographed a golden syrup drop at a liquid paraffin-golden syrup interface and found that the overall shape of the draining film beneath a drop at a liquid-liquid interface was that of a spherical cap. The drop dimensions were not significantly affected by the drainage time nor by the cell size. However, a photograph of a water drop at a glycerol-water mixture/heptane interface (Figure 1.2) demonstrated that the shape was that of an ellipse (102).

To determine the rate of drainage of the light liquid in the film trapped between the drop and the interface, it is important to know the shape and dimensions of the film. Allan, et al (6) estimated the film thickness beneath a nitrogen bubble approaching the free surface of aqueous glycerol and polyglycol oils using interference patterns. The film deformed with time and was eventually thinnest around a ring some distance from the centre. The rate of thinning decreased rapidly with time. Using a similar technique Derjaguin and Kussakov (31) studied the approach of an air bubble in water towards a glass plate. The interference pattern of the film showed that a 'dimple' was formed in the base of the bubble with a barrier ring at a radius  $(3V/4\pi)^{2/3} \sqrt{(2\Delta\rho g/3\sigma)}$ , where  $V$  is the drop volume,  $\rho$  is the density and  $\sigma$  is the interfacial tension. Prokhorov (116) observed a similar dimpling in the surface of two hexane drops pressed together in air.

Because of the radial pressure gradient due to the flow in the draining film, and because the individual surfaces must deform if there is a pressure difference across them, a variation in film thickness with position is to be expected,

Figure 1. 1.



Dimensions of a drop for use with Bashforth and Adams Tables.

$r$  : radial dimension measured from vertical axis of drop  
 $V$  : volume ;  $Y$  : vertical dimension measured from base of draining film;  $Z$  : vertical dimension measured from top of free surface of drop;  $\alpha_c$  : inclination of edge of draining film to  $r$ -axis.

Subscripts  $a$  : maximum diameter of drop;  $c$  : edge of draining film (and spherical cap);  $t$  : free portion of drop (i. e. above spherical cap).

Hartland (54) determined this variation at different drainage times by taking side photographs of the film beneath a liquid drop approaching a liquid-liquid interface. The film shape was very complicated and changed with time. The minimum film thickness occurred at the outer edge. A secondary minimum could occur at the centre of the film, especially with large drops. The drop was usually tilted so that the film thickness was less than  $10^{-3}$  cm. By measurement of the capacitance of the draining film it was demonstrated that the variation of the average film thickness with time changed from drop to drop. At a given time, the average film thickness for 0.1 ml. drops was less than that for 0.5 ml. drops. Smaller drops took longer to coalesce than larger drops of the same liquid and golden syrup drops took longer than glycerol drops of similar size. Several idealised drop/interface profiles, covering rigid or deformable drops and interface, and uniform or non-uniform films have been used to derive mathematical models for the drainage process. These are summarised in Table 1.0. The continuous phase film is, in fact, non-uniform with its thickest part beneath the vertical mid-axis of the drop. Jeffreys and Hawksley used this fact to postulate a mechanism to describe experimentally derived distributions of the coalescence times. This suggested that the drop may approach the interface during the drainage process with its vertical mid-axis tilted as shown in Figure 1.3. The Laplace equation was applied to the profile of the drop to predict the surface pressure. The Navier-Stokes equation was then used on the basis of the film being four microns thick, and the pressure drop in the film was calculated from the mid-central axis to the side of the drop.

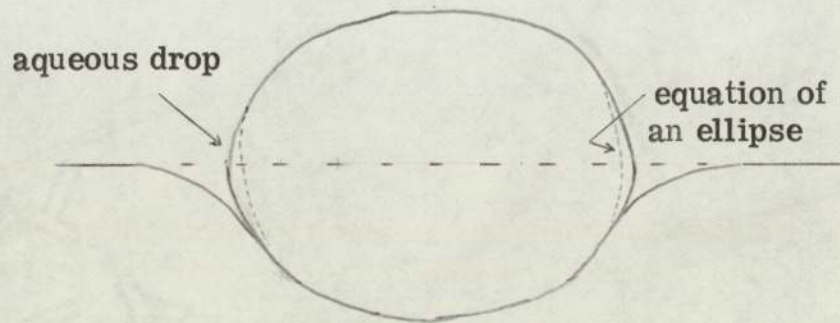


Figure 1. 2.

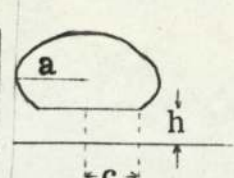
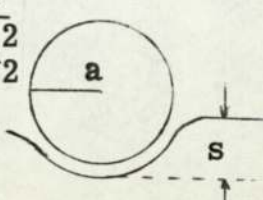
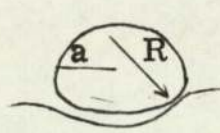
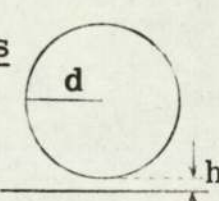
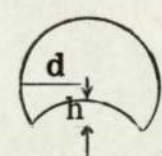
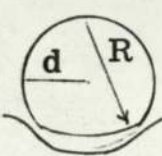
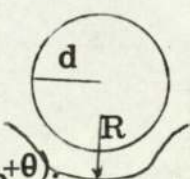
Elliptical shape of a liquid drop at a liquid-liquid interface.  
Aqueous phase drop resting at an heptane-water /glycerol interface.

The pressure in the film at the mid-central axis was found to be greater than that in the drop which would account for the fact that the coalescence always started on the side since the drop was tilted as it approached the interface. Furthermore, a shock wave moved up the drop; the wave was always inclined to the interface as it moved over the drop, which again confirmed that the drop was tilted, and the coalescence was initiated on one side.

The drop was inclined on the interface because the drop would tend to settle at an angle and the film might rupture before it came to rest completely parallel to the interface. However, Hartland considered the drop to tilt because of the instability in the circulation (Figure 1. 4) occurring in the drop and the bulk phase. Because of the deformation of the drop and the bulk interface this circulation was initially towards the centre of the draining film. The drag due to the drainage in the film tended to reverse the circulation. It was possible for the circulation to be outward on one side of the drop and inward on the other side; this caused drainage of the film to be in one direction across the drop which made the drop tilt.

Burrill and Woods (21) proposed four mechanisms for film drainage during coalescence, namely rapid approach, dimple formation, even drainage and rupture. Rapid approach refers to the outflow of the liquid from the film because the bonding interfaces are mobile. Dimple formation refers to the inflow of the liquid into the film because an interfacial tension gradient causes a contraction of the interface which, in turn, drags the bounding bulk fluid into the centre of the film. The initial, large

Table 1.0. Film Drainage Models

		<u>Uniform Film Models</u>	
Deformable drop	$t = \frac{\mu_c \cdot \Delta \rho \cdot g \cdot d^5}{128 \gamma^2} \left[ \frac{1}{h_2^2} - \frac{1}{h_1^2} \right]$		
Rigid interface			
Uniform film			
Rigid drop	$t = \left[ \frac{9 a^3 \cdot (a-s)^2}{(2a^3 - 3a^2s - s^3)(\Delta \rho \cdot g)} \right] \frac{1}{h_2^2}$		
Deformable interface			
Uniform film			
		'a' is the radius of of the drop = d/2	
Deformable drop			
Deformable interface	$t = (\mu_c \Delta \rho \cdot g d^5 / 32 \gamma^2) \cdot 1/h_2^2$		
Uniform film			
		where R=2d	
For large drops:-	$t = (3 \mu_c d^3 / 8 \gamma) (1/h_2^2)$		
		<u>Non-uniform Film Models</u>	
Rigid drop	$t = (\mu_c / 2a \Delta \rho \cdot g) \ln(h_1/h_2)$		
Rigid interface			
Non-uniform film			
Deformable drop	$h=0 \quad 0.096 n^2 \mu_c r_f^6 / t \cdot a \cdot r$		
Deformable interface			
Non-uniform film			
		where 'n' is number of surfaces that resist heat.	
Rigid drop	$t = 6 \pi \mu / 4 \phi^2 F \left[ \frac{\ln(h_2' - \theta) / h_1' - \theta}{\ln h_1' / h_2' + (\theta / h_2' - \theta / h_1')} \right]$		
Deformable interface			
Non-uniform film			
For $\lambda = R/d < 1$ ,			
where $\phi = 1/d(1 - 1/\lambda)$ ; $\theta = (\lambda - 1)(d/2 - s)$			
For $\lambda = R/d > 1$	$t = 6 \pi \mu / 4 \phi^2 F \left[ \frac{\ln(h_2/h_1) + \ln(h_1 + \theta) / h_2 + \theta}{(\theta/h_2 + \theta) - (\theta/h_1 + \theta)} \right]$		
			

interfacial tension gradient is created because of the dissipation of the drop's kinetic energy. Even drainage is the symmetrical outflow of the liquid from the film because of a pressure gradient in the film. One of the bounding interfaces is usually immobile. Uneven drainage is the unsymmetrical outflow of the liquid from the film because of the local interfacial mobility. Film rupture was observed to occur at a film thickness between 300 - 500 Å<sup>0</sup> with the oil-water systems studied.

### 1.1.1. Rest-time distribution

In an oil-water type system, drops of either phase do not normally coalesce spontaneously with their homophase on reaching the phase boundary but rest at the interface for some time (35). The rest-time arises because of the thin film of continuous phase liquid trapped between the drop and the interface as outlined earlier. Mahajan (90) found that the rest-time varied from virtually zero to several minutes. Its magnitude was dependent on several factors such as temperature, drop size, the geometric shape of the interface, the degree of purity of the components and the interfacial tension. For a given system, there is in fact a roughly Gaussian distribution of values of 't' between 't<sub>min</sub>' and 't<sub>max</sub>' (35, 26, 105) (Figure 1.5). The mean rest-time 't̄', the distribution of 't' about 't̄' and the median life 't<sub>1/2</sub>' are influenced by various factors. In an oil-water system the addition of a surfactant (35, 26, 105), a decrease in temperature or an increase in drop size (26) generally increased 't̄' and 't<sub>1/2</sub>'. A change in the curvature from convex to concave with respect to the drop increased the drop stability (105). Electrolytes added to the water phase markedly reduced 't̄' (42). In general the scatter in 't' about the mean value increased as 't̄' and 't<sub>1/2</sub>' increased (26, 144)

Figure 1. 3.

Approach of a liquid drop to a  
plane liquid-liquid interface

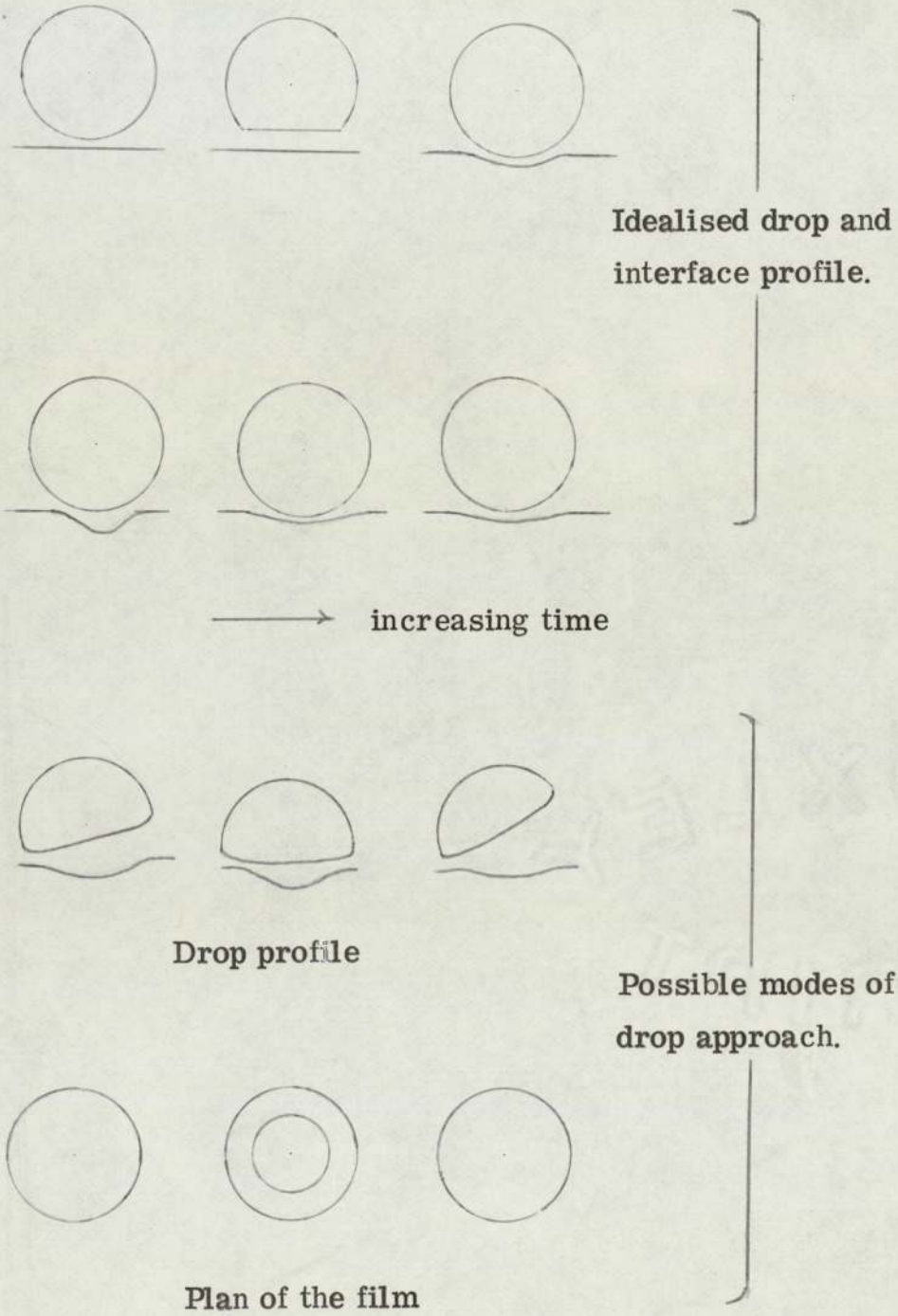


Table 1.1.- Parameters affecting Coalescence of Single Liquid Drops at Liquid-Liquid Interface

<u>Parameter</u> (increasing)	<u>Physical description</u> of effect	<u>Coalescence</u> time	<u>Refs</u>
Interfacial tension	Little deformation of drop, hence area for drainage smaller	Decreases	(5)
	Increases strength of film, hence resistance to rupture	Increases	(78)
Density difference	Greater drop deformation hence area for drainage greater	Increases	(69, 80)
	Greater hydrostatic forces act on drainage	Decreases	(134)
Drop size	Drainage area greater	Increases	(69, 80)
	Smaller area/volume hence surfactant area smaller	Decreases	(67)
	Depends on system investigated	Variable	(78)
	All forces balance	No effect	(99)
Distance of drop fall to interface	Exposure time to surfactants increases	Increases	(80, 59)
	Independent (effect of apparatus design)	No effect	(80)
	Depends upon thermal and vibration disturbance imposed on drainage of film	Variable	(77)
Viscosity of continuous phase	Increases resistance to film drainage	Increases	(122)
Temperature	Decreases all physical properties particularly viscosity	Decreases	(59)

Table 1.1.(continued)

Temperature gradients	Increases instability of film, hence promotes rupture	Decreases	(8)
Vibrational	Renews continuous film Produces random variations	Increases Variable	(8) (77)
Electrical	Effectively produces forces greater than gravity alone	Decreases	(17)
Surfactants	Grouping of surface active molecules creates one mobile and one immobile interface, drop sinks and drainage area greater, or Initial internal circulation causes surface pressure differences, reduction of momentum transfer and consequently retards film drainage	Increases	(55)  (29)
Mass transfer			
Solute from drop	Lowers interfacial tension locally Interface dilates, film drawn inwards	Decreases	(29, 63)
Solute into drop	Bulk phase continues to renew film by mass transfer gradients, hence retards drainage	Increases	(70)

Other factors have been reported to influence the rest-time. For example, temperature gradients and dirty interfaces tended to decrease drop stability (26, 42, 90, 24). Conversely, mechanical vibrations appeared to increase the rest-time (90, 59).

Several theories have been proposed to explain the wide scatter found in rest-time values (90, 59). From a study of systems containing surfactants Cockbain and McRoberts (26) proposed that displacement of adsorbed surfactant molecules from the interface was necessary in order for coalescence to occur. This concept, although supported by other investigators, does not explain the scatter found in pure systems (35, 42, 59, 108).

### 1. 1. 2. Factors affecting coalescence

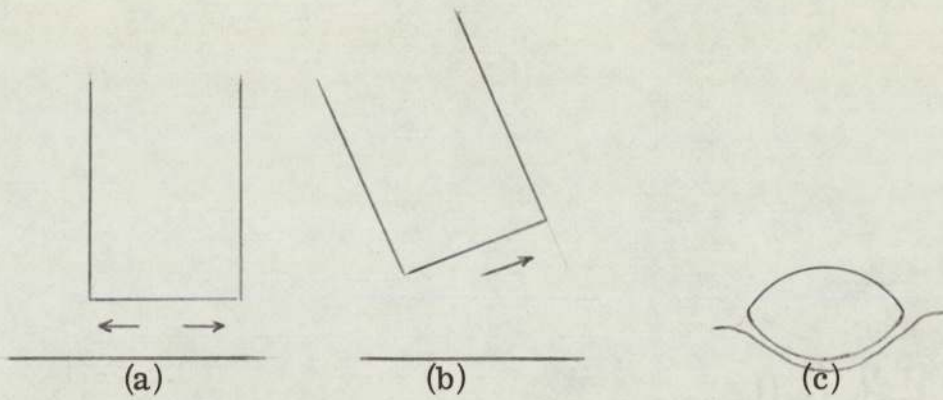
Consideration of factors affecting the rate of coalescence of drops have been mainly based on studies of single drops residing at a plane interface. Similar factors are assumed to control the coalescence of a pair of drops, or the coalescence of a drop at a film of dispersed phase on a solid surface. As already described, the coalescence of a single drop at an interface is accomplished through the drainage and rupture of a film of the continuous phase; the factors that most affect drainage and rupture of the film therefore control the coalescence process. The effects which changing certain variables have on the coalescence behaviour of a system are summarised in Table 1. 1. The factors considered to be overriding are discussed in the following paragraphs.

#### Effect of droplet size:

An increase in the droplet size increases the drainage force due to the weight of the drop, but the volume of the phase-2 liquid in the film also increases. Since an increase in the drop size results in an increase in the coalescence time, the overriding effect is an increase in the film volume. Charles and Mason (24) found that  $t \propto a^3$ , where 'a' is the equivalent spherical radius of the drop. Hawksley (59) determined the exponent as 1.02 and Lawson (80) as 1.5.

Figure 1. 4.

Settling of a liquid drop at a  
liquid-liquid interface



The instability in the circulation in the drop and bulk phase.

- a. Symmetrical flow of liquid between a cylinder and the interface.
- b. Assymmetric flow due to angled approach of cylinder
- c. Final stable position of drop resting at interface.

### Change in drainage rate of film liquid:

The effect of any variable on coalescence may be assessed by considering the change it brings about in the drainage rate of the phase-2 film. This follows because the time taken for the film to drain to some critical thickness at which rupture is initiated is really the 'coalescence time' measured by the stop watch, since with most systems the other processes which occur are virtually instantaneous. Only in the work of Hartland (56) involving a system (liquid paraffin-celacol) with physical properties such that the drainage process and the drop deflation process were very slow, has it been possible to distinguish between them. Gillespie and Rideal (42) found the film had to drain to a thickness of the order of  $10^{-5}$  to  $10^{-4}$  cm. before rupture was likely. Mackay and Mason (88) using an interferometric technique, found the drainage process to be symmetrical and uniform with the film thickness at rupture less than  $5 \times 10^{-6}$  cm. In addition, for drop diameters upto 2,500  $\mu\text{m}$ , the rate of thinning of the film was proportional to the cube of the thickness.

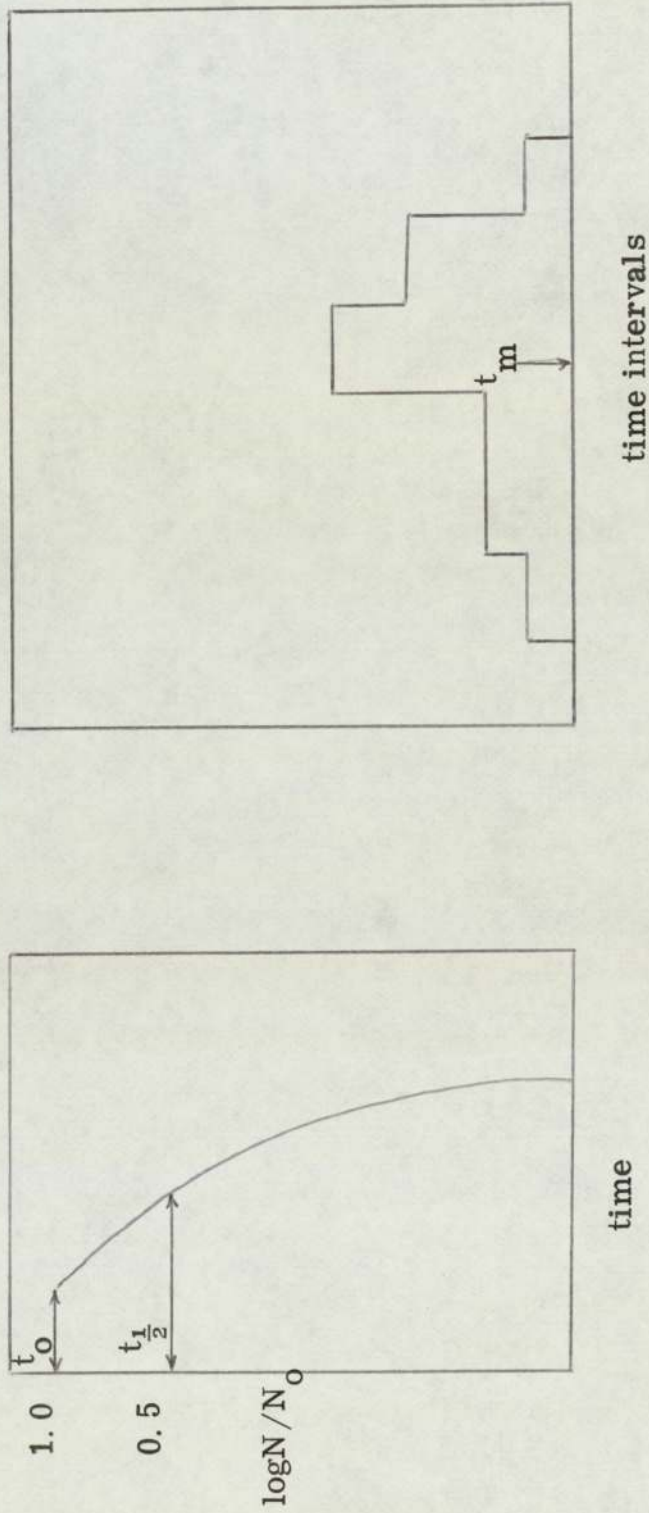
Mackay and Mason (87) and Jeffreys and Hawksley (69) photographed the rupture of the phase-2 film. It usually occurred peripherally but sometimes occurred centrally. Hartland (53) who initiated the rupture of the film by applying a voltage across the drop and interface, found that it always occurred at the edge of the film and never centrally.

### Effect of length of fall of drop:

Drop stability would be expected to decrease with the length of fall from detachment at the nozzle to arrival at the interface. However, the drop apparently bounces relative to the interface for a period after the initial strike has occurred, until the oscillations become damped and the interface is stationary (59, 80). During this time, it is possible that the film is replaced.

Figure 1.5.

Rest-time distributions in coalescence  
of single drops



Typical experimental results and normal method of presentation.

The coalescence time is not a simple function of the terminal falling velocity. The effect may be some function of the energy transmitted by the drop to the elastic interface, which manifests itself in the degree of replacement of the partially drained film. Other explanations include the possibility of the droplet absorbing surface active molecules, or acquiring an electrostatic charge, during fall. These factors can, however, be eliminated by careful preparation and precise experimental techniques.

Effect of the presence of a third component:

The effect of a third component varies dependent upon the nature of the component, and in which phase it occurs. A substance insoluble in either phase may increase or decrease the coalescence rate of a system. Thus the presence of dust particles in the film may promote its rupture, or an absorbed layer of surfactant material might be formed around the skin of the drop causing stabilisation. The presence of a stabilising agent in the film affects both the drainage rate and the probability of rupture. The drainage rate is reduced by an increase in the interfacial viscosity due to the presence of a double layer and electroviscous effects, whilst the probability of film rupture is decreased by variation in interfacial tension. The surface concentration and hence the interfacial tension vary and thus distortions in the film are inhibited since, as the area changes, the interfacial tension varies and takes up the tangential stress (44). High concentrations of the stabilising agents were most effective as shown by the relation ' $t_m$ '  $\propto$  (concentration of the stabiliser)<sup>n</sup> where  $0.4 > n < 0.3$  (42) Elton and Picknett (35) studied the coalescence process with pure binary oil-water systems contaminated with a known concentration of an electrolyte, and found that the stability of the drops increased with increased aqueous phase dilution. The concentration of electrolyte was never sufficiently high to significantly affect the physical properties of the system and experimental rest-time distribution could be correlated by equation,

$$\log N/N_0 = -c \cdot t^q \quad (1.0)$$

Where the exponent 'q' was 2. The effect of the electrolyte content on the coalescence behaviour was also studied; the stabilising effect was a function of electrolyte valency, bivalent ions being the least effective. However, Gillespie and Rideal (42) proposed the relation:

$$\log N/N_0 = -K (t - t_0)^{1.5} \quad (1.1)$$

This was based upon the drop profile observed for air bubbles at a solid plane and an assumption that the probability of film rupture was inversely proportional to film thickness.

Effect of mass transfer on coalescence;

Groothius and Zuideweg (45) studied the effect on coalescence of the transfer of acetic acid in several systems. The concept of foam stability being increased by the development of interfacial tension gradients in the area of contact between the individual bubbles was concluded to apply to the case of liquid drops coalescing at an interface.

When the direction of diffusion is from the drop, the quantity of phase-2 liquid in the film between the drop and the interface rapidly comes to equilibrium with the drop liquid. The diffusing solute will therefore be in its highest concentration in the continuous phase in the trapped film. When this higher concentration is accompanied by a lowering of interfacial tension, liquid is drawn away from the region by interfacial tension forces, Marangoni effects are produced, and coalescence is promoted. In the opposite case coalescence is retarded and the drops are stabilised. Thus in a spray column droplets coalesced more rapidly at the interface when solute was transferred from the drops into the continuous phase (23). Consideration of the results of Gayler and Pratt (40) who studied the efficiency of packed extraction columns also suggests that an increase in coalescence rate can be expected if the component undergoing transfer causes

a decrease in interfacial tension (89).

Mackay and Mason (88) studied the phenomenon of partial coalescence when this was complicated by the process of diffusion which continued throughout the stage-wise process. Their results generally confirmed the mechanisms described earlier. The results of Jeffreys and Lawson (70) could be explained partially by the mechanisms of earlier workers (45, 89) with one exception for step-wise coalescence; the secondary drop, and subsequent smaller ones, did not behave in the same manner as the primary drop and could be stabilised at the interface when mass transfer initially occurred from the primary drop. Dilution of the drop may occur during the process of step-wise coalescence, shown pictorially by Charles and Mason, and Hawksley (24, 59) due to the lower phase component being transferred upwards by the 'upward extending force' (69). The secondary and subsequent drops may be so depleted in solute concentration that it may be lower than the solute concentration in the continuous phase; the direction of transfer and the effect are then reversed.

Effect of electric fields;

Charles and Mason (24) showed that the coalescence of individual water drops at a plane benzene-water, or heptane-water, interface was promoted when an electrostatic field was applied in a direction perpendicular to the plane of the interface (42).

Brown and Hanson (17) equated the electrical forces upon the drop to the rate of drainage of the trapped film of the continuous phase. From this they calculated the initial and final thickness of the film. Their results explain the fact that an electric field only promotes coalescence of a water in oil emulsion, since no charge is induced in an oil drop in an aqueous phase owing to the high conductance of the latter.

Electrically induced coalescence can be applied to industrial processes (146) and may greatly reduce the size of certain types of liquid-liquid contactors (86).

#### Effect of impurities:

Impurities in liquid-liquid systems may take a number of forms. When the impurity is of an 'inert' nature e. g. dirt, or grease, the life times of the drops are in general markedly decreased. Even trace amounts of impurity were sufficient to produce this effect (73, 74). Conversely, Wark and Cox (143) assumed that contamination by grease could stabilise drops resting at an interface.

When the impurity is surface active, the result is invariably a marked decrease in the speed of coalescence. For example, Nielsen (104) found that life times of drops depended approximately upon the cube root of the concentration of the surfactant.

#### Vibrational effects:

Conflicting results have been reported on the effects of vibrations upon coalescence times of single drops at an interface. For the coalescence of groups of drops at an interface relatively large disturbances propagated by the coalescence of one drop tend to stabilise the other drops. Thus Gillespie and Rideal (42) suggested that vibration tended to stabilise drainage of the continuous phase film thereby impeding coalescence. Nielsen (104) observed that room vibrations and mild agitation had only a slight effect on the rate of coalescence and Brown and Hanson (17) concluded, from a study using high energy A. C. fields of varying frequencies that coalescence time was virtually independent of the frequency of vibration. Conversely, Lang (77) proposed that vibration introduced random vibrations in reported coalescence times, thereby explaining the distribution in residence times

found in all experimental results. Lang and Wilke (78) studied the effect of sonic disturbances and found a decrease in drop rest-times when these were applied to the system tributyl phosphate-water.

In conclusion, that vibration tends to stabilise the drops at the interface, resulting in longer rest-times because of constant renewal of the continuous phase film seems most probable. It must be emphasised however that this applies only to single drops, or drops in general at an interface, because the effect of vibration on the coalescence of a pair of drops or of drops in a closely packed dispersion is different. For example, drops travelling freely in a spray column tend to coalesce when vibration is applied to the column (134). Further coalescence of drops is also enhanced in a bed of drops.

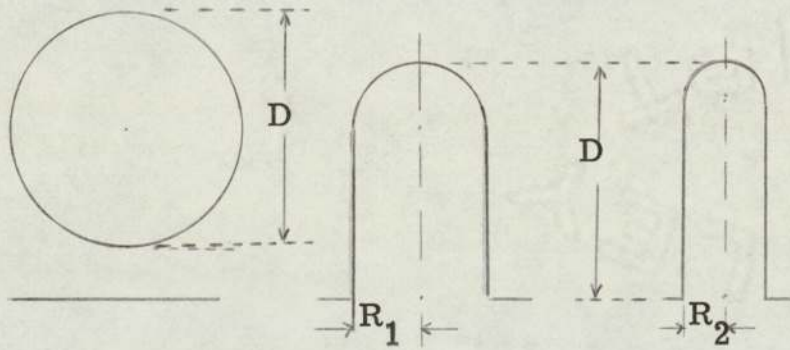
### 1. 2. Stepwise Coalescence

With some systems a smaller droplet is formed after the coalescence of a liquid drop at a liquid-liquid interface (Figure 1. 6). This phenomena of 'partial coalescence' is responsible for many of the settling difficulties encountered in commercial solvent extraction equipment. The cloudiness which often follows the primary 'break' is in part due to the formation of these small secondary drops which take a very long time to settle.

Little quantitative information is available on this phenomenon because few workers have attempted a thorough study of drop break-up during the coalescence process. However Charles and Mason (24) produced high speed cine photographs of the partial coalescence process. The mechanism of the stepwise coalescence was postulated as: The film of the liquid separating the drop from the interface was ruptured and the drop was deflated

Figure 1. 6.

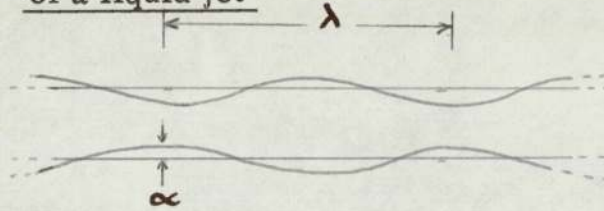
Coalescence of a liquid drop  
at a liquid-liquid interface



Formation of a column of liquid of primary drop during coalescence. The height of the column remains constant but the circumference diminishes.

Figure 1. 7.

Rayleigh's theory of break-up  
of a liquid jet



Undulations in a liquid cylinder which lead to break-up as predicted by Rayleigh.

as a result of the drainage due to the excess internal pressure. In drainage, the drop formed a cylindrical column, the radius of which continued to decrease (Figure 1. 6) until its circumference was less than its height. It then behaved like an unstable jet in which the Rayleigh disturbance could grow (Figure 1. 7). The disturbance was concentrated at a point where the cylindrical column joined the interface and resulted in a reduction of the diameter of the cylinder at that point. When the amplitude of this disturbance became equal to the radius of the cylindrical column, the latter was detached and formed the secondary droplet (Figure 1. 8). Brown and Hanson (19) made similar assumptions in their model to describe the break-up and treated the column of the liquid in the same manner. Rayleigh's theory was used to describe the break-up of the coalescing column of liquid at the liquid-liquid interface in a similar manner to the break-up of an unstable jet of liquid. However, the Rayleigh theory cannot be applied to the break-up of the coalescing column of the liquid since it does not break when the height of the column equals its circumference.

It has been shown that in a normal step-wise coalescence process, only the top half of the drop formed into a column while the bottom half remained stationary. During subsequent drainage the dimensions of the column continued to change until the column tilted about its neck where it was attached to the side of the cavity formed into the stationary pool of liquid of the bottom half of the drop. After this tilt in the column, a break occurred at its neck; the undrained column of liquid fell to the bottom of the cavity (Figure 1. 9). The secondary droplet thus formed subsequently emerged from the cavity as it retreated from the lower phase; due to the kinetic forces imparted to it by the retreating cavity

Figure 1. 8.

Formation of a secondary droplet

Model for the formation of a secondary droplet from the coalescence of a primary drop at a liquid-liquid interface.

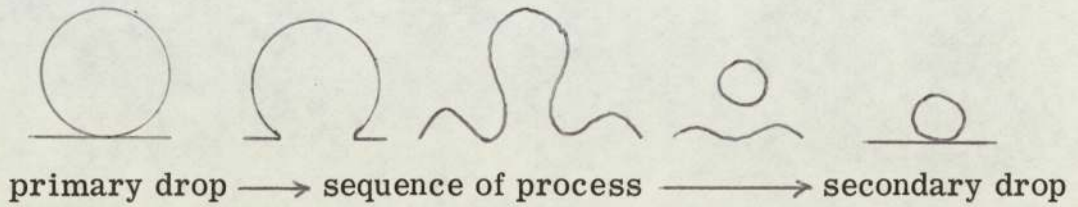
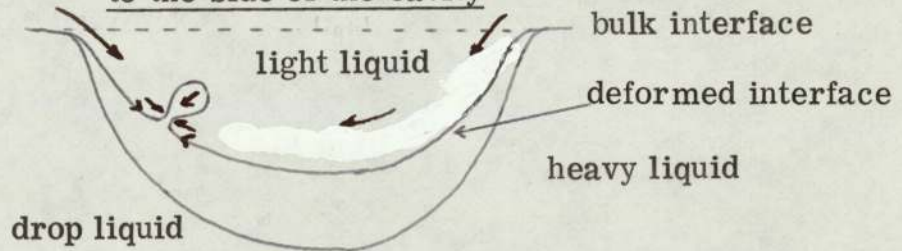


Figure 1. 9.

Draining column of liquid attached to the side of the cavity



The column breaks at its neck to form a secondary droplet which falls to the bottom of the cavity.

the secondary droplet shot above the interface as the deformed interface regained its normal position. The secondary droplet then fell back onto the interface where it rested before undergoing the next stage of coalescence.

In considering drainage from the column of liquid, Brown and Hanson treated it in a similar manner to the flow of liquid through a pipe and assumed the walls of the pipe to be rigid. However, it is not flow through a pipe but flow of one liquid surrounded by another liquid. Therefore, the model suggested by Brown and Hanson (17) cannot be applied to the drainage of the primary drop coalescing at a liquid-liquid interface.

Jeffreys and Hawksley (68) studied stepwise phenomena and suggested that the upward reaction to the downward force on the initial deflation of the drop helped to maintain the cylinder of liquid above the interface until it was detached due to this force to form the secondary droplet. The extent of the downward force was demonstrated using a coloured dye in the drop liquid; as the drop coalesced some of its contents were ejected down into the bulk phase and the dye showed the vortex produced. Charles and Mason (91) using a coloured drop, observed that after the coalescence a vortex ring similar to a smoke ring formed in the lower phase. However, with a coloured drop the cavity formed at the interface during the coalescence cannot be observed since the colourless cavity is surrounded by the coloured drop liquid.

It has recently been observed that during stepwise coalescence of a primary drop after break-up of the draining column the secondary droplet may either fall down to the bottom of the cavity or be recovered to the bulk interface. When the secondary droplet coalesces at the bottom of the cavity, the

tertiary droplet produced may coalesce there (at the bottom of the secondary cavity formed at the bottom of the primary cavity), or coalesce at the bottom of the primary cavity after its emergence from the secondary cavity, or be recovered in the bulk interface as the cavity retreats from the lower phase. In an instantaneous coalescence process, smaller droplets are formed but have not been photographed since coalescence of these smaller secondary droplets occurs below the bulk interface in the primary, secondary or tertiary cavities. According to this description (102) a drop always coalesces in a stepwise manner. All the subsequent cavities formed during instantaneous coalescence are difficult to record simultaneously at the high magnification needed to overcome other optical difficulties.

### 1. 2. 1 Factors affecting stepwise coalescence

Number of stages:

Coalescence appears generally to occur in an indefinite number of stages but becomes single-staged for drops below a certain critical size, dependent on the physical properties of the system (17). Below this critical size, the drop is presumably able to drain before the amplitude of the Rayleigh disturbance becomes sufficiently large to cause break-up of the liquid column. The number of stages observed during the coalescence of a drop is a function of the size of the primary drop and physical properties of the system. The larger the ratio of the diameters of the primary to the secondary drops the larger the number of coalescence stages (17).

Drop diameter ratio

In research studies the equivalent diameter of the primary drop has been calculated from its volume and the diameter of the secondary drop measured from photographs. The drop diameter ratio is the diameter of the primary drop over the diameter of

the secondary droplet.

A small decrease in the drop diameter ratio has been observed with increasing viscosity of the continuous phase but the interfacial tension and the viscosity of the dispersed phase are the primary variables.

Effect of viscosity ratio:

Charles and Mason (24) showed that the viscosity ratio of the drop liquid to that of the surrounding medium was the chief factor determining whether stepwise coalescence occurred. When the viscosity ratio was less than 0.02 or greater than 11, a single stage coalescence was likely to occur. However, Jeffreys and Hawksley (69) observed a two or three stage coalescence processes at a viscosity ratio much less than 0.02.

Effect of temperature on stepwise coalescence:

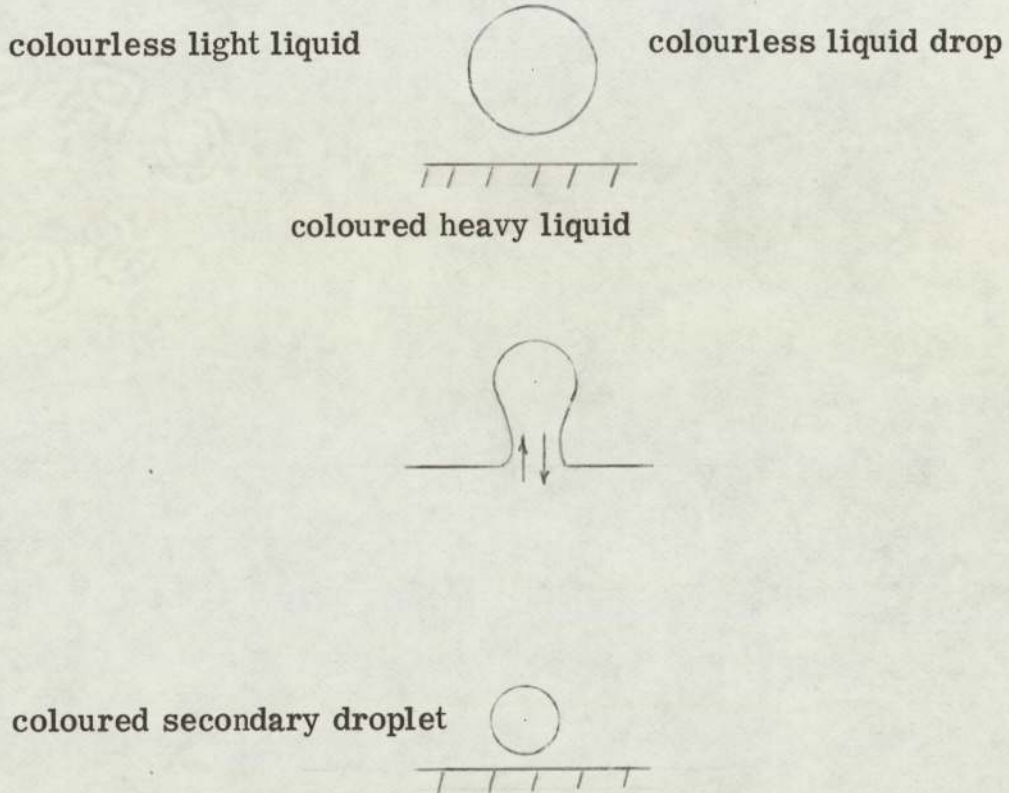
Jeffreys and Hawksley (69) examined the effect of temperature on stepwise coalescence. At 35°C, water drops of radius 0.2 - 0.4 cm. coalesced in a single stage at a liquid paraffin-water interface. At 45°C and 55°C, the coalescence was completed in two or three stages. For both, kerosene and benzene with water the coalescence took place in five steps at a temperature above 20°C.

Flow of homophase liquid into drop during coalescence:

Jeffreys and Lawson (70) observed that in the coalescence of an aqueous phase drop in an oil-aqueous phase system some of the aqueous phase entered the drop during its coalescence. The aqueous phase was coloured with a red dye and a colourless drop allowed to coalesce. They noticed that the secondary droplet was coloured. Therefore, some of the aqueous phase was drawn up

Figure 1.10.

Flow of homophase liquid into the drop during coalescence



Formation of coloured secondary droplet showing the flow of coloured homophase liquid into the colourless primary drop during its coalescence.

(Figure 1. 10) through the centre of the neck and mixed with the contents of the drop during its initial stages of coalescence.

#### Effect of mass transfer on stepwise coalescence.

When mass transfer occurs during coalescence of a single drop, two types of coalescence process are possible, i. e. instantaneous coalescence and delayed coalescence. A true instantaneous coalescence has been observed to occur when the drops did not rest at the interface but appeared to pass straight through it. When this type of coalescence occurred the drop contents, after plunging into the aqueous phase, descended into it and then returned to spread over the interface. However, it has been reported that water drops passed straight through a glycerol-water mixture/heptane interface when a small amount of 'Teepol' was added to the aqueous phase (102). In this case, the drop coalesced after hitting the bottom of the glass cell. An apparent 'instantaneous' coalescence was also observed in which a drop rested at the interface for only a fraction of a second before coalescing (70); in this, after coalescence, the drop contents descended about three times deeper into the aqueous phase and then slowly mixed with the lower phase.

In a delayed coalescence, Jeffreys and Lawson (70) observed that the drop rested at the interface for a measurable time before it coalesced.

#### Effect of electrostatic potential on stepwise coalescence

Brown and Hanson (19) found that the application of an electrostatic potential between the drop and the interface produced a single staged coalescence in a system which had previously exhibited secondary droplet formation. This was attributed to

an electrocapillary effect i. e. a lowering of the interfacial tension due to a repulsion between similar charges.

Simultaneous formation of more than one secondary droplet:

During their investigation of the stepwise phenomena Charles and Mason observed quite often that a large primary drop yielded two secondary droplets of equal size. Edge and Greaves (33) also observed the simultaneous formation of two secondary droplets (Figure 1. 11) but in pure systems only. Simultaneous formation of two secondary droplets has been attributed to two cycles of a Rayleigh type disturbance being present on the column during coalescence. The plateau-spherule drop, which always follows the primary drop from the tip, may be confused with another secondary droplet (102). The plateau-spherule drop remains at the interface even after the completion of the first step of the coalescence of the primary drop; the secondary droplet formed by coalescence has been observed resting side by side with the plateau-spherule drop.

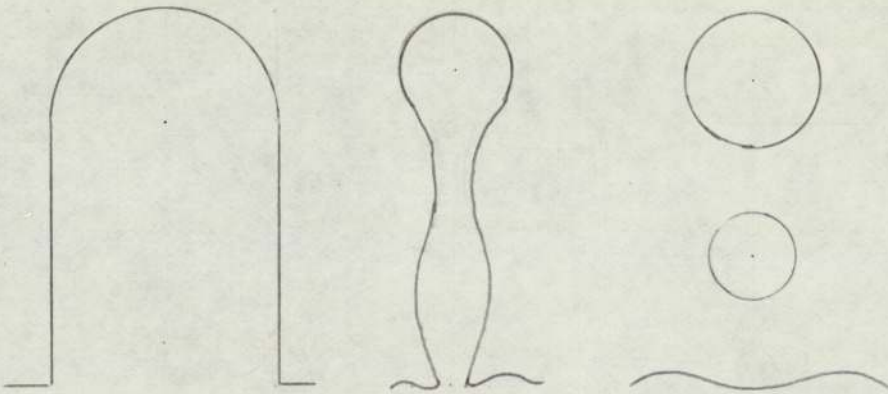
### 1. 3 Drop-Drop Coalescence

Few studies have been made of drop-drop coalescence due to two main experimental difficulties. Firstly, a controlled collision between two drops is extremely difficult to obtain unless one of the drops is restrained in some way. Secondly, the randomness with which the drops rebound and coalesce makes analysis inherently difficult.

Linton and Sutherland (83) noted that small drops (0. 1 cm. ) issuing from two jets would coalesce while larger drops (0. 5 cm. ) would not. The other important factors governing drop-drop coalescence are undoubtedly the drops' terminal velocities and the

Figure 1. 11.

Simultaneous formation of two secondary droplets from a single primary drop



Simultaneous formation of two secondary droplets was attributed to two cycles of Rayleigh type disturbance.

position of contact during collision.

Scheele and Lang (125) investigated experimentally whether two colliding drops would coalesce or rebound. No obvious relation was found between the coalescence probability and the input velocity, but coalescence was very sensitive to the phase of oscillation at the point of contact. The classical parallel disc model (125) would not predict rupture within the apparent time of contact. The controlling factor in the drop-drop coalescence was, therefore, concluded to be the film thinning step, which is in agreement with the findings of Mason (89).

The life times of the drops depend upon the curvature of the specific oil-water interface. Thus Nielsen (105) found that life times were longest when the oil-water interface curved around the drop and shortest when the interface curved to facilitate the flow of the continuous phase away from the interface, as when two drops approach each other. In the case of interdrop coalescence the increase in the quantity of the continuous phase film trapped between the interfaces is a factor.

Allan and Mason (7) studied the coalescence of pairs of drops in a laminar shear field produced in the annulus between two concentric cylinders rotated in opposite directions. The annulus was filled with the continuous phase and, by adjusting the velocities of the cylinders, a static layer of liquid with zero tangential velocity could be produced. The drops were propelled towards each other by placing one on each side of this stationary zone. For any set of conditions the amount of rotation that took place before coalescence of the doublet occurred, and therefore the contact time, showed a distribution of values similar to that observed for coalescence in a gravitational field.

In a simulation of coalescence of pairs of drops two curved surfaces were propelled together at a constant velocity, and the delay times and interface patterns were determined from high speed photographs (7). The reduced delay times that occurred when very small potential differences, of less than 1.0 volt, were applied between the drops were shown to result not from an enhanced rate of drainage of the complete film, but rather enhancement concentrated at the thinnest parts of the film when projections were formed that bridged the film due to the induced charges. Indeed, this normally occurred so rapidly that uniformity of film thickness was not reached.

#### 1. 4. Swarms of Drops

The phenomena involved in coalescence of swarms of drops is complex but deserves special attention, since it represents the real situation in practical equipment. In theory the phenomena is describable in terms of the behaviour of single drops, but is better analysed from a consideration of an incomplete layer or monolayer. This can then be extended to conceive a more complicated multilayer system.

##### 1. 4. 1. Monolayers

Lawson (80) studied the coalescence of groups of drops at an interface and noted that relatively large disturbances, propagated by the coalescence of one of the drops, did not promote coalescence in the others. On the contrary, the existing drops became more stable resulting in longer rest-times. Conversely, other workers concluded that, in general, any factor which causes a vibration or disturbance at the interface, decreases the stability of the drops.

The movement of neighbouring drops affects the drainage and rupture of the film between the surfaces. With other conditions remaining constant, one cause of the disturbance in a monolayer is the arrival or disappearance of a drop or droplets during the time a specific single drop is undergoing the process of coalescence. Davies et. al. (67) studied a group of droplets at an interface i. e. a monolayer. Without injecting any outside disturbance into the system they concluded that the rate of coalescence was inversely proportional to the drop size. With the smaller drops interdroplet coalescence was promoted to a greater extent.

A series of investigations to determine the coalescence characteristics of a single drop and subsequently two or more drops as a layer at an interface have been reported by Robinson and Hartland (120). They investigated the effect of neighbouring droplets in a two dimensional array on the arc length of the draining film between a drop approaching a bulk interface. The arc lengths were calculated from droplet profile measurements from projected photographs. The arc length was least for the drop in the middle of the row: it reached a minimum when there were about four drops present in investigations of a total of one to nine drops in a single array. The arc length for a drop in the middle of a row was about 30 % less than that for a single drop for the systems liquid paraffin-golden syrup and liquid paraffin-glycerol. An aqueous glycerol-silicone system showed twelve per cent difference. Further it was observed that in a row of droplets each of volume less than 0.2 ml., the one at the middle which had the shortest arc length coalesced first with the bulk dispersed phase. However, for larger sizes, drop-drop coalescence occurred prior to the interface.

The decrease in arc length was attributed to the increase in the horizontal forces exerted by the neighbouring droplets. Similar studies with drops in a vertical column, and more than one row of droplets, showed changes in arc lengths. It was concluded that the shape of a liquid drop approaching a deformable liquid-liquid interface was affected by the presence of adjacent drops .

Topliss (140) studied the coalescence behaviour of a monolayer of regular sized droplets at a plane interface using two component systems in a 6" diameter glass column. Drop sizes and coalescence times were evaluated from cine films. In one set of experiments, the droplets were formed continuously but the dispersed phase was not recycled. Fresh and saturated dispersed phase liquid was fed to the distributor by gravity. For the continuous arrival of water droplets at a benzene-water interface, values of  $\log N/N_0$  were plotted versus overall drop-interface coalescence times. Similar curves were obtained to that illustrated in Figure 1. 5 for single drops but of a different magnitude, the variation being dependent on the proximity of adjacent drops. No satisfactory distribution was obtained for drop-drop coalescence, the incidence being low for the continuous production of drops.

With batch-wise production of drops (140) most of the coalescence was observed to be drop-drop followed by a final few large drops coalescing with the interface.

#### 1. 4. 2 Multilayers

The investigations reported in the literature may be grouped into two main sections, viz

- (a) Batch wise (unsteady state) studies and
- (b) Continuous (steady state) studies.

Robinson and Hartland (120) studied droplets in multilayers in both batch and continuous experiments; their results showed a decrease in residence time for a drop of given size at the bulk interface as the dispersion height increased. In the comparison of the coalescence in two and three dimensional beds, the latter was reported to be more rapid.

Komasawa and Otaka (75) concluded from a study involving batchwise experiments, that the stability of a drop layer was independent of the volume of drops arriving at the layer. In the presence of stabilisers, especially sodium oleate, the stability of a drop layer was far less than that of a single drop, but the relation between stability and concentration was analogous to the relation observed with single drops. The stability of a drop layer was defined as the average time that drops could remain in the layer. In the presence of sodium oleate, interdrop coalescence was negligible. However, when polyvinyl acetate was used as a stabiliser in benzene droplets, drop-drop coalescence occurred to such a degree that the diameter of drops about to coalesce with the bulk phase was often 2 - 5 times larger than drops from the inlet nozzle.

Jeffreys, Davies and Pitt (66) investigated the rate of coalescence of swarms of drops in the settler of a single stage mixer - settler. With kerosene dispersed in water the drop size in the settler increased with the distance from the inlet and was dependent upon agitator speed and flowrate. The effect of agitator speed was most significant; the ratio of drop diameter at any position to that at the inlet increased directly with an increase in speed. This ratio varied at the top of the wedge between two and five dependent on operating conditions.

These studies were conducted in either agitated vessel type mixer settlers, horizontal gravity settlers or vertical spray type columns. Binary systems were studied in the absence of mass transfer. When a third component was present it was equilibrated between the two phases merely to allow a controlled variation of a particular physical property, e. g. interfacial tension. However, when mass transfer accompanies coalescence, completely different behaviour can be anticipated (123).

Coalescence of droplets within a swarm necessitates firstly that they approach each other to form a close packed, heterogeneous zone between the two bulk liquid phases. The high initial velocities of the droplets are thus reduced and they move towards the interface in a close packed arrangement. Some interdrop coalescence occurs amongst the densely populated droplets before they reach the two-phase interface where they eventually undergo drop-interface coalescence. Thus coalescence within a swarm of droplets involves both modes i. e. interdrop and drop-interface coalescence.

Batch experiments were used by Meisner and Chertow (93) to study the effect of phase ratio. A mixture of two immiscible liquids was agitated and the time for separation was then determined. Large droplets separated fairly rapidly but the fine droplets remained as a haze that settled extremely slowly.

Ryon, Daily and Lowrie (123) investigated the scale-up of mixer settlers and observed that most of the coalescence in the settler occurred at the interface. However, the system employed in their investigation seems likely to have suffered from contamination; therefore, their results are not of general application.

Smith and Davies (135) studied dispersion bands produced in a 2" spray column with water dispersed in five different continuous phase systems. The following general correlation related the dispersion band height to the physical properties and inlet mean drop diameter,

$$H/d_{12} = 3.5 \times 10^3 (V_d \mu_c / \rho)^{0.85} (d_{12} \cdot g \cdot \Delta \rho / \rho)^{-0.88} \times (\mu_d / \mu_c)^{0.77} \quad (1.2)$$

An equation was also proposed for the case when the column walls were 'non-wetted' by the dispersed phase due to the application of a coating of a silane compound,

$$H/d_{12} = 2.6 \times 10^3 (V_d \mu_c / \rho)^{0.82} (d_{12} \cdot g \cdot \Delta \rho / \rho)^{-0.86} \times (\mu_d / \mu_c)^{0.73} \quad (1.3)$$

Higher dispersion bands were produced when the dispersed phase wetted the column walls. Either an increase in dispersed phase velocity, or a decrease in the inlet mean drop diameter, produced an increase in band height. The effects of the system properties were evaluated in terms of dimensionless groups as given in Equation (1.4.20 and 1.4.21). The limitation of this study was the small column diameter such that wall effects would be more significant than on a larger scale.

Hitit (60) studied phase separation in a continuous flow system. This involved the formation of a flocculation zone comprising three distinct sections. Different droplet behaviour and packing efficiencies were observed in each section. In the droplet entry region rigid drop behaviour pertained and fractional hold-up varied between 0.25 and 0.75. This region extended some 10 to 15 mm. from the inlet plane; in this region the drops moved freely and randomly but the incidence of interdroplet

coalescence was small. The second region constituted the major proportion of the total height and in it a gradual change in the hold-up was observed which was characteristic for each system studied. Interdrop coalescence and drop deformations prevailed in this region. The third region was turbulent and extended to the bulk dispersed phase interface. The fractional hold-up in this region was of the order of 0.90 and droplets underwent maximum distortion; a high incidence of inter-drop coalescence prevailed. Measured hold-up profiles for each section were represented by straight line plots of fractional dispersed phase hold-up  $\phi$  vs. fractional zone height, H, viz,

$$\phi = m \cdot H + C \quad (1.4)$$

For the entry section, m had a value between 1.33 to 1.85; for the mid section m was lower, in the range of 0.06 to 0.24 and was dependent upon the ratio  $g \cdot \Delta \rho / \beta$ . Higher values of m pertained in the third section viz, 0.37 to 1.5. The value of the constant C was 0.30 to 0.70, 0.70 to 0.90 and 0 to 0.64 for each section respectively.

The total flocculation zone heights were correlated by the following equations:

For the toluene-water system,

$$H = 3.28 d_{12}^{-0.062} \cdot V_d^{1.24} \quad (1.5)$$

For diethylcarbonate-water system

$$H = 15.20 d_{12}^{-1.56} \cdot V_d^{1.88} \quad (1.6)$$

For M. I. B. K. -water system,

$$H = 25.0 d_{12}^{-0.15} \cdot V_d^{1.43} \quad (1.7)$$

For the iso octane-water system

$$H = 7.65 d_{12}^{-1.54} \cdot V_d^{2.80} \quad (1.8)$$

For inlet drops of a mean diameter between 0.07 to 0.48 cm., the effect of system physical properties upon flocculation zone height was correlated by

$$H = a. (d_{12} \cdot g \cdot \Delta\rho)^n / \gamma \quad (1.9)$$

with 'a' and 'n' being constants specific for each system.

Countercurrent flow of the continuous phase had no significant effect upon the zone heights. Agreements between results obtained in 6" and 9" columns respectively indicated that wall effects were not significant either when compared with results from a 3" column.

By assuming the overall motion of the flocculated drops to resemble a diverging conduit, the cross sectional area of which was described in terms of the empirical hold-up equations, a model was proposed for the residence time.

$$T = K \cdot \frac{V_d}{H} \quad (1.10)$$

From the above review it is clear that coalescence, especially in multi-drop systems, is a complex process involving interaction between numerous variables. The practical difficulties often encountered in liquid-liquid coalescence may be overcome by liquid-liquid-solid coalescence in which a solid surface is introduced, e. g. in the form of a packing, in the continuous phase medium to aid coalescence. However, the efficiency of a liquid-liquid-solid coalescence process depends on the surface characteristics of a solid which are reviewed in the next chapter.

## CHAPTER TWO

### BEHAVIOUR OF LIQUID DROPS AT A SOLID-VAPOUR INTERFACE

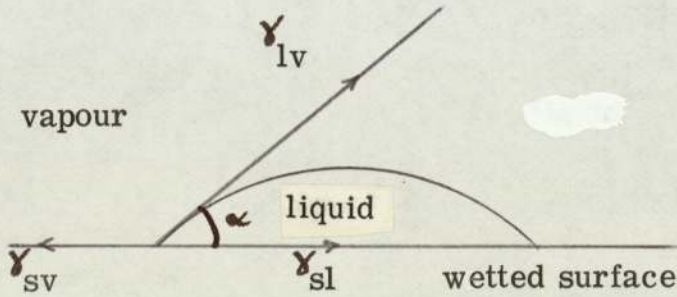
With many liquid-liquid dispersions coalescence under the influence of gravity does not take place readily. To accelerate the process, and to achieve efficient phase separation, methods other than gravity settling or means to aid coalescence efficiency may be employed. One simple and economical method involves passing the dispersion through a coalescing aid in the form of a packed or fibrous bed. The operation of these beds depends upon the fundamental behaviour of liquid drops on solid surfaces. The simplest case to consider is the behaviour of a single liquid drop on a plane solid-liquid interface where the solid surface is placed in a vapour medium.

#### 2.1 The contact angle

When a liquid drop is placed on a clean solid surface, the liquid drop may either spread out as shown in Figure 2.0, forming a thin film of the dispersed phase liquid on the solid surface, or remain 'bunched up' in the form of a segment of a circle, as shown in Figure 2.1. If the drop is very small, surface forces predominate over gravitational forces and the shape of the drop approaches that of a sphere segment. Conversely, if the drop diameter is larger than about 3 mm. gravitational forces predominate and the drop is distorted so that it tends to the horizontal. Drops of intermediate size flatten out partially. Clearly, therefore, the behaviour of a liquid drop on a solid surface is determined by the relative attraction between the drop and the solid surface. Such behaviour is conveniently characterised by the contact angle, an index of the relationship between the solid surface energy

Figure 2.0.

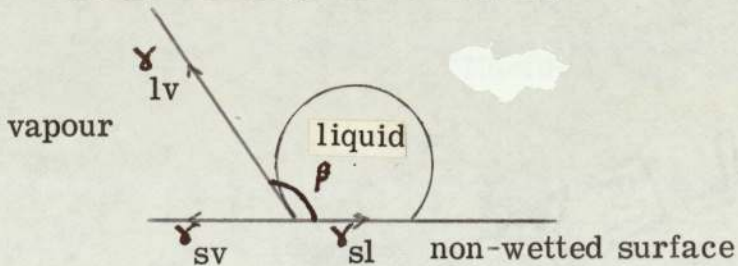
Behaviour of a liquid drop at a wetted solid surface placed in vapour



A contact angle  $\alpha < 90^\circ$ .

Figure 2.1.

Behaviour of a liquid drop at a non-wetted solid surface placed in vapour



A contact angle  $\beta > 90^\circ$ .

and the overall coalescence process. The contact angle is defined as the angle between the tangent to the drop, measured at the junction of the drop and the solid surface, and the surface of a solid. It is measured into the drop as shown in Figures 2.0 and 2.1.

The contact angle is a measure of the phenomena called 'wettability'. A contact angle of zero implies complete 'wetting' in which the dispersed phase liquid spreads out to form a thin film on the solid surface; subsequent drops arriving at the solid surface would coalesce with this film. A contact angle of  $180^\circ$ , which is rarely encountered in practice, corresponds to complete 'non-wetting'; if subsequent drops arrive in the vicinity of the initial drop, coalescence occurs via an interdrop process.

## 2.2 Work of 'cohesion' and 'adhesion'

The work of 'cohesion' is the work required to separate a liquid in a column, one square centimeter in cross-sectional area, to give two surfaces, each one square centimeter in area i. e.

$$W_c = 2\gamma_b \quad (2.1)$$

where  $\gamma_b$  is the surface tension of the liquid.

The work of 'adhesion' is the work required to effect a separation of two immiscible liquids in a column, one square centimeter in cross-sectional area i. e.

$$W_a = \gamma_a + \gamma_b - \gamma_{ab} \quad (2.2)$$

where  $\gamma_a$  and  $\gamma_b$  are the surface tensions of the two liquids and  $\gamma_{ab}$  is the interfacial tension.

Harkins (50) modified Dupre's Equation (2.2) to cover the spreading of liquids. Thus when a drop of a liquid B is placed on the surface of another liquid A, the first liquid may spread out to a film of sufficient thickness so that the interface between the two liquids and the surface of B do not lose their identity. The corresponding change in surface tension, i. e.

$\gamma_a - (\gamma_b + \gamma_{ab})$  is defined as the spreading coefficient 'S' such that

$$S = \gamma_a - (\gamma_b + \gamma_{ab}) \quad (2.3)$$

Harkins' Equation (2.3) implies that liquid B will not spread on liquid A unless  $(\gamma_b + \gamma_{ab})$  is less than  $\gamma_a$ . Therefore, for spreading to occur, the spreading coefficient must have a positive value. However, the work of 'adhesion'  $W_A^{sl}$  for a solid and a liquid has been defined by Harkins such that

$$W_A^{sl} = \gamma_s + \gamma_{lv} - \gamma_{sl} \quad (2.4)$$

where

$\gamma_{lv}$  is the surface tension of liquid surrounded by vapour  
 $\gamma_{sl}$  is the interfacial tension of a solid-liquid interface  
 and  $\gamma_s$  is the specific free energy of the solid surface free from any adsorbed film.

### 2.3. Young's Equation

Young proposed the following equation to relate the surface energy of a solid surface to the physical properties of a liquid drop resting on this plane surface at equilibrium;

$$\gamma_{sv} - \gamma_{sl} = \gamma_{lv} \cos \alpha \quad (2.5)$$

where  $\gamma_{sl}$  is the interfacial tension along the solid-liquid boundary,  
 $\gamma_{sv}$  is the surface tension of the solid covered with a film  
of vapour of the liquid (in equilibrium),  
and,  $\gamma_{lv}$  is the surface tension of the liquid surrounded by  
the vapour.

Young's equation has been a subject of continuing discussion both as to the derivation and the assumptions inherent in it. Binkerman (12) argues that the treatment in Young's equation leaves the vertical component of tension  $\gamma_{lv}$ , namely  $\gamma_{lv} \sin \alpha$ , unaccounted for. From the Second Law of Thermodynamics, this component, if not compensated, would impart a constant acceleration to the solid. Pettica and Pettica (110) commented that the equation for the equilibrium contact angle was only applicable for a spherical drop and that it was invalid in a gravitational field. However, Johnson (71) suggested that adsorption and gravitational effects had no effect on the validity of the equation. Elliott and Riddiford (34) could not understand why so many questions should be raised about a self-evident equation; they suggested that if a three phase system was truly in equilibrium, both before and after drop deposition, then Young's equation must apply.

Goodrich (43) considered Young's assumption that a solid surface has a surface tension analogous to a liquid interface and argued that the equation is only applicable when the drop produces a negligible strain energy in the solid. However, Lester (81) showed that the equation was valid provided the surface was not too deformable.

The basic thermodynamics of a surface, first described by Gibbs (41) were later used by Buff (20) and more recently by Johnson (71) to verify Young's equation. Johnson also presented a thermodynamic proof as to the validity of the equation. It is frequently assumed that  $\gamma$ , the surface tension of an interface, and  $F_s$ , the specific surface free energy are numerically equal. These two are defined as follows:

$$\gamma = (\partial F / \partial A) \quad (2.6)$$

$$\text{and } F_s = (F - F^\alpha - F^\beta) / A \quad (2.7)$$

However,  $\gamma$  and  $F_s$  are related by Equation 2.8

$$F_s = \gamma + \sum_{i=1}^M \Gamma_i \mu_i \quad (2.8)$$

$$\text{when } \mu_i = (\partial F / \partial n_i)_{T, V, sl, n_j} \quad (2.9)$$

and  $M$  is the number of components in the system. For a pure liquid, the surface excess of the solvent can be considered to be zero and the surface tension is numerically equal to the specific free surface energy. For those systems in which adsorption is important,  $\gamma$  and  $F_s$  are not equal. Young's equation is then valid in terms of  $\gamma$  but not  $F_s$ .

Equation 2.5 can be written in the form:

$$\gamma_s - \gamma_{sv} = \gamma_s - \gamma_{sl} - \gamma_{lv} \cos \alpha \quad (2.10)$$

where  $\gamma_s$  is the specific free energy of the film-free solid in a vacuum. The left-hand side of equation 2.10 is termed the 'film pressure';

$$\gamma_s - \gamma_{sv} = \bar{\pi} \quad (2.11)$$

it represents the decrease in the surface tension of the solid when covered with an adsorbed film in equilibrium with its vapour.

Using the above definition of  $\pi$ , Equation 2.11 can be rewritten,

$$\gamma_s = \gamma_{lv} \cos \alpha + \gamma_{sl} + \pi \quad (2.11)$$

If each of the parameters  $\gamma_s$ ,  $\gamma_{lv}$ ,  $\gamma_{sl}$  and  $\pi$  could be determined independently,  $\alpha$  can be calculated; hence the extent to which a specific liquid will wet a given liquid could be predicted. In practice, little is known about the specific free energies of solids and Equation 2.11 is used to assess this parameter. However, if spreading occurs, Young's equation is no longer applicable.

#### 2.4. Surface Free Energy

In any system comprising two phases, there is a surface of separation. While the precise thickness of this interfacial region is unknown, it includes all parts of the system that are influenced by the surface forces. The two bulk phases, which may be two liquids or a liquid and vapour, can for convenience be considered to be separated by a surface phase.

The total free energy  $F$  of a system comprising two bulk phases and an interface is,

$$F = F^\alpha + F^\beta + F^s \quad (2.12)$$

where  $\alpha$  and  $\beta$  refer to the bulk phases and  $s$  to the surface phase. If a small, reversible change occurs in the system, the free energy change  $dF$  is expressed as,

$$dF = dF^\alpha + dF^\beta + dF^s \quad (2.13)$$

For the homogeneous bulk phases, the free energy changes are:

$$dF^\alpha = -S^\alpha dT + V^\alpha dp^\alpha + \mu_1^\alpha dn_1^\alpha + \mu_2^\alpha dn_2^\alpha + \dots \quad (2.14)$$

$$dF^\beta = -S^\beta dT + V^\beta dp^\beta + \mu_1^\beta dn_1^\beta + \mu_2^\beta dn_2^\beta + \dots \quad (2.15)$$

where  $s$ ,  $T$ ,  $V$  and  $p$  refer to entropy, temperature, volume and pressure respectively. The term 'n' refers to the number of

molecules of a component whose chemical potential is  $\mu$ . The subscripts refer to components 1, 2, .....

The surface free energy change must include a term for the work required to increase the area of the surface by an infinitesimal amount  $dA$ , at constant temperature, pressure and composition. The reversible work of surface expansion, done against the surface tension  $\gamma$  is equal to  $\gamma \cdot dA$ . Since the surface contribution to the volume is negligible,  $Vdp$  can be omitted.

Then,

$$dF^S = -S^S dT + \gamma dA = \mu_1^S dn_1^S + \mu_2^S dn_2^S + \dots \quad (2.16)$$

where  $\mu_1^S, \mu_2^S, \dots$  are the surface chemical potentials of the various components of the system.

$$dF = S dT + V^\alpha dp^\alpha + V^\beta dp^\beta + \gamma dA + \sum \mu_i^\alpha dn_i^\alpha + \sum \mu_i^\beta dn_i^\beta + \sum \mu_i^S dn_i^S + \dots \quad (2.17)$$

where  $S = S^\alpha + S^\beta + S^S$  is the total entropy of the system.

At constant temperature, pressure and composition

$$dF = \gamma dA \quad (2.18)$$

$$\text{or } \gamma = \left( \frac{\partial F}{\partial A} \right)_{T, p, n} = F_S \quad (2.19)$$

Equations 2.18 and 2.19 define surface tension, a measure of the work required to increase the surface by unit area, at constant temperature, pressure and composition. The term  $F_S$  is the surface free energy per unit area, expressed in  $\text{ergs cm}^{-2}$ .

Since it is numerically equal to the surface tension for a pure liquid,  $\gamma$  is commonly used to express either surface tension or surface free energy per unit area.

### 2.5 High and Low Energy Solid Surfaces

Solid surfaces which have a high specific surface free energy are referred to as 'high energy surfaces' and solids which have a low specific surface free energy are termed 'low energy surfaces'. Examples of high energy surfaces are metal and glass;

those of low surface energy include plastics e. g. polypropylene, nylon and p. t. f. e.

#### 2. 5. 1. Wetting of high surface energy solid materials

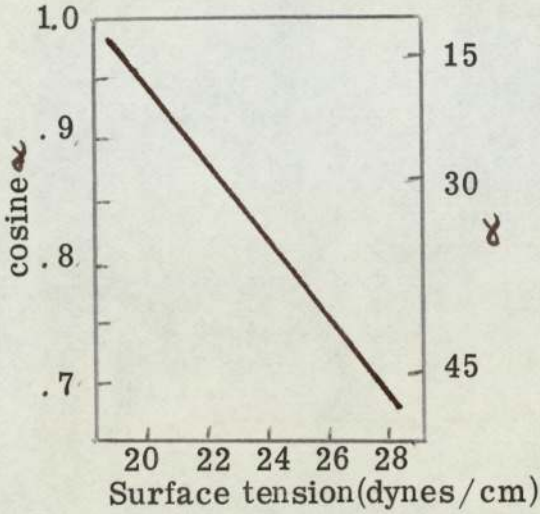
From extrapolation of measurements of the spreading coefficients of liquids on water and mercury, Harkins and Feldman (52) concluded that practically all liquids should spread on clean metals and high melting point solids. Zissman et. al. demonstrated that under certain conditions liquids will not spread on a high energy solid surface. When the liquid is a polar-nonpolar molecule of a certain type, or contains a solute of a certain type, it deposits a low energy surface through adsorption at the solid-liquid interface; it will not subsequently spread on this surface film. Many pure liquids, including the branched and straight-chain aliphatic acids and alcohols, are autophobic (49) in this fashion. When a solid is coated with a nonpolar adsorbed film, liquids which have higher surface tensions than the critical surface tension of the adsorbed film will not spread.

#### 2. 5. 2. Wetting of low surface energy solid materials

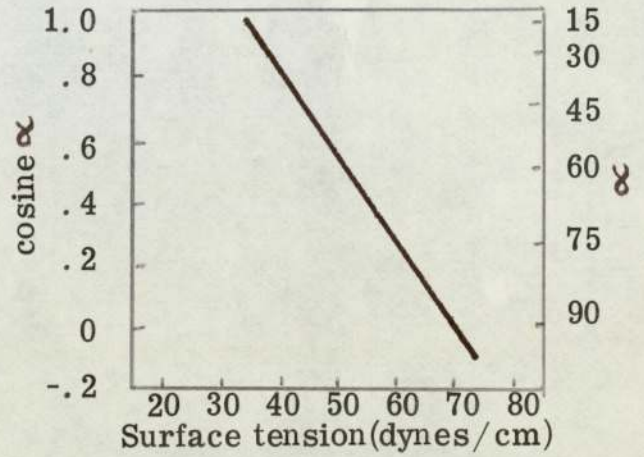
Fox and Zissman (38) investigated the equilibrium contact angles of a variety of pure liquids on particular surfaces of solid organic polymers such as polytetrafluoroethylene. Care was taken in surface preparation to give an extremely clean and smooth condition. The advancing and receding contact angles were identical so long as the liquid drop was advancing or receding sufficiently slowly to be reasonably close to an equilibrium condition. The systems behaved reproducibly. No significant differences were found in the contact angles of n-alkanes on polytetrafluoroethylene when measured in air

Figure 2. 2.

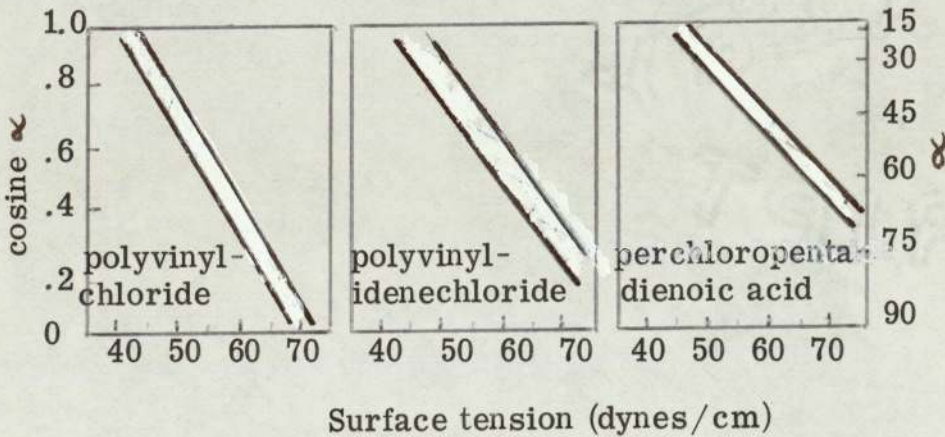
Effect of surface tension on the  
wettability of solid surfaces



Wettability of p. t. f. e.  
by n-alkanes.



Wettability of polyethylene  
by n-alkanes.



Wettability of various surfaces by various liquids.

saturated with the liquid vapour compared with those measured in air. Therefore, measurements of contact angles of high boiling liquids on low energy surfaces could be made in air.

Figure 2. 2. illustrates the relation between  $\cos \alpha$  and  $\gamma_{lv}$  for n-alkanes on polytetrafluoroethylene (38). The intercept of the horizontal line  $\cos \alpha = 1$  with the extrapolated straight line plot  $\cos \alpha$  vs  $\gamma_{lv}$  is equivalent to the critical surface tension,  $\gamma_{cl}$ , i. e. the liquid surface tension below which liquids spread on a given polymer. In general, the graph of  $\cos \alpha$  vs  $\gamma_{lv}$  for any low energy solid is always a straight line, or a narrow rectilinear band, as shown in Figure 2. 2. b. and 2. 2. c.

When rectilinear bands are obtained, the intercept of the lower limb of the band at  $\cos \alpha = 1$  is chosen as the critical surface tension,  $\gamma_{cs}$  of the solid.  $\gamma_{cs}$  has been used to characterise and compare the wettabilities of a variety of low energy solid surfaces. It has been concluded from experimental results that the wettability of low energy organic surfaces, or of high energy solid materials coated by organic films, is determined essentially by the nature and packing of the exposed surface atoms of the solid and is otherwise independent of the nature and arrangements of the underlying atoms and molecules.

## 2. 6. Factors affecting the Contact Angle

### 2. 6. 1. Surface roughness

Bartell and Shepard (9) defined surface roughness in terms of the average height 'h' to which asperities rise above the horizontal surface plane and the mean angle of inclination  $\alpha$  of the sides of the asperities with respect to the horizontal plane of the solid surface. Their investigation of contact angles on a roughened paraffin wax surface indicated that 'h' had no

effect on either the advancing or receding contact angles. However, an increase in the angle of inclination generally resulted in an increase in the apparent advancing contact angle and a decrease in the apparent receding contact angle. Wenzel (147) also investigated the surface roughness and suggested a modified form of Young's equation,

$$r (\gamma_{sl} - \gamma_{sv}) = \gamma_{lv} \cos \alpha' \quad (2.20)$$

where 'r' is the ratio of the actual surface area to the geometrical surface area and  $\alpha'$  is the contact angle on the roughened surface. 'r' is always greater than unity except on an ideally smooth surface when its value is unity. The contact angle  $\alpha$  on a smooth surface is related to that on a roughened surface by,

$$\cos \alpha = \cos \alpha' \quad (2.21)$$

Therefore, if the contact angle on a smooth surface is less than  $90^\circ$ , roughening the surface would decrease the observed angle and vice versa. Binkerman (12) considered that every groove, or scratch, on a solid surface behaves as a capillary tube in which the liquid rises if the contact angle is less than  $90^\circ$  or descends if it is greater than  $90^\circ$ .

### 2.6.2. Interfacial velocity

Yarnold and Mason (149) studied the effect of varying the rate of motion of a water-air interface over paraffin wax. There was only a little change in the advancing angle but the receding angle fell with increasing rate of recession.

Elliott and Riddiford (34) studied the phenomena with glass-water-water vapour and polyethylene-water-water vapour. A drop of water was made to advance between two parallel plates of the same solid surface; the interface was allowed to advance to a certain limit and then halted causing the drop to recede. The

contact angle was shown to be independent of interfacial velocity at low velocities. At higher speeds the rate of change increased linearly and became practically insignificant leading finally to a limiting value.

### 2. 6. 3. Temperature

Since the physical properties of a system vary with temperature, the stability of a liquid drop is also temperature dependent. However, although contact angle varies with temperature, the variations observed are very small.

Davies and Rideal (29) investigated the effect of temperature on contact angle values and found that  $d\theta/dT$  for high energy surfaces was  $-0.06$  degrees/degree C. Fowkes and Harkins (37) noted that the contact angle of water drops on low energy surfaces increased by  $0.06$  degrees/degree C.

Newman found an appreciable decrease in the contact angles of several organic liquids against their saturated vapours, on a siliconed surface, when the temperature was allowed to increase from  $12^{\circ}\text{C}$  to  $28^{\circ}\text{C}$ . Adam and Elliott (2) found no detectable variation for water on various solid hydrocarbons between  $20^{\circ}$  and  $35^{\circ}\text{C}$ .

### 2. 6. 4. Time

Elliott and Leese (34) studied the change of contact angle as a function of time by allowing air bubbles to impinge upon a paraffin wax surface immersed under water. They observed an initial rapid change in the contact angle followed by a very slow change. The angles were receding angles and, since they increased on standing, a movement of the three phase line of contact must have occurred. The increase was concluded to result from an increase in  $\gamma_{lv}$  and possibly  $\gamma_{sl}$ , due to the

adsorption of solute molecules in excess of the equilibrium value prescribed by Gibbs adsorption isotherm.

Borgin (14) studied contact angle variation with time for the system water-cellulose-air. Initially the angle was  $30^{\circ}$  but fell to  $11^{\circ}$  after a period of about 15 minutes; the angle was then stable for a further period of 24 hours. The initial decrease in the contact angle could be attributed to the fact that water penetrated into the cellulose mass so that the results are specific to this system.

### 2. 6. 5 Hysteresis

The term hysteresis applies to a contact angle which exhibits an increase or a decrease from a previously determined value. The contact angle formed when the solid-liquid interface has moved onto a previously dry solid surface is the advancing angle. The angle formed after the solid-liquid interface has moved away from a previously wetted surface is the receding angle. The values of these two angles frequently differ. Some workers consider that hysteresis can be avoided by careful experimental techniques but others assert that it is a fundamental phenomena (39, 111).

Several theories have been proposed to explain hysteresis, for example it has been suggested that the degree of the adsorption at a solid-liquid-liquid interface is different for the advancing and the receding angle (60, 18). Other theories relate to the change in an orientation of the polar groups (76) in the solid surface or the migration of the polar groups of the impurities in the bulk of the solid to the surface.

### 2.6.6 Experimental techniques

A wide variation has been noted in the values of the contact angle of a sessile drop for a given system. Some of the variation is undoubtedly due to the use of different system specifications, e. g. variations in contact angles on a glass surface may result from variations in the compositions of the glass. Hence, values between  $0^{\circ}$  and  $40^{\circ}$  can be obtained for water on silica glasses, dependent on the composition of the glass. Hair (46) investigated the effect of the varying compositions of silica glasses and outlined the difficulty in describing accurately the composition of such surfaces since evaporation of the more volatile compounds occur during the glass cooling process. Furthermore, the composition of a solid surface is altered according to the treatment given to it. Different surface treatments have been favoured by different workers. However, grinding and polishing can produce changes in the surface composition and surface heterogeneity (15).

Similarly, different techniques have been used to clean the solid surfaces. Cleaning with an acid exposes a fresh surface whereas cleaning with a surfactant removes all the surface active compounds from the surface. However, by cleaning the packings with chromic acid, followed by washing with deionised water and finally drying in an oven at  $120^{\circ}\text{C}$ , stainless steel packings were obtained which could be further treated by a preferential wetting technique (100).

The fundamentals of drop behaviour at a vapour-solid interface have been reviewed. However, in liquid-liquid contacting and separation equipment, drop behaviour at a liquid-solid interface is frequently more relevant.

The effect of solid surfaces in coalescers and packed columns is outlined in Chapter Four. Before this it is relevant to consider the manner in which drops may be formed and travel through equipment containing baffles and/or packings; this is discussed in the next chapter.

## CHAPTER THREE

### DROPLET HYDRODYNAMICS IN EXTRACTION EQUIPMENT

Coalescence in practical equipment may occur either as part of the main process, e. g. in efficient phase separation in a settler, or as part of an ancilliary process, e. g. in mass and direct heat transfer equipment and in suspension polymerisation reactors, in which it may or may not be desirable.

If the coalescence effects are deleterious to the main process, then equipment is designed and operated so as to minimise interdrop coalescence. This may be achieved by, for example, continuous agitation. Drop-interface coalescence is also avoided unless repeated surface renewal is required. Although drop-interface coalescence can usually be eliminated from the equipment, drop-drop coalescence may always persist to some extent dependent upon process conditions and system properties. The above applies to conditions in a column or mixer type extraction equipment. In the phase separation zones, e. g. a horizontal settler or the dispersed phase outlet from a continuous countercurrent column, droplet flocculation and coalescence is required. Consideration is then given to the promotion of coalescence by the use of coalescing aids, thus increasing the potential for interdrop coalescence contact and providing larger areas for drop-interface interaction. Since liquid-liquid extraction is the major unit operation involving contacting and separation of immiscible liquid-liquid systems, it is relevant to the present work to briefly review the knowledge of droplet hydrodynamics in the equipment commonly used.

### 3.1 Coalescence in Extraction Equipment

The simplest way of achieving coalescence in any equipment is to form an interface near the dispersed phase outlet. In spray columns, an enlarged diameter section is usually provided for this purpose to increase the area of contact between droplets and the bulk dispersed phase. Either a sudden or gradual conical enlargement may be used. Similar sections are used in the more elaborate pulsed, packed or rotary agitated extraction columns. In any application efficient coalescence at this end of the column is essential in order to avoid the wedge extending into the column proper. Interstage-coalescence may also be utilised in some equipment such as in the cascade type mixer-settler or certain rotary agitated columns. If no separate settler exists, the drop-drop coalescence may be promoted in intermediate sections or calming zones, or in baffled regions remote from the agitator, in order to enhance mass transfer by repeated drop coalescence and break-up (141).

Thus coalescence in practical equipment occurs by both the interdrop and drop-interface modes. In addition, partial coalescence is encountered leading to the production of secondary droplets or a secondary haze. In the following paragraphs, the coalescence phenomena involved in typical equipment designs, viz. horizontal and vertical mixer settlers and agitated systems, and the effects on performance are summarised.

#### **Mixer Settlers:**

A wide range of mixer settler designs are commercially available (141, 97) These may be arranged vertically or horizontally with the driving force for fluid flow being either pumping or gravity. In some types individual agitators are used in others

these are fixed to a common shaft. However, despite these variations, settling or phase separation relies upon the basic processes of droplet flocculation, packing, interdrop and finally drop-interface coalescence.

In simple horizontal settler arrangements, the dispersion is distributed from the inlet port in the form of a heterogeneous wedge which may reside above or below the interface dependent upon the relative densities of the dispersed and continuous phases. The wedge should not cover the whole area but extend over only 70 % of the length of the interface in order to accommodate fluctuations during the normal operation, or changes in throughput. The wedge dimensions are determined by the difference between the input rate of the emulsion and the rate of coalescence of droplets in the wedge with the interface. However, many of the design procedures are based either on hydraulic balances of the two phase flows or upon empirically determined mean residence times. The procedure proposed by Jeffreys et. al. (66) is the only one to take account of the physical processes governing separation, viz. interdrop and drop-interface coalescence, using experimentally determined drop-interface rest-times.

The use of mechanical aids in order to promote coalescence and phase separation in settlers has long been practised (141, 97). Thus a vertical impingement baffle is sometimes inserted adjacent to the inlet port in horizontal settlers, and horizontal baffles may serve to preserve laminar flow and to decrease settling distance (141) Baffles fitted on either side of the phase inlet slot, to form a rectangular duct, have been used to reduce flow disturbances and promote upto a 30 % increase in capacity in a pilot scale settler (64).

Decreased dispersion band widths, and hence increased settling velocities, are achieved in the Lurgi Multi-Tray settler by means of stacked trays to which the dispersion is evenly distributed (85). Similarly, the coalescing aids may be incorporated in a novel design wherein there is a complete hydraulic separation between mixer and settler (72). Settling rafts have also been proposed (48).

#### Columns:

Coalescence rate is one factor affecting the efficiency of mass transfer in agitated systems. Thus a detailed design procedure published for a rotating disc contactor incorporates parameters to allow for coalescence (92, 94). The situation in agitated columns is however complex and there is potential for enhancement of mass transfer by continued droplet coalescence and break-up (3, 98).

The available data on coalescence in agitated columns is limited (99). Davies et. al. (30) found that drop-drop coalescence was not significant in a pilot scale R. D. C. with the system kerosine-water. However, this was with phase ratios of 12 to 16:1, compared with the 0.5 to 4:1 used in practice. Misesk (94) assumed that a dispersion can be characterised by a hydraulic mean diameter, and every collision of the droplets resulted in a coalescence.

The extent of interdrop coalescence of various systems has been investigated in several agitated columns viz. the R. D. C., Oldshue-Rushton and Scheibel (98). In the R. D. C. with three systems in the absence of mass transfer, at rotor speeds from 500 to 1000 r. p. m. and with varying flowrates drop-drop coalescence was found to be insignificant until flowrates reached

the flooding point. Conversely, in the Oldshue-Rushton column, a coalescence-redispersion mechanism predominates (98, 30), and a similar effect was observed in the Scheibel column provided the agitator speed was above a minimum necessary to distribute the droplets across the column-section. Since these findings covered a large range of interfacial tensions of the system material viz. 9.7 to 55.4 dynes/cm., they clearly indicate the importance of coalescence phenomena in the design and operation of agitated columns. Thus design procedures involving the assumption of spherical uniform droplets which do not undergo coalescence are generally ill-founded.

The utility of knitmesh packings of the type used in the Scheibel column for the coalescence of primary dispersions was studied by Mumford and Thomas (100). They confirmed that for maximum coalescence efficiency, the coalescer material should be preferentially wet by the dispersed phase liquid, possess a large surface to volume ratio, have interstices small enough to cover the range of drop sizes encountered, and yet cause as low a pressure drop as possible. The common objection to the use of packings as liquid-liquid coalescing aids is that, even with voidages as high as 98 %, they may be prone to blockage by any solid present. However, practical results indicate that this objection may be overridden by the promotion of the coalescence (99, 100). The increase in droplet size due to drop-drop coalescence on the surface of packings has been studied and confirmed by photographic analysis (63). It has been reported that no interdrop coalescence occurred in the bulk fluid. As would be expected high separation efficiency can only be achieved if the droplets can approach and adhere to a packing surface and reside there long enough for coalescence to take place.

### 3.2 Flow Phenomena in Packed Columns

In packed extraction columns there is, by design, interaction between drops and solid surfaces as the dispersed droplets impact upon, and are distorted to flow through the voids i. e. the packings. It is relevant therefore to note the extensive studies made of flow phenomena in packed extraction columns. These studies cover flooding phenomena, hold-up and pressure drop across the packed bed which is normally of a material wetted by the continuous phase. Gayler and Pratt (39) investigated the relationship between hold-up and the pressure drop for counter-current flow in columns packed with Raschig rings. Hold-up values were determined by a displacement method in which the flow was shut off by quick acting gate valves. Three distinct regions were identified as the flow rate was increased; the first region corresponded to a linear increase in the hold-up. When the flooding point was reached, an increased rate of hold-up occurred and flooding was possible with systems of low density difference. However, with other systems, a third region was observed, in which the hold-up remained constant for a further increase in the dispersed phase velocity.

Flooding was defined as the limiting flow condition; if exceeded, an accumulation of one phase took place. A knowledge of this limiting flow condition is essential for extraction column design. The flooding condition was found to be a function of the particular liquid system and the packing under observation. Many investigations have been carried out, resulting in empirical and semi-empirical correlations of the data (13, 95). Most are presented in the form of graphs with coordinates of the complex functions of liquid properties and phase flow rates. A statistical study by Chin (25) compared all available data with several correlations and concluded that the correlation of Crawford and

Wilke (27) was the most suitable for use. Crawford and Wilke presented their work in two parts. For values of

$$(V_{cf}^{\frac{1}{2}} + V_{df}^{\frac{1}{2}}) \cdot \rho_c / a \cdot \mu_c > 50 \quad (3.1)$$

flooding occurred when,

$$(V_{cf}^{\frac{1}{2}} + V_{df}^{\frac{1}{2}})^2 = (69.4 \Delta \rho \cdot \epsilon^{1.5} / \rho_c^{0.8} \cdot a^{0.5} \cdot \gamma^{0.2}) \quad (3.2)$$

For values  $< 50$ , flooding occurred when

$$(V_{cf}^{\frac{1}{2}} + V_{df}^{\frac{1}{2}})^2 = (79.7 \Delta \rho^{1.33} \cdot \epsilon^2) / (\rho_c^{0.73} \cdot a \cdot \mu_c^{0.33} \cdot \gamma^{0.27}) \quad (3.3)$$

These correlations have been found to be easier to use than the correlations of Hoffing and Lockhart (61) which Chin concluded were best compared to all available data.

### 3.3 Formation of Liquid Drops in an Immiscible Liquid

At the outlet from any coalescer the enlarged drops detach in a manner analogous to that from discrete orifices or nozzles. Furthermore, the drops for single drop studies in the present work were delivered from discrete nozzles, as described in Section 5.1.2. and a composite coalescer for studies of swarms of drops was constructed from an arrangement of nozzles, as described in Section 5.2.2. Therefore, it is relevant to review the literature on drop formation with immiscible liquids.

#### 3.3.1. Variables governing the drop formation

Hayworth and Treybal (57) studied the behaviour of liquid drops on formation at a nozzle in an immiscible liquid and the effect of interfacial tension and density difference of the system on the drop volumes. The variables governing the drop formation were assumed to be: density of both the dispersed and the continuous phases, nozzle design, shape and size; velocity of the

dispersed phase through the nozzle; nature of motion of the continuous phase; and whether heavy or light liquid is dispersed. A drop does not separate from the nozzle or the jet from which it is formed provided:

1. The rising velocity,  $V_r$ , of the drop is smaller or equal to the velocity  $V$  of the dispersed phase through the nozzle. (The rising velocity is the velocity with which the drop rises or falls freely through the continuous phase liquid due to the buoyancy or gravity forces acting upon it.), and

2. The buoyant force,  $F_b$ , acting on the drop is smaller or equal to the force of interfacial tension,  $F$ .

The drop, therefore, breaks away when both  $V_r > V$  and  $F_b > F$ .

Effect of nozzle design:

All five nozzles used by Hayworth and Treybal, ranging in inside diameter from 0.133 to 0.786 cm., were brass tubes with the delivery ends carefully chamfered, or beveled at  $45^\circ$ , to a sharp edge. This design was based on experience with sharp edged nozzles selected such that the dispersed phase does not spread over or wet the outer surface.

Effect of velocity of the dispersed phase liquid:

At low linear velocities of the dispersed phase through the nozzle, a drop is formed immediately at the tip of the nozzle. As the velocity is increased, a short jet or stem of the dispersed phase extends from the nozzle and the drops form by 'necking-in' at the top of the stem. Drop size and uniformity then fall rapidly with increased velocity upto approximately 30 cm. per second. At higher velocities the drop size is non-uniform; this tendency begins at velocities of 10 cm. per second. Below the velocities of 30 cm. drop size increases with increased nozzle diameter and increased interfacial tension. A continued increase in the dispersed phase velocity does not change the situation greatly until such a high velocity is reached that the stream is 'atomised', producing a cloud of very fine droplets.

#### Effect of the dispersed phase liquid:

Hayworth and Treybal noted that the choice of the dispersed liquid, i. e. whether a light phase drop was formed upwards or a heavy phase drop was formed downwards, had no influence on the drop formation mechanism.

Hayworth and Treybal, and Null and Johnson (106) attempted to predict drop size as a function of operating parameters, e. g. interfacial tension, viscosity of the continuous phase, nozzle diameter and the flowrate of the dispersed phase liquid through the nozzle. The wetting characteristics of the material of the nozzle were not taken in account i. e. metallic nozzles were used to deliver the organic liquid drops. However, the equation developed by Hayworth and Treybal (Section 3.3.3) is semi-empirical, based on a force balance made by expressing the various contributory forces acting on the drop as fractions of the total drop volume. This procedure is not wholly justified since the exact instant at which the forces act is not known, nor is their quantitative contribution to the total volume. Null and Johnson based their model on the geometry of the drop formation process. This model neglects the effect of viscosity of the continuous phase which seemed to play an important role in the model proposed by Hayworth and Treybal. This might explain why Hayworth and Treybal found only one peak on the flowrate vs. drop size curve, whereas Null and Johnson found two peaks.

Rao, Kumar and Kuloor (118) developed a correlation (Section 3.3.2) based on a two-stage drop formation process. In the static stage, the drop is assumed to expand until the buoyancy force balances the interfacial tension force. During the second stage, when the drop is detaching from the nozzle, the drop continues to grow.

For cases in which velocity effects become important, there are two widely accepted correlations (Section 3.3.2.) Treybal and Hayworth extended the analysis of Harkins and Brown while Null and Johnson used a geometric approach, to obtain a correlation for drop volume.

However, Meister and Scheele (126) found that the Hayworth and Treybal and Null-Johnson correlations did not satisfactorily predict the drop size over a wide range of liquid properties and nozzle diameters. This result is consistent with the observations of Null and Johnson who found maximum average errors of 94% and 377% when they compared experimental data with their analysis and that of Hayworth and Treybal respectively.

Each primary drop is usually followed by a satellite drop from the nozzle. Scheele and Meister ignored the volume of satellite drops during their analysis of the drop volume, since they did not affect the uniformity of the primary drops and their contribution to the interfacial area was negligible.

### 3.3.2 Mathematical modelling of drop formation

Hayworth-Treybal Model: (37)

All forces acting on a drop at a nozzle can be expressed in terms of the equivalent drop volumes, in as much as the volume of the submerged drop in another liquid represents a buoyancy force. The total volume  $V_f$  of a forming drop can be considered to be made up of the following partial volumes:

(a) The volume,  $V_s$ , necessary to overcome the interfacial tension,

(b). The additional volume,  $V_r$ , necessary to produce a rising velocity at least equal to the velocity of the dispersed phase through the nozzle, and

(c). The negative volume equivalent  $V_k$  of the kinetic energy supplied by the incoming stream.

$$\text{Therefore } V_f = V_s + V_r - V_k \quad (3.4)$$

Calculation of  $V_s$ :

In their simplified approach Hayworth and Treybal considered the forces acting on the drop as  $F_s$ , due to the interfacial tension,  $F_b$  the buoyancy force and  $F_k$  the force due to the kinetic energy of the stream entering the drop. The force due to the interfacial tension is given by,

$$F_s = \pi D_n \sigma \quad (3.5)$$

and the volume of the drop with sufficient buoyancy force to overcome  $F_s$  will be,

$$V_s = \pi D_n^3 / \Delta \rho g \quad (3.6)$$

Harkins (50) observed that at zero velocity through the nozzle not all of the drop will separate and move away; a certain fraction will remain behind at the nozzle. This fraction left behind was determined and expressed graphically as a function of the volume of the drop formed and the nozzle diameter. The volume  $V_s$  of the drop under static conditions, i. e. zero velocity of the dispersed phase, will be

$$V_s = (\pi D_n^3 / \Delta \rho g) \psi (D_n / D_s) \quad (3.7)$$

where  $\psi (D_n / D_s)$  is Harkins' correction factor.

Calculation of  $V_r$ :

A drop of given size and shape will rise or fall at a certain velocity  $v_r$  through the continuous phase, depending



upon the viscosities and densities of the fluids.

$$v_r = (1/18K)(D_r^2 \Delta \rho g / \mu_c) \quad (3.8)$$

Solving this equation for  $D_r$  and substituting  $v$  for  $V_r$  results in,

$$D_r = (18vK \mu_c / \Delta \rho g)^{\frac{1}{2}} \quad (3.9)$$

$$\text{from which } V_r = 0.523(18vK \mu_c / \Delta \rho g)^{1.5} \quad (3.10)$$

Calculation of  $V_k$ :

The liquid stream forming the drop enters it with a velocity  $v$ , as a result of which a certain amount of kinetic energy is supplied to the drop acting in the direction of flow, i. e. away from the nozzle. The kinetic energy can be expressed as

$$Wv^2/2g = V \rho_d v^2/2g \quad (3.11)$$

The total kinetic energy supplied to the drop then becomes,

$$V_f \rho_d v^2/2g = V_k \rho_d v^2/2g \Delta \rho D_f \quad (3.12)$$

$$V_k = V_f \rho_d v^2/2g \Delta \rho D_f \quad (3.13)$$

Calculation of  $V_f$ :

Substituting the values of  $V_s$ ,  $V_r$  and  $V_k$  in Equation 3.4. the value of  $V_f$  is then given by,

$$V_f + 4.11(10)^{-4} V_f (\rho_d v^2 / \Delta \rho) = 21(10)^{-4} (3 D_n / \Delta \rho) 1.069(10)^{-2} \cdot (D_n^{0.747} v^{0.365} \mu_c^{0.186} / \Delta \rho)^{1.5} \quad (3.14)$$

which can be used to calculate  $D_f$ .

Rao-Kumar-Kuloor Model:

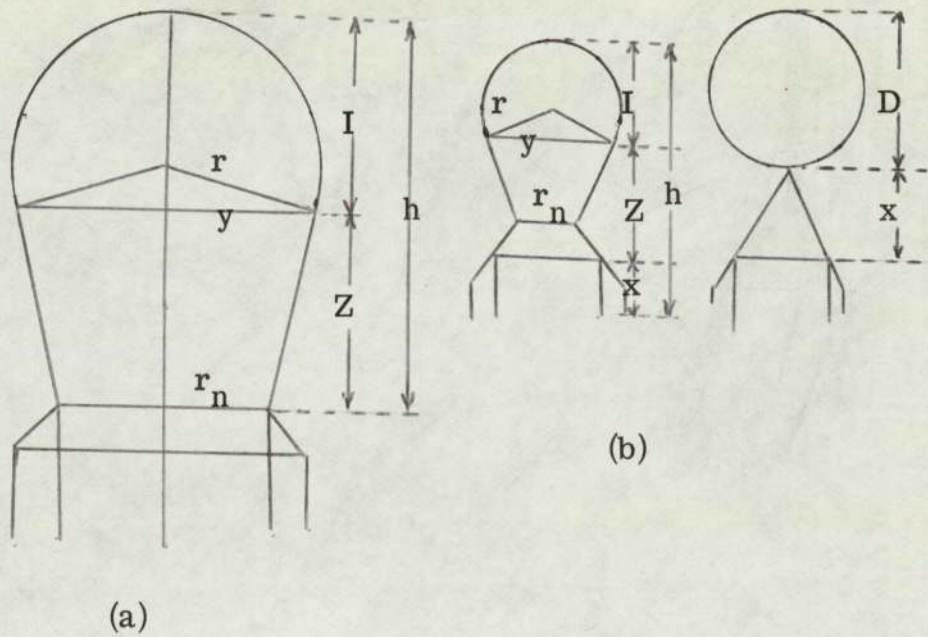
The final volume after the break-off (Figure 3.1) is given by

$$V_f = V_s + V_d = V_s + Q \cdot t \quad (3.15)$$

$$\text{where } V_s = \kappa D_n^3 / \Delta \rho g \quad \psi D_n / D_s \quad (3.16)$$

Figure 3.1.

Rao-Kumar-Kaloor Model of a drop  
at a nozzle.



- (a). Geometry of the drop before the break off, and  
 (b). Geometry of the drop during the break period.

$\psi(D_n/D_s)$  is the Harkins-Brown's correction factor and  $Q$  is the volumetric flowrate through the nozzle. The value of 't' may be calculated from one of the following equations.

$$v = C/A + B(t/A - 1/A)^2 + (B/A^2 - C/A)C \cdot \exp(-At) \quad (3.17)$$

where  $A = 6\pi v\mu/m$ ,  $B = Q(\rho_c - \rho_d)g/m$ ;  $C = Qv_c \rho_d/m$   
and  $t = (2A \cdot D_s/B)^{1/2}$

Scheele-Meister Model:

The drop volume after the break-off is given by,

$$V_f = \psi(D_n/D_s)(V_{fs} + V_{fn}) \quad (3.19)$$

where  $V_{fs} = \pi \beta D_n/g \Delta \rho + K_d \mu_c Q/D_f g \Delta \rho (D_n/D_s)^n$   
 $- 4 \rho' Q U_n/3g$  (3.19. a)

$V_{fs}$  is the volume of the liquid on the nozzle tip at equilibrium. If the drop breaks off instantaneously, multiplication of  $V_{fs}$  by  $\psi(D_n/D_s)$  gives the volume of the separated drop. However, Scheele and Meister observed from high speed cine films that a considerable amount of the liquid flowed into the drop during the process of drop break-off, i. e. after the net lifting forces exceeded the net restraining forces. To predict  $V_f$ , it is necessary to estimate this additional flow given by,

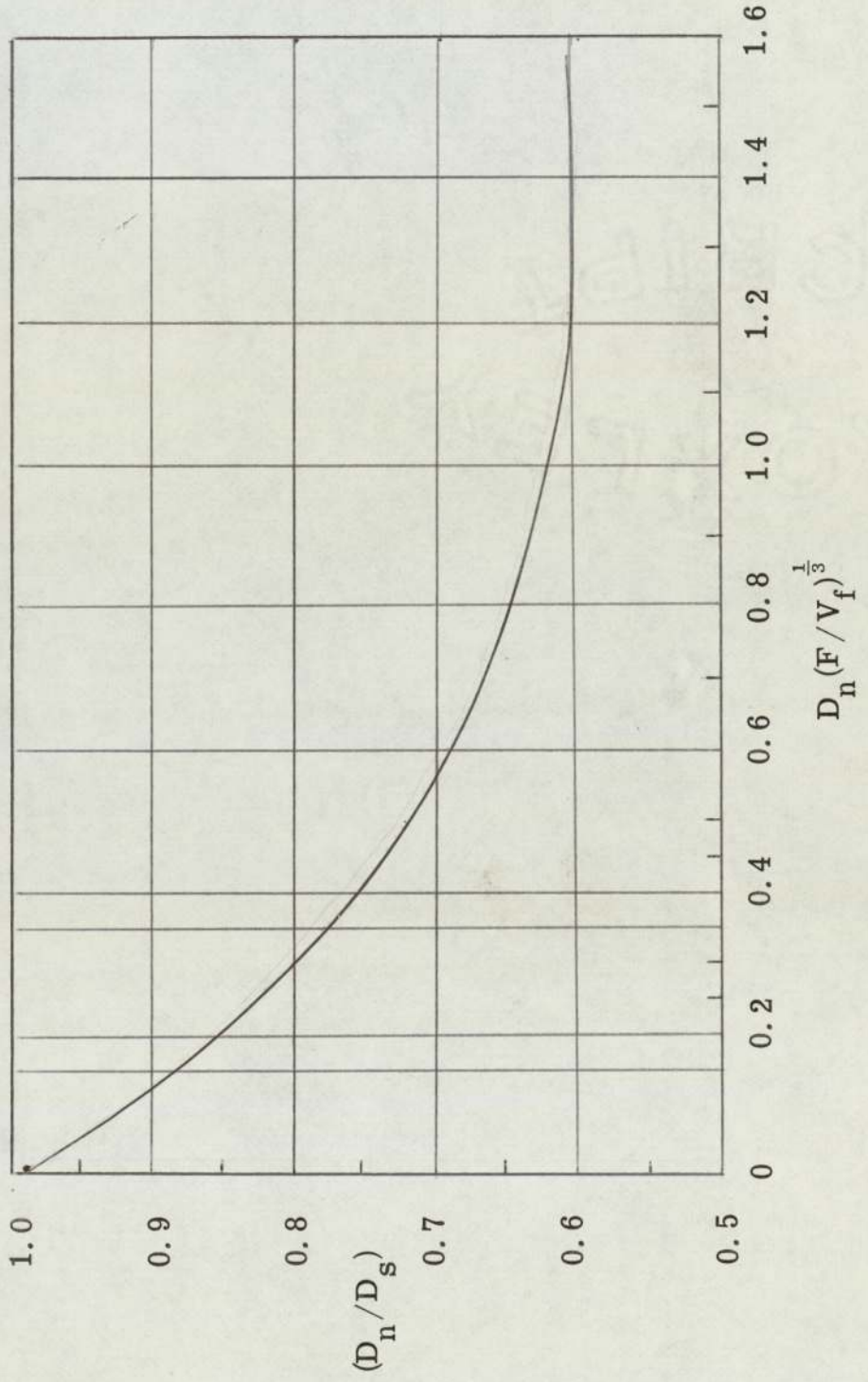
$$V_{fn} = K_3 (Q^2 D_n^2 \rho' \beta / (g \Delta \rho)^2)^{1/3} \quad (3.20)$$

The value of  $V_f$  is given by substituting the values of  $V_{fs}$  and  $V_{fn}$  from Equations 3.19. a and 3.20. into Equation 3.19.

$$V_f = \psi(D_n/D_s) (\pi \beta D_n/g \Delta \rho + 20 \mu_c Q D_n/D_f g \Delta \rho - 4 \rho' Q U_n/3g \Delta \rho + 4.5 (Q^2 D_n^2 \rho' \beta / g \Delta \rho)^{1/3}) \quad (3.21)$$

The Harkins-Brown's correction factor is generally plotted as  $\psi$  vs.  $(D_n/V_f^{1/3})$  which is not convenient to use with Equation 3.21. Therefore, the correction factor has been replotted (Figure 3.2) as  $\psi(D_n/D_s)$  vs.  $D_n(F/V_f)^{1/3}$ .

Figure 3.2.  
Harkins and Brown's correction factor.



None of the above models take into account any effect of two-phase cocurrent or countercurrent flow on drop formation and the flow of the dispersed phase liquid. Within the channels of a packing both the phases are in motion even when the bulk of continuous phase is kept stationary.

During the formation of a drop at the exit of a packing element, 'graping' also occurs to some extent when some continuous phase is entrapped within the growing droplet. In this case, both the phases coexist within the boundary of the same drop.

Although the general mechanisms by which the drops grow at, and detach from the exit surface of, a coalescer are similar to those described above, there are other important features. Therefore the factors, including the wetting characteristics of the solid surface, which control the flow hydrodynamics of the dispersed phase liquid through a packed coalescer are discussed in detail in the next chapter where the operation of specific packings generally used as separating aids are outlined.

## CHAPTER FOUR

### COALESCENCE OF LIQUID DISPERSION IN PACKINGS

Although dispersions have been divided arbitrarily into two categories depending on the size of the droplets, any dispersion may contain droplets of both primary and secondary sizes. Therefore, coalescence of both types of dispersion are reviewed in this chapter.

#### 4.1 Primary Dispersions

The potential advantages of introducing solid surfaces in the form of packings into any liquid-liquid coalescence process is evident from the review presented in Chapters 1 to 3. Solid-liquid-liquid coalescence can overcome the inefficiencies of liquid-liquid coalescence. These inefficiencies result, firstly, from the skewed type rest-time distributions of the drops at the interface and, secondly, from the production of a haze due to the formation of secondary droplets left behind during coalescence. In the design of an effective solid-liquid-liquid coalescer, there is a need for a suitable solid material. The nature of the solid surface is vital since the mechanism of coalescence varies with wetting characteristics of the solid. In practice, under certain conditions, a surface can be made to be preferentially wetted by either the continuous or the dispersed phase. Furthermore coalescence is apparently enhanced with a composite surface which includes both wetted and non-wetted components.

Early attempts to use solid surfaces to aid coalescence involved baffles. However, the action of baffles in promoting coalescence has been ascribed to the preservation of laminar flow and a decrease in the settling distance (141). A review of the various methods devised to assist settling is presented in Section (4.3)

The packings used to promote coalescence of primary dispersions, do not act as a filter media and their effectiveness can be assessed by comparing the mean outlet drop diameter with the mean inlet diameter. The mean size is used since in almost all processes, there is a distribution of droplet sizes, both in the inlet and the outlet streams. The main factors affecting the overall performance are the surface properties of the liquid system and the solid packings, the system hydrodynamics, inlet drop size and the packing geometry i. e. surface/volume ratio and percentage free volume (65).

There are basically two distinct mechanisms of coalescence for droplets on a packing surface. The wetting properties of the system may be used to distinguish between the two mechanisms. These are determined by the surface of the solid and the liquid-liquid system. In the first case, if the surface is wetted by the dispersed phase, the entering droplets coalesce on it to form a film of the dispersed phase liquid; subsequent drops arrive at this film and coalesce with it following a drop-interface coalescence mechanism. Drainage of the dispersed phase film takes place continuously across the bed and the droplets detach from the packing at the outlet by a drip-point mechanism. In the second case, when the dispersed phase does not wet the packing, interdrop coalescence takes place in the interstices of the packing; the packing merely acts as a mechanical aid to restrain the drops in close contact and thus promote the interdrop coalescence.

The degree of separation in packing, defined by the ratio of the mean outlet drop diameter to the mean inlet drop diameter, depends on the coalescence mechanism. The ratio is generally higher if the dispersed phase liquid wets the packing. The effects of the various parameters are reviewed in detail in Sections 4.1.1 and 4.1.2

#### 4.1.1. Coalescence in packed beds

In packed beds, the coalescence essentially takes place within the packed section. However, some coalescence also occurs at the inlet and exit of the bed. The composition of the bed depends largely on the type of the dispersion to be treated. A range of materials may be used for the packing including fibrous beds which consist of cotton, glass wool, metal and polymer strands, knitted mesh packing formed by inter-locking the loops of metals and or polymeric materials, particulate packings such as ballotini beads, pebbles, gravels and the conventional packings such as ceramic Raschig Rings and Berl Saddles.

Wilkinson et al (148) investigated the coalescence behaviour of liquid dispersions in glass ballotini. Two techniques were used to change the wetting characteristics of the glass packings. The first was the preferential wetting technique described by Thomas and Mumford (100). The ballotini was cleaned in chromic acid, thoroughly washed with distilled water and dried in an oven at 150 °C for 8 hours. This surface, when immersed in either an organic or aqueous phase, was preferentially wetted by the liquid which first came into contact with the surface; this effect was possible irrespective of the solid surface energy. Therefore, glass, which has a high surface energy and is normally wetted by water, was made to be wetted by the organic phase. The other technique to change the wetting characteristics of the glass packing involved the adsorption of silane molecules on to the glass surface to render it hydrophobic.

A two dimensional mathematical model was proposed to predict the upper and the lower limits of the size of the drop that would be retained by a given packing. The model was presented in graphical form in terms of drop size and packing interstice size with the group ( $\Delta P_g/2\gamma$ ), characterising the physical properties of the system, as parameter. Statistical treatment of the experimental results indicated

that the depth of the packing in the bed, the superficial velocity of dispersed phase, preferential surface treatment, and inlet drop size had only minor effects on the drop size in the effluent dispersion.

#### Coalescence in Knitted Mesh Packings

The primary use of knitted mesh packings is to enhance coalescence of primary dispersions. Research efforts have, therefore, been directed mainly to coalescence studies. However, such packings are also used to separate the mixing sections in Scheibel column. They generally serve to isolate the mixing sections and prevent back mixing within the column (127). However, if the packing is wetted by the dispersed phase the column can function as a vertical mixer-settler, with essentially discrete stages, but with a very much reduced volumetric capacity.

The mean exit drop size is dependent upon the packing height but independent of the inlet drop size and the dispersed or continuous phase flowrates (62). The droplet flow characteristics are similar to those in conventional packings greater than the critical size. Both, Piper (112) and Slater (133) found that the limiting flow was dependent on the inlet drop size. They used packings of known voidage in the range of 97.5 - 98.75 % and found that the limiting flowrate increased as the voidage increased.

#### Coalescence on packings wetted by dispersed phase

Jeffreys and Davies (67) studied the effect of wetting and non-wetting characteristics of packings on the coalescence of primary dispersions. With the wetted packing the drops coalesced on reaching the surface and formed a film of the dispersed phase liquid on the packing surface. Coalescence of subsequent drops took place with this film via a drop-interface coalescence process. The film eventually drained through the bed when the buoyancy forces were greater than the solid-liquid adhesion forces. The exit drops thus formed left by a drip-point mechanism. The condition of a packing wet by the

dispersed phase was characterised by a contact angle  $< 90^\circ$ .

With a packing wetted by the dispersed phase, the size of the mean exit drop increased to ten times the mean inlet drop size and it is now generally considered that a packing wetted by the dispersed phase liquid enhances coalescence. However, the adhesion forces holding the dispersed phase liquid to the packing can increase the hold-up and pressure drop. Consequently, the maximum throughput before flooding occurs will be lower for a wetted packing than for a non-wetted packing. Hence the reduced volumetric capacity of a Scheibel column with wetted packing if flooding is to be avoided. At high hold-up values and above a certain fraction of dispersed phase volume, phase inversion may occur. For most systems, there is a range of phase ratios, the ambivalence range, where it is possible to disperse either phase. Thus the packing must be specified for the particular phase to be dispersed.

Mumford and Thomas (100) investigated the hydrodynamic behaviour, and in particular the breakdown coalescence mechanisms, of drops in knitted mesh packings. A variation in the wetting properties of the packing was obtained by modification of the method of preparation. The precleaned packings were either soaked in the dispersed phase liquid for one hour prior to operation, to produce a packing preferentially wetted by the dispersed phase, or in distilled water to produce a packing preferentially wetted by the aqueous continuous phase. After such treatment, the wetting properties were found to remain constant despite prolonged use.

A primary dispersion from a distributor was then passed through the packed section. Following impaction between a drop and the

packing surface, the fibre element was covered with a film of the dispersed liquid and coalescence occurred into this film. Movement of the coalesced dispersed phase was governed by flow of this film under the influence of gravity and flowstream drag forces.

The effect on the outlet drop size was also studied by varying the bed height of a stainless steel packing which was subjected to a preferential wetting treatment technique. With a packing treated to be wetted by the dispersed phase liquid, the outlet drop size was three to four times larger than with the same packing treated to be wetted by the continuous phase liquid. The droplets either broke down or grew to the size of an equilibrium droplet with the bed height. Therefore, for any given system there is a critical bed height below which the droplets are still either breaking down or growing. Below this height they will not have reached an equilibrium size when they appear at the packing outlet. The droplet break-up phenomena involved are discussed in the next section.

The results confirmed that coalescence and hydrodynamic behaviour were dependent upon the wetting properties of the packing material; the most efficient coalescers were those wetted by the dispersed phase. For packings wet by the dispersed phase, coalescence predominates and enlarged exit droplets are produced. The exit mechanisms are dependent upon system and packing physical properties. The exit drop size, in a stationary continuous phase, at low dispersed phase flowrates has been correlated as

$$d_{vs}^0 \frac{\Delta\rho\gamma}{\mu_c^2} = 2.44 \left( \frac{\Delta\rho\gamma}{\mu_c g} \right)^{0.523} \quad (4.1)$$

### Coalescence on packings non-wetted by the dispersed phase

Mumford and Thomas (100) also investigated the coalescence behaviour of liquid drops in the packings wetted by the continuous phase. With non-wetted packing, the extent of dispersed phase spread over the packing was reduced. Dispersed phase droplets remained discrete and growth occurred by random collisions between moving drops in the continuous phase and stationary drops attached to the packing element, or collisions within the restricted paths through the packing. In this case, the packing acted to promote interdroplet coalescence. Behaviour of packings wetted by the continuous phase was analogous to the droplet behaviour in conventional packed columns viz. Raschig rings and Berl saddles. The breakdown/coalescence equilibrium was dependent upon packing and system physical properties. The existence of a 'characteristic' exit drop was related, for high voidage packings, 95 % by

$$d_{vs}^0 \cdot \Delta\rho \cdot \gamma / \mu_c^2 = 0.92 \left( \Delta\rho \cdot \gamma^3 / \mu_c^4 \cdot g \right)^{0.503} \quad (4.2)$$

Jeffreys and Davies (63) were the first to analyse the importance of solid surface energy in relation to its effect on coalescence. The technique used was to vary the concentration of acetone in a toluene-acetone-water system to produce a change in the interfacial tension values.

The effect of disperse phase wetting and non-wetting on the resulting drop diameter formed was demonstrated by formation at an orifice. They investigated the size of the drop leaving a perforated plate under various conditions. For non-wetting conditions, the drop did not pass through the perforations when the ratio of the nozzle to drop diameter was

$< 0.4$ . However, the drops could deform and pass through the hole when this ratio was between 0.4 - 0.8. From a force balance, they suggested the relationship:

$$V = \pi d_n (\gamma / \Delta \rho \cdot g) \quad (4.3)$$

Two important observations were: the importance of surface:volume ratio for the non-wetted situation and that interdrop coalescence did not take place. In a non-wetted packing the drop must be held up in the interstices against the hydrodynamic forces long enough for adjacent drops to collide and coalesce. Thus with the non-wetted packing the function of the packing is merely to hold the drops together where they coalesce via a drop-drop coalescence mechanism.

Theoretical considerations and the experimental observations of the behaviour of droplets at single orifices showed that the hydrodynamics can be characterised by a process of drop retention-coalescence-release. In principle, this behaviour can be used to describe the more general conditions of dispersion within a packed bed coalescer. However, in unrestricted drop passage, the inlet drop is smaller than the packing aperture, therefore, the drop passes through the bed without retention or coalescence taking place. But in a restricted drop passage, drops enter the packing and may initially pass through the first few apertures which would normally promote retention, owing to the combined effect of kinetic and buoyancy forces. At each packing restriction, energy is lost by the drop on impact and deformation and also with oscillation about its equilibrium shape, after penetration has taken place. Likewise, energy is also dissipated on passage through

the restriction by drag forces acting on the drop. The kinetic forces are consequently reduced and drop retention depends largely on a balance between buoyancy and surface forces.

In an inlet drop restriction, penetration of the packing is by the same mode as in a restricted drop passage, but hold-up occurs at the bed inlet because the buoyancy, and hence the kinetic forces, are low. Alternatively, a drop with a large diameter compared to that of the packing aperture, may also be retained at the inlet to the bed. Drops accumulate at the packing inlet and penetration occurs when the buoyancy forces overcome the surface forces. At this point, the bed continues to operate without further increase in the layer of drops at the bed inlet. However, once the drop has been retained, its behaviour is dependent on the local geometric structure and the physical properties of the system.

In the retention-impact-release mechanism, an inlet drop which has been retained is near to the critical point of passage. Under these conditions, passage may be initiated by impact from a following drop. The initial drop is pushed through the restriction and its place is taken by the following drop. In this way, the drop may pass through the packing without coalescence taking place.

After the retention has occurred, then droplet growth takes place by coalescence with following drops. On release, provided the penetrating meniscus is able to accelerate, drop formation takes place as from a standard nozzle or orifice.

But in a restricted drop release, the advancing interface of a drop held in the bulk of the packing is restricted by the packing above the orifice. Therefore, acceleration and drop formation is not possible and a rivulet of dispersed phase is formed which "snakes" through the bed. The rivulet may pass through to the packing exit where break-up occurs by acceleration of the penetrating interface into an unrestricted medium. Passage or retention of the rivulet is dependent on packing geometry and the physical properties of the system.

The path chosen by the droplet is always dependent to some extent on the packing configuration. Drop retention occurs at a restriction, and coalescence and subsequent drop growth occurs. If the volume of the retained mass is sufficient to extend to a second, larger opening, then subsequent drops, before coalescing, may seek this preferential route.

At low volumetric throughput, only the largest exit voids are active, and the exit drop size is at its maximum. As the volumetric flowrate increases, more exit voids of decreasing diameter become active. The average exit drop diameter therefore falls to a minimum corresponding to the maximum number of active voids. At higher flowrates, a band of the inlet dispersion is formed at the bed inlet, but the packing continues to operate without flooding occurring. The packing is now analogous to a series of nozzles, and the exit drop diameter increases in a manner similar to that of drop formation at single nozzles as shown by the Meister and Scheele (126) correlation.

The existence of unstable drop release processes compound the difficulties of relating the exit drop sizes to the

void size distribution in the exit layer. Drop formation by normal release and jetting has been observed, but in neither case has it been clear which mechanism of release was operating. Jetting may be caused by excessive hydrostatic forces or break-up of rivulet flow from within the bulk of the packing. In jetting, a neighbouring orifice may be acting under normal release and the drops formed are larger than those produced by jetting.

#### 4. 1. 2. Break-up in the packings

For a given system with a packing preferentially wetted by the continuous phase and above a critical size, that is the size for which the mean void size is equal to the mean droplet size, the droplets move freely within the interstices and are brought to rest periodically by random collisions with the packing elements. The energy dissipated may result in droplet break-up. Therefore, the droplet movement through the packing results in a gradual reduction in the Sauter mean diameter with height.

Pratt and Lewis (82) studied the behaviour of liquid drops and their break-up/coalescence during flow through a 2-inch diameter extraction column with a three feet packed height. The column was packed with Raschig rings of different sizes, all preferentially wetted by the continuous phase. Nine aqueous-organic systems were investigated and for each pair of liquids, there was a critical packing size, defined as

$$d_c = 2.42 (\gamma / \Delta\rho \cdot g)^{0.5} \quad (4.4)$$

Droplet behaviour within the packing depended upon whether the packing was greater or smaller than this critical size. The mean diameter of the drops leaving the packing was independent of the inlet drop size but dependent on the critical packing size. For a packing larger than the critical packing size, the exit drop size was independent of the packing size

and the flowrate. In this situation, the drops passed through the packing voids and either broke down to an equilibrium size upon an impact at the packing element or, in the case of small drops coalesced until the equilibrium size was attained. The Sauter mean diameter of the exit drop was given by,

$$\Delta\rho \cdot \gamma d_{VS} / \mu_c = 1.62 (\Delta\rho \cdot \gamma^3 / \mu_c \cdot g)^{0.475} (4.5)$$

$$(1 + 700 \mu_c \cdot U_c / \gamma)$$

and at zero flowrates

$$d_{VS}^0 = 0.92 (V / \Delta\rho \cdot g)^{0.5} (4.6)$$

Gayler and Pratt (39) related the equilibrium drop diameter to the physical properties by,

$$d_{VS}^2 \cdot \Delta\rho \cdot g / \gamma = 1.25 (4.7)$$

Based on the collision theory, they found that the diameter of the drop varied directly with its velocity relative to the packing, so that

$$d_{VS} = d_{VS}^0 (\bar{V} / V) (4.8)$$

where  $\bar{V}$  is the mean velocity of the droplet in relation to the stationary packing and  $d_{VS}$  is the characteristic droplet diameter i. e. the drop diameter at substantially zero flowrate. Since

$$\bar{V} = V_d / \epsilon \cdot x (4.9)$$

$d_{VS}$  was expressed as,

$$d_{VS} = d_{VS}^0 (V_o \cdot \epsilon \cdot x / V_d) (4.10)$$

which gave further,

$$d_{VS} = 0.92 (\gamma / \Delta\rho \cdot g) \cdot (V_o \cdot \epsilon \cdot x / V_d) (4.11)$$

This was only applicable for packings greater than  $d_c$ .

Ramshaw and Thornton (117) studied the behaviour of organic liquid drops in the diameter range of 0.23 - 0.70 cm. upon impact at their terminal velocities on a thin stainless steel baffle 0.004 inch thick and a glass microscope slide 0.045 inch thick immersed in distilled water. The droplets ruptured

unequally on striking the baffle until, at a certain critical displacement, droplets no longer ruptured but were deflected to either side of the baffle. A minimum drop size was measured for each baffle below which no further break-up occurred; this was designated the critical drop size. Whether or not splitting occurred depended upon whether the total energy of the droplet was sufficient to provide the excess surface energy to produce two smaller droplets. No breakdown occurred when the initial drop size was smaller than the critical droplet size. The case of an initially spherical droplet forming two equal drops thus yielded the following approximate expression, neglecting friction,

$$1.8 d_{ec}^2 \Delta \rho \cdot g + d_{ec} \cdot V_t^2 \cdot \rho_d = 3.12 \beta \quad (4.12)$$

where  $V_t$  is the terminal droplet velocity in an infinite medium from the drag coefficient measurements. In practice, the impact velocity  $V$  is a function of hold-up and continuous phase superficial velocity  $V_c$ .

$$V = \phi V_t - V_c / \epsilon \cdot (1 - x) \quad (4.13)$$

where  $\phi$  is a correction factor for a droplet moving in a restricted medium. Values of  $d_{ec}$  were calculated from Equation (4.12) using impact velocities given by Equation (4.13). For the system toluene-water in the absence of mass transfer, the equilibrium droplet size  $(d_{vs})_{eq}$  was related to the critical value by Equation (4.14).

$$(d_{vs})_{eq} = 0.85 \cdot d_{ec} \quad (4.14)$$

Clearly the numerical constant is specific to the system and the analysis applies to a droplet striking a baffle symmetrically, since when the droplet is offset, two unequally sized droplets are produced. However, from an energy balance it was concluded that there was a critical drop size for any one system, below which droplets did not break-down on impact with the baffle (40).

Thornton found experimental values of  $d_{ec}$  to be generally higher than those predicted. This was attributed to the dissipation of energy in the form of friction eddies within the droplet.

The concept of critical drop size was developed further for a number of aqueous hydrocarbon solvent systems by Ramshaw and Thornton (117). In a packed extraction column, droplets larger than the equilibrium size broke down on impact with the column packing. With a toluene-water system, the equilibrium droplet was established after several feet of packing. The change in the Sauter mean drop diameter with the column height,  $h$ , was approximated by,

$$d_{vs} = 0.45 + 0.27 \exp - (0.0157 h) \quad (4.15)$$

Whilst the main purpose of their work was to enable the mean drop size and hence interfacial area for mass transfer in the packed columns to be predicted, the hydrodynamics described do provide useful background to the present study.

These considerations of the interaction between the physical properties of the liquids, the solid surface energetics, and the packing geometry and their effects upon droplet hydrodynamics represent a considerable step forward in understanding the fundamental behaviour in a packed bed.

#### 4.1.3. Coalescence in universal packings

Composite packings have been investigated to achieve an improved separation of liquid dispersions. These packings have also been claimed to be universal in nature, since they comprise both the wetted and non-wetted components, and this renders them suitable for use irrespective of which phase is dispersed.

During studies on the dispersed phase bands in vertical settlers, a rather interesting feature of a coalescence phenomena was observed at the junction of high and low surface energy materials. Ali (4) observed that an enhanced rate of coalescence took place at the junction of the surface of the glass column and that part of it which was treated with dichlorodimethylsilane to render the surface hydrophobic. The observation led to the development of a composite knitted mesh packing consisting of high and low surface energy filaments crimped together. Davies, et. al. (66) found that a composite packing could separate both, an oil in water and a water in oil, dispersion. The packing performance was hence independent of the phase dispersed. However, further work on different ratios of high to low surface energy material showed that with ratios outside 1:3 or 3:1 the coalescence efficiency decreased.

No explanation has been given for this enhanced coalescence effect in a composite packing. Therefore, the junction effect was studied thoroughly in the present work and the mechanism of coalescence at a junction determined. Although only primary dispersions were studied, composite packings may also be expected to improve the coalescence of secondary dispersions discussed in the next section.

It is well known that when the drop size in a primary dispersion is less than that of the interstice in the packing, the coalescence rate is very low, even when the dispersed phase wets the packing. This is due to the low adhesion force, compared with the other forces, acting on the relatively large drops. Furthermore, the drops of the size found in a primary dispersion are elastic and tend to bounce off the strand of packing rather

than adhere. Consequently, in order to ensure that coalescence occurs in the packing, irrespective of whether the dispersed phase wets the packing, the drop size in the entering dispersion must be larger than the interstice. The drop will be trapped, at least momentarily, and must undergo distortion in order to pass through the space in the packing. If it resists distortion, the drop will be retained in the aperture until either the film of the continuous phase between it and the packing ruptures, or, as other drops in the dispersion will soon accumulate around the stationary drop, until interdrop coalescence occurs.

Repeated interdrop coalescence will be necessary to increase the size of the retained drops sufficiently to provide the packing buoyancy to force the drops through the aperture in the packing, and unless the dispersed phase wets the packing, it will most probably flood. Davies and Jeffries (63) have shown that when the ratio of the aperture diameter to drop diameter is less than 0.4, the drop will not pass through the space.

The single nozzle studies have shown (148) that the effective surface forces per unit area are smaller on the larger drops so that greater deformation is required for penetration and passage. It may be that the inertial forces, associated with the increased flowrates of these larger drops become significant and produce some slurp penetration effects when passage occurs immediately after a drop coalescence; the enlarged drop suddenly accelerates through the aperture to emerge as a jet which subsequently breaks up into smaller drops. Furthermore, as the rear of the elongated drop emerges from the aperture, it tends to draw some of the inlet drops through the space between the packing elements. However, this will not occur within a packed bed because the packing beyond the retention coalescence point will dissipate the kinetic energy required by the drop.

Wilkinson, Mumford and Jeffreys (148) studied the coalescence mechanisms of primary dispersions in a 15" diameter bed packed with glass ballotini. It was shown that the ballotini size had a significant effect on the drop size in the dispersions leaving a packed bed. This is to be expected if the exit drops are formed at a series of orifices in the exit layer of the packing. The increase in the exit drop size with the increase in the ballotini diameter followed from the fact that mean void diameter increases as the particle size increases. This effect was investigated by placing a layer of ballotini 1.2, 0.9, or 0.6 cm. diameter on the discharge side of the packed bed, and the results obtained for different bed depths and packing sizes in the bed confirmed that the drop size in the effluent dispersion leaving the packing depended to a very great extent on the void size in the exit layers of the packing. This factor is of great importance in the design of packed bed coalescers since, providing drop retention and coalescence occurs within the bed, it is desirable to install a layer of packing at the exit with as large a space between the particles as possible.

The dispersed phase flow rate affects the phase separation efficiency of packed bed coalescers, but the behaviour pattern is complex, depending on the properties and the geometry of the packing and on the retention-release mechanism in the packing (148). At low flowrates of upto  $1.5 \text{ cm. s}^{-1}$  the exit drop size varied considerably with flowrate. With these flowrates the drops emerged from only a small number of points. Mumford and Thomas (100) referred to this as channeling and suggested that it might be related to preferential wetting of some of the packing by the dispersed phase. However, preferentially wetted

channels had little effect on the exit drop release mechanism. The active exit release sites may be related to local fluctuations in the aperture size between packing elements, but these active sites were observed to be distributed randomly over the exit of the bed. If the space between the packings was the dominant factor, the sites would be located near the column walls, since Ridgway and Tarbuck (119) found a high voidage region within two particle diameters of the wall. It must therefore be concluded that, although the exit layers of the packing affect, and largely control, the exit drop size in the dispersion the release sites also depend on flow within the packing. However, it was shown that irrespective of the ballotini size the largest drops were released at low flow rates, and these were found to emerge from a small number of sites. As the flowrate was increased, the number of release sites increased and, since on average these were slightly smaller, the mean drop size in the effluent dispersion was also smaller.

#### 4.2 Secondary Dispersions

A dispersion of 20 micron size is usually referred to as a secondary dispersion, the size of the drops always being less than 100 microns. Such fine dispersions do not settle readily under gravity; therefore, they are sometimes termed 'stable emulsions' or hazes. Depending upon the drop size and the physical properties of the liquid-liquid system, such a dispersion may not separate even after a period of days.

Although only primary dispersions were studied during the present investigation, in a practical situation, e. g. in a liquid-liquid settler a dispersion may contain a mixture of both primary and secondary dispersion droplets. In the coalescence of secondary dispersions, the drops normally grow to the size range of primary dispersions before detaching from the outlet of the bed. In an ideal situation, one thread feeds a droplet at the downstream face of a bed. A balloon-shaped drop then grows until the hydrodynamic forces exceed the interfacial forces. Rupture

occurs at the balloon's neck, the size of the released drop being dependent upon the flow velocity, interfacial tension and the wetting property of the surface at the position of release. Another release is pointing in which the fingers of the collected droplets project beyond the bed face. These fingers taper to a point, vibrate and kick small droplets from the tip. Langdon and Lindenhofen (79) reported a graping release mechanism. This is found at high dispersed phase concentrations or with certain additives. Fibres preferentially wetted by the dispersed phase tend to encourage graping. Therefore, a knowledge of the processes of coalescence of secondary dispersions, and the mechanisms of formation and detachment of the droplets at the exit layer, are relevant to the present study.

A variety of processes may be used to separate secondary dispersions (109, 113). These include alternating electric fields, magnetic fields, centrifugation, addition of chemical coagulants and flow through close packed beds. Some of these applications have had limited success, but are often too specialised, or too expensive, when applied to general industrial use. Increased attention is therefore focussed on the most simple form of coalescing aid, viz packed beds. This type of coalescer can be divided into three categories:

- (a) Porous media (including porous rock, sponge etc. );
- (b) Fibrous beds (including cotton, glass fibre, polymeric and metal threads); and
- (c) Particulate packings (pebbles, gravel, polystyrene cubes etc. ).

#### Flow through porous media

Many processes involve the capillary action associated with the flow of immiscible liquids within the interstices of porous solids. Whilst principles of capillary action have been fully explained (128, 129), their application to practical problems

is often limited by the complicated geometry associated with porous solids. The difficulties are compounded by uncertainty as to the surface energetics or the wettability of the solids.

However, the theory has been used for the basis of a model to predict coalescence of a secondary dispersion in a fibrous bed (137). It is likely that the dispersed phase droplets do not even come into contact with the non-wetted surface of the bed since it will be more difficult for such small droplets to replace the continuous phase which wets the surface.

Davies and Jeffreys confirmed that the small droplets (65) adhere to the surface where coalescence takes place and that no interdrop coalescence takes place in the bulk phase flowing through the packing. For a high separation efficiency droplets must approach and adhere to the packing surface and reside there long enough for coalescence to take place with an adjacent drop. Depending on the relative sizes of the fibres, capillary spaces and droplets, and on the local flow velocities, droplets arrive at the surface either by direct interception or, in the case of submicron drops, by Brownian movement. Electrostatic charges may also affect the migration of small drops to a surface in water-oil dispersions.

#### Coalescence in fibrous beds

Fibrous beds have been extensively used to coalesce secondary dispersions (138, 121). Several prerequisites have been proposed for successful operation, e. g. the bed should have a high voidage consistent with a close packing arrangement, combined with a high surface area to volume ratio. Coalescence efficiency increases with the bed height and pressure drop across the packing.

The effect of fibre wettability has been the subject of some controversy. Successful operation was considered independent of the wetting properties of the fibre (65) but this

was based on a definition of an equilibrium drop size (107), which was considerably larger than those found in secondary dispersions.

Fibre roughness and fibre diameter are important factors affecting the coalescence efficiency (137). Coalescence rates have been found to increase with decreasing fibre diameter and increasing surface roughness. In this respect, cotton fibres have been very successful in coalescing secondary dispersions but the beds suffer from compression, and hence voidage reduction, at high flowrates; composite beds of cotton and p. t. f. e. fibres have been used to overcome this problem.

For a given packing there is an optimum flowrate, above which the efficiency of separation decreases. This is due to the local shear forces within the bed exceeding the drop-fibre adhesion forces so that breakthrough of smaller droplets occurs at a critical velocity.

#### Flow through particulate beds

Packed beds of pebbles, quartz, gravel and polymeric material such as polythene chips, have been used to coalesce secondary dispersions. Douglas and Elliot (32) and later Farley and Valentine (36) reported that particulate beds were satisfactory for coalescing oil in water secondary dispersions. However, these investigations were mainly concerned with the industrial usage and little quantitative analysis was reported. Smith (136) has reviewed the extensive work in this area.

There is no accepted theory as to the mechanism involved in the coalescence of micron size drops during their passage through a fibrous bed.

Burtis and Kirkbride (22) considered the rupture of the continuous phase film between the drops when flowing through the small passages to be a factor as well as preferential wetting of the packing by the dispersed phase liquid. Subsequently Voyutski (142) proposed the following steps for the coalescence process:

- (a) Collision of the droplets with the bed fibres
- (b) Adhesion of the droplets to the fibres
- (c) Coalescence of the micron sized droplets whilst retained on the fibres.
- (d) Adhesion of the coalesced drops to the fibre surface.
- (e) Trickling down of the coalesced drops from the bed.

The mechanism of coalescence was divided by Hazlett into three stages i. e. approach of a drop to a fibre, the attachment of a drop to a fibre or a droplet already attached to a fibre, and the release of an enlarged drop from a fibre.

Approach: This mechanism was subdivided into direct interception, diffusion and inertial impaction. Electrostatic movement and the effects of gravity were neglected since Vinson proved these phenomena to be insignificant for the approach mechanism with fine mesh screens, although Sareen and Davies and Jeffreys (63) considered electrostatic phenomena participated in the coalescence process. For the attachment process to be effective the dispersed phase must displace the continuous phase liquid from the packing and preferentially wet it.

The basic requirements, therefore, of a coalescer with regard to operating conditions and packing properties comprise (119).

- a. The bed should possess a high surface to volume ratio and be closely packed.
- b. The bed should, on balance, be preferentially wetted by the dispersed phase and, if possible, presoaked before operation.
- c. Coalescence is more complete as fibre diameter is decreased. Surface roughness is an important factor affecting drop collection, fine fibres with high surface roughness being most efficient. The fibres should of course be chemically inert and mechanically strong.
- d. Surfactants and high viscosities of either phase tend to significantly reduce coalescence but the latter may be alleviated by operation at higher temperatures. As would be expected, a high interfacial tension system is more easily coalesced than one of low interfacial tension.
- e. Whilst packing surface free energy affects the performance of a coalescer, mixed beds of high and low energy surface materials have proved successful. Composite beds of e. g. cotton and polypropylene are used but the latter is intended as a mechanical support for the deformable cotton fibres.
- f. The superficial velocity should be maintained between certain minima and maxima; a typical range is 0.1 to  $2.5 \times 10^{-2} \text{ m. s}^{-1}$ . The minimum velocity places a practical limitation on coalescer area whereas the permissible maximum velocity increases with bed depth, as does capture efficiency. However, there is an optimum thickness for each application as excessive bed depths cause redispersion of the coalesced drops. Also, operation at high velocities is associated with high pressure drops and a reduction in exit drop sizes thus imposing tighter

limits on settler design. If the critical separation velocity is exceeded, breakthrough of the secondary dispersion occurs.

Examples of the fibrous packing materials employed as coalescence media are shown in Table 4.0 together with their performance under typical operating conditions.

Table 4.0 Typical performance of packings in secondary dispersion coalescence.

Packing type	Bed thickness $\text{m} \times 10^{-2}$	Max. Operating Vel. $\text{ms}^{-1} \times 10^{-2}$	Pressure Drop bar
Reticulated ceramic	1.5	1.0	0.25
Cotton/Glass fibre (cartridge)	5.0	0.45	0.75
Glass fibre (compressed)	0.2	2.0	1.5
Carbon/Metal	15.2	0.5	0.05
Glass fibre	4.0	2.0	0.8
Glass fibre (woven)	0.35	0.5	0.25
Glass fibre mats	0.3	1.5	0.06
Stainless steel meshes	0.25	2.5	0.08
Fibre diameters		3- 35 $\mu\text{m}$	
Voidages		0.4 - 0.95	
Phase ratio		0.07 - 7 % v/v	

#### 4.3 Coalescing Aids

Coalescence is normally brought about by gravity forces moving the dispersed phase drops to an interface where flocculation, interdrop coalescence and subsequently drop-interface

coalescence takes place. This is the principle of the gravity settlers which are commonly used for primary dispersions. However, due to the prolonged times required to settle secondary dispersions and the large volumes needed for treating large throughputs of primary dispersions, a need has arisen for more efficient methods of settling.

#### Addition of chemicals

The addition of certain chemicals can assist the coalescence in one or more of the following ways (58):

- (a) Phase inversion
- (b) Neutralisation of the surface charges
- (c) Weakening, or dissolution of, the protective film which surrounds each droplet.

There is however, a possibility of the liquid system being contaminated by the chemical additives. This must be considered prior to the addition of such chemicals and it is preferable if they are easily recoverable.

#### Mechanical aids

The addition of horizontal baffles to settlers has been found to significantly improve coalescence performance with primary dispersions. This has been attributed to the creation of laminar flow and a reduction in the distance through which the droplets must settle (141) It was found that the residence time was reduced with the addition of baffles. As would be expected, these baffles have no significant effect with permanent emulsions.

Most of the design procedures available for settlers are based either on the hydraulic balances of the two-phase flows or upon an empirically determined mean residence time. However, a mathematical model has been developed to take into account the physical processes governing the separation, viz. interdrop and drop-interface coalescence using albeit experimentally determined drop-interface rest-times (66). In coalescing swarms of drops, interaction effects would result in some deviation from the model.

### Centrifugation

More rapid separation of primary or secondary dispersions can be brought about by substitution of centrifugal for gravity forces. Thus centrifugation may be utilised either for complete removal of a contaminant or to effect a separation of two liquids having a low density difference. However, centrifuges have a relatively high initial cost and running costs and may be uneconomical. Thus use of a centrifuge tends to be limited to where a low holding time is essential (47), e.g. when space is limited, as on oil production platforms or tankers.

### Induced coalescence

In certain cases, coalescence of primary or secondary dispersions can be induced by the addition of an excess of the dispersed phase liquid. Meissner and Chertow (93) have shown that this method can be successfully employed to clarify a polar dispersed phase. Thus a system in which both the components are polar is totally recoverable, whereas a system which is composed of a polar and a non-polar component is semi-recoverable.

### Separating membrane

Separating membranes may be used when the membrane pore size is such that the liquid which preferentially wets the solid may flow through the capillaries readily while the strong interfacial film which separates the wetting from the non-wetting liquid blocks the capillaries for the flow of the non-wetting liquid (131). Secondary dispersions may be treated by this method provided the pore size is less than the micron size droplets.

### Electrostatic coalescers

Electrostatic coalescers rely upon the application of an electric field to dispersions of water in a nonconductive continuous phase. The force inducing the approach of the droplets and coalescence results from either the induced dipoles or a unidirectional applied field in which the droplets have a net charge. The droplets are polarised and align into chains along the line of the force. The increased collision rate enhances the coalescence of secondary dispersions as the chains make contact (146).

Clearly from the above the surface phenomena studied in the present work are more relevant to drops  $> 100 \mu\text{m}$ .

Whether or not wettability by the dispersed phase is important for secondary dispersions collection and coalescence is unclear. However, since the drops grow to the primary dispersion size at some plane in the packing, and are released as large drops, it will be important in the exit layers; the phenomena then applicable are as discussed for Knitmesh coalescers.

## CHAPTER FIVE

### EXPERIMENTAL INVESTIGATION

The literature review, for both single drops and liquid dispersions (Chapter 1 - 4), highlighted the difficulties generally encountered during the analysis of experimental observations. Although it is often misleading to relate the behaviour of single drops to liquid dispersions, single drop studies were used in this work to establish the fundamental mechanisms of coalescence at a composite surface. These would have been difficult to study in the presence of swarms of drops. The more precise work on single droplet behaviour was carried out using a specially designed laboratory apparatus (Section 5.1.2). The coalescence behaviour of primary dispersions with composite packings was then investigated using laboratory scale equipment (Section 5.2).

#### 5.1 Single Drop Studies

Detailed study of the fundamental coalescence behaviour of single liquid drops at solid surfaces of various materials, and geometries, involved determination of:

- a. Liquid-liquid contact angles of liquid drops, having a range of physical properties, at various plane solid surfaces immersed in an immiscible liquid. The information obtained was then used as a basis for the selection of the solid components constituting a junction.
- b. The ratio of the outlet drop diameter of the void of an idealised packing which was 'wetted' or 'non-wetted' with respect to the dispersed phase. Various geometries of the void were examined including cubical, rectangular or spherical geometries. An equivalent void diameter of the cubical or rectangular void was

estimated and used to calculate the above ratio. The drop behaviour at a void of a packing with a junction was generalised from these studies.

- c. The effect on coalescence of a thin film of dispersed phase liquid on the packing surface. This was to investigate the enhanced coalescence effect reported (15) on packings immersed in a dispersed phase liquid before lowering into the continuous phase,
- and d. Junction mechanisms, in order to propose an explanation for the enhanced coalescence effect at composite surfaces.

The single drop studies were later extended to the practical situation involving simultaneous arrival of liquid dispersions at a composite packing and the coalescence within it.

#### 5.1.1 Selection and preparation of solid surfaces

The history of a solid surface at which drops arrive is an important factor affecting coalescence behaviour. The solid surfaces used in this work, and the procedure adopted in their preparation, are described below.

Plane solid surfaces of both high and low surface energy material were used to study liquid-liquid-solid contact angle phenomena. The high surface energy solid materials, which were used in the form of flat plates, were: stainless steel, copper and glass. The low surface energy solid materials were polytetrafluoroethylene (p. t. f. e. ) and polypropylene. Each solid surface was 3 cm. x 3 cm. x 1.25 cm. thick.

The behaviour of a solid surface varies with the treatment given during preparation. The pretreatment technique has varied between workers investigating the phenomena (60). Grinding and polishing tends to alter the surface properties since the cavities of an uneven surface are filled up with carborundum;

conversely washing and cleaning with an acid exposes fresh surface due to etching. However, since a 'smooth' horizontal surface was essential, grinding and polishing was used in this work.

The surfaces of p. t. f. e., polypropylene and glass were not rubbed with emery paper, since they were naturally smooth; they were however polished on a diamond wheel. The stainless steel and copper plates were ground to reduce the surface roughness using emery paper of varying gradations, commencing with 100 and finishing with 420. Finally all the plates were polished on a diamond wheel.

The surface roughness of each plate was measured at different points on the surface using a scanning technique with a Telesurf machine and a mean value was taken. The mean value for the asperity height for the stainless steel plate was 0.0058 and for copper 0.0071 micrometers. Therefore, the surface conditions of stainless steel and copper were considered to be satisfactory. (The stainless steel plate and copper values were compared with those for naturally smooth surfaces of glass (0.0032)). Indeed any further attempt to improve the condition resulted in a loss of symmetry in some planes on the surface.

The plates were washed with phenol and dried, washed again with filtered, distilled and deionised water, and then with acetone followed by water. They were finally dried in a dust-free, electrically heated cupboard for 5 hours at 20°C.

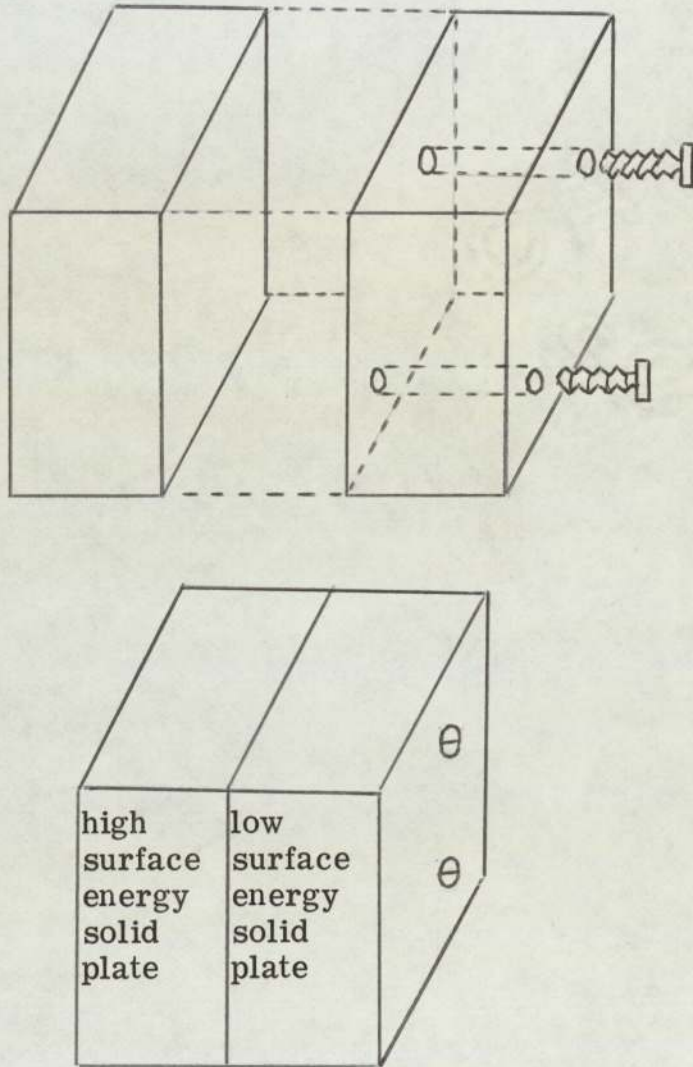
The single drop studies were also devised to provide some understanding of the coalescence mechanisms which occur in packings of different geometries and void sizes. It was, therefore, necessary to study the conditions governing the passage

and coalescence of single liquid drops at a single aperture of knitted mesh packings. For this purpose single meshes of various materials, i. e. nylon, polypropylene, stainless steel and copper were used, their size and wire diameter are given in Table G. 1 .

A junction surface was constructed from two dissimilar plates (Figure 5.1), one wetted and the other non-wetted with respect to the liquid of the dispersed phase. Selection of the components of each junction surface was based upon the observations and measurements made with single drops at single solid plates. From the range of high and low surface energy materials, p. t. f. e. and glass were the surfaces found to yield extreme contact angle values; this was, therefore, an ideal pair to provide a junction.

Each plate was precisely cut to give sharp edges at  $90^{\circ}$  to each other. The two plates were bonded together with an adhesive and two bolts. The adhesive was 'Araldite' (AV 138M + HV 998) ex Ciba-Geigy and was insoluble in most organic liquids. However, whilst it provided a bond of great strength to the high surface energy solid material it did not bond to the low surface energy material. Application of a thin layer of this adhesive to about 3 mm.<sup>2</sup> between the plates gave a junction which had a surface free of any contamination and an air gap which was removed by pressing the plates against each other. Two holes of 2 mm. diameter were drilled in the low surface energy solid plate and two bolts, each of 2 mm. diameter and 1.25 cm. long, were wrapped by the adhesive and pushed into the drilled holes in the plate. When the high surface energy solid plate was pressed onto the other side of this low surface energy solid plate, the adhesive at the ends of the bolts bonded with the high surface energy solid plate.

Figure 5.1.

Construction of a junction.

Construction of a junction of plane solid plates of high and low surface energy materials by tightening the air gap between the plates using bolts wrapped in Araldite adhesive.

The two plates were pressed together until the adhesive cured and the junction strengthened. The surface of the junction was subsequently cleaned as described above.

Various attempts were made to construct a void from mixed components. However, it proved difficult to obtain the correct tension in strings of a mesh packing woven from mixed filaments to give a surface with a minimum surface roughness. Junctions in glass beads of various sizes were made by coating the beads with a p. t. f. e. spray (Figure 5.2). However, the surface obtained with the spray was not uniform, or smooth and firm. In addition the sprayed, dried layer tended to absorb the organic liquid. This was not therefore followed up since in any event, the surface of the bead was curved which would have hindered assessment of the kinetic forces imparted to the liquid drop by the low surface energy material.

Finally, nozzles of glass and p. t. f. e. were prepared such that they could be fitted into each other to give a spherical void with a smooth surface junction.

The solid components could be arranged in various geometries to simulate the conditions in a commercial composite packing. The arrangements in which the junctions were formed were:

A horizontal junction; a junction surface in which both the components were arranged side by side and horizontal with respect to the drop arrival at the junction (Figure 5.3. a)

A vertical junction; a composite surface of two dissimilar materials arranged at right angles to each other. The vertical component was normally a wetted and the horizontal a non-wetted material (Figure 5.3. b).

Figure 5.2

A junction of glass beads

Four glass beads; ratio of high to low surface energy varied by coating with p. t. f. e. aerosol (e. g. in this example three glass beads were coated to give a ratio of 1:3 and a cubical aperture).

A parallel junction; both the solid components were arranged parallel to each other and at right angles to the direction of fall of the drop. In this case the drop could first 'rest' at the non-wetted surface before an interdrop coalescence took place with another drop at the wetted surface of the junction (Figure 5.3.c) Mixed junctions; an arrangement which incorporated horizontal, vertical and parallel junctions (Figure 5.3.d)

Junction voids were also constructed from cylindrical rods of 4.0 mm. diameter of mixed components (Figure 5.4) to note the effect of varying surface area of the solid junction upon the drop behaviour. Finally junction voids were made from 1.0 mm diameter plastic insulated metallic wires, i.e. 0.5 mm. tin wire insulated with P. V. C., in an attempt to simulate composite packing, by peeling off the insulation from only part of the wire. This provided a junction between the uncovered metallic surface and the insulated plastic surface. A packing matrix was made by soldering together the metallic surfaces.

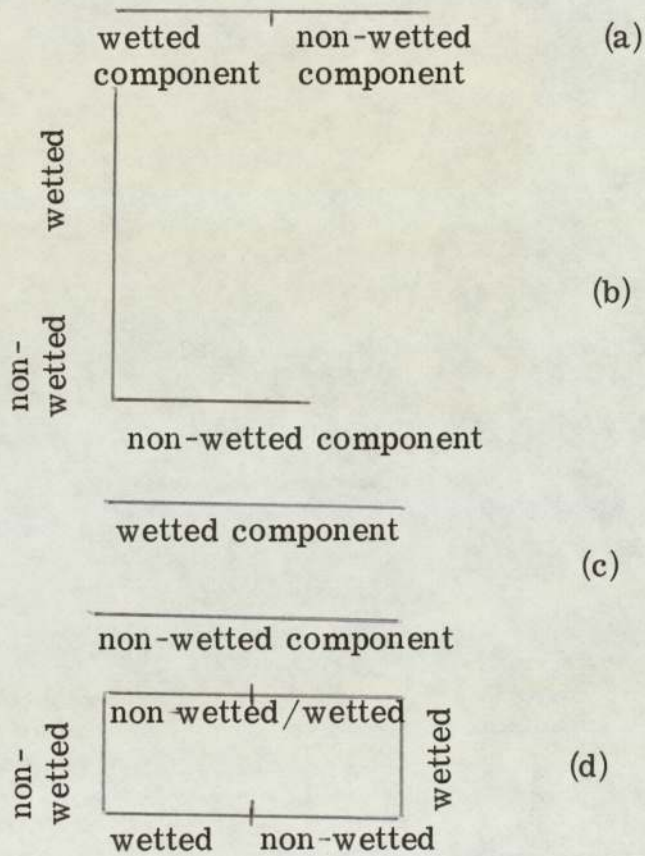
### 5.1.2 Experimental apparatus

The initial considerations in devising the apparatus were: the necessity for relatively stable conditions, constant temperature, and freedom from vibrations. A further requirement was to accurately control the drop volume with a good reproducibility and to deliver the drops at the required spot.

Various workers have experienced difficulty in obtaining reproducible results in fundamental liquid-liquid studies. One of the major factors responsible for such difficulties is inadvertent contamination in the systems. This contamination may result from materials of construction selected to suit the experimental study, for example, from the leaching of 'inert' adhesives used to bond the walls of a glass cell or leaching of plasticisers from plastics.

Figure 5.3.

Some arrangements to form a junction.



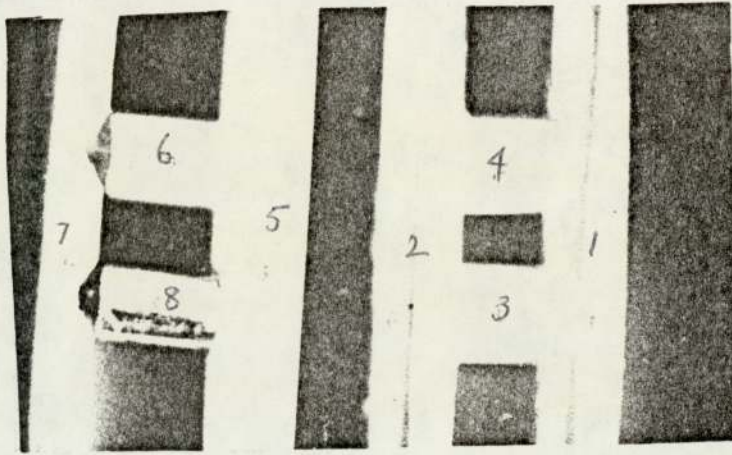
- (a). Horizontal junction      (b). Vertical junction  
 (c). Parallel junction      (d). Mixed junction

Great care was therefore taken to select materials of construction to minimise surface active contamination. The materials which came into contact with the liquid-liquid systems were restricted to glass, p. t. f. e. and stainless steel.

The apparatus used to form and deliver single liquid drops is shown in Figure 5.5 It consisted of two reservoirs, in which the drop phase and continuous phase liquids were stored inside the temperature controlled cabinet, a drop forming flask and the ancillaries. The drop forming flask was connected to the drop liquid reservoir, an Agla micrometer syringe, a vent and a nozzle to deliver the drop. Since contact angle varies with drop size, it was necessary to control and measure accurately the volume of the drop delivered. The Agla micrometer syringe was found to be very convenient and satisfactory for these purposes; by revolving the head of the micrometer attached to the syringe, the volume of the drop could be controlled. The movement of the micrometer head advanced the plunger in the syringe, and the volume delivered could be calculated from the number of revolutions of the micrometer head. Each complete revolution delivered only ten microlitres of the liquid.

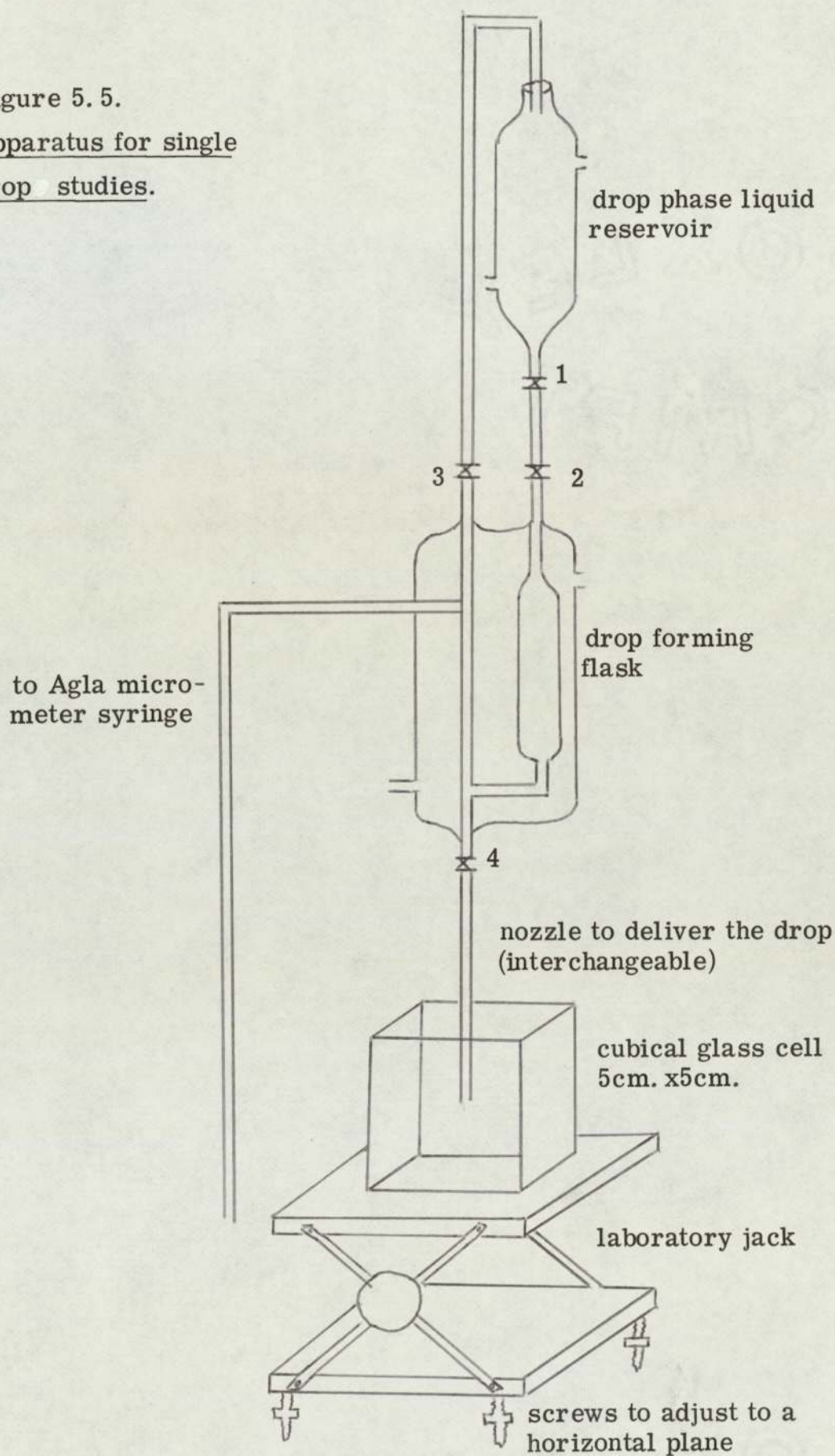
To check whether the contact angle value became constant below a certain minimum, or above a certain maximum, drop diameter a range of sizes of nozzles were used to form the drops. Single liquid drops were delivered individually from three hypodermic syringe needles of sizes 20G, 27G and 32G corresponding to 0.05, 0.1 and 0.3 mm. inside diameter and glass nozzles of inside diameter of 0.5, 1.25, 2.08 and 3.15 mm. respectively. The glass nozzles had polished tips, and the needles had bevelled ends to assist detachment of the drop.

Figure 5. 4.

Construction of junction of solid bars .

Junctions were constructed with 0.225 cms. diameter stainless steel and p. t. f. e. bars. This figure shows the various ways in which solid surfaces were arranged. Numbers 3, 4, 5 and 6 refer to p. t. f. e. surface and numbers 1, 2, 7 and 8 refer to stainless steel surface.

Figure 5. 5.  
Apparatus for single  
drop studies.



Most workers have examined only a limited number of liquid-liquid systems to study coalescence; this restricted generalised conclusions from their results. The present study involved examination of a number of systems to cover a range of physical properties and hence permit generalisations to be made regarding the coalescence behaviour of single liquid drops at plane solid surfaces, with and without junctions, and to extend this to the behaviour of dispersions in composite packings. Addition of surfactant was avoided to keep the liquid-liquid systems pure.

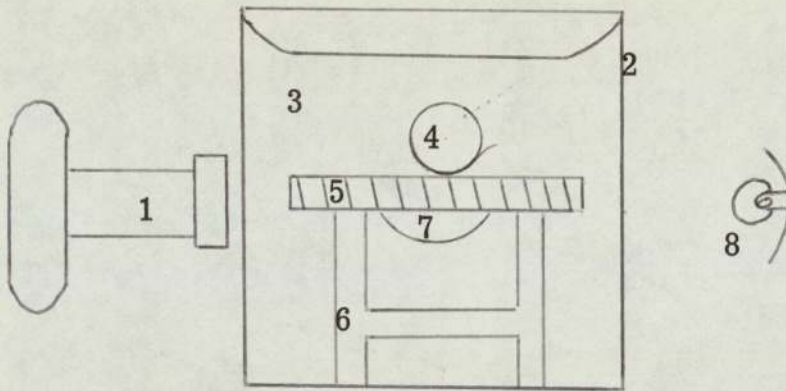
Five organic liquid-water systems were chosen which provided a suitable range of values of liquid-liquid interfacial tension and density (Appendix A). This combination actually provided ten coalescing systems i. e. water dispersions in organic liquids and vice versa. With this range of physical property values, it was considered unlikely that any other system would differ significantly in its coalescence behaviour except for very viscous liquids, or liquids contaminated by surfactants or solids. The liquids used were of Analar grade; the deionised water was obtained from a laboratory distillation column.

To determine the effect of density difference between the dispersed and continuous phase liquids upon the liquid-liquid contact angles, the density of the organic liquid could conveniently be varied by gradual additions of carbon tetrachloride (Appendix B), since it did not increase the interfacial tension by more than 5 %.

Each pair of the above ten pairs of liquid-liquid system was examined separately. The organic liquids were redistilled in a laboratory scale glass distillation column before use; the

Figure 5.6.

Photographic arrangement for liquid-liquid-solid contact angle measurements.



- |   |                           |
|---|---------------------------|
| 1. Still camera                             | 2. Cubical glass cell     |
| 3. Continuous phase liquid                  | 4. Dispersed phase liquid |
| 5. Solid surface                            | 6. Glass stand            |
| 7. Dispersed phase (organic)                |                           |
| 8. Lighting arrangements (200 W flood lamp) |                           |

distillate being collected at  $\pm 1^{\circ}\text{C}$  of the recognised boiling point. Each pair of liquids was mutually saturated by shaking them together over a period of 24 hours to ensure that mass transfer effects were eliminated, that complete saturation was achieved was confirmed by analysis, using chromatography, and by surface tension measurements using a Du Nouy Tensiometer.

The studies of the coalescence behaviour of single liquid drops at solid surfaces were carried out in a cubical glass cell measuring 5 cm. x 5 cm. The walls of the cell were free from optical distortions and were bonded together at the corners with a non-surface active Araldite cement. Repeated use of the glass cell resulted in some leaks along the cemented corners, these were sealed with a special Araldite Av 138 + hardener Hv 998. It was advantageous to use this cell because of its optical properties and the small volume of liquid required to fill it. Above all, it was convenient for photographic purposes.

A specially constructed glass stand was placed inside the glass cell as shown in Figure 5.6. The solid surface under investigation was held on this horizontal stand. The glass cell was then filled with the appropriate continuous phase liquid.

Since temperature fluctuations have a significant effect on coalescence time and contact angle, the complete apparatus was enclosed in air bath which was temperature controlled. Temperature control was facilitated by a Fi-monitor control module. This consisted essentially of a temperature sensitive head in conjunction with a capacitance cell connected to the control module itself. When the electrical circuit was completed this was linked with a heating element. A 60W electric bulb proved adequate for the heat required. The Fi-module was found to be simple and effective, and a temperature control of  $20 \pm 0.2^{\circ}\text{C}$  was obtained.

### 5.1.3. Cleaning technique

Cleaning techniques were followed meticulously for all the surfaces which came directly into contact with the liquid-liquid systems.

The apparatus design for both single drops (Section 5.1.2) and drop swarm studies enabled cleanliness to be achieved very conveniently. Prior to each 'single drop' experimental run, the glassware was dismantled for washing and cleaning. Flask reservoirs used to store both the liquids, drop forming flask, glass nozzles and syringe, p. t. f. e. tubing and control valves, and cubical glass cell were soaked over night in a 2 % Decon 90 solution in distilled water in a tank. After draining off the solution, the tank was repeatedly filled with tap water to remove any traces of the solution. Each item was removed by hand and, using gloves to avoid contact with the surfaces, washed thoroughly in distilled water in a separate container. Finally, each item was washed with filtered, deionised, distilled water before leaving the glassware and the ancilliary apparatus to dry in a dust-free, electrically heated oven at 40<sup>0</sup>C for about 5 hours. After drying was complete, the glassware was reassembled onto the wooden frame with holding clips and supports.

### 5.1.4. Experimental technique

The dispersed phase and the continuous phase glass reservoirs held at the top of the frame were filled via a long stemmed funnel. Flow control valves 1 and 2 (Figure 5.5) were opened. The plunger was not inserted into the glass syringe and the syringe was dipped into a beaker containing the dispersed phase liquid. The dispersed phase liquid thus flowed down to fill the drop-forming flask and then via the syringe into the beaker. Valve 2 was shut.

The plunger was inserted into the syringe which was then clamped into a syringe holder on the wooden wall of the temperature controlled cabinet. The holder was designed such that only the micrometer head, to control the drop volume, was outside the cabinet.

Valves 2 and 3 were then opened so that the remainder of the drop-forming flask was filled up and the liquid rose up past valve 3 into the glass tube. Both the valves 2 and 3 were then shut. A beaker containing the dispersed phase liquid was placed on an adjustable laboratory jack such that the drop forming glass nozzle dipped into the liquid in the beaker. Valves 2 and 4 were opened to fill up the nozzle with the drop phase liquid. During these stages, air bubbles could be trapped either in the inlet to the nozzle or in the drop-forming flask. By moving the plunger in and out of the syringe, keeping the delivery end of the nozzle in the liquid in the beaker, and operating valves 2, 3 and 4 one at a time, any air bubbles in the line escaped into the glass tube past valve 3. Valve 3 was shut, and the plunger pulled back to its starting point to fill up the syringe with liquid.

The glass stand designed to hold the solid surface accurately in a horizontal position, was placed inside the cubical glass cell. The solid surface was placed on the glass stand, and the glass cell was thus placed on the adjustable laboratory jack. This jack plate was levelled using a spirit level by adjusting the fine adjustment screws fixed to its legs. Now valve 5 and then valve 6 were opened to fill up the glass cell with the continuous phase liquid. The elevation of the glass cell was adjusted by revolving a knob fixed to the jack until the solid surface was only 2 to 3 mm. from the drop. A drop of the required size was

delivered by revolving the micrometer head. Once the drop had attained a stable condition, generally after two minutes, the lights were switched on and the characteristic photograph taken. Three photographs were taken of each drop and a mean value of the contact angle was taken from projections of negatives.

#### 5.1.5. Measurement of size of single drops and voids

Single drops were delivered from either a glass nozzle or hypodermic needle (Section 5.1.3), depending upon the size of the drop. Drops larger than three millimeters diameter were generally delivered from a glass nozzle. The drop forming tip was connected to an Agla micrometer syringe via drop forming flask and ancilliary apparatus (Section 5.1.3). The whole assembly was completely filled with the drop phase liquid, care being taken to ensure that no air bubbles were trapped in the flow line. When the micrometer head attached to the glass syringe was rotated, it pushed the glass plunger; liquid in the syringe was gradually forced out as a growing drop at the tip.

The volume of each single drop delivered from the tip could be calculated from the distance the plunger advanced in the syringe. The distance moved was calibrated so that the volume of the drop could readily be calculated, since each complete revolution of the micrometer head produced a volume of ten microlitres.

In experiments in which drops were required to pass through an aperture, some of the liquid had to be taken out or added to, the known volume of the drop to obtain the characteristic drop size. The volume of the liquid added, or subtracted from, the existing drop could also be found from the micrometer syringe. The diameter of the drop,  $D_d$ , was subsequently calculated from the adjusted volume.

The single drop studies were carried out with apertures of various geometries and solid materials. To assess the size of the single drop that passed through a given aperture, it was necessary to determine accurately the sizes of both the drop and the aperture. The drop size was determined as explained above. A travelling microscope was used to determine the size of the void. With rectangular apertures, the length, width and thickness were measured and an overall equivalent mesh diameter,  $d_e$ , calculated by equating the length parameter of the aperture to the circumference of a circle. The diameter of the circle was taken as the equivalent diameter of the aperture as shown in Appendix G. With circular apertures the diameter of the void and the thickness of the solid surface were measured.

## 5.2 Drop Swarms Studies

In the laboratory scale equipment only the coalescence of water dispersions in organic media was studied in a QVF glass column packed with the junction coalescer especially constructed from the mixed components (Figure 5.7.). The main features of the apparatus, and the construction of the composite coalescer, are described below.

### 5.2.1. Experimental apparatus

To avoid system contamination via the materials of construction only glass, stainless steel and p.t.f.e. were used with the exception of brass distributor plates.

The distributor plates were designed to produce a primary dispersion with a narrow drop size distribution; fabrication of the plate with the sharp edged orifices required was best carried out using brass. Distributor plates with 3.1, 1.6, 0.8 and 0.4

Figure 5.7.  
Apparatus for coalescence of swarms of drops.

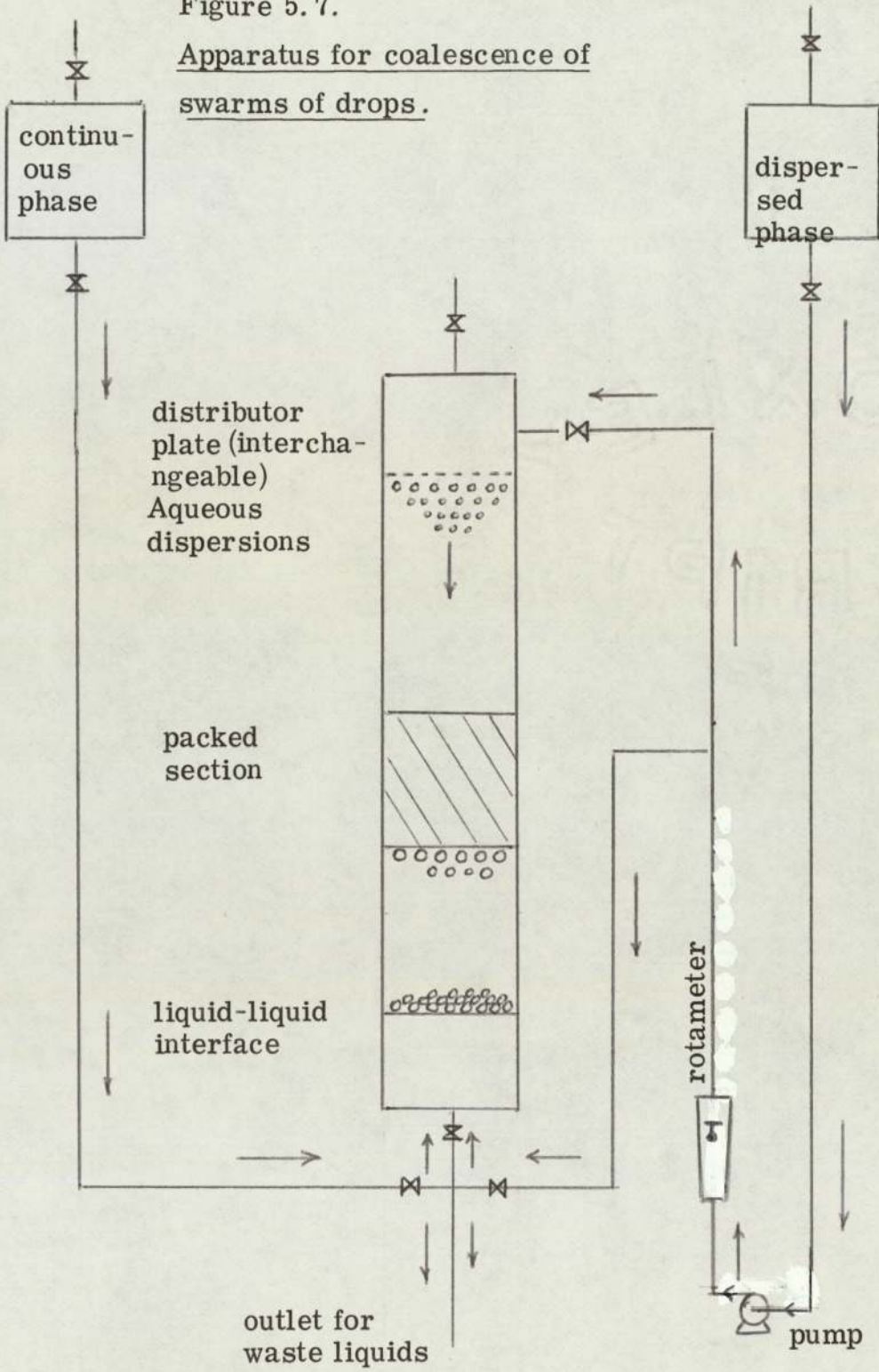
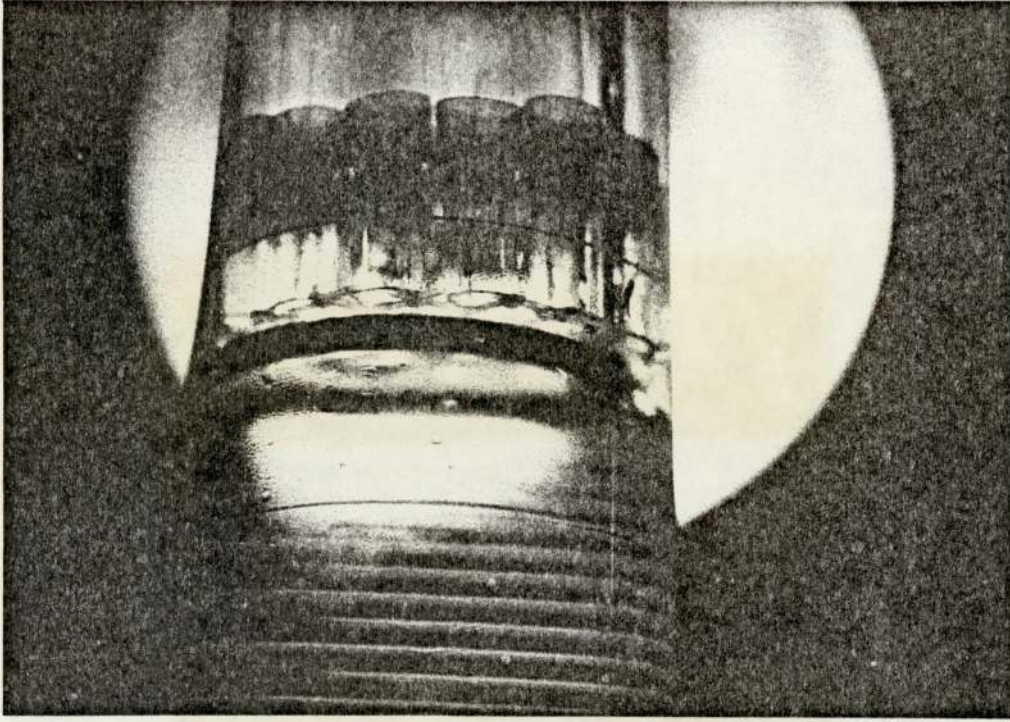


Figure 5. 8.

Heterogenous geometrical junctions



This figure shows the heterogenous composite packings consisting of a number of junction nozzles.

mm. diameter orifices were used in this study to produce inlet drop size in the range 0.8 - 0.1 cm.

The coalescence of swarms of drops was studied in a glass column of 3" diameter. The coalescer element comprised an arrangement of nozzles supported on a special stainless steel holder secured at the top of the column; this enabled the coalescer to be held at any required position in the column. The coalescer was positioned beyond the plane at which the drops in the size range 0.8 - 0.1 cm. reached their terminal velocities i. e. 30 cm. from the distributor.

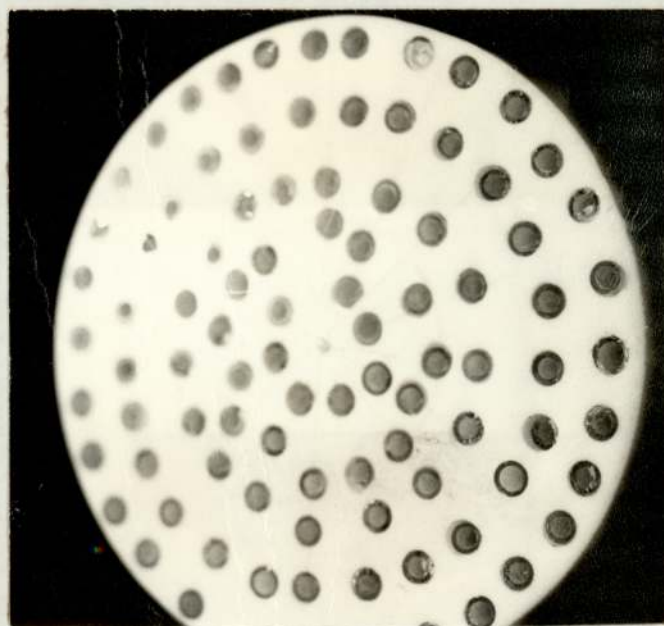
Special attention was given to the distillation, storage and handling of all the liquid systems. Periodic checks of phase purity were made using a Du Nouy Tensiometer to determine the interfacial tension values. When a deviation in the value was detected, the organic liquid was redistilled and left for saturation with fresh deionised, distilled water.

The organic systems selected covered a range of interfacial tension values from  $8.2 \times 10^{-3}$  to  $52.1 \times 10^{-3} \text{ Nm}^{-1}$ , and a range of density difference values from  $1.0 \times 10^2$  to  $3.4 \times 10^2 \text{ Kgm}^{-3}$ . Non-viscous liquids i. e. with viscosities in the range  $4.69 \times 10^{-4}$  to  $6.57 \times 10^{-4} \text{ Nsm}^{-2}$  were selected to minimise the pressure drop associated with flow through the packed bed. The organic liquids and their physical properties are listed in Appendix A. A further advantage of the systems used was that of general convenience. They were all relatively non-toxic, non-corrosive, readily available and economic to use in laboratory scale studies.

Prior to use, the organic phase was distilled twice with a distillation cut  $\pm 1^\circ\text{C}$  around its theoretical boiling point. It was then stored prior to use in clean containers in a darkened cupboard

Figure 5. 9.

Ideal coalescer with junctions



In this 'ideal' coalescer, glass nozzles were inserted firmly into the holes drilled in p. t. f. e. circular plate.

to avoid any polymerisation due to sunlight, which Hitit (60) concluded was important to phase purity. The aqueous phase, consisted of laboratory tap water which had been passed through a filter to retain all particles  $> 10 \mu\text{m}$ ; it was then deionised and distilled. Distillation was at a rate of 8 litres per hour with collection in a special sealed container of 40 litres capacity. All parts of the apparatus in contact with the liquid phases were cleaned thoroughly before each experimental investigation. A surface active cleaning solution, Decon 90, was found to be most suitable for cleaning purposes. Before each series of runs, the apparatus was filled with a 2 % solution of Decon 90 in distilled water and allowed to soak for 24 hours with periodic recirculation of the cleaning solution. After soaking, the whole apparatus was rinsed thoroughly with tap water; this was effective since there were no dead-legs in which solution could be retained. The apparatus was then rinsed with distilled water and finally filtered, deionised, distilled water, and the coalescer element was dried in a dust-free oven for 8 hours at  $20^{\circ}\text{C}$ .

### 5. 2. 2. Construction of junction coalescer

For the single drop studies, a spherical void with a junction was constructed by the insertion of a glass nozzle through a p. t. f. e. nozzle. However, when a number of these individual junction nozzles were packed (Figure 5. 8) into the column to provide a composite packing, the voids obtained were nonhomogeneous. Moreover, such an arrangement gave a packing of junctions interspersed with p. t. f. e. channels.

An ideal coalescer was therefore constructed (Figure 5. 9) from a  $\frac{1}{4}$ " thick p. t. f. e. plate and glass nozzles. Holes were drilled in the p. t. f. e. plate and the glass tubes were inserted

firmly into these holes to provide junctions between the aqueous non-wetted (p. t. f. e. ) and wetted (glass) materials. The diameter of the holes drilled in the p. t. f. e. plate was equal to the outside diameter of the glass nozzles so that the glass nozzles were a push fit. The minimum distance between the edges of adjacent holes in the p. t. f. e. was made equal to the hole diameter; this ensured the drops acquired enough kinetic energy from the non-wetted surface and avoided interdrop coalescence between two drops growing adjacent to each other at the exit of the packing. The dimensions of the glass nozzles used are shown in Table K.

The coalescer was held between two vertical bars of a stainless steel holder which did not interfere with the coalescence mechanism since they occupied only two voids on opposite sides of the coalescer and only near the column wall.

This coalescer enabled the following factors to be controlled conveniently:-

- (a) Geometry and symmetry of the void and the junction in relation to the drop.
- (b) Coalescence mechanism at the inlet and exit of the packing.
- (c) Height of the bed.
- (d) Formation of the drop at the exit of the coalescer.

### 5.2.3 Experimental technique

The stainless steel holder and the coalescer were lowered into the column from the top. The saturated dispersed and continuous phase liquids were transferred, using a long stem funnel into their respective reservoirs above the height of the distributor plate to facilitate gravity flow as shown in Figure 5.7.

Before each series of experimental runs the continuous phase liquid was first admitted to the column to the required height and then the dispersed phase liquid. The latter was admitted gradually and slowly to avoid a dispersion, in order to maintain a liquid-liquid interface at a constant level near the bottom of the column. This prevented escape of the continuous phase liquid with the dispersed phase liquid through the column outlet which could have created an emulsion during their flow through the pump. In this way, the coalescer surface came into contact first with the organic liquid. The dispersed phase liquid line from the outlet was connected via a No. 10 Stuart Turner pump to the inlet at the top of the column where it was admitted to the column as a dispersion from the distributing plate. After coalescence in the packing, drops detached from the outlet of the coalescer and were collected at the liquid-liquid interface maintained at a constant level near the bottom of the column.

A measure of the coalescence efficiency of a packing is the ratio of the outlet to inlet mean drop diameter. Throughout this study the size distribution of droplets entering or leaving the packing was evaluated from photographic records. The inlet dispersions were produced from distribution plates with equal sized, sharp edged orifices and as such had a small distribution of sizes around the mean value. Consequently, the analysis of the mean inlet drop diameter was carried out at selective intervals from each flowrate and liquid system. From the exit of the packing, the droplets detached also from equal sized, sharp edged orifices but the drop size in the outlet dispersion was dependent on system hydrodynamics. This made the size distribution much wider due to fluctuating conditions across the channels of the packing.

During any experiment, five minutes were allowed following any change in the operating parameters for the system to regain hydrodynamic equilibrium before photography commenced. Mean droplet diameter was determined directly by measuring the drop dimensions with a graduated scale from an enlarged photographic negative. The number of drops recorded on any one negative was a function of the flowrate. Therefore, in the case of very low flowrates, three or more photographs were obtained at 15 second intervals so as to record sufficient drops for analysis.

It was found on analysis of the exit dispersion that the drops were irregular in shape; for purposes of analysis a drop shape equivalent to an oblate spheroid was assumed. Hence the individual drop diameters were determined by measuring the horizontal and vertical dimensions. The diameter was then evaluated from the following equation.

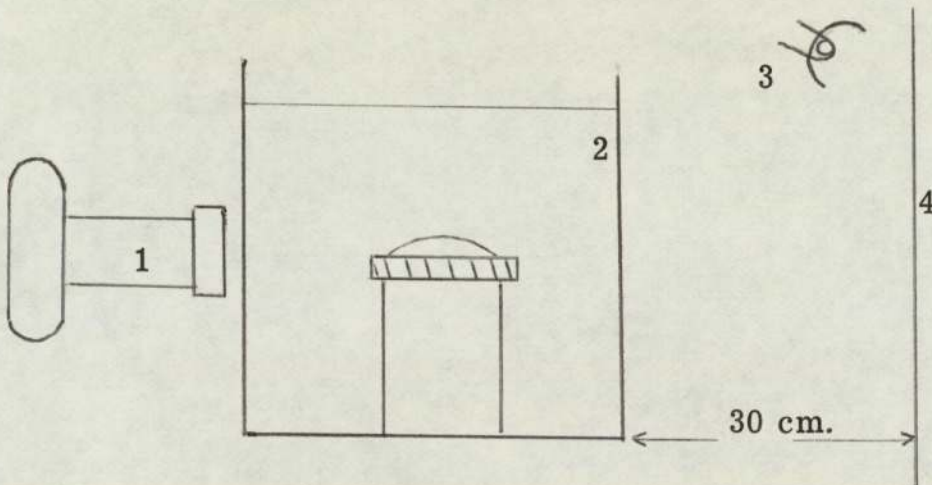
$$d = a^2/2 + (b^2/4.e) \ln (1+e)/(1-e)$$

where 'a' and 'b' are the major and minor axes of an oblate spheroid. The eccentricity 'e' which is always less than one, is defined by,

$$e = (a^2 - b^2)^{0.5}/a^2$$

For any one set of experimental conditions, approximately 50 drops were measured and their arithmetical mean was computed. The number of drops required to be measured to produce a representative mean was evaluated using an experimental technique. Several tests were made on a large number of drops to evaluate the mean diameter. It was found for all cases investigated, that the difference between the mean

Figure 5. 10

Arrangement for colour photography

1. 'Hyspeed' camera (pedestal mounted)
2. Cubical glass cell
3. Lighting (200W floodlamp)
4. White-matt screen (40cmx40cm)

of a large sample and that for 50 drops was always less than 5 %. The size distribution around the mean 'd' was calculated using a 95 % confidence limit. This was obtained from the general equation of 0.95 probability that all the individual diameters lie within  $1.960/\sigma \cdot N$  of the mean drop diameter 'd' where N = number of drops measured, and  $\sigma$  is the standard deviation.

### 5.3 Photographic Technique

Most of the results presented in this work were obtained by photography. The accuracy of the analysis of the results therefore depends on the quality of the photographs and hence the photographic technique. One of the major requirements in terms of the quality of a photograph, irrespective of whether it is with a still camera or high speed camera, is good definition of the image with a high contrast. This was more difficult with coloured film and high speed cine photography.

A 'Miranda' still camera was used for the determination of contact angles in liquid-liquid-solid systems, behaviour of single drops at single apertures and filaments in liquid-liquid-solid systems and drop size distributions in liquid-liquid systems. A 'Hyspeed' cine camera, capable of exposing up to 40,000 frames per second, was used for more detailed studies to determine the mechanisms of coalescence of single liquid drops at solid surfaces and single packings. Coloured and high speed photography was used to determine the coalescence mechanisms at composite surfaces and to show the extent of mixing which took place during the interdrop coalescence process (Figure 5.10).

The coalescence mechanisms at a liquid-liquid interface have been studied (102) by matching the refractive indices of both the continuous and dispersed phase liquids to overcome optical reflection and interference from the mirror-like liquid-liquid interface. However, it was found difficult to match the refractive indices of both the liquids and the solid surface. Therefore, other means were employed to overcome the optical reflections from the polished solid surfaces and from the mirror-like spherical drop surfaces which reflected the objects around them. Direct rear lighting was used with still photography for recording liquid-liquid-solid contact angles and the behaviour of liquid drops at solid surfaces and single packings. Front lighting was used for photography of drop size distributions in liquid-liquid dispersions.

Rear indirect lighting was used for all high speed photography. In this case, the flood lamps were directed on to a white matt screen facing the camera. For coloured and high speed photography, the cubical glass cell was wrapped with a black paper, a 1.5 cm. x 1.0 cm. slit was made in the paper for the light reflected from the matt screen, and the camera view was aligned horizontally with the solid surface. The 'Hyspeed' camera was operated at 10,000 to 12,000 frames per second. The camera speed did not remain constant throughout any run since it was synchronised with the electric drive motor. However, the cine processed films showed timing interval marks to enable the determination of the speed at which any particular length of film was shot.

## CHAPTER SIX

### RESULTS AND DISCUSSION

The experimental investigation covered various aspects of the coalescence behaviour of liquid drops at solid surfaces immersed in another immiscible liquid (Figure 6.0). The solid surfaces were of different single or composite materials and different geometries. The aim was to explain and correlate the mechanisms, and efficiencies, of collection and coalescence of primary dispersions. The work was carried out in the following sequence:

#### 1. Single drop studies

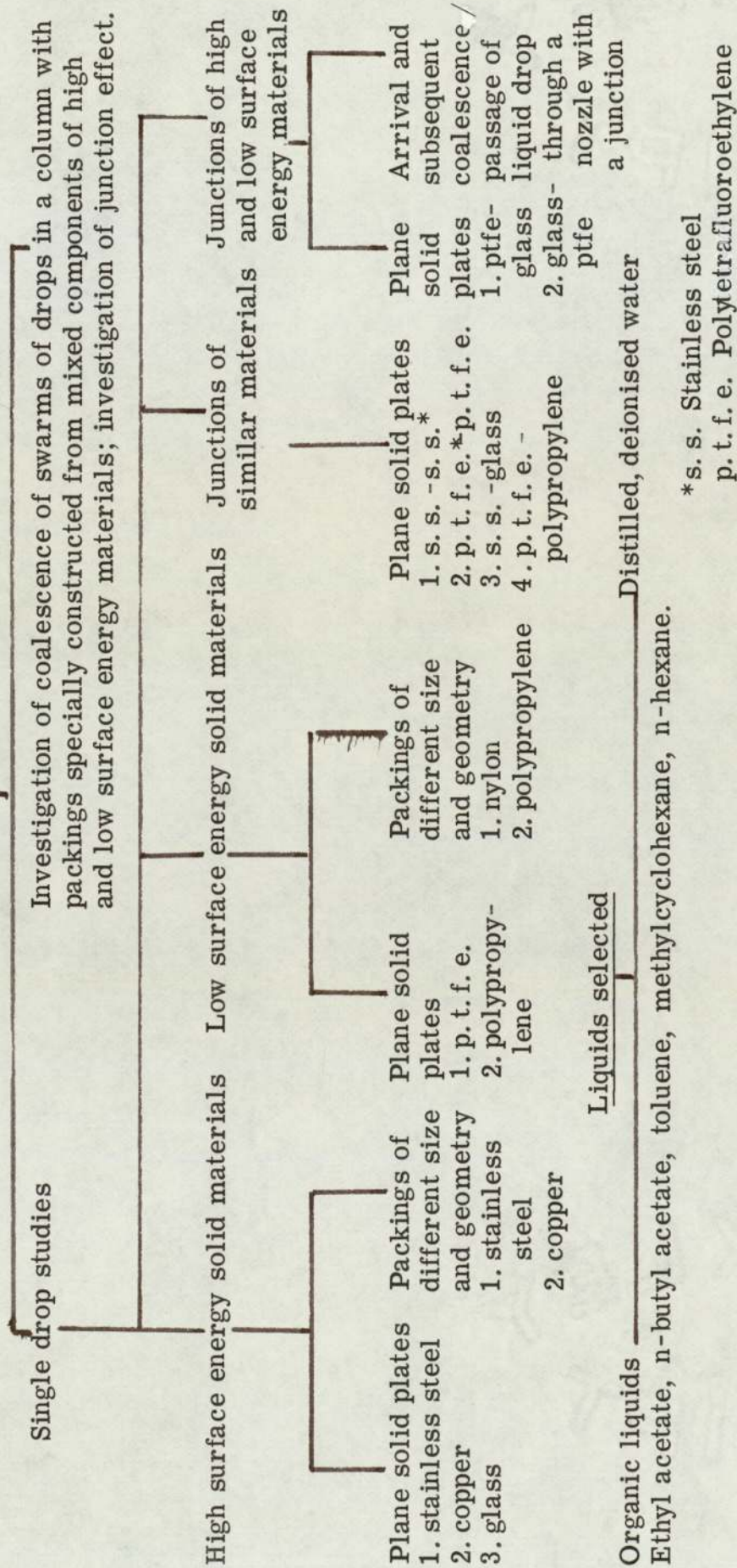
- (a). Measurement and characterisation of liquid-liquid contact angles of liquid drops at wetted and non-wetted solid surfaces (Sections 6.1.1.a & 6.1.1.b).
- (b). Measurement and correlation of the maximum diameter of a single drop able to pass through an aperture of a packing of single material. Determination of the effect of soaking the packing in the dispersed phase liquid before coming into contact with the continuous phase liquid (Section 6.1.2.).
- (c). Investigation of the mechanism of 'junction effects' (Section 6.1.3.).

#### 2. Studies of swarms of drops

- (a). Preliminary investigation of the coalescence performance of various packings incorporating junctions (Section 6.2.1.).
- (b). Investigation of coalescence mechanisms and correlation of exit drop size from an idealised junction coalescer (Section 6.2.2.).

Figure 6.0. Summary of experimental investigation

Coalescence behaviour of liquid drops at solid surfaces immersed in an immiscible liquid



### 6.1. Single Drop Studies

Young's Equation (6.0) relates the vapour-liquid to the solid-liquid and solid-vapour properties via the 'contact angle', as shown in Figure 6.1.

$$\gamma_{sl} - \gamma_{sv} = \gamma_{lv} \cos \alpha \quad (6.0)$$

The numerical value of the contact angle has been used to describe the wetting conditions in similar systems.

Young's Equation and the contact angle are equally important for characterising the coalescing behaviour of liquid dispersions in packed extraction columns and in liquid-liquid coalescers. However, little information is available on such quantitative characterisation of wetting conditions. Single drop studies were therefore carried out for the measurement and characterisation of solid-liquid-liquid contact angles, and for determination of coalescence behaviour of liquid drops at single flat solid plates of both high and low surface energy materials. In addition to original measurements of contact angles in solid-liquid-liquid systems (Section 6.1.1.), it was necessary to modify Equation (6.0) for application to solid-solid-liquid-liquid systems.

In describing liquid-liquid phenomena at surfaces, the term 'wetting' and 'non-wetting' generally refer to the dispersed phase liquid behaviour, unless otherwise stated, and this convention is used throughout this text.

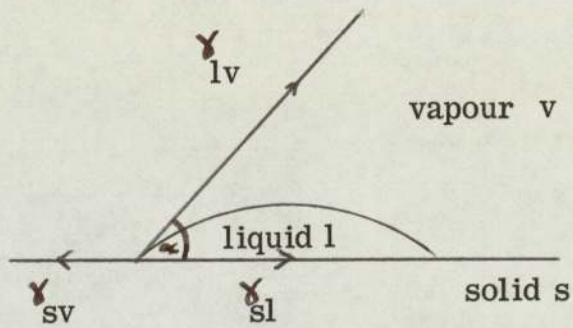
#### 6.1.1. Behaviour of liquid drops at flat solid plates

##### Solid-Liquid-Liquid Contact Angles:

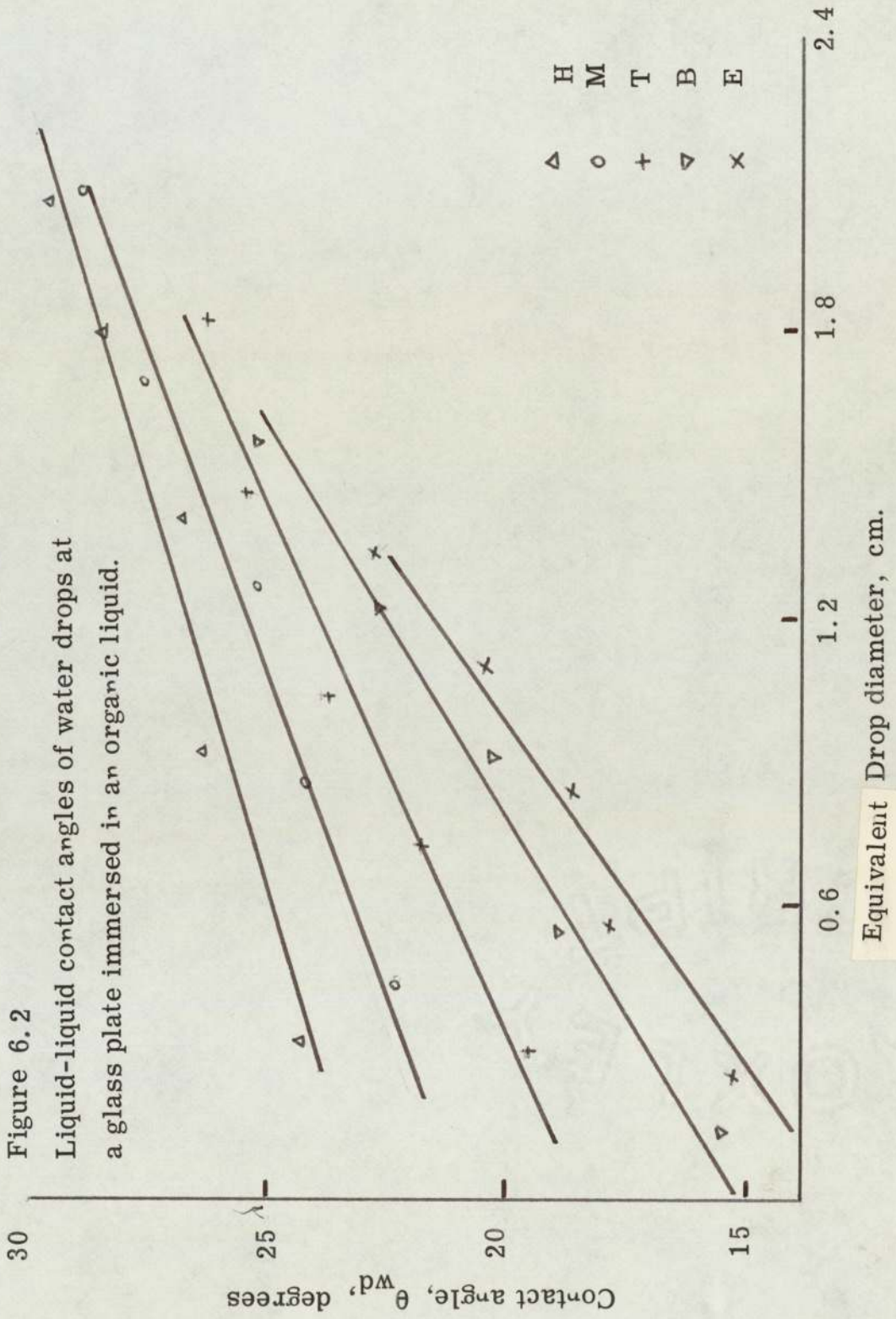
The solid-liquid-liquid contact angles of water drops were measured at each of the following plane solid plates immersed in organic liquids: glass, stainless steel, copper, p. t. f. e. and polypropylene. The experimental values of these angles are shown in Figures 6.2 to 6.6. In these figures, the following symbols are used for organic liquids: H - n-hexane; M - methylcyclohexane; T - toluene; B - n-butyl acetate; and E - ethyl acetate.

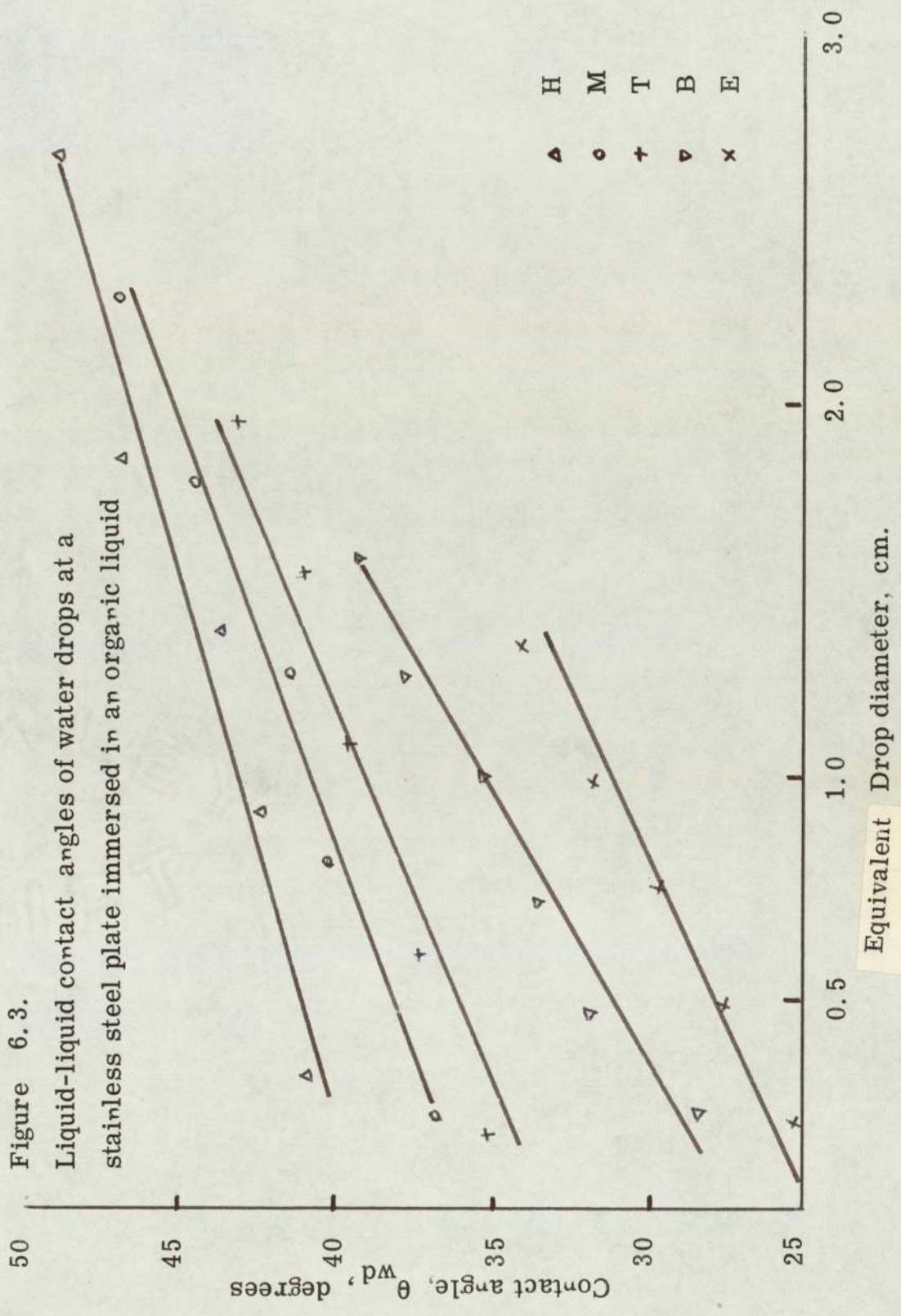
Figure 6.1.

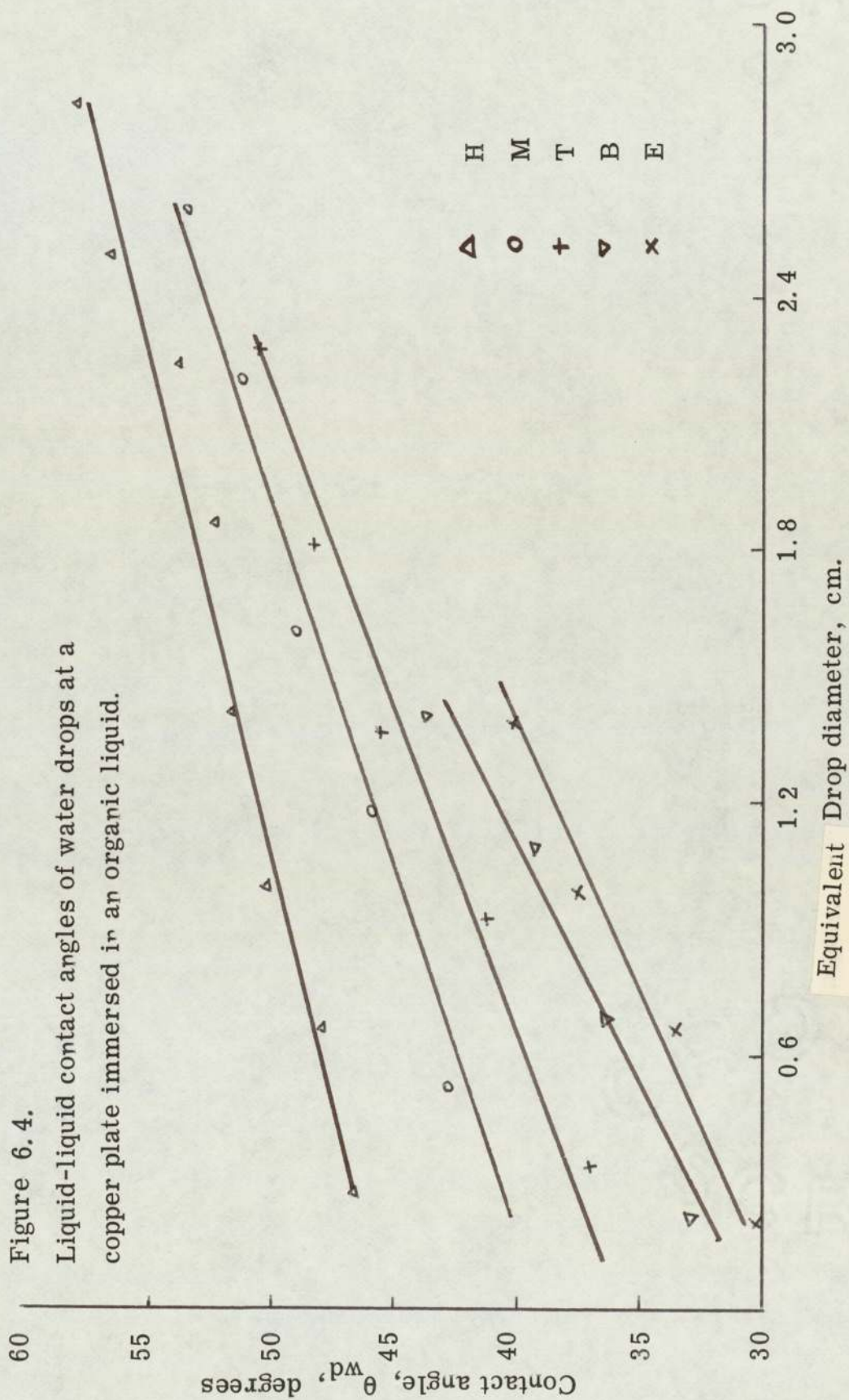
Vapour-solid-liquid system defined by Equation 6.0.

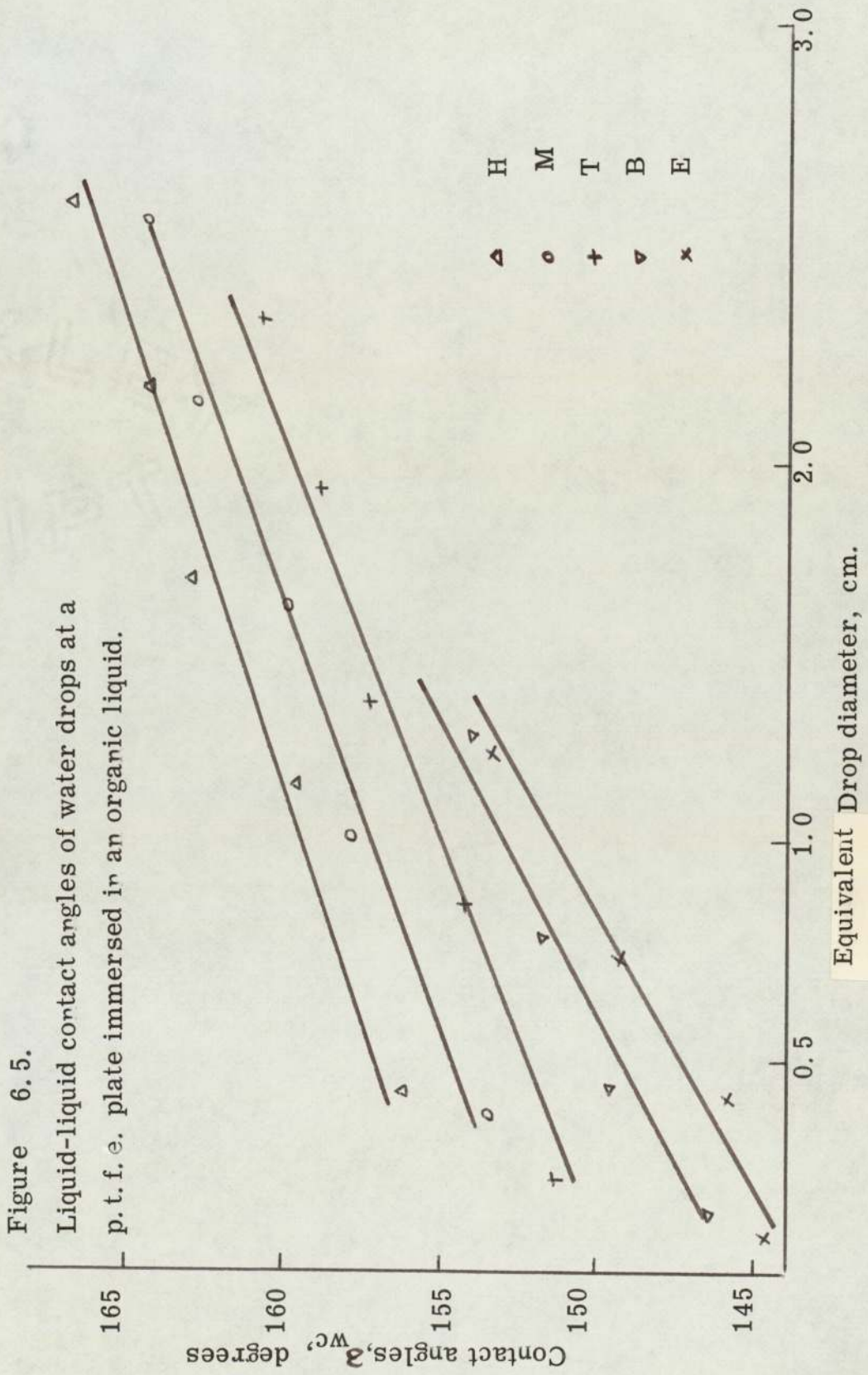


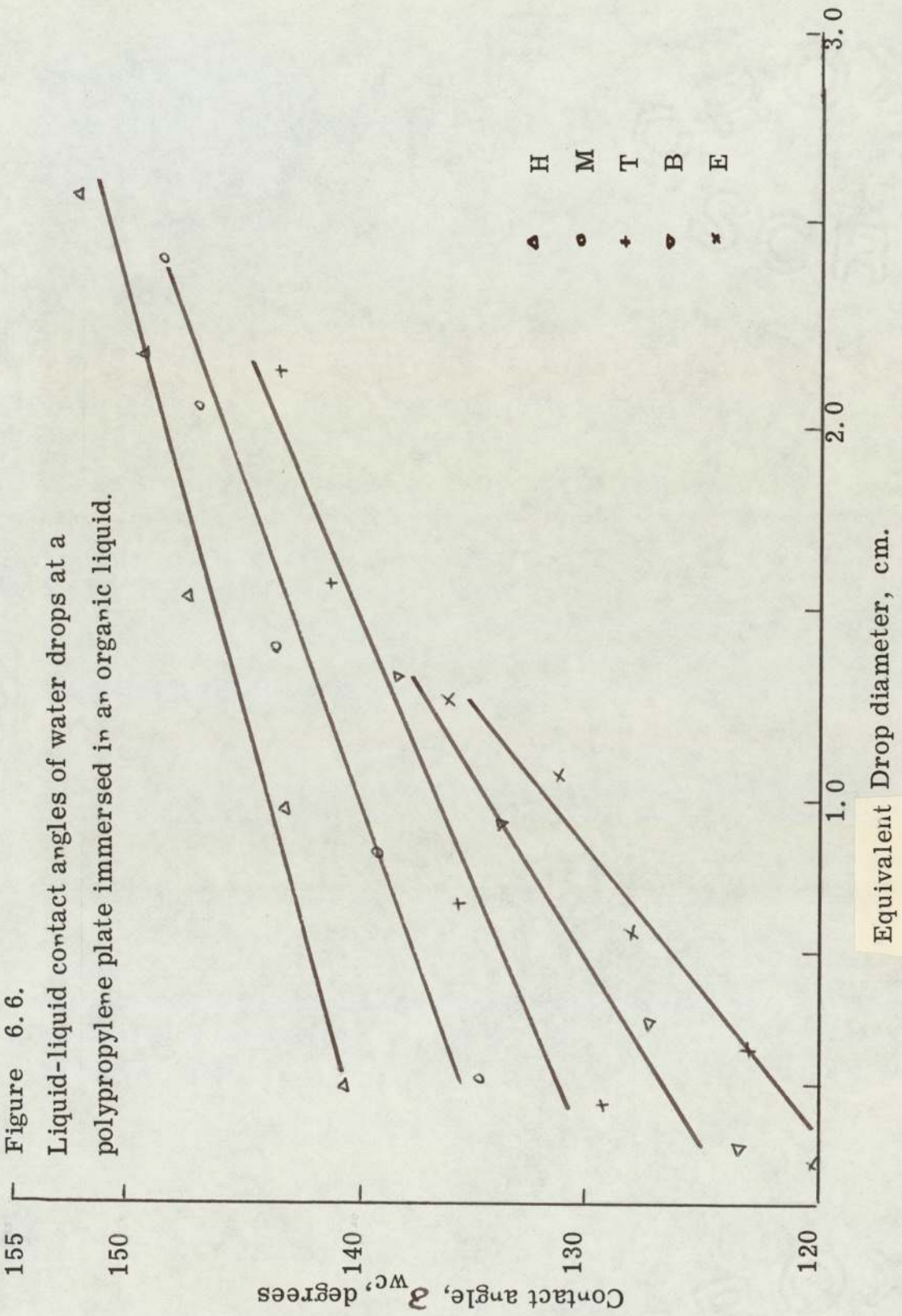
A liquid drop of contact angle  $\alpha$  at a solid surface placed in a continuum of vapour.











The contact angles of drops of each of five selected organic liquids were also measured at the above plates immersed in filtered and deionised water. The experimental values of these angles are shown in Figures 6.7 - 6.11. The tabulated values of solid-liquid-liquid contact angles measured during this work have been bound and deposited in the Departmental library.

Modification of Equation 6.0. :

Figure 6.12 shows a drop of liquid 2 in an equilibrium condition at a smooth, horizontal solid surface 3 immersed in an immiscible liquid 1. The cosine of the contact angle (at the triple point and measured in the drop) is the ratio of  $\gamma_{32}$ , if it were acting alone, to  $\gamma_{12}$ . Since  $\gamma_{31}$  is also acting along the same straight line as  $\gamma_{32}$  but in the opposite direction, the resultant is  $\gamma_{32} - \gamma_{31}$ . Writing the cosine of the contact angle in terms of these forces gives Equation 6.1, analogous to Equation 6.0.

$$\gamma_{32} - \gamma_{31} = \gamma_{12} \cos\theta \quad (6.1)$$

#### 6.1.1. a. Solid surface wetted by the dispersed phase liquid

For a system in which the solid surface is wetted by the dispersed phase liquid and non-wetted by the continuous phase liquid, as in Figure 6.13, Equation 6.1 becomes

$$\gamma_{wd} - \gamma_{nc} = \gamma_{dc} \cos\theta_{wd} \quad (6.2)$$

The experimental observations showed that  $\theta_{wd}$  was always less than  $90^\circ$  for liquid drops at solid surfaces which were wetted by the dispersed phase liquid, e. g. an aqueous phase drop at a glass surface as shown in Figure 6.14, or an organic liquid drop at a low energy solid surface, e. g. p. t. f. e., as shown in Figure 6.15. When  $\theta_{wd}$  is less than  $90^\circ$ , it lies in the first quadrant, therefore, cosine  $\theta_{wd}$  is always positive. Since  $\gamma_{dc}$  is a positive quantity, the right side of Equation

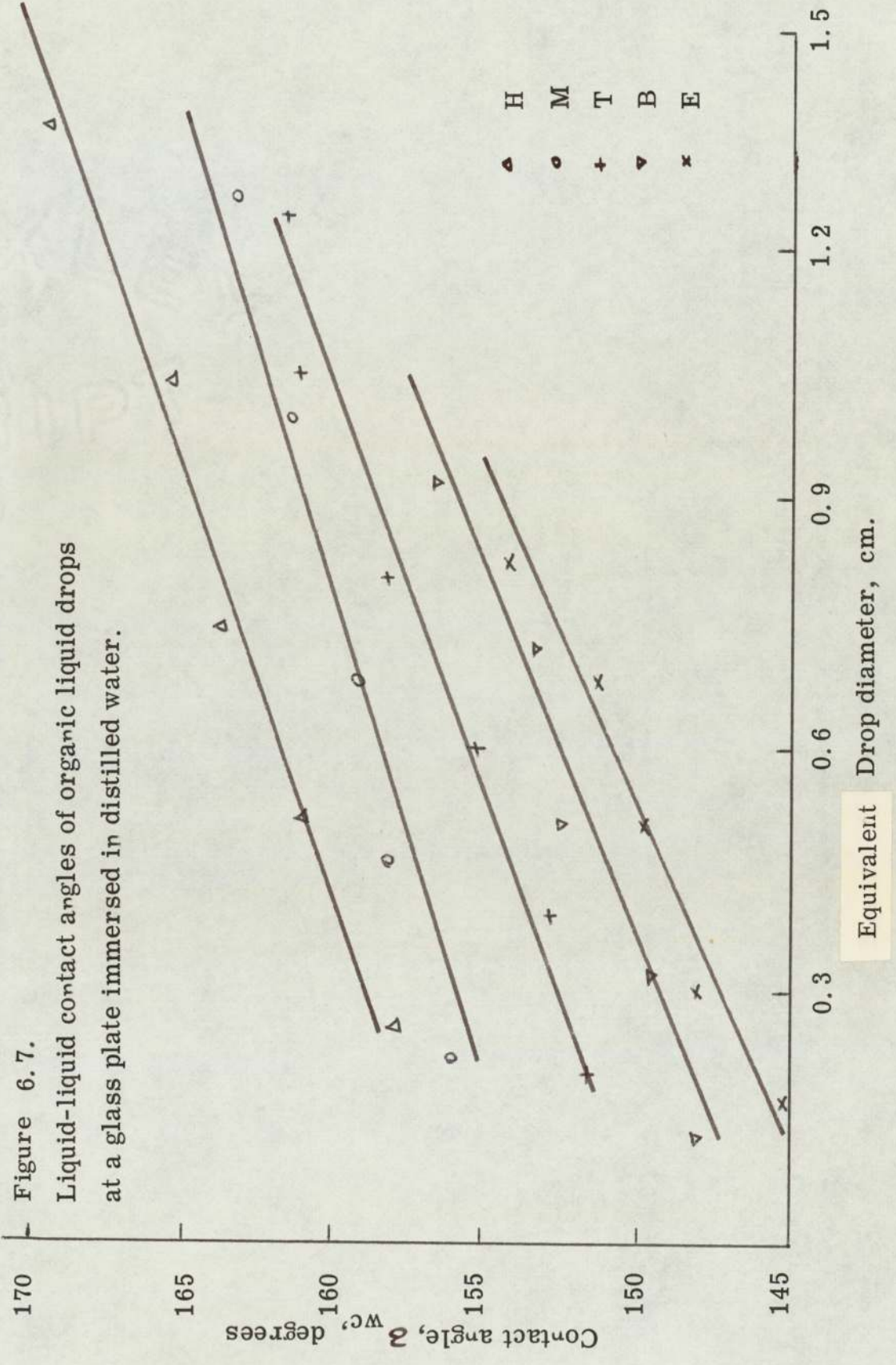
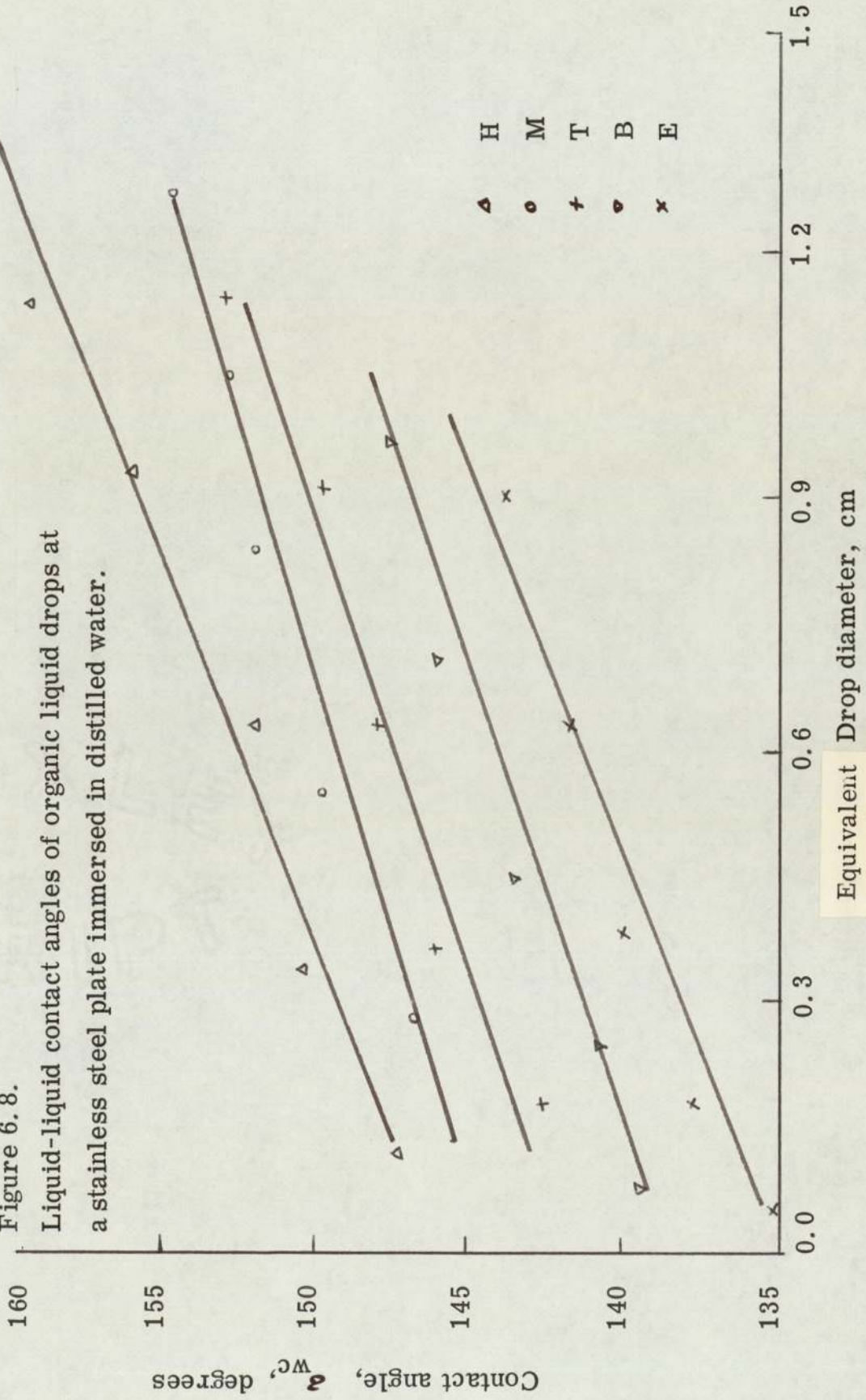


Figure 6. 8.

Liquid-liquid contact angles of organic liquid drops at a stainless steel plate immersed in distilled water.



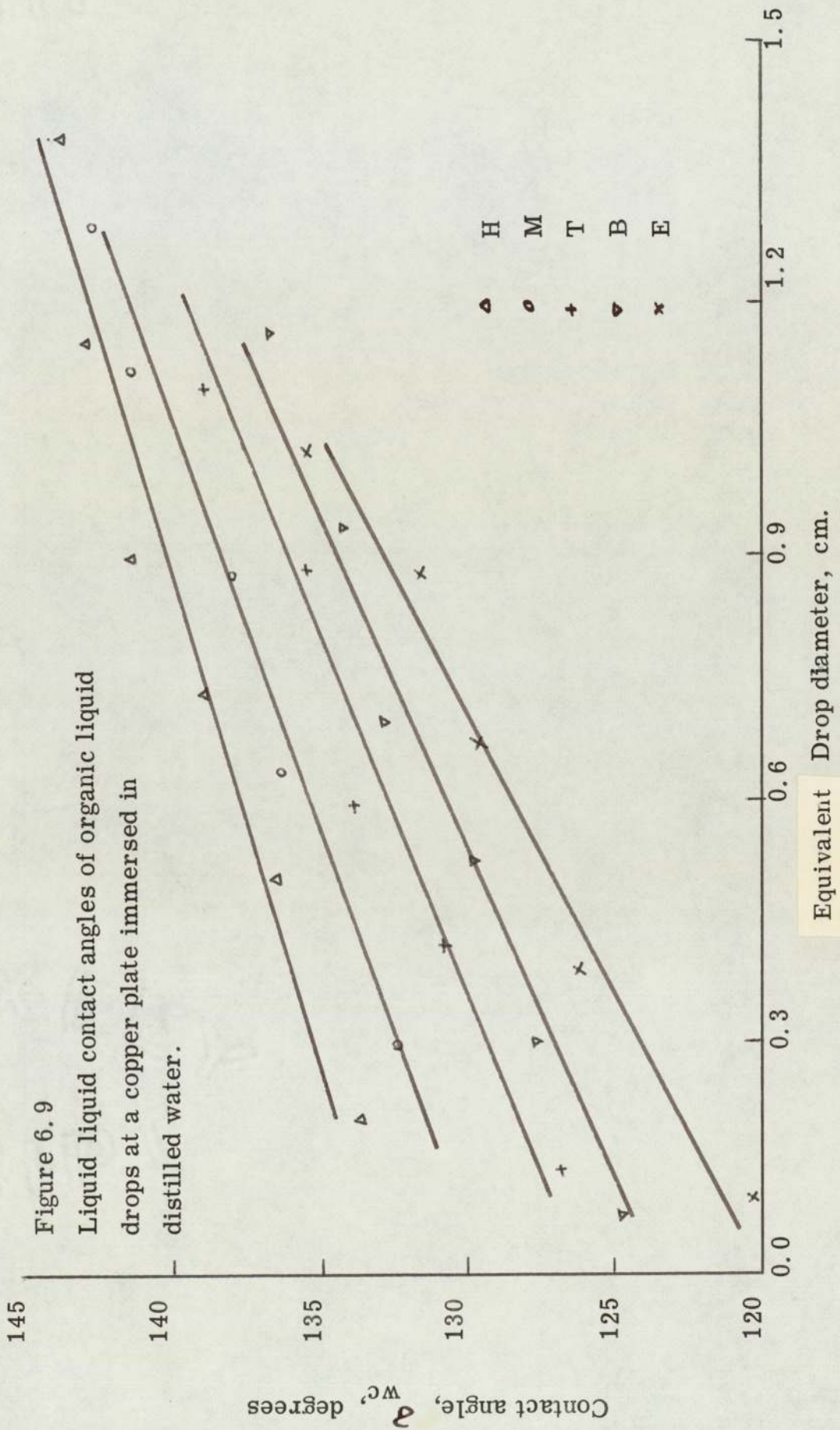
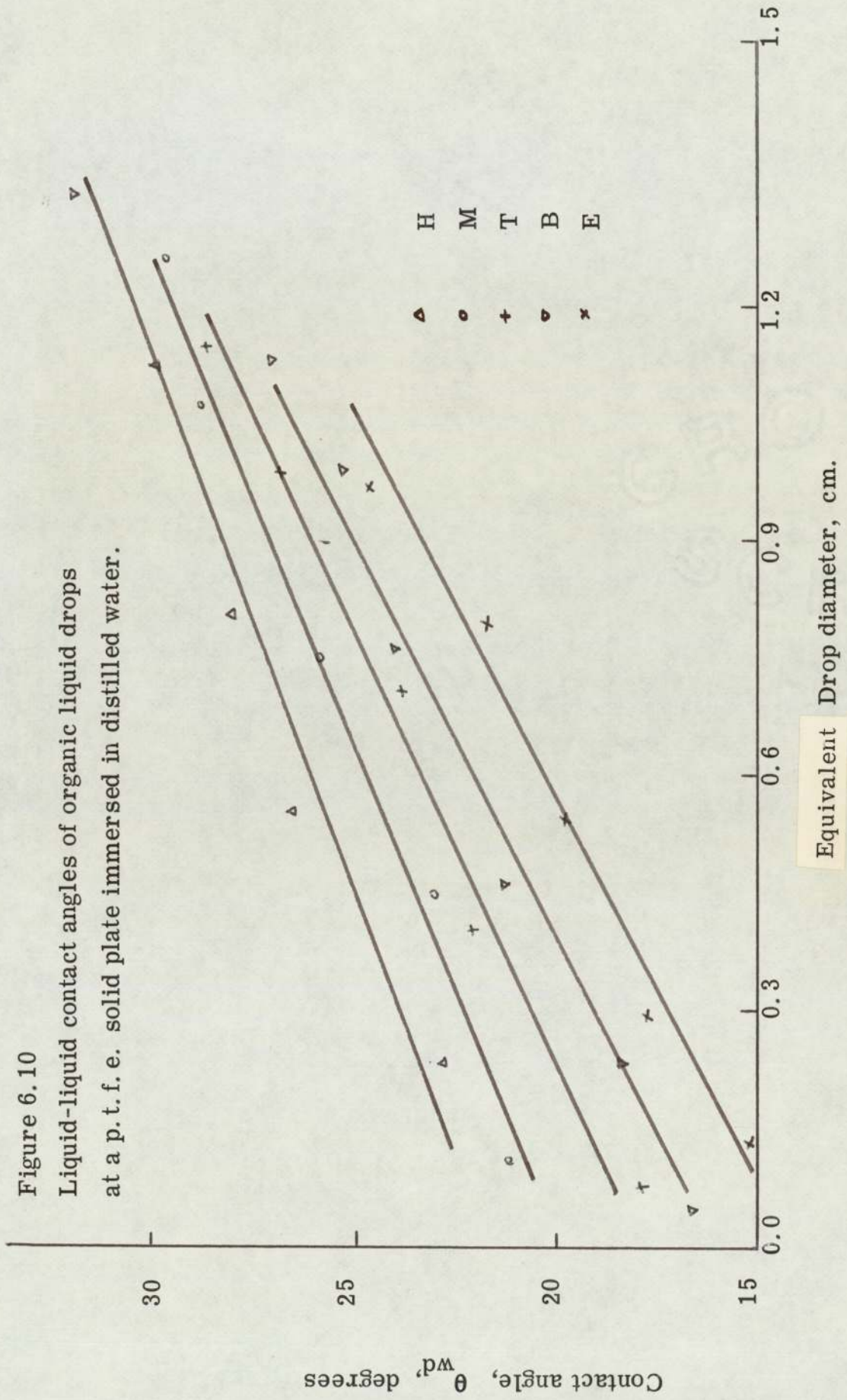


Figure 6. 10

Liquid-liquid contact angles of organic liquid drops  
at a p. t. f. e. solid plate immersed in distilled water.



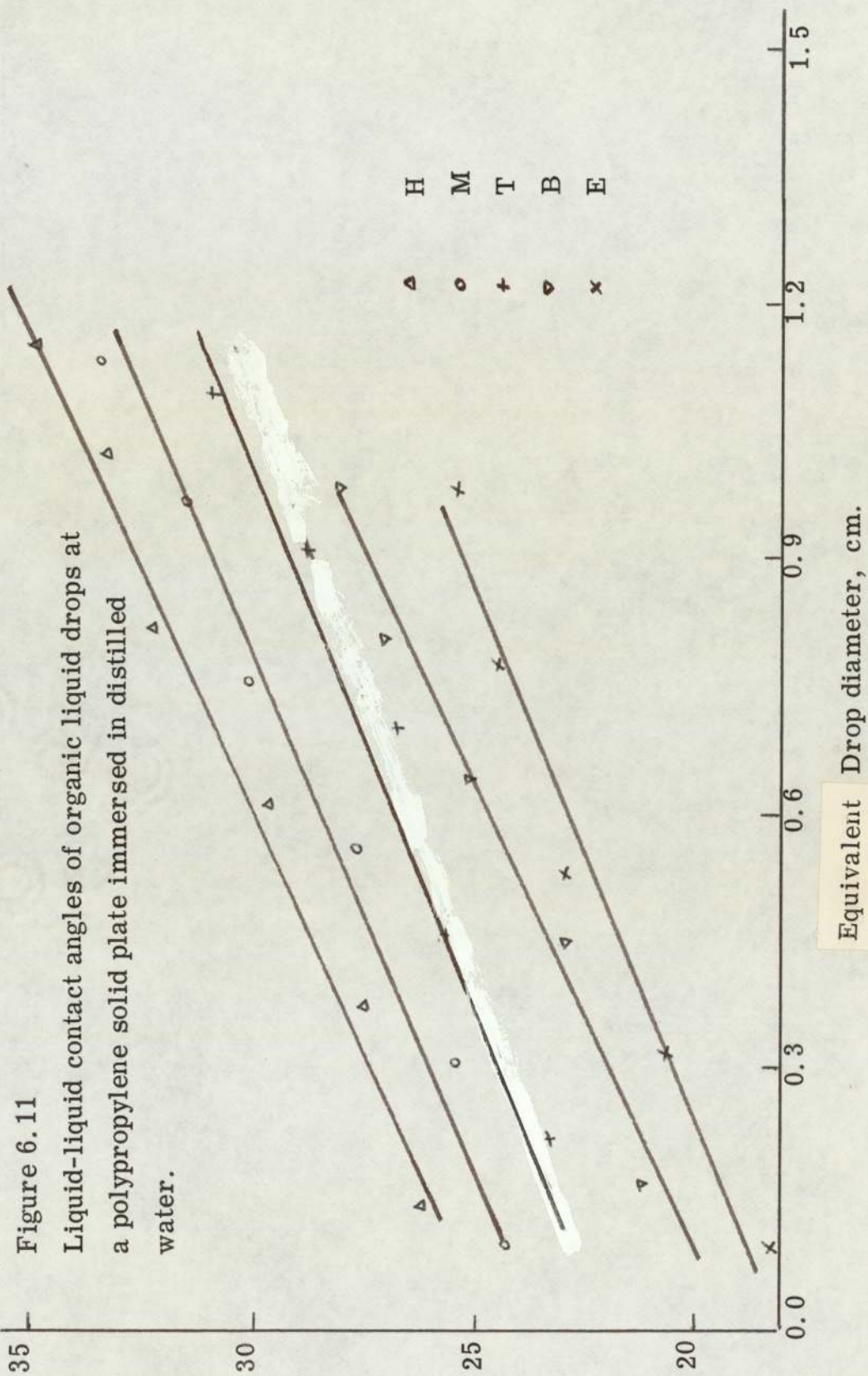


Figure 6.12.

Solid-liquid-liquid system defined by Equation 6. 1.

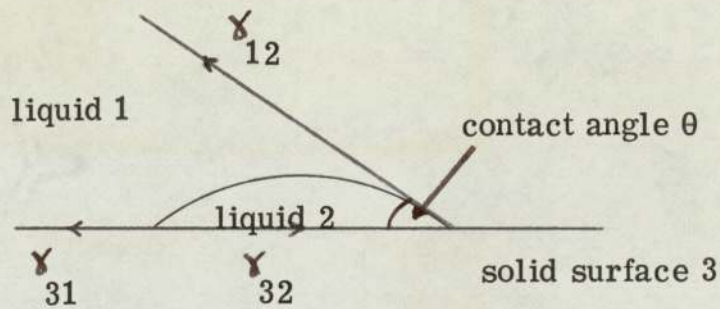
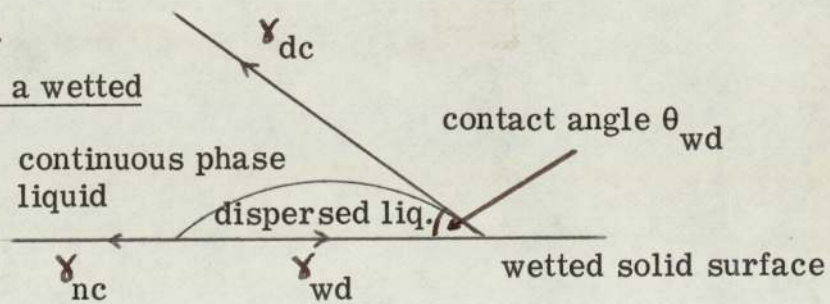


Figure 6.13.

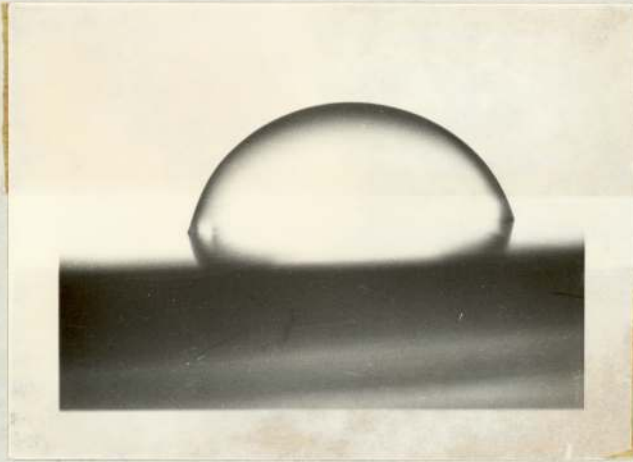
A droplet on a wetted surface



Liquid drop of contact angle  $\theta_{wd}$  at a solid surface wetted by the dispersed phase liquid, and immersed in a continuous phase liquid, subtends an angle less than  $90^\circ$

Figure 6.14

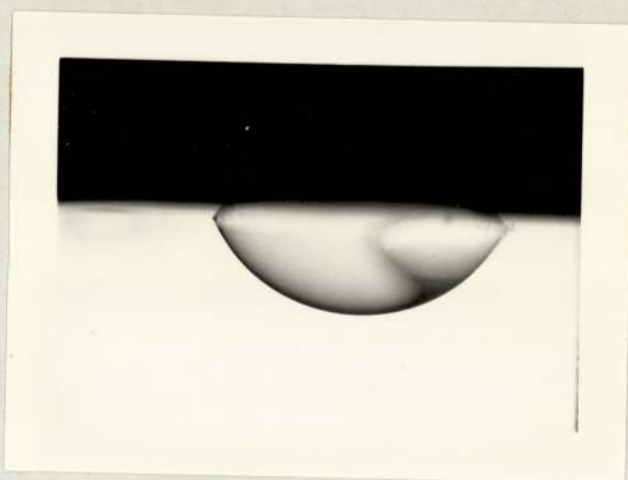
Behaviour of a liquid drop at a high surface energy material 'wetted' by the dispersed phase liquid.



Dispersed phase liquid	: distilled, deionised water;
Continuous phase liquid	: toluene;
Solid surface	: glass plate;
Drop dia.	: 3.03 mm.

Figure 6.15

Behaviour of a liquid drop at a low surface energy material 'wetted' by the dispersed phase liquid.



Dispersed phase liquid	: n-hexane;
Continuous phase liquid	: distilled, deionised water;
Solid surface	: p. t. f. e. plate;
Drop dia.	: 2.78 mm.

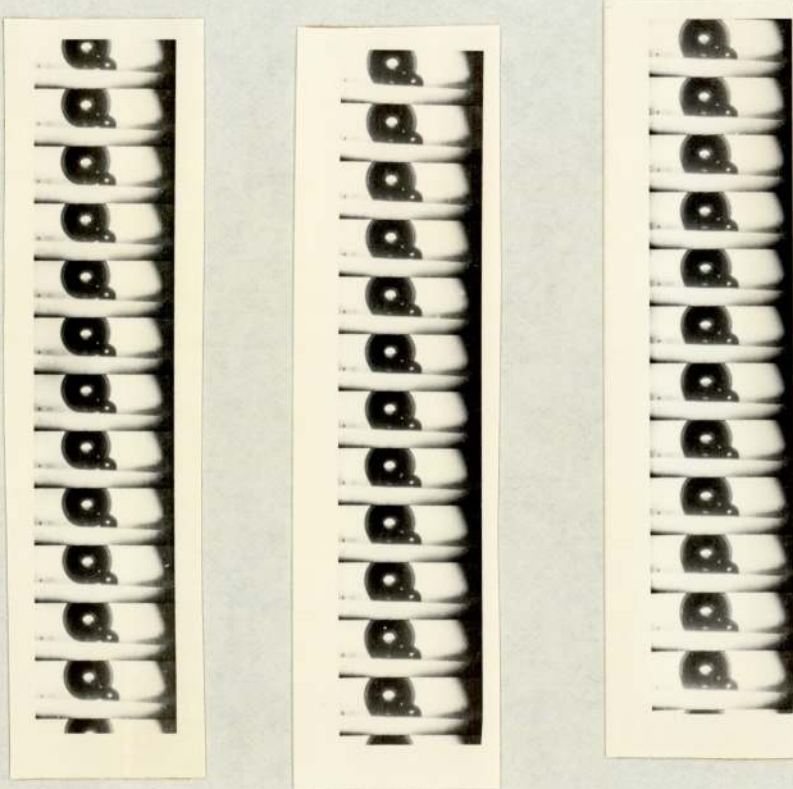
6.2. i. e.  $\gamma_{dc} \cos\theta_{wd}$  is always positive for a surface which is wetted by the dispersed phase liquid. This quantity was calculated from the experimental values of  $\gamma_{dc}$  and the contact angle. The numerical value of  $\gamma_{dc} \cos\theta_{wd}$  thus calculated is equal to  $\gamma_{wd} - \gamma_{nc}$  in Equation (6.2). For example, by reference to Table D.1, water drops in the size range  $0.546 \times 10^{-2}$  to  $0.910 \times 10^{-2}$  m in ethyl acetate gave  $\gamma_{dc} \cos\theta_{wd}$  values of  $7.882 \times 10^{-3}$  to  $7.680 \times 10^{-3}$   $\text{Nm}^{-1}$  respectively. However, when  $\theta_{wd}$  is zero the drop liquid completely spreads to form a thin film at the solid surface. Therefore, for complete wetting to occur, the interfacial tension between the dispersed phase liquid and the solid surface must be sufficient to remove the continuous phase from the surface allowing advancement of the liquid-liquid interface. As a matter of interest, for  $\theta_{wd} = 90^\circ$  it follows from Equation (6.2) that the interfacial tensions of the solid surface with each of the two liquids must be equal.

In practice after a drop arrived at a solid plate it underwent a short period of oscillation about both axes. It travelled a short distance of about 1 mm. along the plate until these oscillations became damped and the film of the continuous phase liquid trapped under the drop ruptured; this allowed it to rest there permanently. The instant, when the thin film of the continuous phase liquid ruptured, could not be ascertained from the still photographs. The phenomena was investigated further using the 'Hyspeed' camera and a typical photographic record is shown in Figure 6.16. The film was shot at 6,000 frames per second. Analysis of the photographs demonstrated a distinct difference in behaviour of a liquid drop at a wetted compared with a non-wetted surface (Figure 6.17). This difference in behaviour provides one fundamental meaning to the terms 'wetting' and 'non-wetting'.

At a liquid-liquid interface, the coalescence of a liquid drop usually occurs at some location other than where it is delivered; this has been attributed to the internal circulation of liquid within the drop and the elastic nature of the liquid-liquid interface upon which the drop bounces. The drop and the interface therefore mutually deform

Figure 6.16.

Solid-liquid-liquid contact angle phenomena  
at a wetted surface



Dispersed phase liquid	:	distilled, deionised water
Continuous phase liquid	:	toluene
Solid surface	:	glass plate
Drop size	:	4.17 mm.

(Figures 1.0 and 6.18). However, in solid-liquid coalescence, there can be no deformation in the solid surface (Figure 6.14).

Figure 6.16 is from a cine film of a liquid drop approaching a wetted surface immersed in an immiscible liquid. As in the liquid-liquid (Figure 6.18) coalescence, a thin film of continuous phase liquid was trapped, between the drop and the solid surface following the drop's arrival. Frames 1 to 12 show the drop resting at the interface prior to the rupture of the film.

The rest-time at a solid-liquid interface depends largely on the surface energy of the solid surface and the interfacial tensions of both the liquids to the solid surface. However, a shorter rest-time indicates

(a) the ease with which the continuous phase liquid is removed from the solid surface. This depends upon the relative magnitude of the attraction between the dispersed phase liquid and the solid surface compared with that of the continuous phase liquid and the same surface.

(b) the effect of a low liquid-liquid interfacial tension during the displacement of the continuous phase liquid from the solid surface and the flow of the dispersed phase liquid from the drop to the surface.

The behaviour of a drop impinging upon a solid-liquid interface, is immediately dependent upon the wetting or non-wetting nature of the surface (Figure 6.17), i. e. upon the surface characteristics.

At a liquid-liquid interface, the drop usually rests, in a stable state; the rest-time varies from a few seconds to a few minutes depending upon the system properties. During this rest-time, the thickness of the trapped film of liquid reaches its minimum value at which it ruptures and the contents of the drop liquid are deposited into its homophase. At a solid surface wetted by the dispersed phase,

Figure 6.17.

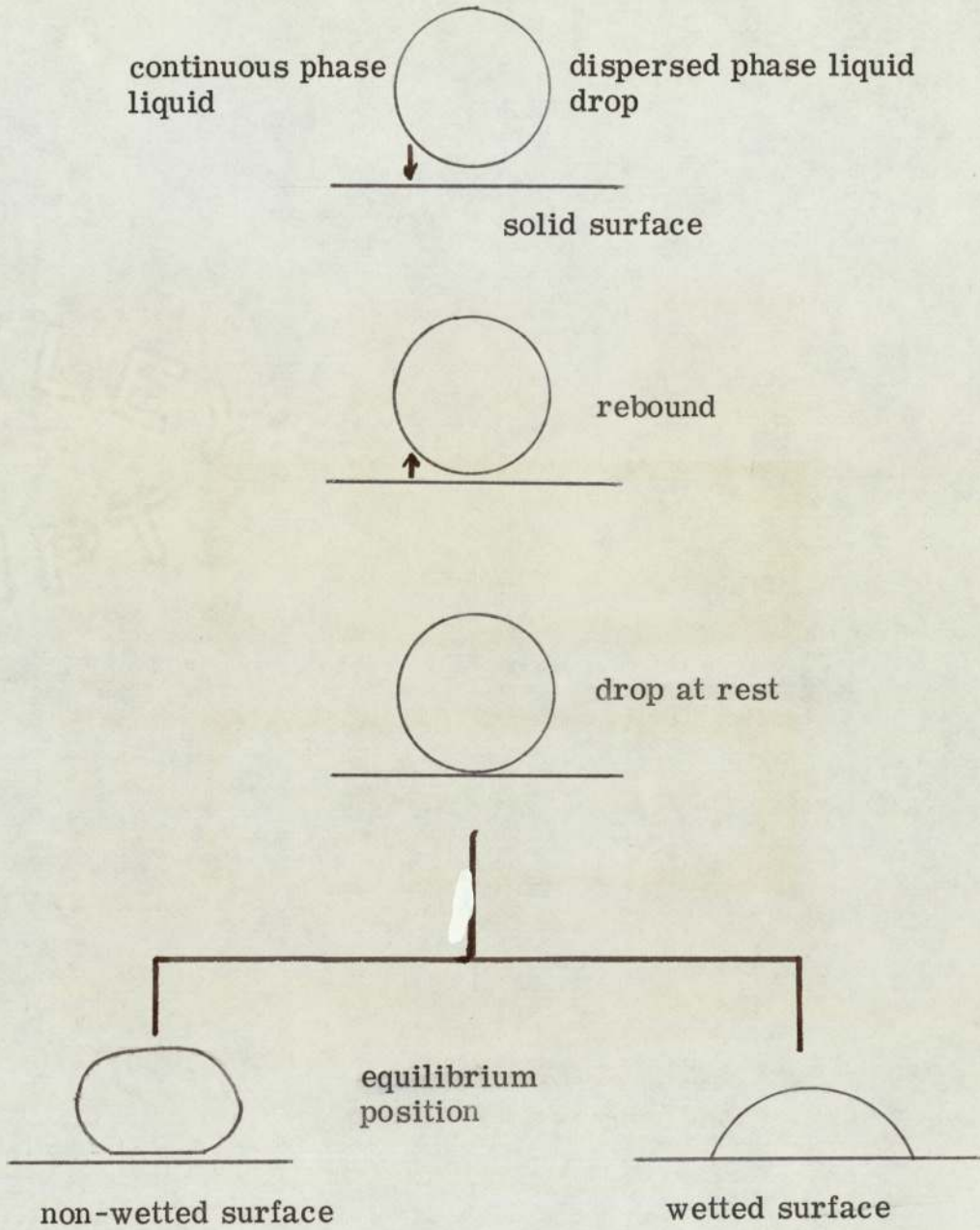
Behaviour of a liquid drop at a solid surface.

Figure 6.18

A liquid drop at a liquid-liquid interface

Dispersed phase liquid	:	distilled, deionised water;
Continuous phase liquid	:	toluene;
Drop dia.	:	2.15 mm.

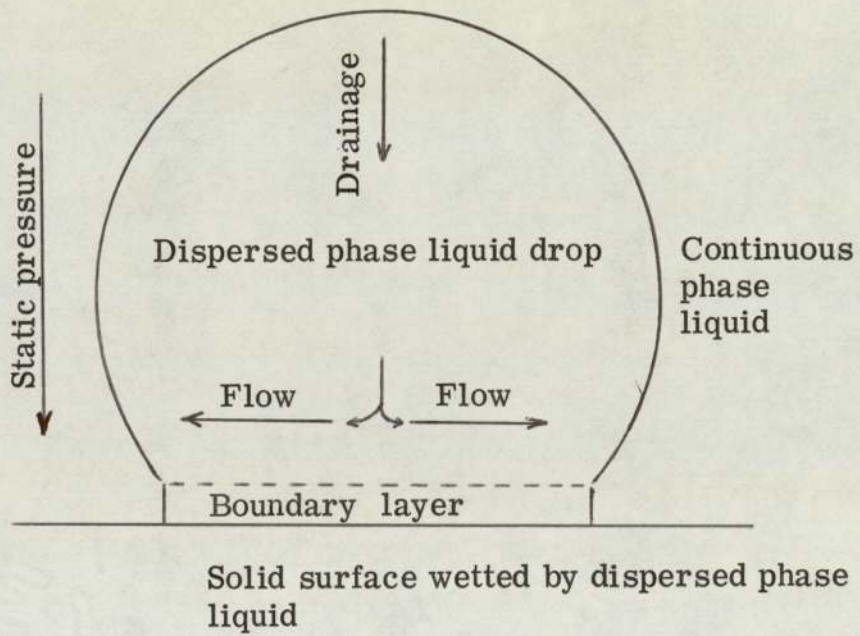
the magnitude of the rest-time was very small, normally less than a second. Conversely, at a surface which was not wetted, the rest-time was infinite, i. e. the film trapped under the drop did not rupture, therefore, no coalescence took place as explained in Section 6.1.1.b.

At a wetted surface, before the drop could deform the film of the continuous phase liquid, which was trapped between the drop and the solid surface, had to rupture. It eventually ruptured under the forces due to gravity on the drop and the solid-liquid interfacial tension, and the contents of the drop began to be deposited at the solid surface. The drop liquid in the vicinity of the ruptured film came into an intimate contact with the solid surface (Figure 6.19), thus setting up a boundary layer of the drop liquid to the solid surface. The drainage of the liquid occurred from the drop to the boundary layer at the solid surface. To accommodate this, the direction of drainage of the liquid changed so that it flowed outwards parallel to the surface and hence displaced the continuous phase liquid. Loss of pressure head would occur at the bend. The liquid subsequently flowed over the existing boundary layer and onto the solid surface thus increasing the area of contact of the dispersed phase on the solid.

Flow of the drop liquid is complicated since it must overcome at least two opposing forces, namely, the frictional force with the boundary layer and secondly the pressure force exerted by the continuous phase liquid static head at the surface. The boundary layer, which is in contact with the solid surface is stationary and tends to retard the flow of the liquid flowing above it. Before the drop liquid can come into contact with the solid surface, not previously covered by the boundary layer liquid, it must remove the other liquid from the surface. With a horizontal surface the drainage of the drop liquid occurs under gravity, proportional to the mass of the drop. Therefore, the drainage and the flow pressures would be

Figure 6.19.

Hydrodynamics of a liquid drop  
at a wetted surface.



greater with the larger drops, the diameter of the base of the drop will also be greater giving a larger boundary layer.

At a liquid-liquid interface, the diameter of the draining column decreases during drainage (Section 1. 2) of the liquid whereas at a solid-liquid interface, the diameter of the base of the drop increased (Figure 6.16). This arose because the drop base would expand as long as the flow pressure of the drop liquid could overcome the pressure exerted by the other liquid at the solid surface and the drag force of the boundary layer.

The drainage from the liquid column at a liquid-liquid interface ceases with the formation of a secondary droplet (Figure 1. 8.). At a solid-liquid interface, it ceased as the advancement of liquid-liquid interface stopped when the forces in favour of drainage and flow were balanced by drag forces and the resistance of the continuous phase. This resulted in a sharp and constant contact angle (Figure 6.14 or 6.15) without any hysteresis effect at a smooth and clean surface. Because of this mechanism, contact angle measurements for drops of a specific size would be expected to differ depending upon whether they were formed singly or by accumulation. This was confirmed in separate experiments (Table 7.0 ). Cumulative drop contact angles are higher than those for single drops because once a drop is adhering to a surface there is a resistance to expansion of the solid-liquid contact area and addition of liquid results in increase in free area.

There was a certain force of attraction or repulsion between the liquid of the drop, in the presence of an immiscible liquid, and the solid surface. This force varied with the system under investigation. To demonstrate the force of attraction between the molecules of liquid and that of the solid plate, a drop was pushed sideways to disengage it from the surface. After it was displaced,

Table 7.0

Contact angle of single drop vs. cumulative drop

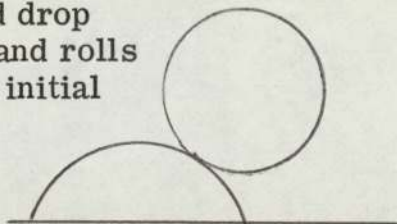
Drop diameter

cm.	Single drop degrees	Cumulative drop degrees.
Dispersed phase: deionised, distilled water; Continuous phase: toluene; Solid plate: glass.		
0.129	18.00	18.00
0.213	18.25	18.50
0.325	18.50	19.00
0.408	19.00	19.50
0.521	19.50	20.00
0.632	19.50	21.00
0.729	20.00	21.50
0.843	20.50	22.00
1.025	21.00	23.00
Dispersed phase: toluene; Continuous phase: deionised distilled water; Solid surface: glass		
0.072	151.00	151.00
0.225	153.00	153.50
0.351	154.00	155.00
0.427	154.50	155.50
0.536	155.00	160.00
0.618	156.00	161.00
0.749	157.50	161.50
0.860	159.00	162.00
1.024	160.00	163.00

Figure 6. 20.

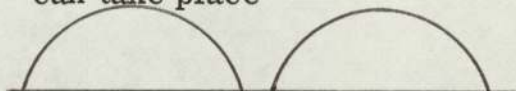
An interdrop coalescence at a wetted plate.

A second drop arrives and rolls over the initial drop



(a)

The second drop rests away from the initial drop, therefore, no interdrop coalescence can take place

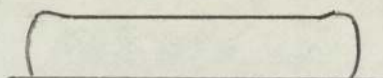


(b)

Figure 6. 21.

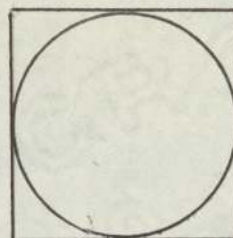
A stagewise coalescence at a wetted plate.

(a)



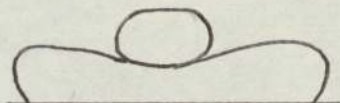
By carefully placing one drop on another, a film of dispersed phase liquid builds up at the surface

(b)



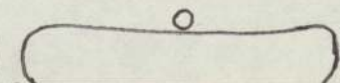
Projected view of the film at the surface

(c)



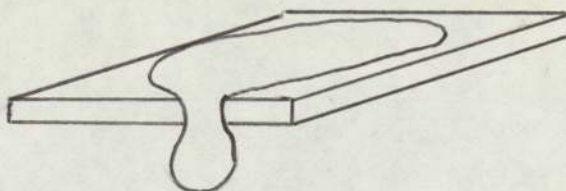
Subsequently arriving drops coalesce with the liquid film at the surface

(d)



A daughter droplet is left behind to coalesce in a stagewise manner

Figure 6. 22.

Coalescence efficiency with a wetted plate.

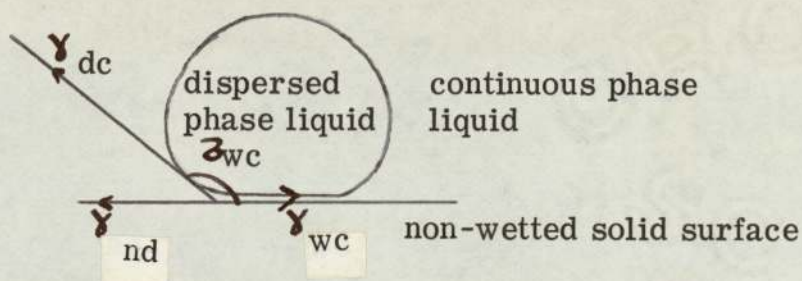
Part of the film may flow down the surface leaving a larger drop at the surface to grow.

a few tiny patches of drop liquid remained adhering at the surface from which the drop was displaced.

When single drops were made to impinge on a wetted plate, the later drops hit the initial drop on the surface, and either coalesced with it or rolled over its curved surface to fall onto the plate and rest a few milli-meters away from the initial drop (Figure 6.20. b.). However, by carefully placing the drops an inter-drop or drop-interface coalescence could be achieved with the initial drop at the wetted plate. Hence a thick film of dispersed phase liquid could be maintained at a clean and smooth surface (Figure 6.21a). The plate was square but with an aqueous drop the projected shape of the thick film on it was always circular (Figure 6.21. b). The thick film of liquid appeared as a single drop with an almost horizontal top but curved along the sides giving a sharp contact angle. Once this film was present, providing it was greater than a certain critical thickness i. e. sufficient to resist complete penetration, subsequent drops coalesced in stages (Figures 6.21. c, 6.21. d. ) leaving behind a secondary droplet at this film as in normal drop-interface coalescence processes.

Only single drops arrived at the liquid film, but once the film reached a certain thickness it flowed down the plate, breaking on reaching the edge of the plate (Figure 6.22). The broken part of the film dripped down the plate as a single larger drop; the ratio of this drop size to the inlet drop size was three to five which is some measure of coalescence efficiency. Slight extraneous frequency vibrations at the plate could lead to a total removal of the entire film from the smooth surface of the plate. In this case, the film flowed away breaking into three almost equal parts. The size ratio was hence even greater.

Figure 6.23.

A droplet on a non-wetted surface

Liquid drop of contact angle  $\theta_{wc}$  at a solid surface non-wetted by the dispersed phase liquid, and immersed in a continuous phase liquid, subtends an angle greater than  $90^\circ$ .

An attempt was made to spread a thin film (i. e.  $\leq 1 \mu\text{m}$ ) of dispersed phase liquid on a wetted solid plate so that the coalescence behaviour of a liquid drop could be observed when such a thin film of liquid was already present on a surface. However, a thin film could not be maintained at the surface but shrank instantly to random patches. When this surface was lowered into the continuous liquid phase, the patches shrank to form tiny droplets; these were able to coalesce with a subsequently arriving drop at the surface exhibiting a hysteresis. The contact angle was, therefore, advancing after coalescence took place with these tiny droplets.

#### 6.1.1.b. Solid Surface Wetted by the Continuous Phase Liquid

Equation 6.1 may be rewritten for the case of a solid surface 'non-wetted' by the dispersed phase liquid (Figure 6.23),

$$\gamma_{nd} - \gamma_{wc} = \gamma_{dc} \cos \theta_{wc} \quad (6.3)$$

The experimental observations showed that the contact angle,  $\theta_{wc}$ , of a liquid drop at a solid surface not wetted by the dispersed phase liquid, e. g. organic liquid drop at a glass surface (Figure 6.25) or a water drop at a p. t. f. e. surface (Figure 6.24) was always greater than  $90^\circ$ . Droplets smaller than 1.5 mm. diameter were almost spherical. The angle for larger drops lies in the second quadrant where  $\cos \theta_{wc}$  is always negative. This makes the right hand side of equation 6.3 negative, suggesting that  $\gamma_{wc}$  is greater than  $\gamma_{nd}$ . Since the force between the continuous phase liquid in the film trapped under the drop and the surface wetted by it is greater, the liquid of the drop fails to rupture the film. The dispersed phase liquid does not come into contact with the solid surface. The liquid drop actually rolls over the immiscible liquid film on the surface. For a condition of complete non-wetting, when  $\theta_{wc}$  is equal to  $180^\circ$ , the interfacial tension between the liquid of the continuous phase and the solid surface wetted by it,  $\gamma_{wc}$ , and

Figure 6. 24.

Drop behaviour at a non-wetted surface

Continuous phase liquid : toluene;  
Dispersed phase liquid : deionised, distilled water;  
Solid surface : P. t. f. e. plate;  
Drop dia. : 2.351 mm.

Figure 6.25

Drop behaviour at a non-wetted surface

Continuous phase liquid	: distilled, deionised water;
Dispersed phase liquid	: toluene;
Solid surface	: glass plate;
Drop dia.	: 1.013 cm.

the liquid-liquid interfacial tension,  $\gamma_{dc}$ , add up together to the interfacial tension between the dispersed phase liquid and the solid surface non-wetted by it. The interfacial tensions between the non-wetted surface and the liquids of the continuous and the dispersed phases are equal when  $\theta_{wc}$  is equal to  $90^\circ$ .

$$\gamma_{nd} = \gamma_{wc}$$

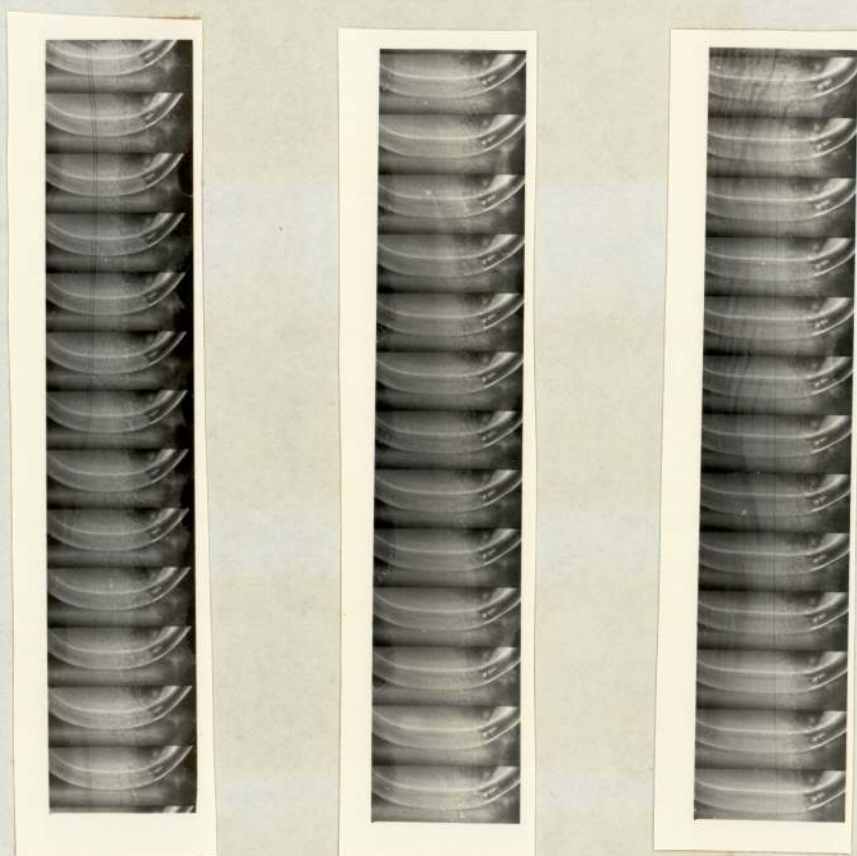
The rolling action of drops at horizontal flat plates is attributable to a force of repulsion between the molecules of the liquid of the drop and those of the solid surface. This force varies from surface to surface but can initially be assessed from the velocity with which the drops were observed to travel. The drops appeared to travel faster at a p. t. f. e. plate than at a polypropylene plate, without leaving any traces of dispersed phase liquid at the surface.

The phenomena of drop approach to a non-wetted surface was investigated further using 'Hyspeed' camera. A typical photographic record, Figure 6.26, shows a liquid drop approaching a non-wetted solid surface. When the drop arrived at the surface, its boundary deformed solely due to the gravitational action of the mass of the drop. The film of the continuous phase liquid trapped under the drops thinned out with the approach of the drop until it reached  $< 1 \mu\text{m}$  thickness but did not rupture. The drop rested on this thin film. The non-rupturing action of this film on non-wetted surfaces can be attributed to molecular adsorption of the organic liquids on such surfaces. The contact angle varied as the shape of the drop resting at the non-wetted surface changed (Figure 6.25).

The variations in the contact angle of liquid drops was further investigated by matching the densities of the drop and continuous phase liquids. As explained in Section 5.1, the density of the organic phase was conveniently varied by gradual additions of carbon tetrachloride (Appendix B).

Figure 6.26

Solid-liquid-liquid contact angle  
phenomena at a non-wetted surface.



Dispersed phase liquid  
 Continuous phase liquid  
 Solid surface  
 Drop dia.

distilled, deionised water;  
 toluene;  
 p. t. f. e.  
 : 4.315 mm.

Figure 6.27.

Effect of density difference on the contact angle  
of a liquid drop on a non-wetted surface.



Drop dia.  
 =2.35 mm.



Drop dia.  
 =5.21 mm.



Drop dia.  
 =10.35 mm.

Drops of 2.0 mm. to 10.0 mm. ;

below the critical  $\Delta\rho$ , therefore, spherical.

Dispersed phase liquid : distilled, deionised water; continuous  
 phase: toluene; solid surface: p. t. f. e.

On a wetted surface, the density difference made no difference to the contact angle. However as the density difference decreased the rest-time of the drop on the solid surface increased since the velocity of flow of the continuous phase in the film decreased. This followed from the reduced approach velocity of the drop to the surface due to a decrease in the gravitational force of the drop in a medium of close density.

On a non-wetted surface as the densities of the two liquid phases became closer, the drop remained spherical irrespective of its size (Figure 6.27), and the line of the tangent drawn to the liquid circle at the triple-point coincided with the plane of the non-wetted surface i. e. a contact angle of  $180^{\circ}$ . (Appendix I.)

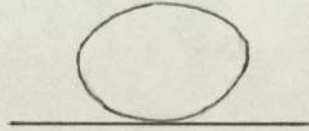
To supplement the above investigations, drop behaviour with respect to its non-wetting characteristics was also studied by first delivering the liquid drop at the solid surface and then gradually increasing the density of the continuous phase liquid. As the density was increased, the drop shape gradually lifted away from the solid surface to give a sphere.

Thus, contrary to some reports, it is possible to have a surface completely non-wetted by the dispersed phase, since it is relatively easy to match the densities of the two phases. When the density of the organic liquid was varied by 0.05 % above or below that of the other liquid, the drop raised or lowered itself gradually from the solid surface leaving no trace of the dispersed phase liquid at the surface. This observation, and others, confirmed the presence of a film of continuous phase liquid under the drop at a non-wetted surface.

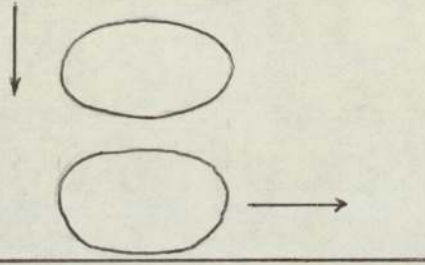
These observations were made with drops upto 1 cm. diameter, i. e. the maximum order of size in coalescers or packed columns, but there is no reason, in theory, why there should be any limit on the diameter.

Figure 6. 28.

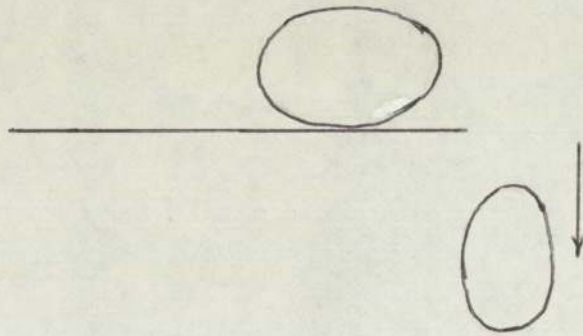
Sequence preventing interdrop coalescence at a  
non-wetted surface.



An initial drop at the surface



A second drop hits the initial drop



Both the drops leave the surface  
as individual drops.

The result leads to the following relationship of proportionality correlating the value of the contact angle at a non-wetted surface to the density difference between the two liquids.

$$\text{Contact angle} = 180 \cdot e^{\Delta\rho}$$

As the value of  $\Delta\rho$  tends to zero,  $e$  tends one, thus giving a constant value of  $180^\circ$  for all drops irrespective of their size.

A film of dispersed phase liquid could not be spread at a non-wetted surface since the dispersed phase did not adhere to this surface. Unlike at a wetted plate, a thick film of liquid could not be maintained at a non-wetted surface because when any subsequent drop arrived at the surface 'touched the initial drop, both the drops rolled over the surface and left the plate as individual drops (Figure 6.28).

Unlike the projected circular shape of the liquid film at a high energy wetted solid plate, the projected shape at a wetted low energy solid plate was in line with the edges of the rectangular plate.

From the experimentally determined contact angles, it was concluded that high surface energy solid plates when placed in a medium of organic liquid were wetted by aqueous phase drops but were non-wetted by the organic liquids when placed in the aqueous phase. The order, in which the high energy solid plates can thus be ranked depending on their degree of wettability by aqueous phase or non-wettability by the organic phase, is: glass, stainless steel, copper. Similarly, the low energy solid plates placed in aqueous phase were wetted by the organic liquids and were non-wetted by the aqueous phase. The low energy solid plates, according to their degree of wettability by organic liquids or non-wettability by aqueous phase were: p. t. f. e., polypropylene.

### Factors affecting contact angle

The solid surface upon which a liquid drop exhibits a contact angle of less than  $90^{\circ}$  has been regarded as wetted by the dispersed phase liquid. In this respect, any variation in the contact angle value means a change of the wetting conditions in the same system, which was not expected. The contact angle increased as the size of the drop of the same liquid at the same solid surface was increased. Since the contact angle has been regarded as a thermodynamic property, the value of which should remain constant at a constant temperature and pressure, a variation in the contact angle would therefore be expected to result from a variation in either temperature or pressure.

### Pressure of continuous phase liquid

Figure 6. 29 shows the effect of the pressure exerted by a static head of the continuous phase liquid upon liquid drops of different sizes.

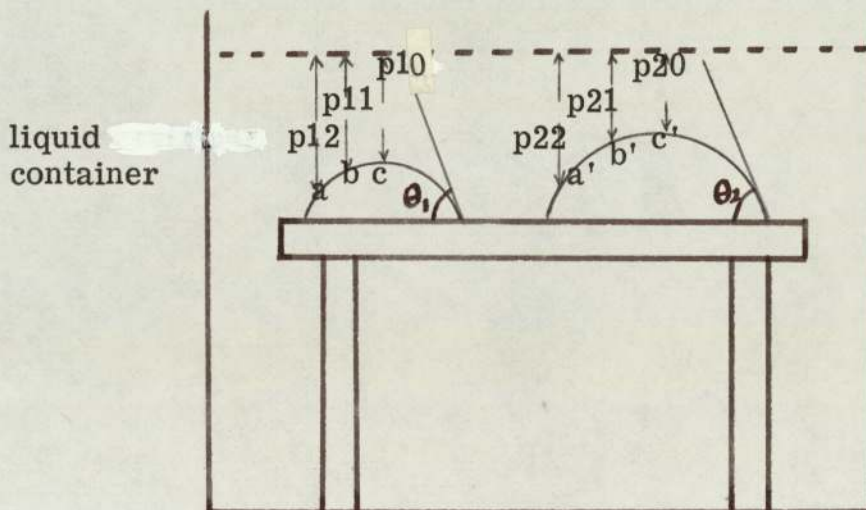
Two different effects therefore arose in determining contact angles with the cell always filled to a constant level:

- (i). The effect of differing heads of continuous phase associated with different drop sizes.
- (ii). The effect inherent in different drop sizes.

The results given in Figures 6. 2 to 6. 11 do not differentiate between different heads. This would have been impracticable due to the different densities of the liquids used and the differing displacements of drops. However, since the maximum density difference between dispersed and continuous phase was only  $0.325 \times 10^3 \text{ Kg. m}^{-3}$  and the maximum head difference, in the worst case of a non-wetted surface, was only 9 mm., this was considered justified.

Figure 6.29.

Effect of variation of pressure head along the curved boundary of a liquid drop at a wetted solid surface.



$p_{10}$ ,  $p_{11}$ ,  $p_{12}$  are the static head pressures at various points  $a$ ,  $b$ ,  $c$  along the boundary of the drop. The net pressure differential ( $p_{12} - p_{10}$ ) or ( $p_{22} - p_{20}$ ) also affects the contact angle  $\theta_2$  or  $\theta_1$ .

(For example, a typical difference in contact angle between a 10 mm. and 5 mm. drop, involving a head difference of approximately 5 mm., was only  $3^{\circ}$  of which most was attributable to the drop size itself.).

Furthermore, the main objective was not to determine absolute contact angles but to obtain an indication of the gradation of wetting properties between surfaces.

For future reference, the variation of contact angle with drop size can be correlated, neglecting head effects, by

$$\text{Contact angle} \propto \text{drop size}^f$$

The values of the exponential factor 'f' are given in Appendix F.

However, in some practical situations, e. g. in tall extraction columns, pressure head may be significant.

#### Radius of curvature of the drop

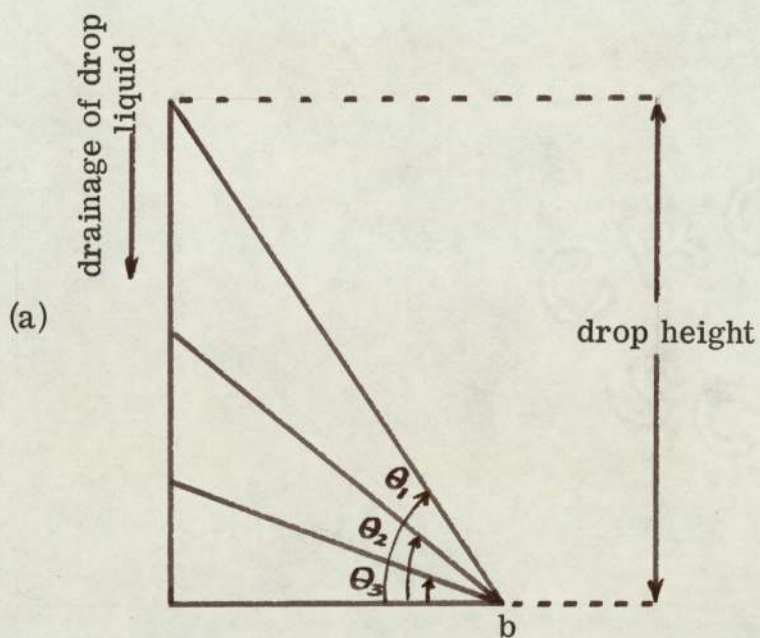
The radius of curvature of the surface of a drop varies with its size; therefore, the tangents at the corresponding points at the curvature act in different directions. The forces of varying magnitude, resulting from the action of tangents in different directions, act along the triple point boundary which itself varies with the drop size. This is the predominant effect causing a change in contact angle with the drop size.

#### Loss of pressure between drainage and flow

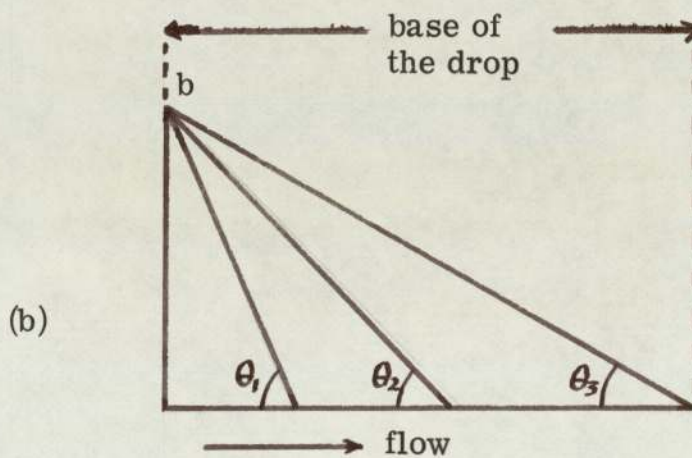
The analysis of forces acting on a drop, the liquid of which wets the solid surface, during its drainage and subsequent flow (Figure 6.19) are complex. After rupture of the film of the continuous phase, the drop liquid comes into contact with the solid surface and the subsequent flow of the drop liquid is retarded

Figure 6.30.

Effect of drainage of drop liquid on the contact angle.



Effect of flow of the drop liquid on the contact angle.



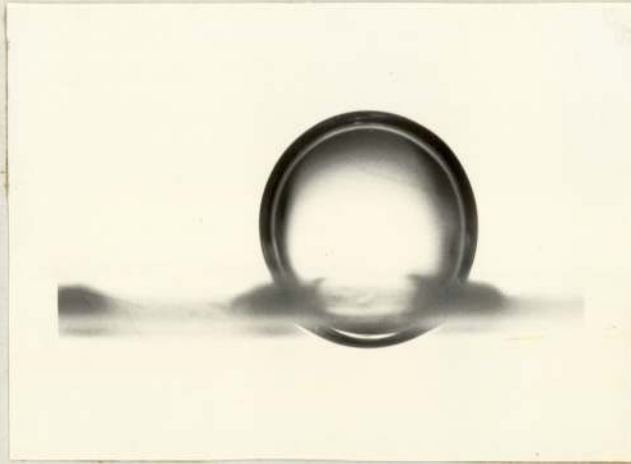
due to the presence of the boundary layer. This loss in the pressure of flow is in addition to that suffered earlier when the draining liquid of the drop changes its direction to flow parallel to the solid surface. For the flow of the drop liquid to continue, the pressure force along the triple-point boundary has to be overcome by the pressure of the flow of the drop liquid along the surface. The flow of the drop liquid at the solid surface ceases when the flow pressure equals the pressure of the continuous phase liquid at the solid surface.

#### Drainage and flow of drop liquid

Figure 6.30a shows the effect of drainage of liquid from the drop on the contact angle. The height of the drop decreases as drainage proceeds. This results in a decrease in the contact angle assuming the diameter of the base of the drop is constant (i. e. point 'b' is fixed), which is a hypothetical situation. Similarly, Figure 6.30b shows the effect on the contact angle of the drop liquid on the solid surface; provided the height remains constant, a prolonged flow results in a narrower angle. This again is a hypothetical situation.

With a larger drop, the initial height of the drop is higher and there is a larger mass of the liquid in the drop to drain. The dimensions of the boundary layer set up immediately after rupture of the film are greater and subsequently the flow is higher. The liquid has to overcome the increased loss in the pressure at the point of change in the direction from drainage to flow and the drag force from the boundary layer. The fluctuating conditions within the drop boundary must also overcome the induced fluctuations outside and along the boundary.

Figure 6.31.

A liquid drop at a non-wetted packing

(a)

Dispersed phase liquid : deionised, distilled water;  
 Continuous phase liquid : methylcyclohexane;  
 Drop dia. : 1.173 mm.;  
 Eq. aperture dia. : 1.124 mm.;  
 Solid material : [redacted]



(b)

Dispersed phase liquid : deionised, distilled water;  
 Continuous phase liquid : toluene;  
 Drop dia : 4.317 mm.;  
 Equivalent aperture dia : 2.251 mm.;  
 Solid material : polypropylene [redacted]

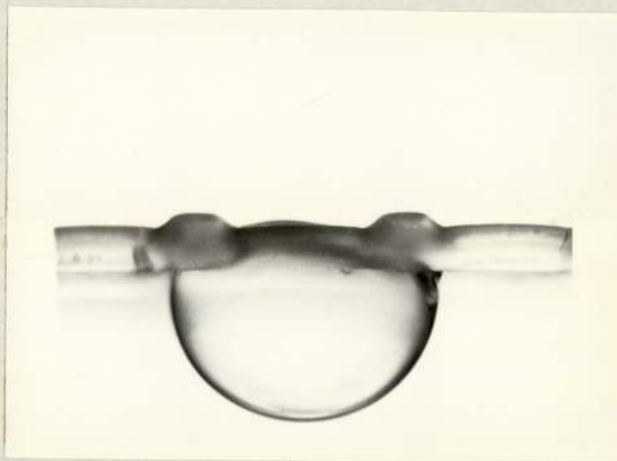
From the above discussions, the height and the base of the drop are inversely related until the drop attains a stable position. A constant value of contact angle irrespective of the size of the drop, can only occur if the ratio of the draining height to the length of flow remains constant. The practical situation involves a combination of Figures 6.30. a and 6. 30. b.

#### Effect of liquid-liquid interfacial tension

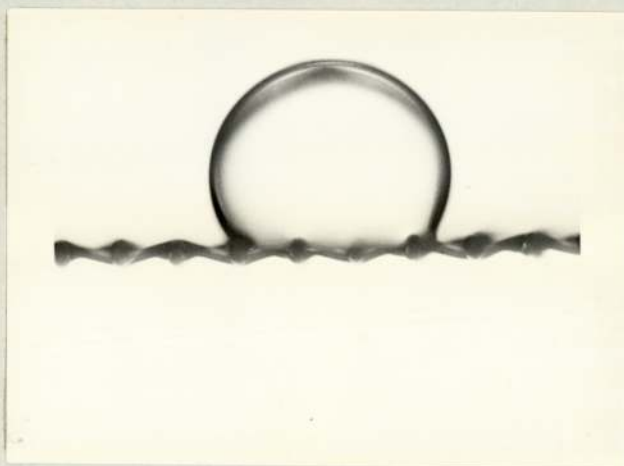
The values of the contact angles at the same solid plate increased with the liquid-liquid interfacial tension as shown in Figure 6.31. The average gradient is 0.202 for the systems where the organic liquids were dispersed. With the low surface energy solid plates, the gradient is lower than the average. The average gradient for the aqueous drops is 0.205. The effect of the liquid-liquid interfacial tension on the contact angles at glass and p. t. f. e. surfaces, at two extremes of the contact angle values for the solid plates investigated, is below this average and at polypropylene, copper and stainless steel plates, above the average.(Appendix E.)

The effect of interfacial tension arises since, after the rupture of the continuous phase liquid film under the drop at a solid surface wetted by it, dispersed phase from the drop flows over the surface. The liquid-liquid interface is thus moved away when the continuous phase liquid is removed from the surface by the flowing liquid of the drop. However, the average value of the gradients show that the overall effect of interfacial tension on the contact angle was not so pronounced as of the other factors discussed earlier, in particular the drop size.

Figure 6. 32.

A liquid drop at a wetted packing

- (a)
- |                          |                               |
|--------------------------|-------------------------------|
| Dispersed phase liquid   | : toluene;                    |
| Continuous phase liquid  | : deionised, distilled water; |
| Drop dia.                | : 3.411 mm. ;                 |
| Equivalent aperture dia. | : 3.380 mm. ;                 |
| Solid material           | : polypropylene packing.      |



- (b)
- |                          |                               |
|--------------------------|-------------------------------|
| Dispersed phase liquid   | : deionised, distilled water; |
| Continuous phase liquid  | : toluene;                    |
| Drop dia.                | : 3.973 mm. ;                 |
| Equivalent aperture dia. | : 1.693 mm. ;                 |
| Solid material           | : stainless steel packing.    |

### 6.1.2. Behaviour of a liquid drop at a packing

Irrespective of the wettability of the void, the behaviour of single drops was characterised by whether or not they passed through a void. Generally there is a range of drop size that may pass through a given void. Drops larger than this size reside at the void. Therefore, the smallest drop in the latter range is close in size to the largest drop in the former. And between these two lie the size of the drop which will not pass freely through nor will reside indefinitely at the void. After a short residence time, any drop in this range deforms and squeezes through the void. The size of such a drop was designated the 'maximum drop diameter'.

The ratio for the passage of a maximum diameter drop to the equivalent aperture of a rectangular packing, or the diameter of the void of a circular nozzle, was determined experimentally. Values of  $D_d/d_e$  are shown in Appendix G. Similarly, values of  $D_d/d_v$  are also shown in Appendix G for circular voids. Clearly, both these ratios approximate to one. This suggested that single drops of a size almost equal to the void size represent the maximum diameter to pass through. This differs from the observations of Wilkinson (148) with ballotini voids because in that case there was some pre-deformation of the drops; hence  $D_d/d_e < 1$ .

These results were expected since it was demonstrated with flat plates that a liquid drop was in intimate contact with a wetted surface (Figures 6.14 and 6.15) but not in contact with a non-wetted surface (Figures 6.24 and 6.25). The behaviour is similar at an aperture.

At a wetted aperture a drop larger than the aperture size can only come into contact with the solid surface after a finite rest-time (Section 6.1.1. a.) During this time it is supported

on the film at the solid surface and by the continuous phase on the opposite side of the aperture. Drops smaller than the aperture size are not supported, and therefore remain unaffected by the solid surface, and are able to pass straight through.

At a non-wetted aperture a drop larger than the aperture size does not come in contact with the solid surface but rests on a thin film of the continuous phase on the surface; this, plus the continuous phase on the opposite side of the aperture, support the drop (Figure 6.31).

In general, therefore, the process of passage of a drop appears to be independent of the wetting characteristics of the surface and to depend only on the relative size ratio. In theory, however, the mechanism involved in drop retention differs.

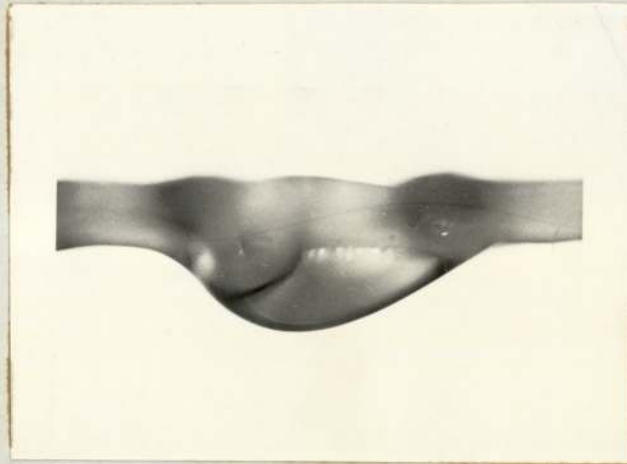
Although a given drop size was expected to be retained on spherical voids, where the surface forces are symmetrical to the drop shape, it was also found to be retained on other geometrically different apertures where it was expected to deform and squeeze through. The minimum distance between two opposite points around the aperture and the ability of the aperture to accommodate deformed drops are important parameters. In practice a larger drop may be retained at more than one aperture (Figure 6.32) distributing the mass of the drop and hence the driving force (gravity) across the voids.

#### 6.1.2.a. Effect on coalescence of a thin film of dispersed phase liquid on the packing.

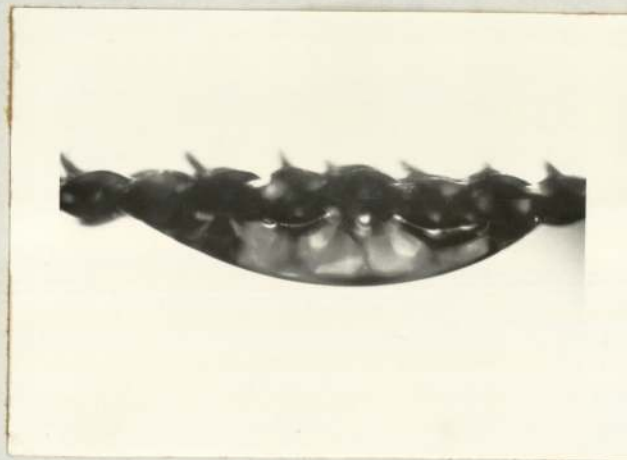
An enhanced coalescence effect has been reported (100) with packings which were first soaked in the dispersed phase liquid before immersing them in the continuous medium.

Figure 6. 33.

Coalescence behaviour of a liquid drop at a wetted  
packing pre-soaked in dispersed phase.



Dispersed phase liquid	: n-hexane;
Continuous phase liquid	: deionised, distilled water;
Drop dia.	: 3.517 mm. ;
Equivalent aperture dia.	: 3.380 mm. ;
Solid material	: polypropylene packing.



Dispersed phase liquid	: methylcyclohexane;
Continuous phase liquid	: deionised, distilled water;
Drop dia.	: 2.985 mm. ;
Equivalent aperture dia.	: 1.124 mm. ;
Solid surface	: nylon packing.

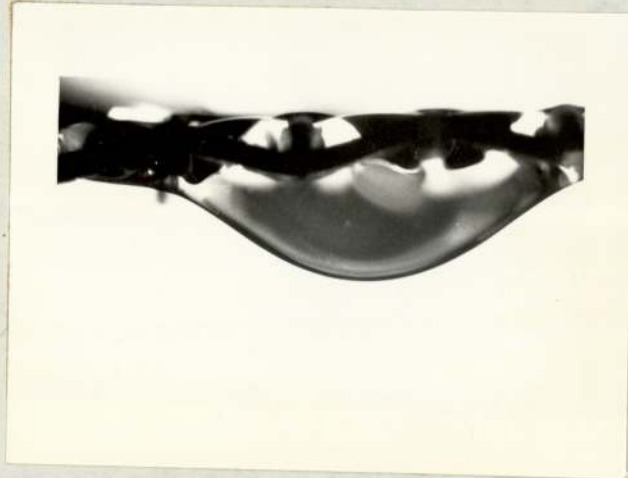
In the major part of the present study no attempt was made to alter the natural wetting characteristics of the solid surfaces. However, some experiments were conducted to investigate qualitatively the mechanism which leads to the above effect. The packings wetted by the dispersed phase liquid behaved differently from those which were non-wetted. The behaviour at a single aperture which would normally be wetted by the dispersed phase liquid but without a film of the dispersed phase on it could be judged from the ratio of the 'maximum drop diameter' that passed through (Section 6.1.2). However, with a film of the dispersed phase liquid, the behaviour could not be judged from  $D_d/d_e$  or  $D_d/d_v$  because drops of various sizes passed through and bulged out onto the other side of the packing (Figure 6.33).

Analysis of the cine photographs showed that the thin film of the dispersed phase liquid at the packing surface shrank to tiny droplets as the packing was lowered into the continuous phase liquid. Since the packing was of a solid material which was wetted, these droplets adhered to various sites at the packing filament and provided a bridging effect for larger drops to coalesce; the enlarged drops then passed through the aperture to the other side of the packing where they bulged out, because the surface forces exceeded the gravity or buoyancy forces. The dispersed phase liquid thus remained suspended from the outlet side.

When a subsequent drop arrived and coalesced at the same site then, after bulging through the packing, the contents of the coalesced drop were added to the existing mass, thus increasing the gravity or the buoyancy force of the mass of the liquid to enable part of this liquid to detach in the form of a larger drop.

Figure 6.33. (contd.)

Coalescence behaviour of a liquid drop at a wetted packing pre-soaked in dispersed phase liquid.



Dispersed phase liquid : deionised, distilled water;  
 Continuous phase liquid : toluene;  
 Drop dia. : 3.742 mm. ;  
 Equivalent aperture dia : 1.693 mm. ;  
 Solid material : stainless steel packing.



Dispersed phase liquid : deionised, distilled water;  
 Continuous phase liquid : toluene;  
 Drop dia. : 3.975mm. ;  
 Equivalent aperture dia : 2.251 mm. ;  
 Solid material : copper packing.

For the packing which was not wetted by the dispersed phase liquid, it was difficult to have a thin film distributed over it. Any traces of liquid which were retained on the rough surface became fine spherical droplets. These droplets coalesced with any drop that arrived subsequently at the packing and the drop did not bulge out through the other side of the packing aperture.

However, these observations confirm the earlier findings that wetted packings pre-soaked in dispersed phase liquid exhibit an enhanced coalescence performance.

### 6.1.3. Behaviour at flat composite surfaces

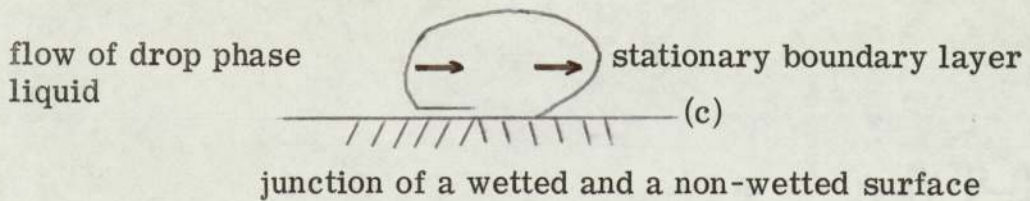
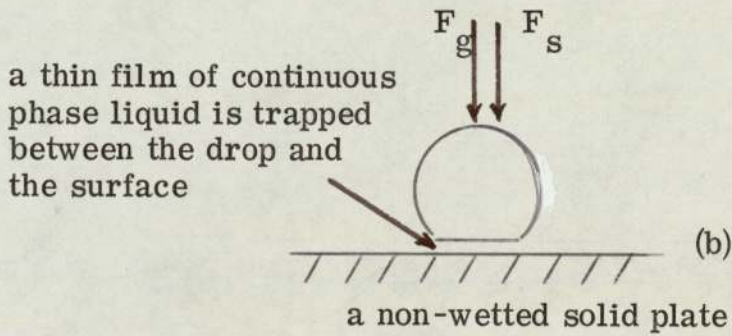
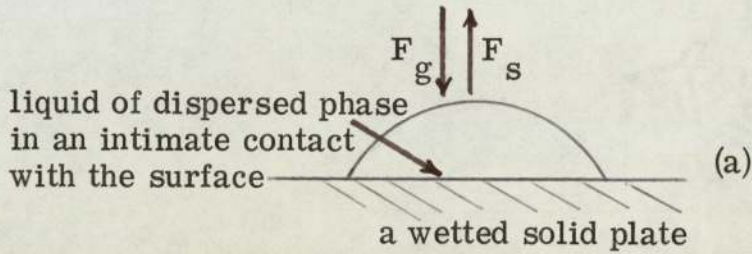
Drops impinging on a smooth and horizontal plate non-wetted by the dispersed phase liquid, rolled over the surface in any direction, as explained in Section 6.1.2. The direction depended upon the angle at which the drop hit the surface before it started travelling on the surface. The direction of travel also depended on the geometry with which it arrived at the surface. However, at a junction surface when the drop travelled from a non-wetted towards a wetted component, its behaviour was much more interesting to observe and analyse. The junction phenomena explained in this section, depend upon the inherent 'wetting' and 'non-wetting' characteristics of single surfaces explained in Sections 6.1.1. and 6.1.2.

#### 6.1.3.a. Horizontal junction

As the drop arrived at a junction (Figure 6.34), only a part of the base of the drop crossed over the junction. The molecules of the dispersed phase liquid in the boundary layer at the base of the drop at the wetted material were in intimate contact with the surface as explained in Section 6.1.1.a. Therefore, the motion of the drop ceased since the drop base

Figure 6.34.

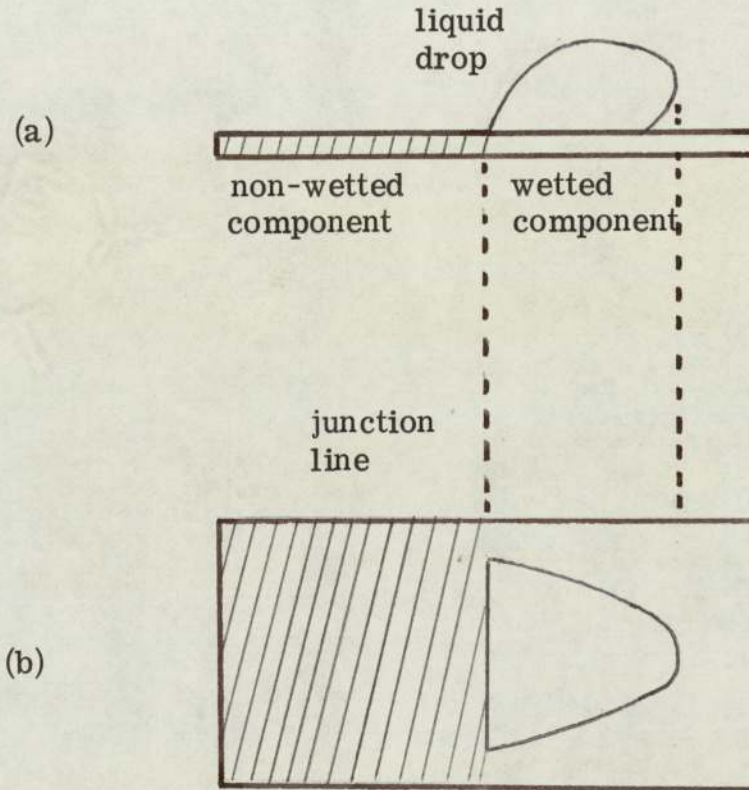
The behaviour of a liquid drop at a junction of a wetted and a non-wetted surface and at individual surfaces.



there adhered to the surface. But the liquid above this boundary layer in the drop was still in motion in the forward direction. A variation in the velocity of the liquid of the drop along the height of the drop would be expected since the velocity would be zero at the base and a maximum at the top. Conversely the liquid at the base of the drop at the non-wetted component of the junction was not in contact with the surface, as explained in Section 6.1.1. b. ; therefore, the velocity there would not be expected to be zero. Correspondingly a higher velocity variation along the height of the drop can be expected on this side of the drop.

In summary, the liquid of the drop at the non-wetted component tended to force the drop forward to the wetted side of the junction, but the base of the drop adhering there resisted this force. As a result the drop was deformed at the junction. This deformation resulted since, after the redirection had occurred, the drop base along the junction lost its sphericity and became parallel with the junction line (Figure 6.35.). The process of redirection occurred when the drop on the non-wetted component was about 2 mm. from the junction line. Once the drop was within this range of the junction, the velocity of the drop increased many fold until the initial part of the drop had crossed over the junction line and physical movement of the drop ceased abruptly. The process of physical transfer of the drop from the non-wetted to the wetted plane of the junction occurred over a very small distance of about 2 - 4 mm. and in a few microseconds, hence it would normally be observed as a redirection.

Figure 6.35.

Redirected liquid drop at a junction surface.

- (a). View parallel to the plane of solid surface and the junction line.
- (b). View normal to the solid surface and the junction line. After the redirection, the drop boundary at the junction line is parallel to the line.

Equation (6.1.) was also applied to characterise the behaviour of a liquid drop at a plane junction of high to low surface energy material since the wetting behaviour was not similar at these materials. For this purpose, it was necessary to estimate the resultant effect of the junction on the liquid drop. Observations of the actual behaviour of a liquid drop, as outlined in Sections 6.1.1.a. and 6.1.1.b., at a wetted and a non-wetted surface, were used in evaluating the resultant of the surface forces of these solid components at a junction. The resultant effect at a junction was demonstrated by the fact that after the redirection, the drop did not roll over at the surface but adhered there (Figure 6.36.) since the force between the liquid of the dispersed phase and the solid component wetted by it overcame the force between the liquid of the dispersed phase and the solid component non-wetted by it. Under these circumstances, the resultant force was, therefore, given by subtracting Equation (6.3) from (6.2).

$$F_r = \gamma_{wd} - \gamma_{nd} = \gamma_{dc} (\cos\theta_{wd} - \cos\theta_{wc}) + (\gamma_{nc} - \gamma_{wc}) \quad (6.4)$$

With the junction effect Equation (6.4) there are still four unknowns with two Equations i.e. (6.2) or (6.3) and (6.4). It was necessary to make use of at least two more equations to solve for these four unknowns.

The deformation in a drop at a junction (Figure 6.36) resulted in a rearrangement of the angles of contact along the boundary of the drop base at the junction. The rearranged angle at the line where the drop was still under the influence of the non-wetted component will be  $\theta_h$ , where  $\theta_h = \theta + \Delta_h$  and  $\theta$  is the angle of the liquid drop at a wetted plate and  $\Delta_h$  the increase in this angle due to the pressure of flow of the drop liquid towards the wetted surface material of the junction.

Figure 6. 36.

Coalescence at a junction surface

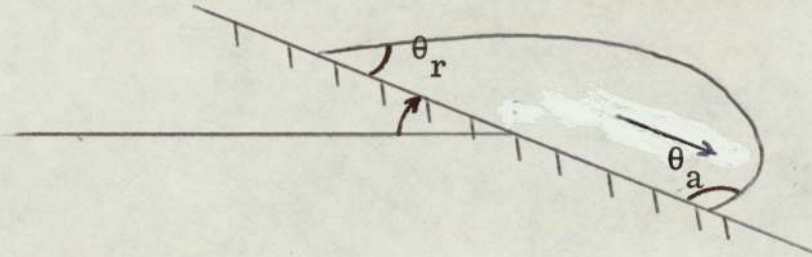
Dispersed phase liquid	: deionised, distilled water
Continuous phase liquid	: toluene;
Drop dia.	: 2. 715 mm.
Solid (junction) surface	: p. t. f. e. glass composite plate.

The value of  $\Delta_h$  will clearly depend upon the magnitude of the flow pressure; the higher the flow pressure the larger  $\Delta_h$  will be. The value of  $\Delta_h$  was almost constant along the boundary of the drop which lost its sphericity at the junction line (Figure 6.35). Conversely, the value of the contact angle of the drop at the non-wetted component decreased correspondingly to  $\mathcal{Z}_h$ , where  $\mathcal{Z}_h = \mathcal{Z} - \Delta'_h$ , and  $\Delta'_h$  is the decrease in the angle  $\mathcal{Z}$ . Clearly,  $\Delta'_h$  will depend upon the magnitude of the flow pressure away from the non-wetted material. The contact angles at the junction line were not measured since their practical and theoretical significance was lost.

The shape of a deformed drop at a junction is comparable to the profile of a drop at a wetted single material plate which is tilted (Figure 6.37). Because of this tilt in the plate, the flow pressure of the liquid of the drop increases in the downward direction. However, in this case, unlike that of a junction, the drop surface maintains its curvature. The deformations in the drop shape at a tilted plate result from at least two forces. The surface forces act in one direction, parallel to the surface, and as a result of these forces the drop adheres to the surface. The gravity forces due to the tilt, which tend to disengage the drop from the surface, act in the same line but in an opposite direction to the surface forces. The surface forces to hold the drop are proportional to the size of the drop and the wetting characteristics of the surface but the forces to disengage the drop are proportional to the angle of inclination. The magnitude of deformation in the drop shape clearly depends upon the above relative forces. However, at a certain tilt, the downward flow pressure of the drop liquid eventually overcomes the intermolecular attractive forces between the molecules of the drop liquid. Consequently, the bulk of the drop liquid breaks away, leaving only the boundary layer adhering to the surface.

Figure 6.37.

Drop profile at a wetted, tilted plate.



Due to a tilt in the surface, different contact angles are formed as a result of flow pressure of the liquid in the drop parallel to the surface.

The deformations, which occurred in a drop after a redirection at a smooth and horizontal junction surface, resulted purely from the action of the surface forces of the wetting and non-wetting components. The assymmetric nature of the surface forces at a junction plate produced assymmetric deformations in the drop shape.

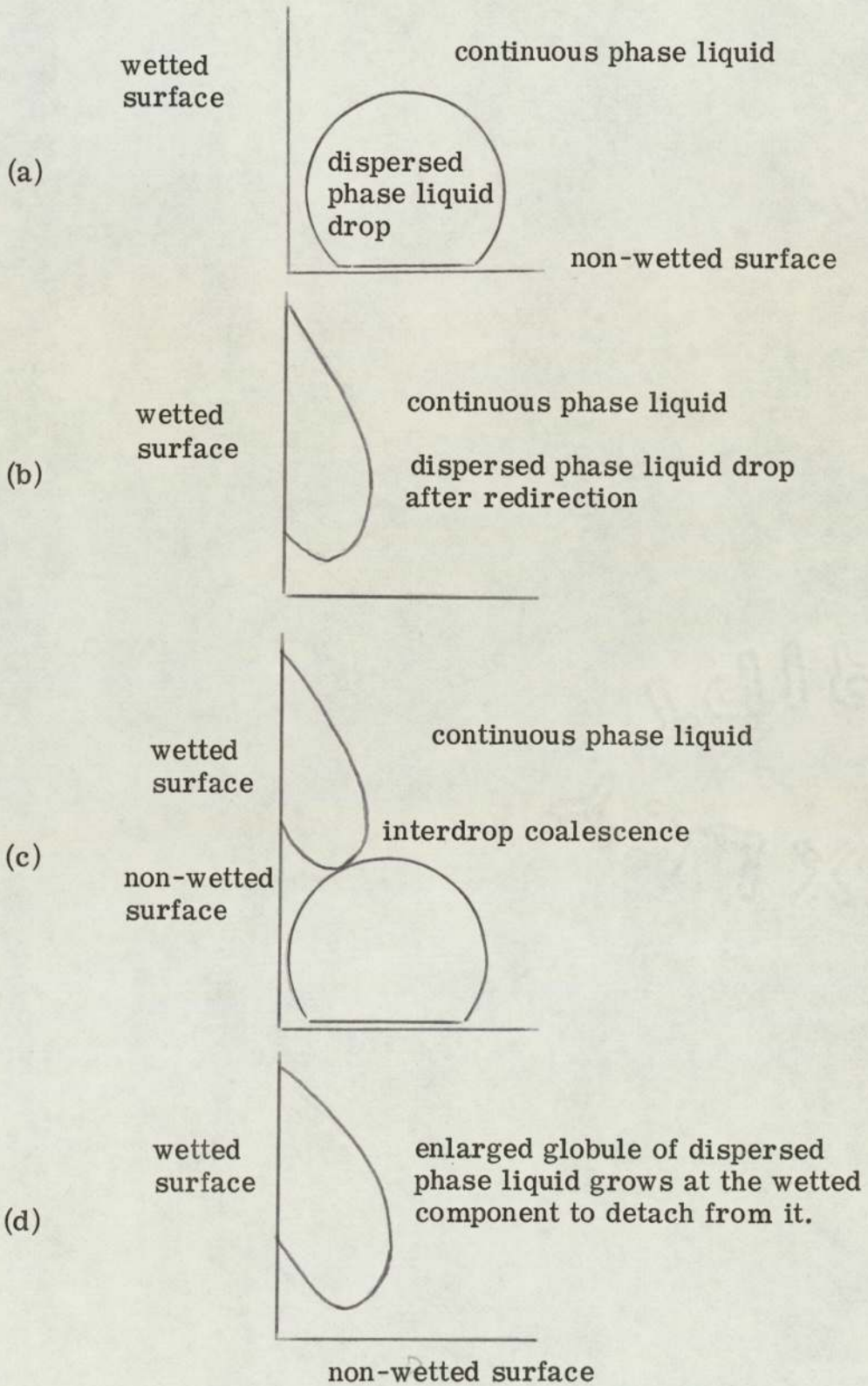
The junction effect is without doubt repeated many times over in different situations. This was demonstrated in a trial in which a number of one centimeter long p. t. f. e. tubes were inserted, about two centimeters apart, into a one meter long and  $1.25 \times 10^{-3}$  m diameter QVF glass pipe to give radial junctions. When an oil-in-water dispersion was passed through this junction pipe, the oil droplets in the dispersion coalesced at the p. t. f. e. component. The larger oil droplets thus formed at the p. t. f. e. surface were detached and carried forward by the flowing dispersion, in a horizontal direction. However, there appeared to be a critical flowrate of  $0.0184 \text{ ms}^{-1}$  of the dispersion above which droplet coalescence decreased because of the increased flow pressure which restricted the contact of oil droplets to the p. t. f. e. surface, and aided the renewal of the continuous phase film beneath the drops trying to approach the surface. When the flowrate was below this critical value, the coalesced mass did not detach from the surface thus causing an increased hold-up. A similar process of drop growth occurred in a vertical junction pipe but in this case, the coalescence of larger droplets resulted in a two-phase plug flow in the pipe.

A junction surface not only provides a far more effective drop coalescence but also a better collection of drops compared with flat plates of single materials. The collection or the coalescence of liquid drops at the non-wetted solid plate was

very rare. A liquid drop did not rest at such a surface (Section 6.1.1. b. ), therefore, it was difficult for any two drops to reside together to coalesce (Figure 6.28). In the absence of a coalescence, impact from a second drop resulted in a drop already at the surface moving away faster than its velocity before impact. On a wetted solid plate, however, the second drop impacted upon the first drop and then rested at the surface, usually away from the first drop. Thus interdrop coalescence in a monolayer dispersion at a wetted solid plate occurred only when the drops were closely packed, but at a non-wetted plate, a slight disturbance to the surface caused the drops to redisperse. However, the practical situation with wetted or non-wetted packings in separating columns is different to that with single drops or monolayers at smooth and horizontal plates. In practical columns coalescence does occur. This is because the drops are packed closely in multilayers and are restricted in their movement by the column walls and by the uneven packing surface.

In preliminary investigations into what comprised junctions between two high surface energy materials, i. e. stainless steel-stainless steel with different surface preparations or glass-stainless steel, or two low surface energy materials, i. e. p. t. f. e. -p. t. f. e. with different surface preparations or p. t. f. e. -polypropylene were investigated. However, these results exhibited no junction effect i. e. plates functioned as 'wetted' or 'non-wetted' surfaces depending upon the dispersed/continuous phases. It is clear from these trials that a certain minimum difference in the surface energies of the component surfaces is required to produce a junction effect.

Figure 6.38.

Coalescence in a vertical junction.

### 6.1.3. b. Vertical junctions

The junction effects were not restricted to component surfaces arranged horizontally adjacent to each other. They were observed with other geometrical arrangements as well. Figure 6.38 shows the two components arranged at right angles to each other, the non-wetted component normally being horizontal. Referring to the arrangement in Figure 6.38. a. , provided the nearest point on the drop was within two millimeters, horizontally, from the wetted surface, redirection of the drop occurred across this vertical junction as shown in Figure 6.38. b. An interdrop coalescence between two drops occurred at a vertical junction, in which the two components were a drop diameter away, vertically, from each other (Figure 6.38. c. ). In this case, flow of the liquid during interdrop coalescence between the two drops occurred against gravity or buoyancy from the horizontal non-wetted component to the drop at the vertical wetted component.

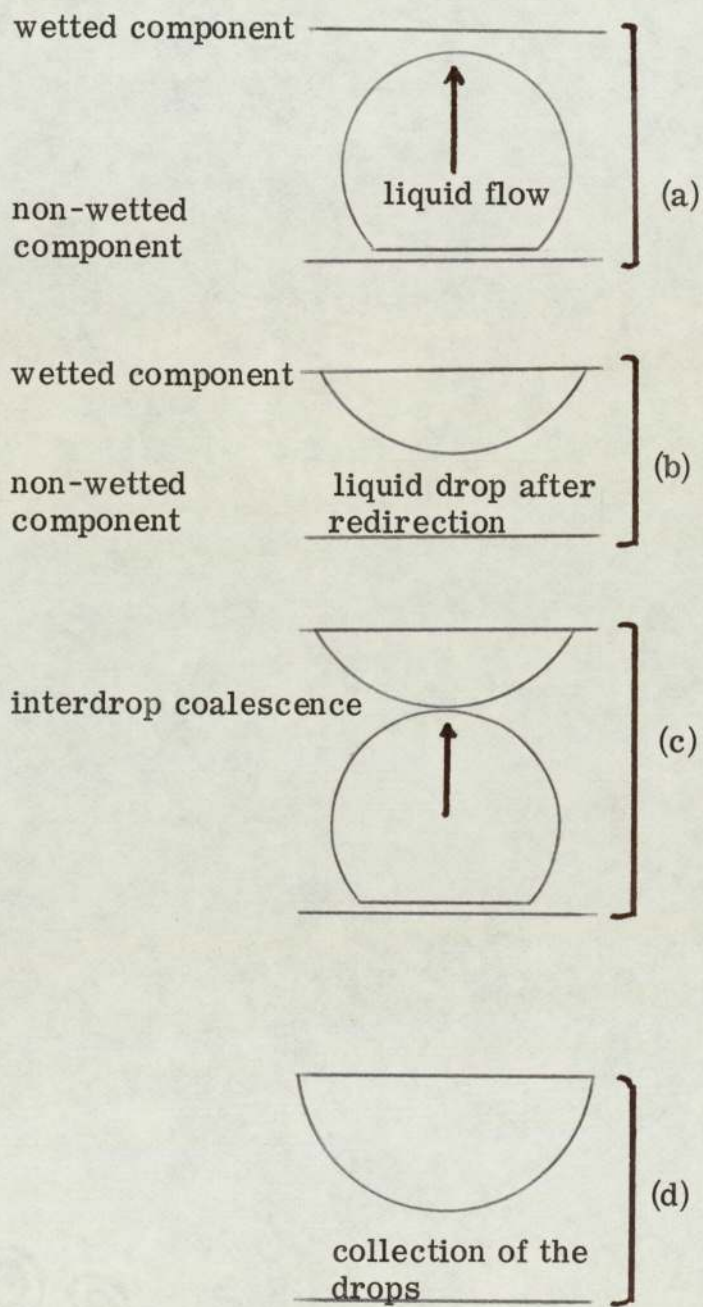
### 6.1.3. c. Parallel junctions

The redirection of a drop or interdrop coalescence between two drops also occurred with a parallel junction as shown in Figure 6.39.

In a vertical, parallel or mixed junction, the general coalescence mechanism was the same as for a horizontal junction. However, at a horizontal junction, the flow of the liquid during coalescence occurred parallel to the junction surface. In other arrangements, it occurred against the force of gravity/buoyancy, at right angles from the non-wetted component.

It is relevant to mention here observations made with parallel plates during experimentation associated with the studies of the behaviour of liquids in space.

Figure 6.39.

Coalescence in a parallel junction.

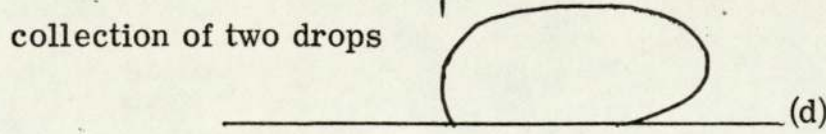
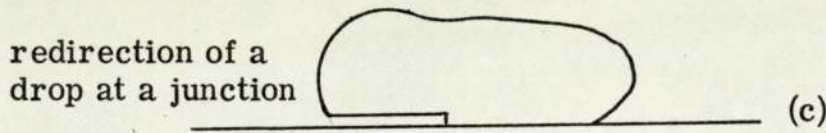
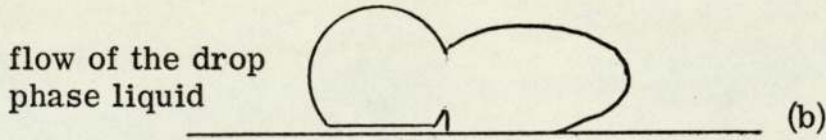
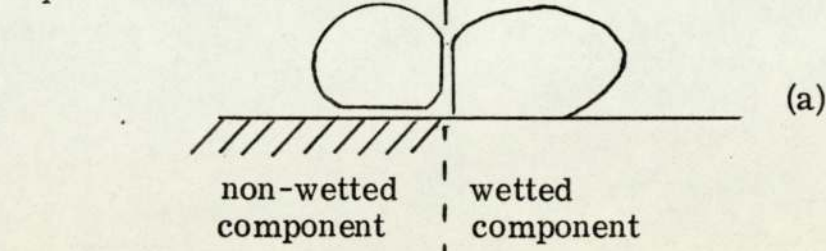
In normal circumstances, liquids are poured into containers under the action of gravitational force. Difficulty arises in space, in the absence of gravity, in retaining the liquid in the receiving container. In space, a wetted container will retain the liquid due to the forces of attraction between the liquid and the solid surface. Liquids cannot be retained in non-wetted containers. In a simple experiment, two equisized wetted plates faced each other and held two equisized organic liquid drops. The plates were surrounded by an aqueous phase liquid. The densities of the two liquids were closely matched to simulate conditions in space. The upper plate was lowered gradually until it touched the other drop. Both drops were deformed to force out the aqueous phase liquid trapped between them. The aqueous phase liquid had similar physical properties to water and it took the film almost one minute to rupture. After inter-drop coalescence occurred, the two drops formed a liquid cylinder with both ends 'attached' to the plates. However, when the process was reversed, by gradually retracting the upper plate, the diameter of the liquid cylinder decreased at its centre to form a neck. The neck ruptured after a further separation of the plates. By this process, two equal sized droplets were reproduced at the plates together with some satellite droplets when the neck ruptured.

The above experiment confirmed that the forces of attraction between a dispersed phase and a wetted surface are greater than the forces between the molecules of the dispersed phase liquid themselves, since stretching caused the liquid column to break at its neck whilst the dispersed phase remained adhering to the plates.

Figure 6.40.

Coalescence and collection of liquid drops at a junction.

flow of continuous phase liquid in the film (Refer also to Figure 6.41.)



#### 6.1.3.d. Interdrop coalescence at a junction

The coalescence between any two subsequently arriving drops at a junction (Figure 6.40) was governed by two main factors. Firstly, the magnitude of the force with which the second drop was forced against the first drop across the junction and secondly, the rate of the outward flow of the continuous phase liquid in the film trapped between the two drops. Once this film thickness reached a minimum, it ruptured and coalescence occurred between the two drops. During this coalescence process at a junction, the flow of the drop phase liquid occurred (Figure 6.40. a.) always from the drop at the non-wetted material to the drop at the wetted material. It is evident, as already explained in Section 6.1.3.a., that after the redirection of a single drop at a junction, the deformation in the drop resulted because of the flow pressure from the non-wetted to the wetted material. Similarly once the film between the two drops (6.40. a.) was ruptured, then the single globule of the coalescing liquid (Figure 6.40. c.) from these two drops behaved as one single drop (Figure 6.40. d.) approaching the junction.

Figure 6.41 records the process of an interdrop coalescence at a junction. Both drops in the photographs were of the same liquid but were dyed with different non-surface active chemicals to give a red coloured drop at the wetted and a blue coloured drop at the non-wetted component of the junction (for details refer to Figure 6.41.). The colouration was intended to give an insight into the extent of mixing between the liquids during coalescence between the two drops.

The range of drop sizes investigated for interdrop coalescence was the same as for single drops, i. e.  $2 \times 10^{-3}$  to  $1.0 \times 10^{-2}$  m and the ratio of the two drop sizes investigated for interdrop coalescence was 1:3, 3:1 or 1:1.

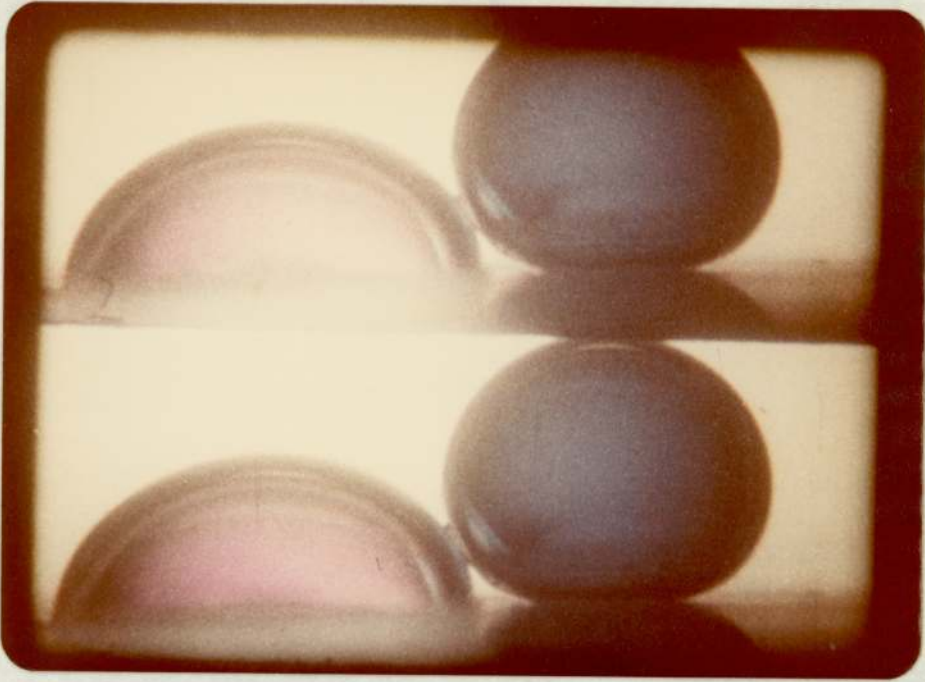
Figure 6.41.

Interdrop coalescence at a junction

Dispersed phase liquid	deionised, distilled water;
Continuous phase liquid	toluene;
Drop dia. ratio.	(wetted : non-wetted) 1:1;
Drop diameter	3.725 mm. ;
Red dye	
Blue dye	
Camera speed	9,500 frames per second;
Wetted component of junction	glass plate;
Non-wetted component of junction	p. t. f. e. plate;
Geometrical arrangement of junction components	horizontal.

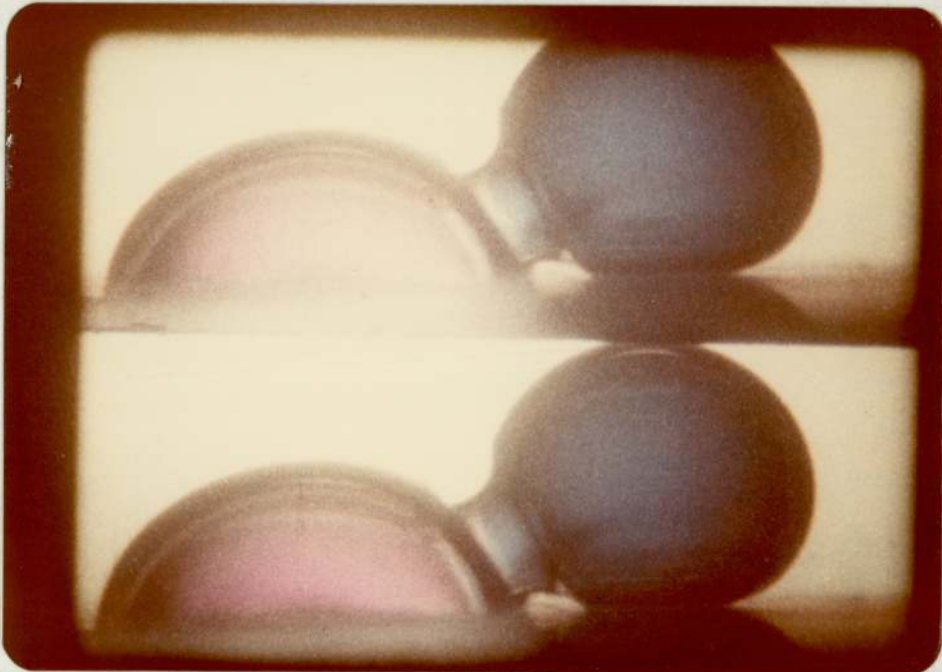
Figure Interdrop coalescence at a junction

(a)



Blue drop is at a non-wetted and red drop is at a wetted surface. Blue drop is approaching the red drop. A film of continuous phase liquid is trapped between the drops.

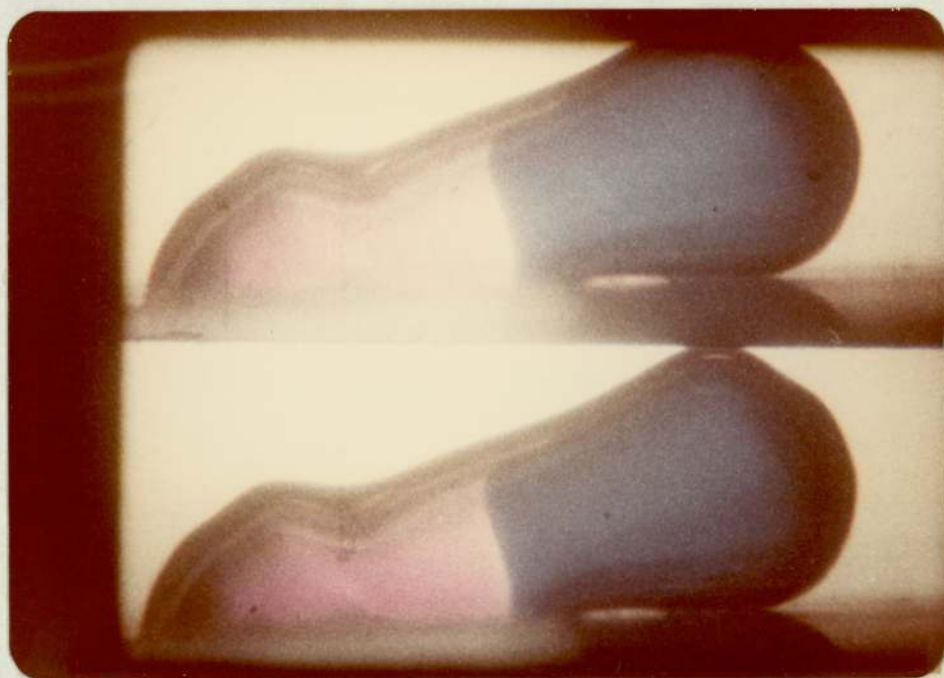
(b)



A common neck for the flow of the blue liquid into the red is formed between the two drops after the rupture of the continuous phase film.

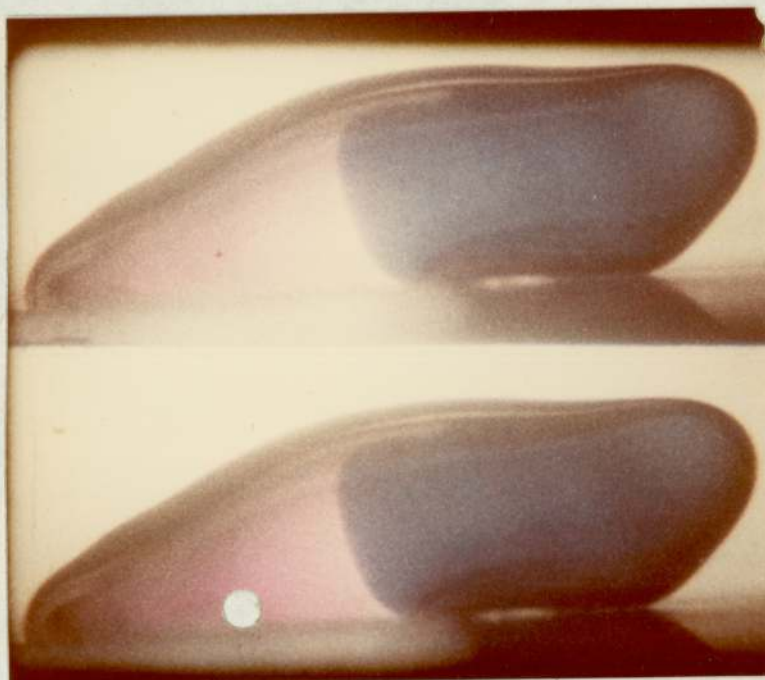
(Figure 6. 41. contd. )

(e)



As the cross-section area of the neck increases under the flow pressure of blue liquid, waves are transmitted over the surface of the red liquid.

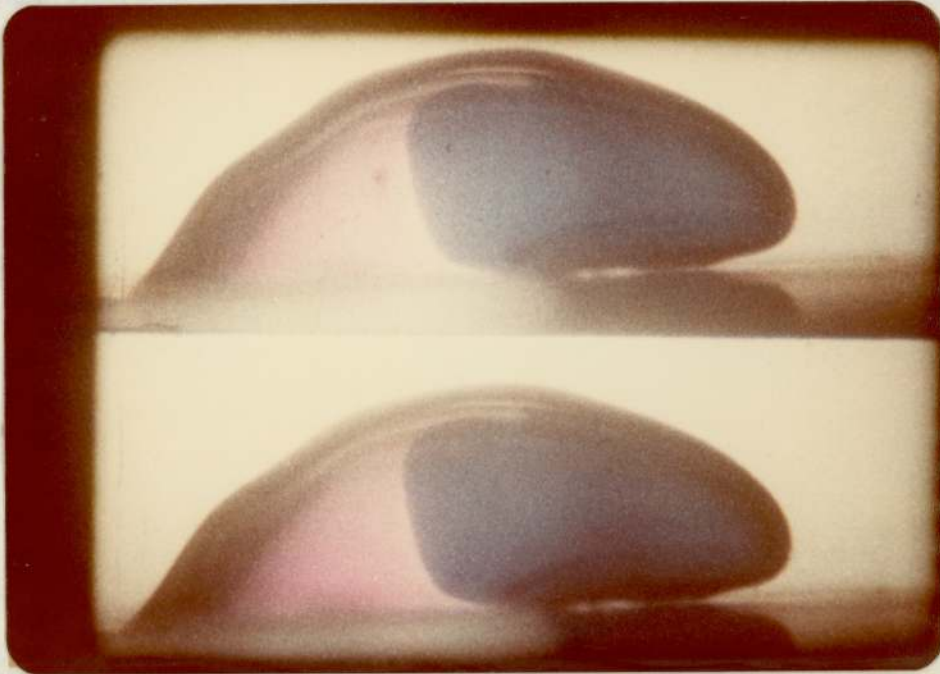
(d)



After the initiation of the interdrop coalescence in(b), the liquid of the two individual drops becomes a single globule which is then redirected from non wetted to wetted component.

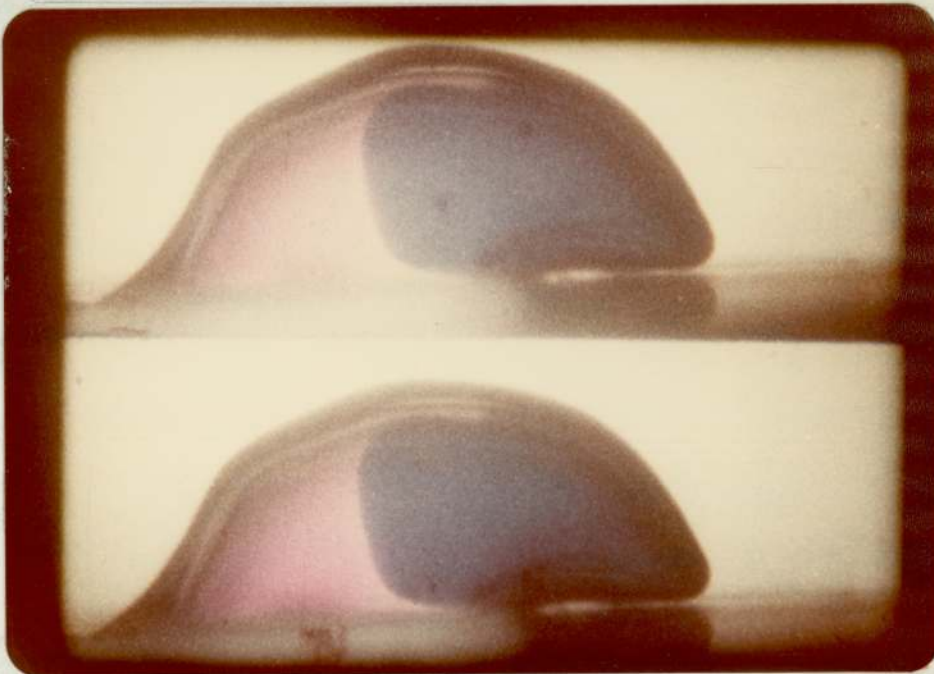
(Figure 6.41. contd.)

(e)



As the gravity force of the blue liquid on the non-wetted component decreases, and the flow pressure increases, the blue liquid lifts away from the surface.

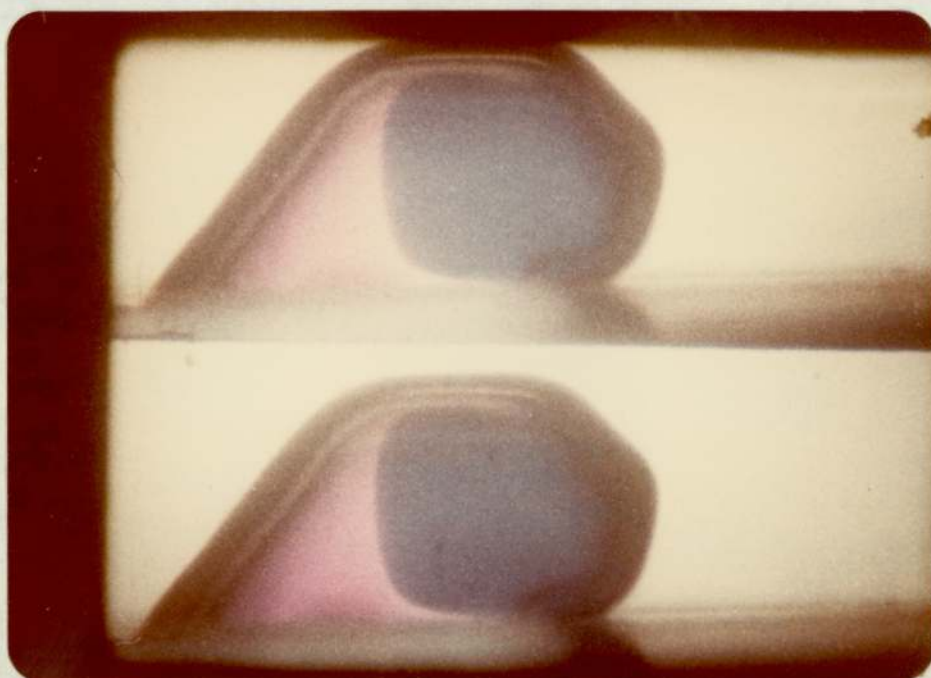
(f)



The flow pressure is insufficient to disengage the red liquid from the wetted surface. To accommodate the additional mass of liquid, the overall height of the red drop increases. As a result of interdrop coalescence, the blue drop has lost and the red drop has gained height.

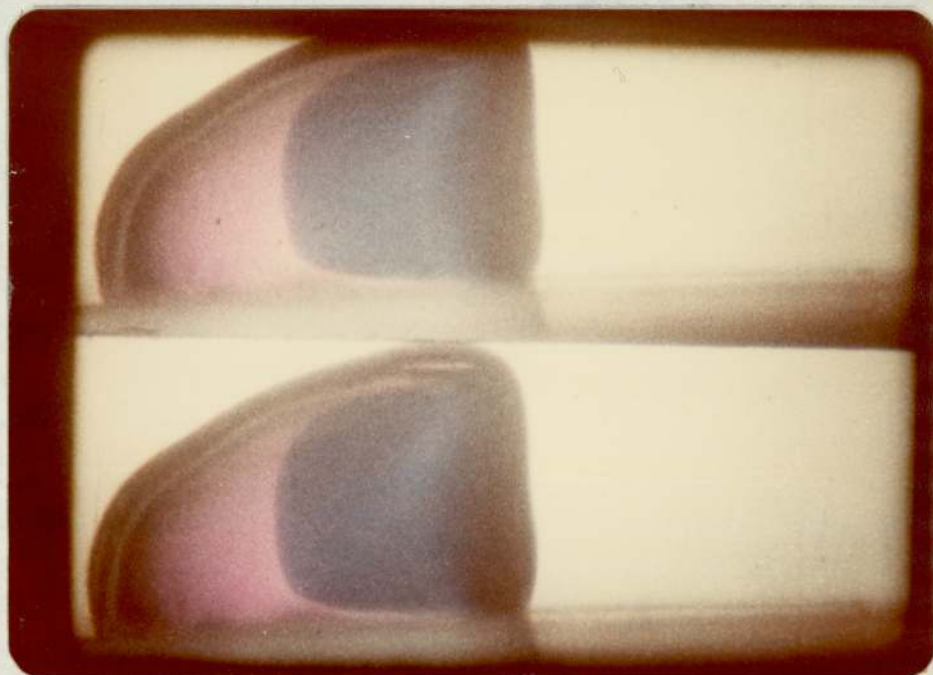
(Figure 6. 41. contd. )

(g)



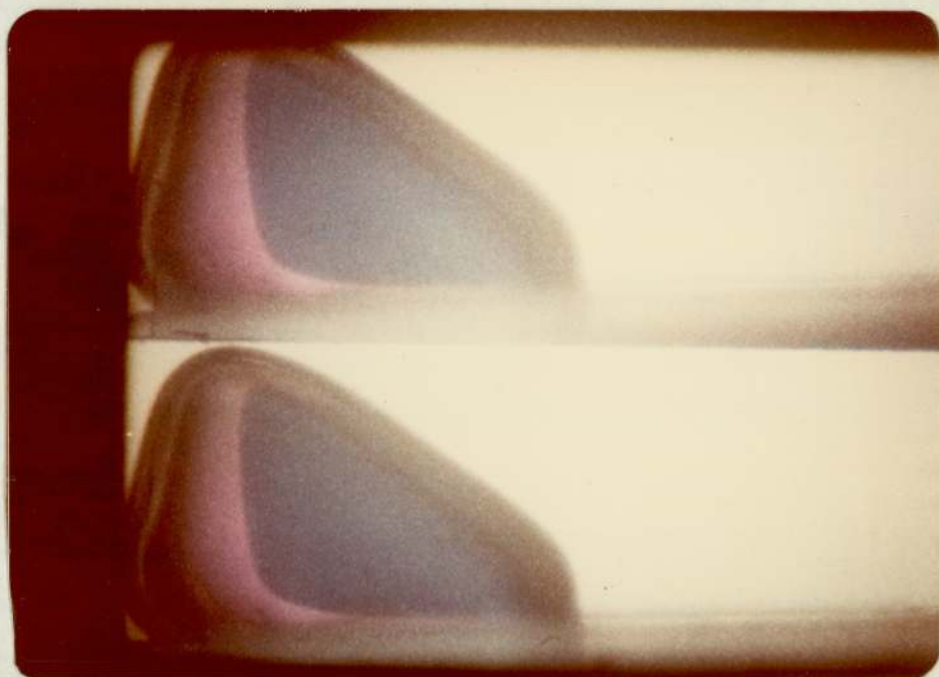
The force or the kinetic energy with which the drop is being moved away from non wetted component is displayed by the additional increase in the overall height, and the plane formed as the red drop minimises its surface. A sudden bend along the blue drop shows the position along the surface where most force is being concentrated.

(h)



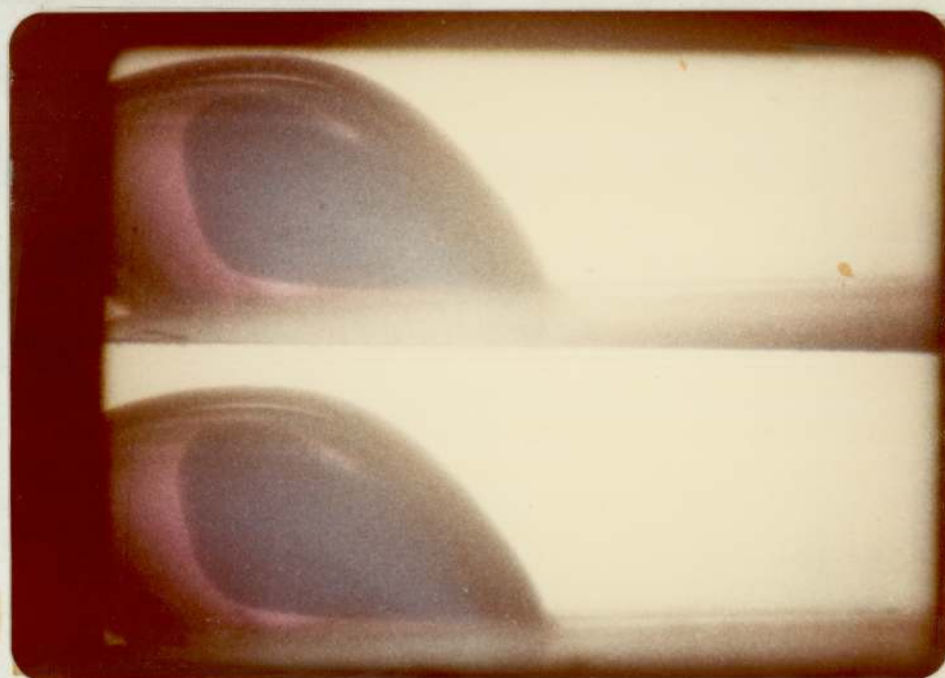
One side of the blue liquid stands vertical to the non-wetted surface. A sphericity reappears along the red liquid boundary to show the direction of the pressure force of flow. The contact angle of red liquid is almost  $90^\circ$  at the wetted component since the triple point boundary there is not displaced.

(i)



Blue liquid under the influence of the red boundary layer and the wetted component underneath it. The rotation of the blue vertical line in (h) to (i) shows the continued action of pressure force.

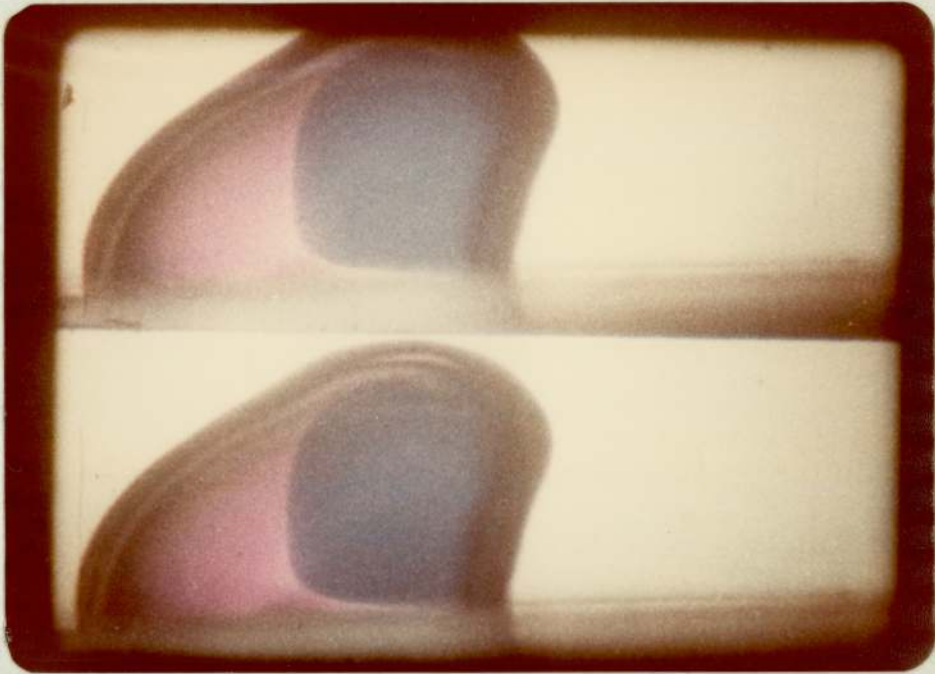
(j)



The liquid globule (blue + red) rotates as a whole about the base to which it is adhering.

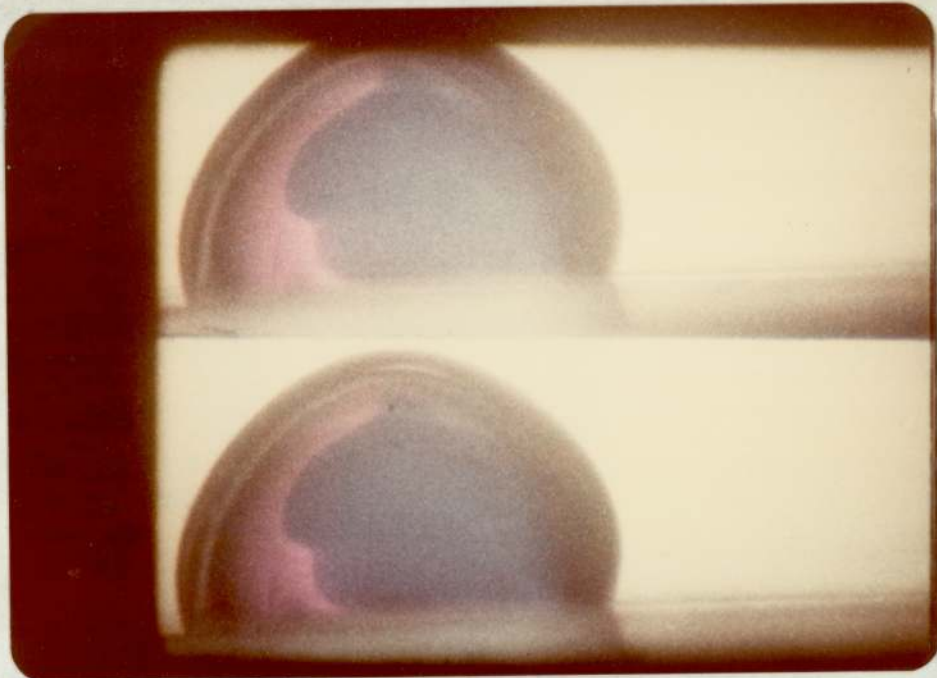
(Figure 6. 41. contd. )

(k)



The reaction from the red liquid is to push the blue liquid back towards its origin, but the blue liquid is now adhering to the wetted component. The direction of reaction is shown protruding of the blue liquid, but the base of the blue liquid cannot cross

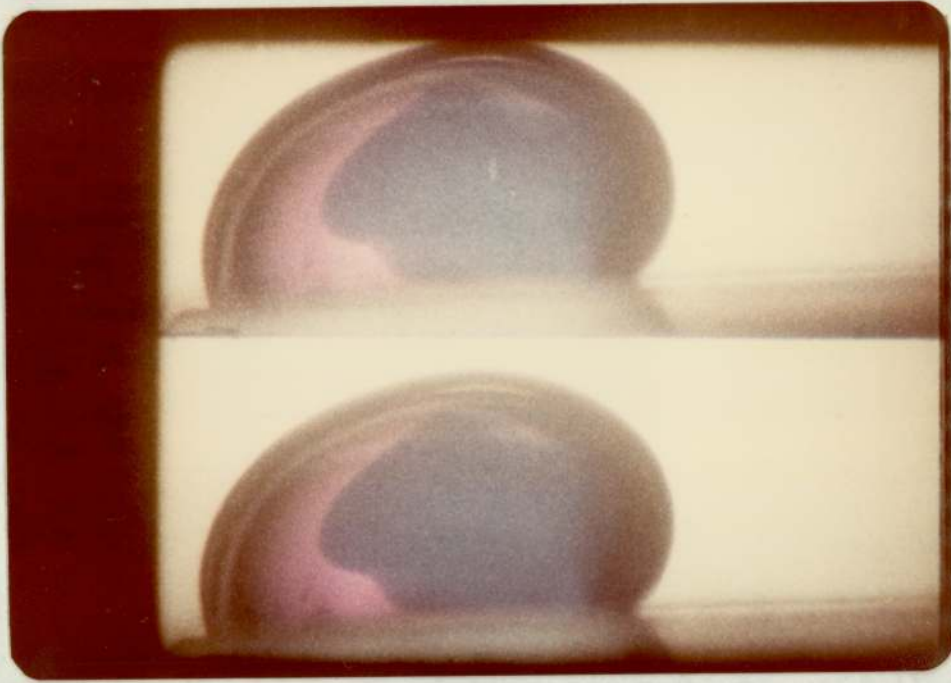
(l)



over the boundary. The red and blue liquids now coexist and intermix by diffusion.

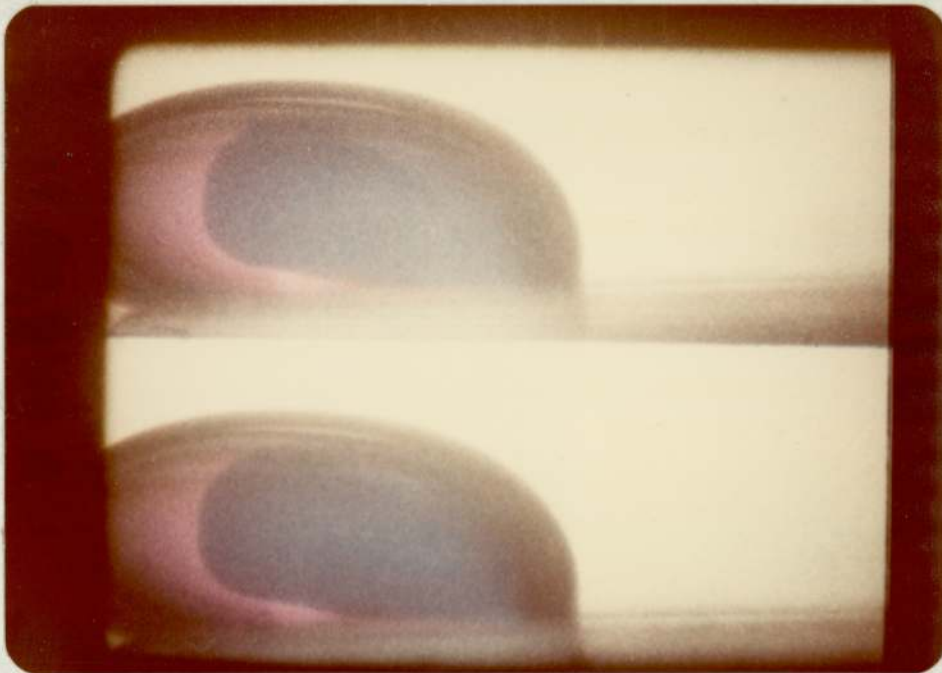
(Figure 6. 41. contd)

(m)



The internal flow in the red (red + blue) drop is still fluctuating backwards and forwards.

(n)



The intensity of internal flow circulation is clearly illustrated.

Photographs 6.41. c. to 6.41. n. illustrate that no mixing of the contents of the two drops took place during the coalescence time (i. e. there was no penetration of the colours deep into each other). This was because turbulence could not develop within the drops in the short time ( $< 100\mu\text{s}$ ) available. The profile of the concentration gradient differed with the ratio of the drop sizes. With equal sized drops, the sharp dividing line between the two colours is almost vertical showing that mixing, which took place later, was through molecular diffusion. However, when the size ratio was 1 : 3 between the drop at the non-wetted to the drop at the wetted component, the interdrop coalescence occurred with much less turbulence than with a ratio 3 : 1; in the former case, the larger droplet wrapped round the smaller droplet.

The phenomena involving the formation of secondary droplets in a liquid-liquid system is explained in Section 1.2. Such secondary droplets were not formed in liquid-liquid-solid-solid systems. Secondary droplets apparently only form when the drops coalesce at a film of dispersed phase liquid at the solid surface. When the surface of a wetted packing is clear of this film, then the solid surface does not allow the formation of a cavity (Figure 1.8) at the interface because in this case, the flow of the drop liquid during coalescence occurs within the solid-liquid boundary and the solid is non-deformable and stationary. In liquid-liquid systems, the mass of the liquid column, the pressure of flow of the liquid and the local turbulence caused in the continuous phase liquid are sufficient to deform the elastic liquid-liquid interface.

Secondary droplets were not observed during interdrop coalescence at a junction. In this case, the flow of liquid from one drop to the other does not occur under gravity but against it. Moreover, the neck formed during coalescence enlarges with drainage whereas for a secondary droplet to form, the 'orifice' must narrow down to interrupt the flow. In this respect, the solid surfaces perform better than liquid-liquid interfaces so that packing coalescing aids should reduce secondary haze formation in settlers.

### 6.1.3.e. Rest-time distributions at a junction

The rest-time between two drops for coalescence whilst residing in contact i. e. excluding travel before contact, at a horizontal junction depends on (Figure 6.42):

- (a) The ratio of the drop diameters and the individual drop diameters.
- (b) The surface energies of the solid surfaces of the junction
- (c) The liquid-liquid interfacial tension

#### Drop diameter ratio

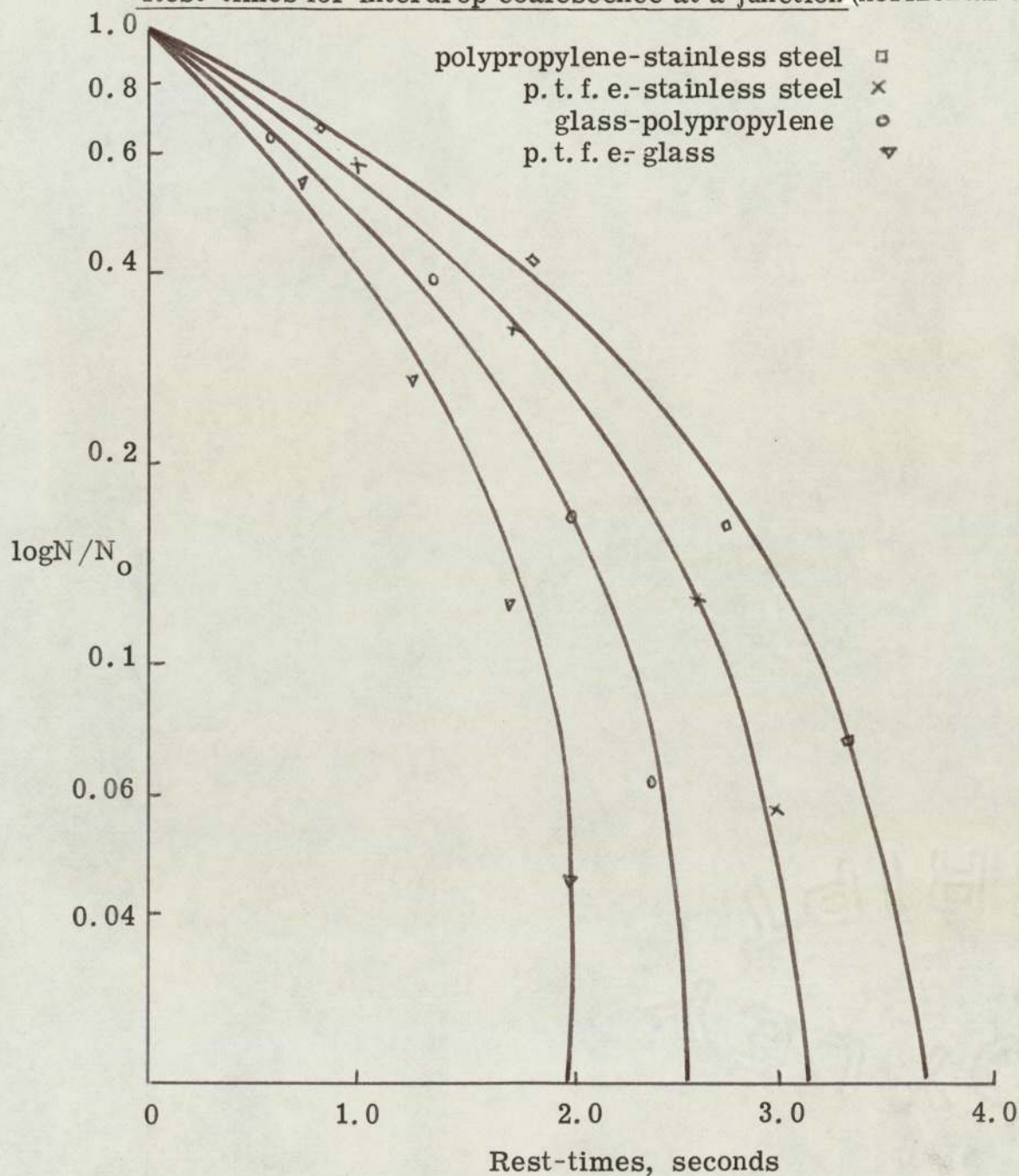
With either a horizontal, vertical or parallel non-deformable smooth junction surface, the approach of a liquid drop from the non-wetted component to a second drop at a wetted component differs from the approach of a drop to a plane liquid-liquid interface under gravity. At a junction the masses of both drops act downwards or upwards and the flow of the liquid in the film occurs from the common sides between the drops.

Whereas with a plane liquid-liquid interface, a drop approaches with its major axis parallel to the interface, at a junction a drop approaches a curved interface with its minor axis parallel to the minor axis of the drop already present. At a liquid-liquid interface, a liquid film is trapped under almost 50 % of the surface area of the drop whereas the surface area of the liquid in the film between two drops at a junction is less than 1 %. In the latter case the flow of the liquid of the film occurs because the drop at the wetted component adheres to the surface in opposition to the pressure exerted by the approaching drop.

When a drop approaches a drop already at a junction, the kinetic energy of the approaching drop is converted into pressure force to cause the outward flow of the liquid film. The impact imparted to the resident drop is greater when the second drop

Figure 6.42. a.

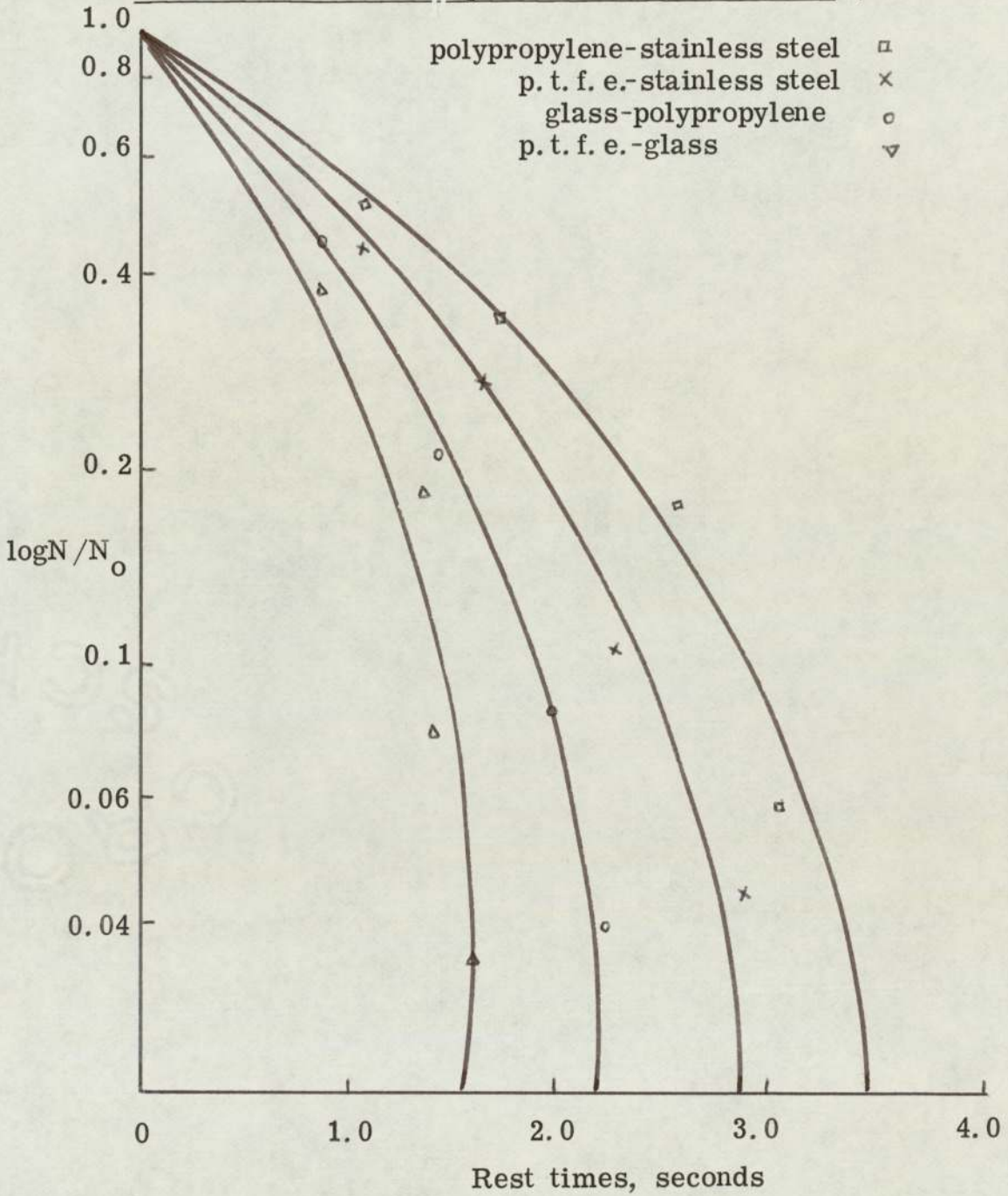
Rest times for interdrop coalescence at a junction (horizontal only).



Dispersed phase liquid: distilled water; continuous phase liquid: n-hexane; drop diameter ratio 1:3 (low surface energy to high surface energy solid plate).

Figure 6.42. b.

Rest-times for interdrop coalescence at a junction (horizontal only).

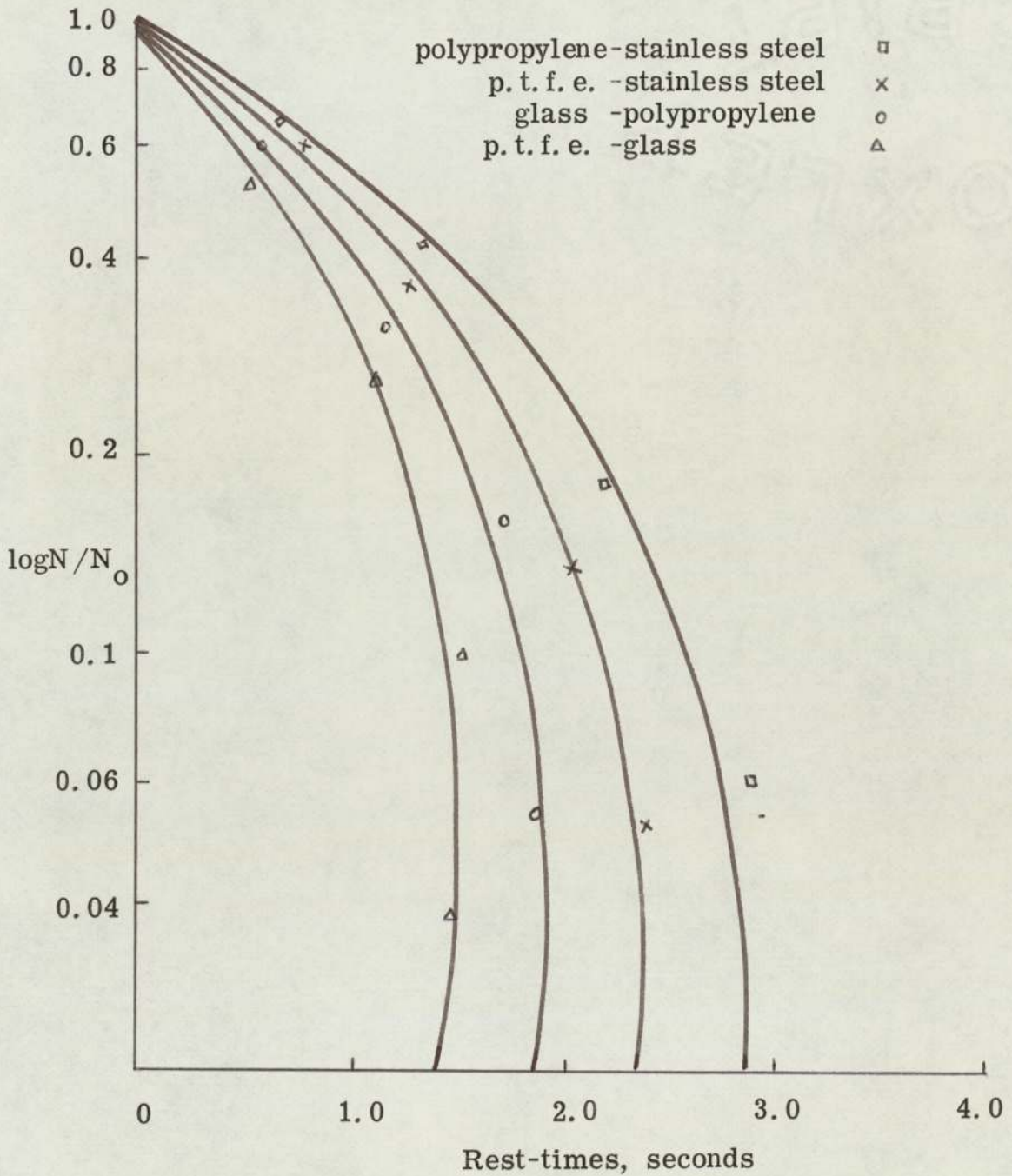


Dispersed phase liquid: distilled water; continuous phase

liquid: n-hexane; drop diameter ratio 3:1 (low surface energy to high surface energy plate).

Figure 6.42. c.

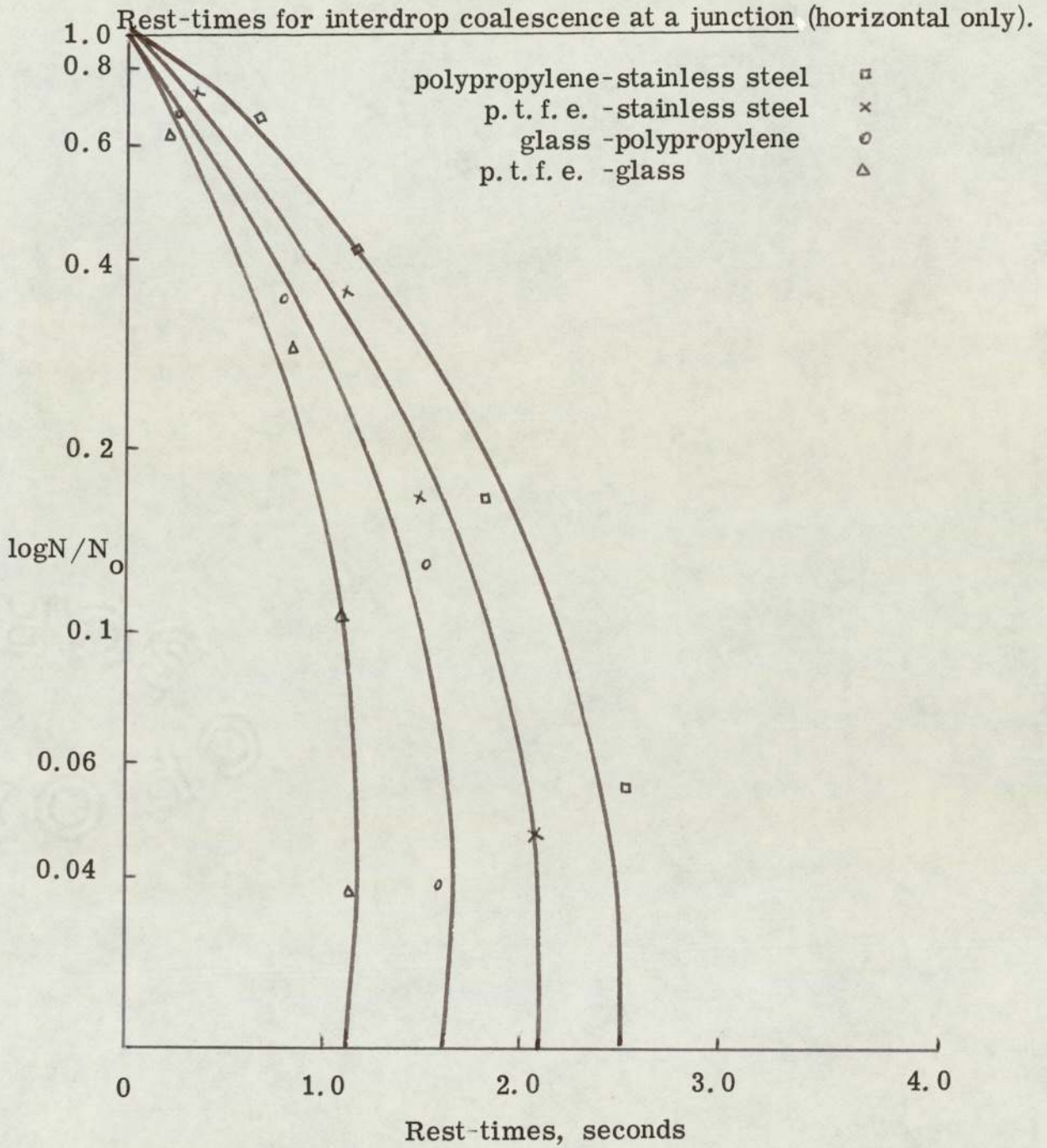
Rest-times for interdrop coalescence at a junction (horizontal only).



Dispersed phase liquid: distilled water, continuous phase

liquid: n-hexane; drop diameter ratio 1:1 (low surface energy to high surface energy solid plate).

Figure 6.42.d.

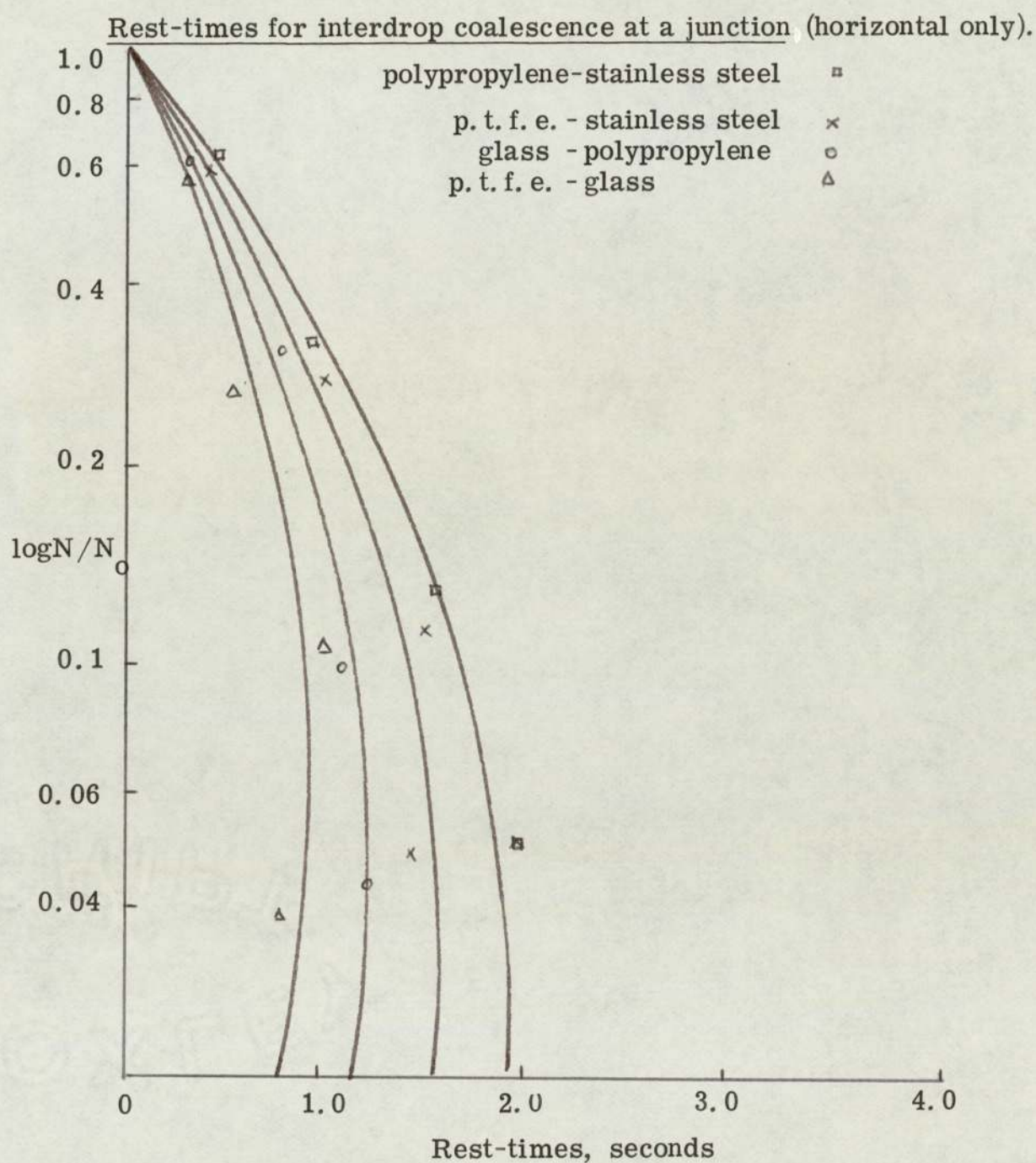


Dispersed phase liquid: distilled water; continuous phase

liquid: ethyl acetate; drop diameter ratio 1:3 (low surface energy

to high surface energy solid plate).

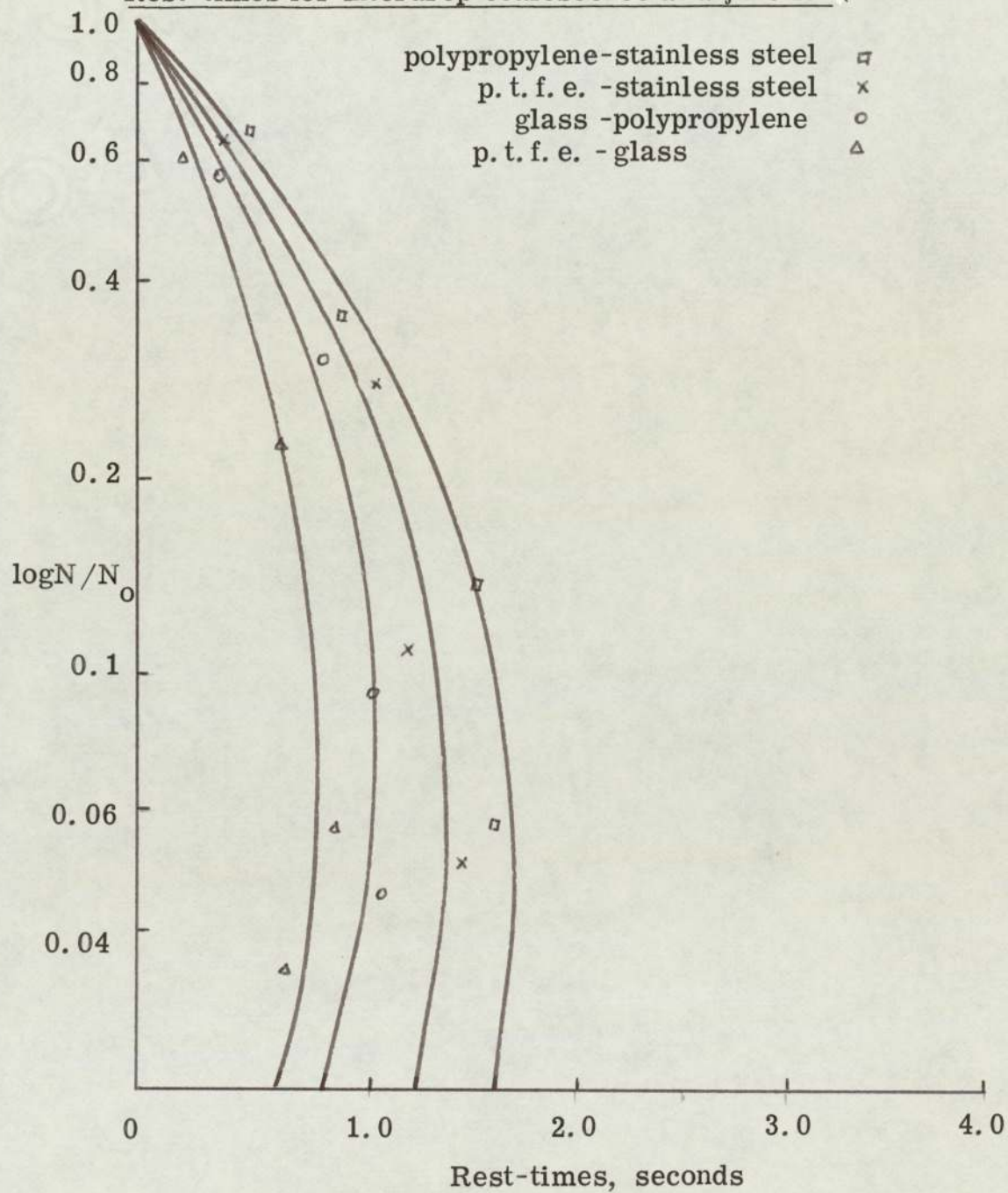
Figure 6.42.e.



Dispersed phase liquid: distilled water; continuous phase liquid: ethyl acetate; drop diameter ratio 3:1 (low surface energy to high surface energy solid plate).

Figure 6.42.f.

Rest-times for interdrop coalescence at a junction (horizontal only).



Dispersed phase: distilled water; continuous phase: ethyl acetate; drop diameter ratio 1:1 (low surface energy to high surface energy solid plate).

approaches in a direction parallel to the solid surfaces than when it approaches from any other angle, since in the latter case it is only the residual force parallel to the surface which is effective. If the approaching drop is very much larger than the first drop, the force causing film displacement will also be significantly less (Figure 6.43). The ideal situation for coalescence, i. e. the maximum impact from the approaching drop, is exerted when the deformed and approaching drop collides at a point of maximum diameter parallel to the junction surface with a point on the curvature of the other drop which is almost vertical to the direction of approach, as shown in Figure 6.43.

The radii of curvature of drops originally of equal size do not remain similar following contact with the different surfaces on either side of the junction. The radius will always be greater on the dispersed phase wetted side (Figure 6.43).

The points at the two curvatures at which the drops collide determine the surface area of contact between the drops. A small area results in a smaller volume of continuous phase liquid in the film and therefore a shorter rest-time. With a large ratio in the diameters, almost 50 % of the surface area of a smaller drop at a wetted component is contacted since it just fits the lower part of the approaching drop (Figure 6.43).

#### Surface energy of solid surface

The liquid in the film trapped between the drops at a junction flows under the influence of,

1. The force with which the liquid drop is adhering to the wetted surface, and
2. The kinetic force imparted by the approaching drop at the non-wetted surface.

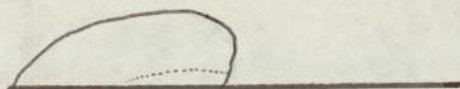
Figure 6.43.

Interdrop coalescence, between unequal sized liquid drops, at a junction

(a)  
Drop at wetted component drop at non-wetted component.

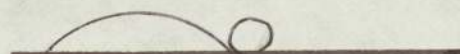


wetted component      non-wetted component  
The force imparted by the larger drop is almost parallel to the solid surface.



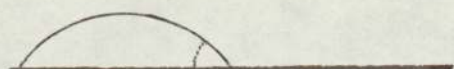
After coalescence, the larger droplet wraps round the smaller droplet. The smaller droplet is shown by a broken line.

(b)  
Drop at wetted component drop at non-wetted component.



wetted component      non-wetted component

The force imparted by the smaller droplet is tangential to the larger drop.



The smaller droplet coalesces in from a side to the larger droplet.

It is shown in Section 6.1.4.a. and Appendix D, that the interfacial tension between a liquid drop and a solid surface immersed in another immiscible liquid varies with the surface energy of the solid material. The force of interfacial tension corresponds to the force of attraction between the liquid and the solid surface and therefore to the force required to disengage the liquid from the solid surface. The higher the interfacial tension of the wetted component, the higher the force in the liquid drop to oppose any deformation in its surface. The liquid in the film is thus squeezed rapidly to give a short rest-time.

From the above discussion, the rest-time is shortened at a junction with two solid components, one of which gives a maximum and the other a minimum contact angle value.

Liquid-liquid interfacial tension: Liquid-liquid interfacial tension is effectively the force required to separate two liquids. For flow of the liquid in the film to occur, the flow pressure of the film liquid must overcome the force required to separate this liquid from the drop on either side of the film. Therefore, the lower the interfacial tension the higher is the flow pressure of the liquid in the film to reduce the rest-time between the drops.

The data in Figure 6.42, although limited in range since the main purpose was to assess the practical requirements for photography, can be correlated by an equation similar to Equation 1.1. This represents a way of ranking the junction efficiency.

$$\log N/N_0 = K. (t_0 - t)^n \quad (2.4.a.)$$

Clearly, the values of constants K and n will depend on the system properties. The time interval,  $t_0$ , during which no coalescence takes place can be determined by a junction with a maximum difference in the surface energies of the components.

#### 6.1.4. Coalescence behaviour at composite packings

The experimental results and observations of droplet behaviour at flat plates and packings of single material, and at plane composite surfaces were extended to behaviour in composite packings. As explained in Section 5.1., the composite packing for single drop studies consisted of a junction nozzle with a void.

The drop behaviour at such a packing is illustrated in Figure 6.44, which shows the drop arrival, passage and coalescence at this junction nozzle placed in a continuous phase liquid.

#### 6.1.4.a. Nozzle with a junction

Through the analysis of the forces acting on a drop at a void of a junction nozzle (Equation 6.5.), a third Equation (6.8.) was obtained. This involved determination of volume and surface area of the deformed drop at the void. The shape of this deformed drop was approximated to a geometrical model (Figure 6.45.), and the volume calculated from this model compared with the drop volume delivered (Appendix D) by the 'Agla' micrometer syringe.

The forces acting on a drop which has arrived at the junction with a nozzle were assumed to be gravity and buoyancy forces, and the surface forces of the two surfaces of the solid junction and of the liquid-liquid interfaces. The junction surface for coalescence did not consist merely of the mixed solid components, the surface of the void was also involved. The drop passed through the nozzle when gravity overcame the surface and the buoyancy forces. These forces were in a balance just prior to passage of the drop and the force balance equation may be written,

$$F_g = F_b + F_s \quad (6.5)$$

Gravity force,  $F_g$ , was calculated from the mass of the drop 'm' suspended in another immiscible liquid,

$$\begin{aligned} F_g &= m \times g \\ &= V \times \Delta\rho \times g \\ &= V.(\rho_1 - \rho_2).g \end{aligned} \quad (6.5.1.)$$

where 'V' is the volume of the drop given by Equation (C.8)

Substitution of the value of V from Equation (C. 8) into Equation (6. 5. 1.) yields the following expression for the gravity force.

$$F_g = \left[ 4\pi R^2 \cdot (R/3 = C\pi/4) + 2\pi R \cdot C^2 + \pi d^3/12 \right] (\rho_1 - \rho_2) \cdot g \quad (6. 5. 2.)$$

Surface forces.  $F_s$ : These resulted when a drop was in Contact with both a solid and a liquid surface,

$$F_s = F_r + F_i \quad (6. 6.)$$

where  $F_r$  is the force due to the surfaces of the junction materials. Since there were two solid surfaces involved in a junction, the resultant effect was given by  $F_r$  as in Equation (6. 4)

At a liquid-liquid interface, there is a force of tension from one liquid to the other. A horizontal bulk interface between the two liquids results since the tension from each liquid is equal but in an opposite direction. Both the drop and the interface deform as the drop approaches. Assuming that the dispersed phase liquid exerts a force  $\gamma_d$  in one direction and the continuous phase a force  $\gamma_c$  in the other, the resultant of these two was taken as the force of interfacial tension between the two liquids, i. e.  $\gamma_{dc}$

$$F_i = \gamma_{dc} \cdot S \quad (6. 6. 1)$$

Substitution of 'S' from Equation (C. 19) into Equation (6. 6. 1) yields the expression for  $F_i$

$$F_i = \left[ 4\pi R \cdot (R + \pi C/2) + \pi C^2 + \pi d_v^2/2 \right] \cdot \gamma_{dc} \quad (6. 6. 2).$$

Substitution of  $F_r$  from Equation (6. 4) and  $F_i$  from Equation (6. 6. 2.) into Equation (6. 6.) yields,

$$F_s = \gamma_{dc} (\cos \theta_{wd} - \cos \theta_{wc}) + (\gamma_{nc} - \gamma_{wc}) + 4 \gamma_{dc} \pi R (R + \pi C/2) + \pi C^2 + \pi d_v^2/2 \quad (6. 6. 3).$$

Buoyancy force,  $F_b$ : The force which tended to propel the drop upwards (or downwards) is given by,

$$F_b = \Delta \rho \cdot g \cdot h^2 / 2 \cdot \gamma_{dc} = (\rho_1 - \rho_2) \cdot g \cdot h^2 / 2 \cdot \gamma_{dc} \quad (6.7)$$

where 'h', the height of the drop, was taken as equal to the diameter of the original drop. 'h' was calculated from Equation (C. 8) which gives the drop volume V.

$$V = \pi \cdot h^3 / 6 \quad (6.7.1)$$

$$h = (6 \cdot V / \pi)^{0.33} \quad (6.7.2)$$

Substitution of 'h' from Equation (6.7.2.) into Equation (6.7.) yields,

$$F_b = (\rho_1 - \rho_2) \cdot g \cdot (6 \cdot V / \pi)^{0.66} / 2 \cdot \gamma_{dc} \quad (6.7.3)$$

Now substitution of the value of  $F_g$  from Equation (6.5.2.),  $F_s$  from Equation (6.6.3.) and  $F_b$  from Equation (6.7.3.) into Equation (6.5.) yields,

$$\gamma_{nc} - \gamma_{wc} = K \quad (6.8.)$$

where 'K' is given by,

$$K = F_g - F_b - F_s \quad (6.8.1.)$$

A fourth Equation (6.9.3.) was obtained by modifying an Equation (6.9.) proposed for vapour-liquid-solid systems.

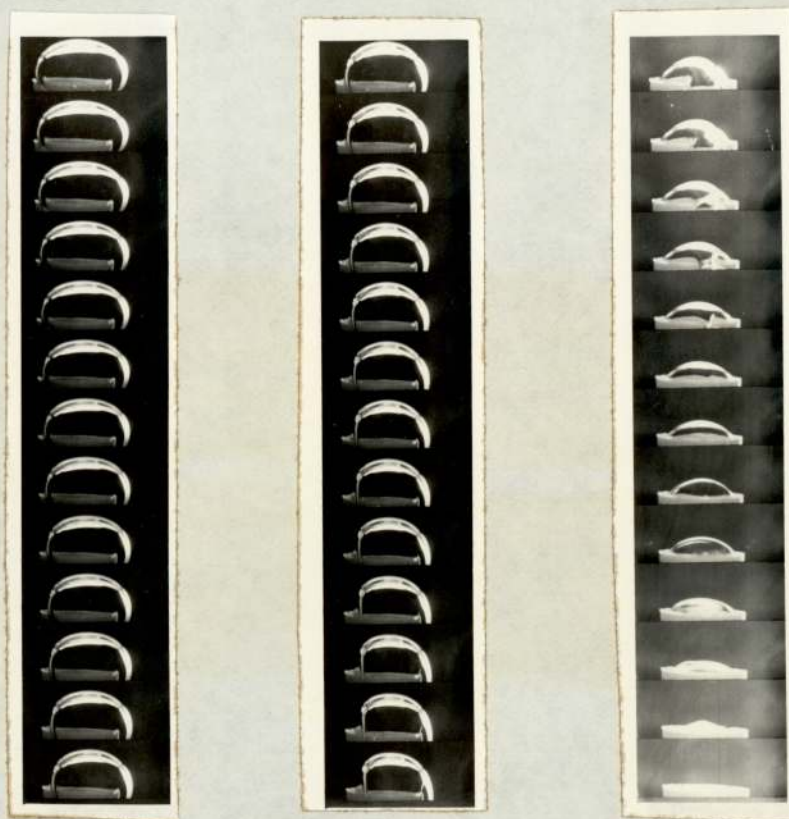
Conditions in a liquid-liquid system have been related by Equation (6.9) to conditions in the corresponding vapour-liquid system by,

$$\gamma_{da} \cdot \cos \alpha_{wda} - \gamma_{ca} \cdot \cos \beta_{wca} = \gamma_{dc} \cdot \cos \theta_{wd} \quad (6.9)$$

Equation (6.9) should enable the calculation of the contact angle of a liquid drop at a solid surface immersed in another immiscible liquid from the values of the contact angles of the two liquids at the same solid plate placed in air.

Figure 6.44.

Coalescence of a liquid drop at a void  
with a junction



(a) passage through a junction nozzle.

Void surface : p. t. f. e. (outside)- glass (inside);

Dispersed phase : deionised, distilled water;

Continuous phase : toluene;

Ratio of drop dia to void size : 3.013.

Figure 6. 44. a.

Passage of a liquid drop through a junction nozzle

Dispersed phase liquid	: deionised, distilled water;
Continuous phase liquid	: toluene;
Junction materials	: p. t. f. e. (outside)- glass (inside);
Void diameter	: 3.27 mm.
Drop diameter	: 8.76 mm.

Figure 6.45. a

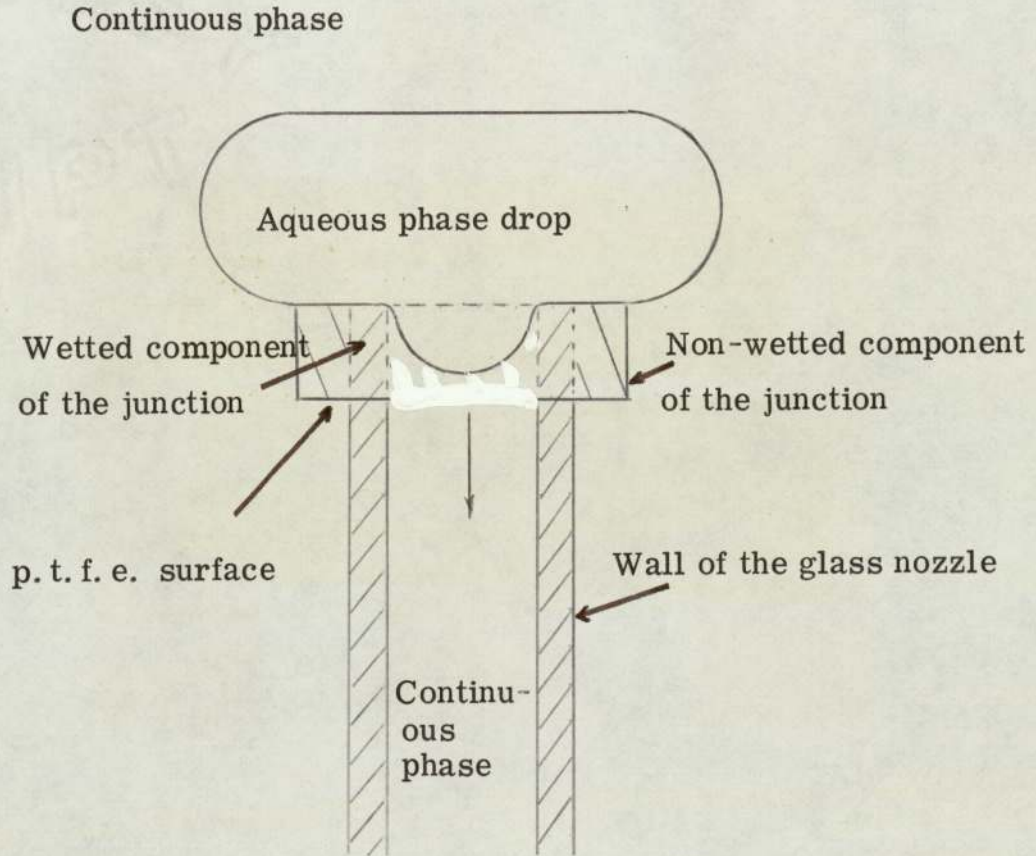
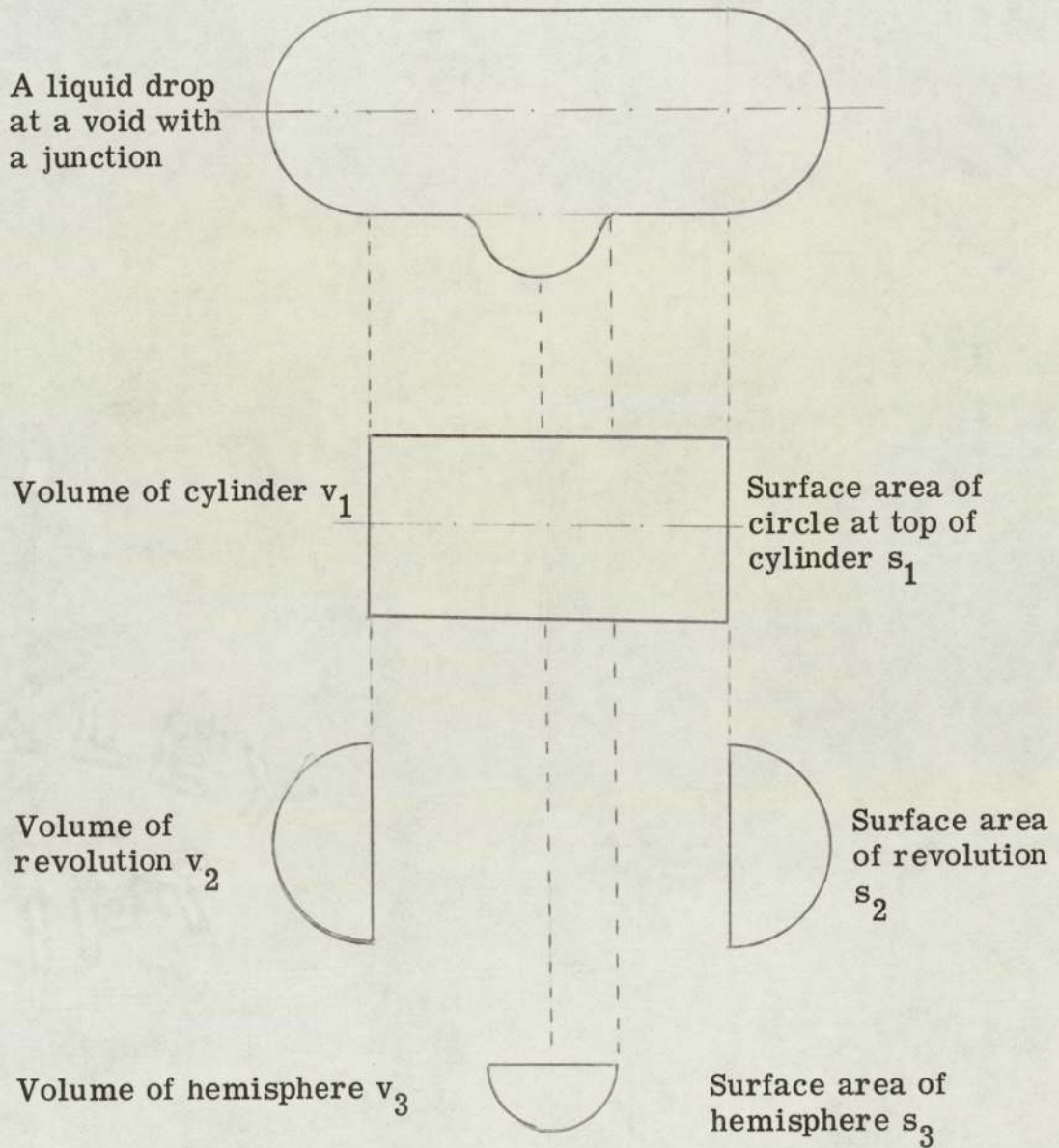
A liquid drop at a nozzle with a junctionA liquid drop at a void with a junction.

Figure 6. 45. b.

Calculation of drop volume,  $V_c$ , and liquid-liquid interface surface area,  $S$ .



Rearrangement of Equation (6. 9) gives,

$$\cos \alpha_{wda} = ( \gamma_{dc} \cdot \cos \theta_{wd} + \gamma_{ca} \cdot \cos \beta_{wca} ) / \gamma_{da} \quad (6. 9. 1.)$$

The interfacial tension of an air-solid system has been related by Equation (6. 9. 2. ).

$$2. \gamma_{wda} = \gamma_{da} ( 1 + \cos \alpha_{wda} ) \quad (6. 9. 2)$$

Substitution of the value of  $\cos \alpha_{wda}$  from Equation (6. 9. 1. ) into Equation (6. 9. 2. ), and by replacing  $\gamma_{da}$  by  $\gamma_{dc}$ , Equation (6. 9. 3. ) results.

$$\gamma_{wd} = \gamma_{dc} / 2. \gamma_{da} ( \gamma_{da} + \gamma_{dc} \cos \theta_{wd} + \gamma_{ca} \cdot \cos \beta_{wca} ) \quad (6. 9. 3.)$$

Equation (6. 9. 3. ) required the air-liquid contact angle values of the systems investigated. These values were measured experimentally and are shown in Appendix L.

The individual values of the interfacial tensions of the solid components of the junction and the liquids of the continuous and dispersed phases i. e.  $\gamma_{wd}$ ,  $\gamma_{nc}$ ,  $\gamma_{nd}$  and  $\gamma_{wc}$ , were calculated using four equations i. e. (6. 2), (6. 3), (6. 8) and (6. 9. 3). The calculated values are shown in Appendix D.

According to Equations 6. 2 and 6. 3, the values of  $\gamma_{wd}$  and  $\gamma_{wc}$  should be higher than the corresponding values of  $\gamma_{nc}$  and  $\gamma_{nd}$  respectively for any given drop size. The calculated values of  $\gamma_{wd}$ ,  $\gamma_{wc}$ ,  $\gamma_{nc}$  and  $\gamma_{nd}$  (Appendix D. ) satisfied this requirement.

The derivation of  $\gamma_{wd}$ ,  $\gamma_{wc}$ ,  $\gamma_{nd}$  and  $\gamma_{nc}$  from experimental data enabled a comparison to be made, for the first time, between the 'real' values of, e. g.  $\gamma_{wd}$  and  $\gamma_{wc}$  and the calculated difference between them using Equations (6. 2) or (6. 3)

$$\gamma_{wd} - \gamma_{nc} = \gamma_{dc} \cos \theta_{wd} \quad (6.2)$$

$$\gamma_{nd} - \gamma_{wc} = \gamma_{dc} \cos \theta_{wc} \quad (6.3)$$

On rearrangement, Equations (6.2) and 6.3) yield,

$$(\gamma_{wd} - \gamma_{nc}) / \gamma_{dc} = \cos \theta_{wd}$$

$$(\gamma_{nd} - \gamma_{wc}) / \gamma_{dc} = \cos \theta_{wc}$$

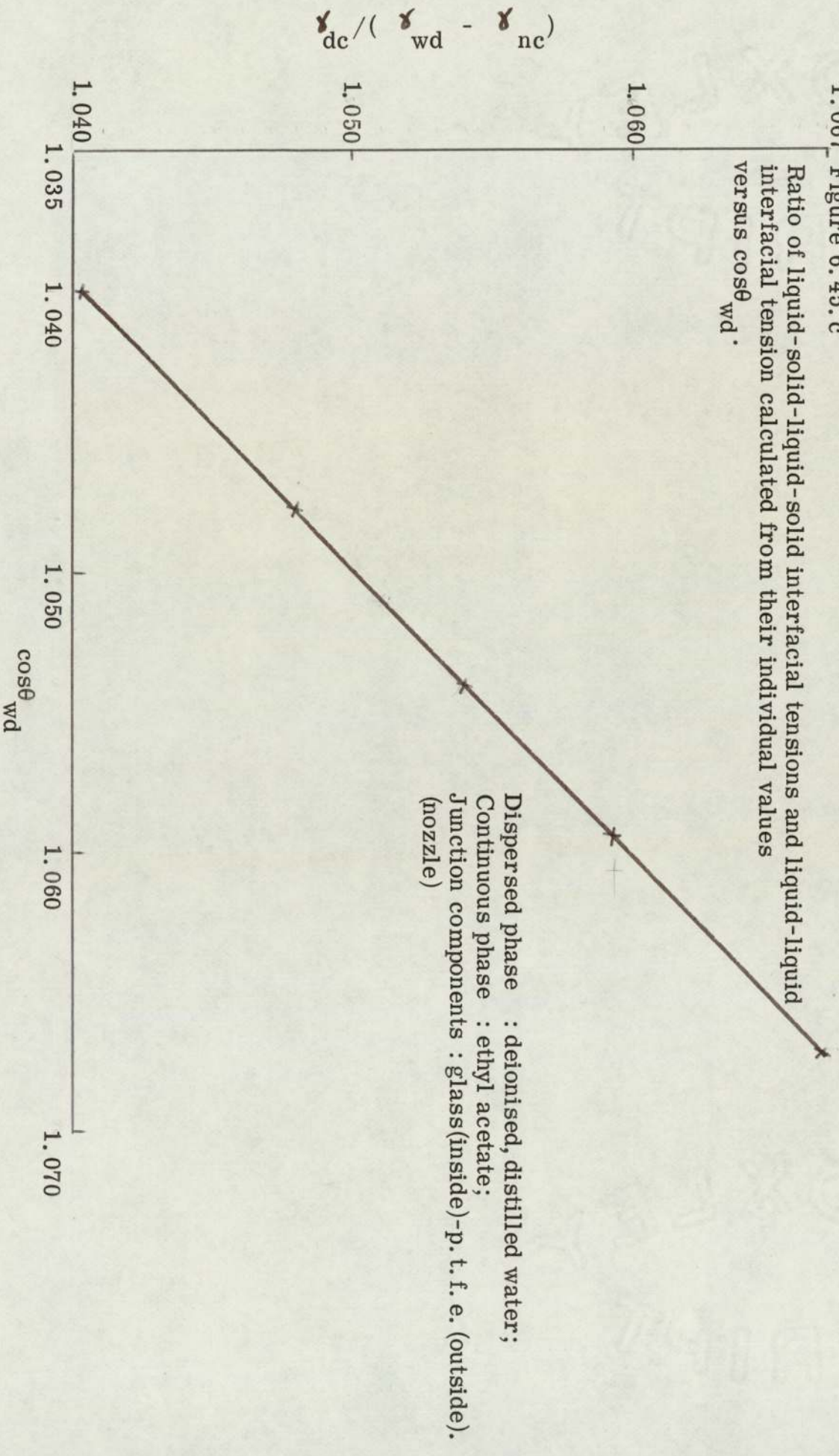
For convenience, comparison was made in terms of the ratios of the respective interfacial tension of the liquid-liquid system to the difference between the liquid-solid/liquid-solid interfacial tensions. All the results are shown in Appendix D. The plots, of ratios of liquid-liquid interfacial tension  $\gamma_{dc}$  to the difference between solid-liquid interfacial tensions i. e.  $(\gamma_{wd} - \gamma_{nc})$  calculated from their individual values versus experimental values of  $\cos \theta_{wd}$ , in Figures 6.45c. to 6.45.g confirm that the ratios coincided upto fourth decimal place in almost 80 % of the cases examined and the divergence in the other 20% of the cases was less than 10%. This confirms that the calculated values of the solid-liquid interfacial tensions are consistent and adds support to the background theory. By analogy with liquid-liquid interfacial tension, solid-liquid interfacial tension may be regarded as the force required to separate a specific liquid from a specific solid. The values of the solid-liquid interfacial tensions were relatively high for those systems where the contact angle of the dispersed phase liquid drop at the solid surface was less than  $90^\circ$ . The higher the interfacial tension the smaller was the angle. The contact angle may therefore be regarded as a means to quantify the forces of attraction between the molecules of a liquid and a solid. As the surface area of contact between a drop and a solid surface is increased, i. e. with a larger drop or a roughened surface, the force of attraction also increases with increasing drop size.

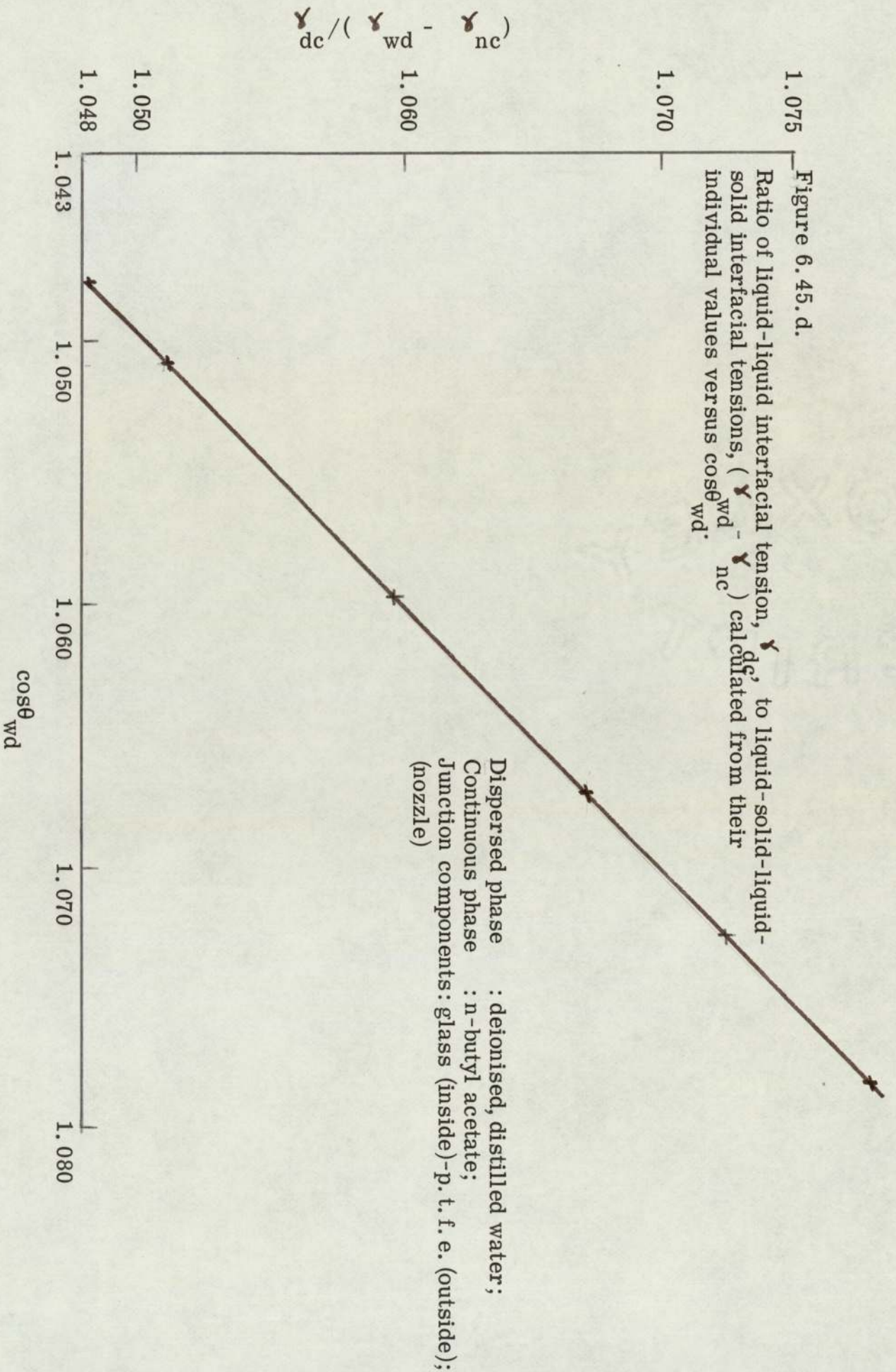
#### 6.1.4. b. Other geometrical arrangements

As mentioned earlier, no information has been published on the enhanced coalescence effect observed with packing of

1.067 Figure 6.45. c

Ratio of liquid-solid-liquid-solid interfacial tensions and liquid-liquid interfacial tension calculated from their individual values versus  $\cos\theta_{wd}$ .



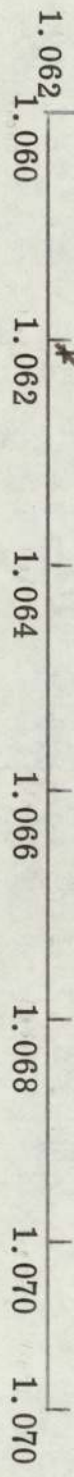


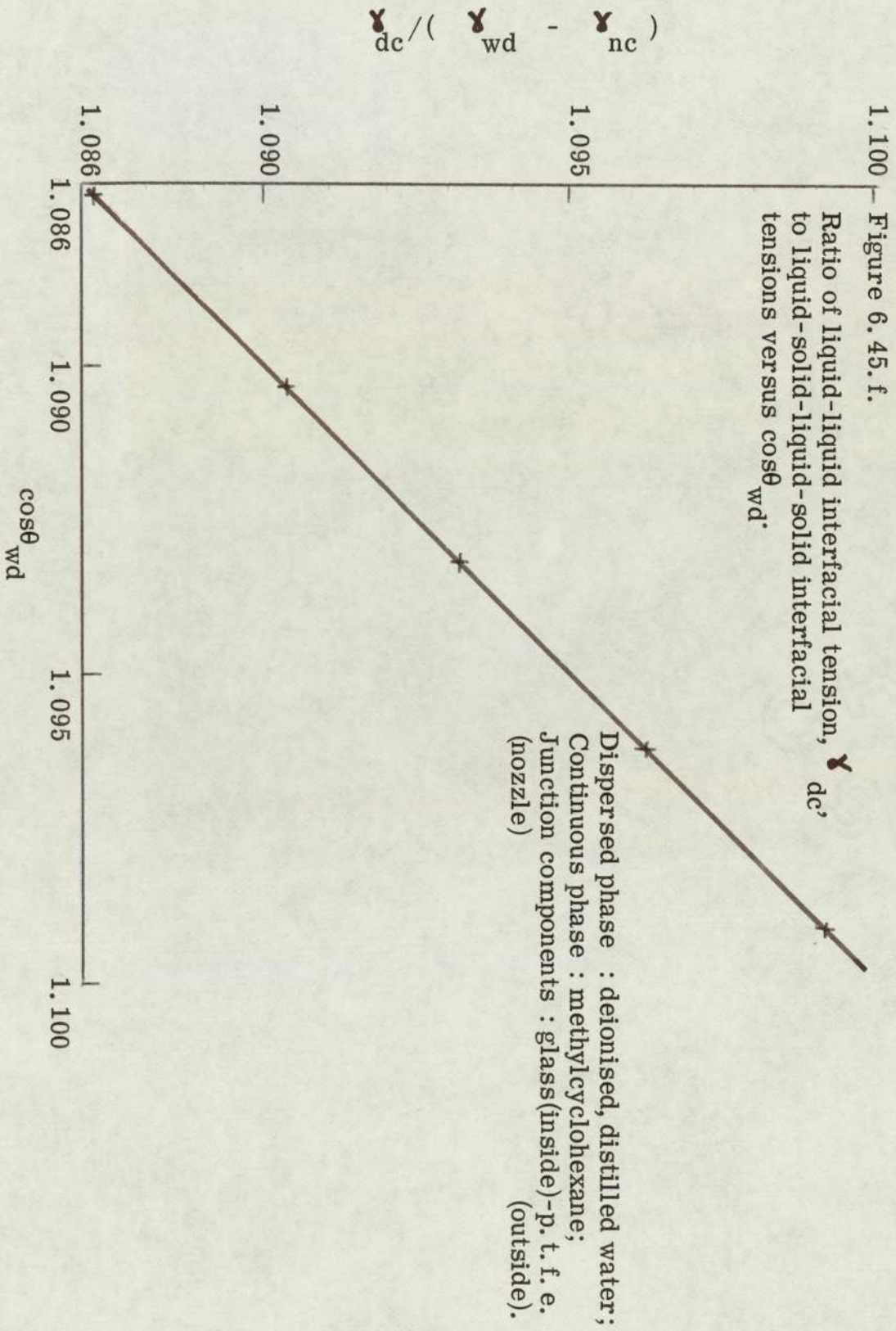
$$\frac{\gamma_{dc}}{(\gamma_{wd} - \gamma_{nc})}$$

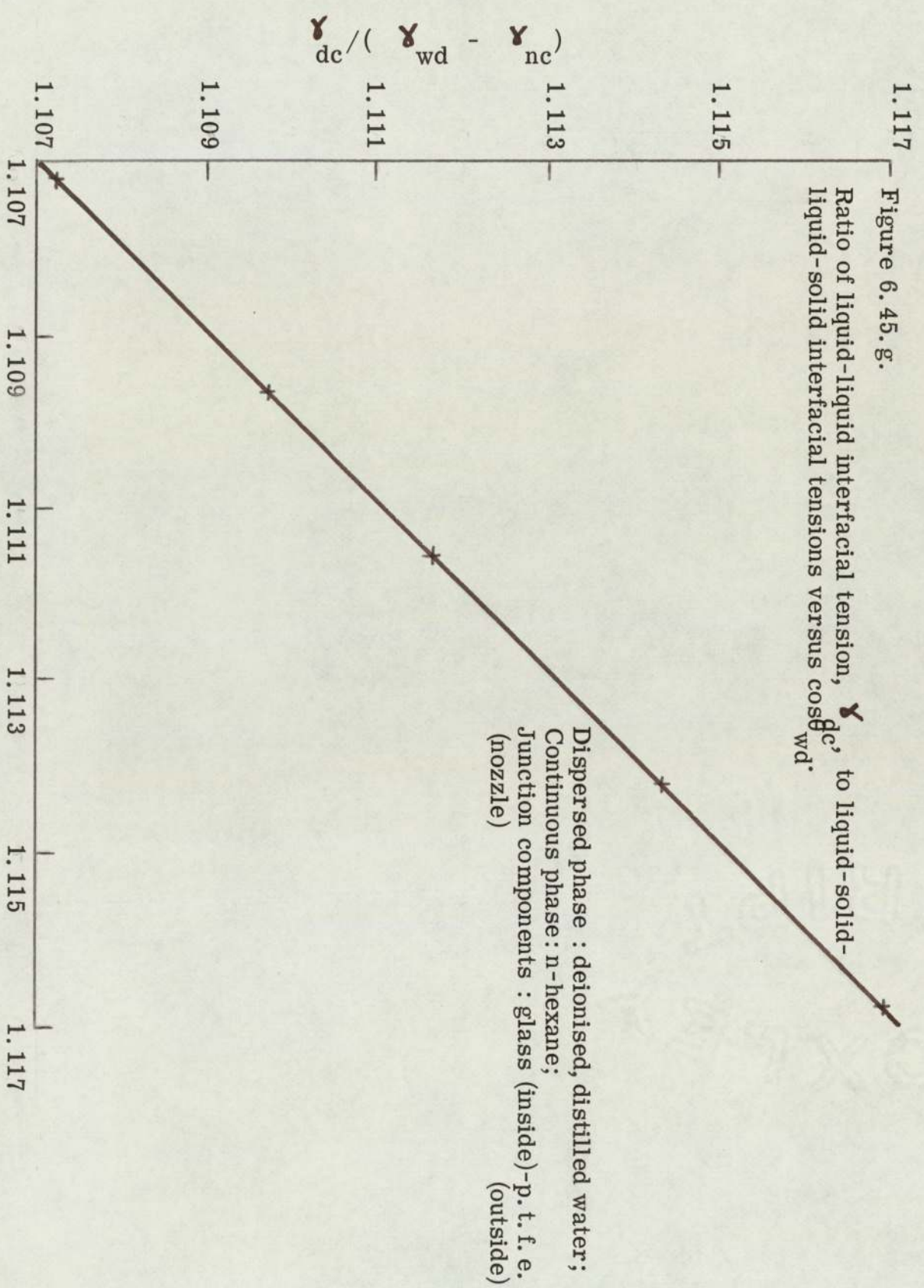
Figure 6. 45. e.

Ratio of liquid-liquid interfacial tension,  $\gamma_{dc}$ , to liquid-solid-liquid - solid interfacial tensions,  $(\gamma_{wd} - \gamma_{nc})$  versus  $\cos\theta_{wd}$ .

Dispersed phase: distilled, deionised water;  
 Continuous phase: toluene;  
 Junction components: glass (inside)-p. t. f. e.  
 (nozzle) (outside)







mixed components i. e. high and low surface energy solid materials. The effect of a junction on coalescence was investigated with flat composite surfaces and the mechanisms are explained in Section 6.1.3. and in Figure 6.41. However, in an industrial coalescer, packings are generally used rather than plane solid surfaces. Therefore, the observations and results obtained with plane solid composite surfaces were extended to meshes of special construction as described in Section 5.1.1.

The behaviour of single liquid drops on a thin horizontal metallic wire of 0.31 mm. diameter and wetted' by the drop phase depended upon the relative ratio of the drop diameter to the diameter of the wire filament. It also depended upon the energy with which the drop arrived at the wire. Drops larger than 3 mm. diameter and travelling about 4 cm. distance to reach the wire ruptured into two segments on impact. When the distance of fall was decreased to less than half a centimeter to deliver a similar drop gently, it did not balance on the wire but rolled over and left from one side. However, drops of less than 1.5 mm. diameter stayed at the wetted surface of the wire but rolled over and adhered to the underside.

As expected drops allowed to impinge upon a non-wetted filament, over a range of sizes and diameter ratios, were never retained by a filament. The only possible exception to this would be on a filament so roughened that cavities were somehow created and filled with dispersed phase so as to create drop-liquid interfaces.

At a crosswire junction of filaments of the same wetted material the size of the drop that resided at the junction was greater than that with a single filament. This would be expected because of the increased area of contact and the increased number of support points. With a cross wire junction of 0.31 mm. diameter wire, drops of upto 2.75 mm. diameter stayed

at the cross since the diameter at the cross was not the same as that of the single wire. However, as expected, the single drops did not stay at a non-wetted cross wire.

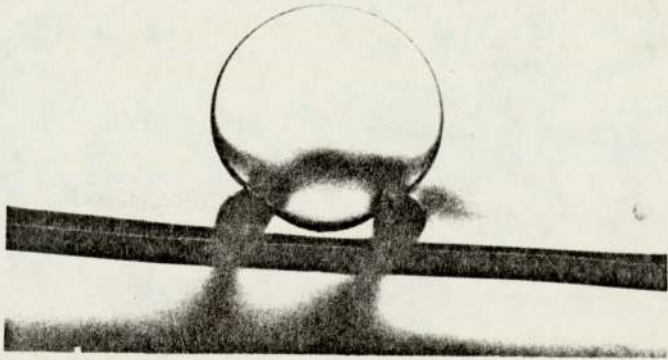
With cross wires of mixed components, with the non-wetted filament uppermost, the drops tilted away gradually from the non-wetted to the wetted surface, and with the exception of small drops of less than 1.75 mm. diameter left the wire. The small drops were retained since they adhered to the underside of the wetted component.

At a single aperture woven from 'wetted' wire, drop behaviour was similar to that discussed in Section 6.1.2. where single drops larger than the equivalent aperture size could not pass through it. Similarly, with a square-shaped aperture of mixed components, with the opposite sides of the same material, the drops larger than the aperture size rested at the aperture (Fig. 6.45c). This was unlike the behaviour at a nozzle with a junction (Section 6.4.) where drops much larger than the circular void could pass through the nozzle due to the effect of junction symmetry. With an aperture woven from wires with adjoining pairs of sides of similar materials, a drop larger than the aperture size could still not pass through. However, it was deformed slightly since it inclined towards the wetted component.

A cubical aperture was made by soldering together pieces of thin insulated wire of equal lengths. The plastic material (pvc) of insulation was peeled off from alternate threads to expose metallic surface to form the junctions  
In this manner, a double-storey aperture was provided. Any drop larger than the first aperture was of course retained. This was not

Figure 6.45. c.

A liquid drop at a composite packing



The drop is resting at non-wetted filaments only  
and is not in contact with the wetted filament.

altered by the addition of further drops which merely resulted in a deformed globule. A large drop delivered to the second aperture was not displaced by subsequent delivery of a large drop to the first aperture; indeed no coalescence occurred.

This confirmed that drop behaviour in a three-dimensional bed containing junctions can be generalised from the single wire, cross wire and single aperture mechanisms. The behaviour of single liquid drops at apertures of mixed components could not, however, be predicted from the mechanisms observed with junctions at flat plates or nozzles. This was because two factors were not common. Firstly, the ratio of the free surface of the drop to the surface in contact with the solid for the same size drops was at least ten times higher on an aperture than on a flat junction plate. Secondly, the geometrical shape of the solid surfaces is important which was different in the above cases. These factors tend to enhance or diminish the junction effect.

The junction mechanism was determined with flat surfaces which is an ideal situation. With a woven aperture, the solid surface is neither smooth nor horizontal i. e. the surface of the wire is circular. With a composite packing, the relatively small kinetic force available to assist drop passage from a small area of contact with the non-wetted filament is distributed on either side of the filament. In an ideal situation at a junction nozzle, the composite surface is distributed symmetrically to coincide with the symmetry of the base of the drop; hence the forces act along the base to enhance the passage. Conversely, at an aperture, the directions in which these forces act are not symmetrical; they are distributed depending upon the geometrical shape of the aperture. It follows that better coalescence performance should be possible from a composite packing if the

geometrical shape of the void coincides with that of the base of the drop. The best situation would be where the inlet layer of the packing is of mixed components to enhance passage, collection and coalescence, and the exit layer of single material either wetted by the dispersed phase to obtain large drops or of non-wetted material for smaller drops at a larger throughput. In either case, the intermediate zone should consist of non-wetted material alone to accelerate the flow of the dispersed phase through the packings. In practice drops travelling to the inlet of a packing tend to move away from the column/pipe wall. Hence on arrival at the packing, the drops are not equally distributed across the inlet. This can be overcome by using a convex shaped inlet layer of composite material. This will distribute the drops away from the centre; in this manner more surface of the packing can be utilised by the coalescing drops thus avoiding flooding. A further improvement to limit complete distribution to the column wall would be a convex composite inlet surface with equally spaced indentations of the order of one drop diameter across.

## 6. 2. Coalescence of Swarms of Drops

One aim of this work was to extend the preliminary findings of the behaviour of single drops at flat surfaces (Section 6. 1. ), meshes (Section 6. 1. 2. ) and nozzles (Section 6. 1. 4. ) to packed columns incorporating a bed constructed of mixed components i. e. high and low surface energy materials. This involved observation of the behaviour of swarms of drops at the voids of a junction bed.

Only aqueous dispersions were investigated since the single drop studies showed that the general mechanisms of coalescence were the same irrespective of the liquid in the drop.

### 6.2.1. Prediction of exit drop size

The coalescence of aqueous dispersions was studied in a 3" diameter QVF glass column packed with a junction coalescer (Section 5.2) constructed from mixed components.

The factors which were considered to affect the coalescence of liquid dispersions in a composite packing are analysed in Appendix J. Contact angle was used as a characterisation of 'wetting' conditions. Dimensional analysis was performed on these variables and ten dimensionless groups were obtained. The regression coefficients of these ten groups were evaluated using a statistical analysis Mark 2 computer program (Appendix J.) The values of regression coefficients of groups 2, 3, 6 and 7 were found to be zero. The other six groups were renamed as follows:

Group 1 & 4	Bond Number
Group 5	Height Number
Group 8	High Surface Energy Number
Group 9	Low Surface Energy Number
Group 0	Drop Number

Regression analysis was carried out on these groups but a satisfactory correlation could not be obtained because of two separate groups for the junction effect i. e. high and low surface energy groups. These two groups were therefore combined to give the Junction Number.

$$\text{Drop Number} = K. (\text{Bond Number})^a. (\text{Height Number})^b. (\text{Junction Number})^c \quad (\text{J. 11})$$

Experiments were designed based upon Graeco-Latin squares (Appendix J). Experimental values were then substituted in the Bond Number, Height Number and Junction Number respectively.

The values of constant K, a, b and c were evaluated by carrying out a multiple regression analysis (Appendix J.) on the above three independent dimensionless groups at 99% significant level, with Drop Number as the dependent variable, for the coalescence of aqueous dispersions in each of the four organic liquids i. e. butyl acetate, toluene, methylcyclohexane and n-hexane. The method of analysis of results is fully explained in Appendix J. Evaluation of K, a, b and c, in this way (Equation J. 11), yielded the correlation:

$$d_o/d_i = K. (\Delta\rho \cdot d_i^2 g/\gamma)^a \cdot (d_i/h_b)^b \cdot \left[ \left\{ (d_{nd}^2 - d_{wd}^2) \cdot \cos \theta + (d_{wd}^2 - d_v^2) \cdot \cos \alpha \right\} / d_i^2 \right]$$

where  $d_o/d_i$  = Drop Number;  $d_i/h_b$  = Height Number;  
 $\Delta\rho \cdot d_i^2 g/\gamma$  = Bond Number; and

$$\left[ (d_{nd}^2 - d_{wd}^2) \cdot \cos \theta + (d_{wd}^2 - d_v^2) \cdot \cos \alpha \right] / d_i^2$$

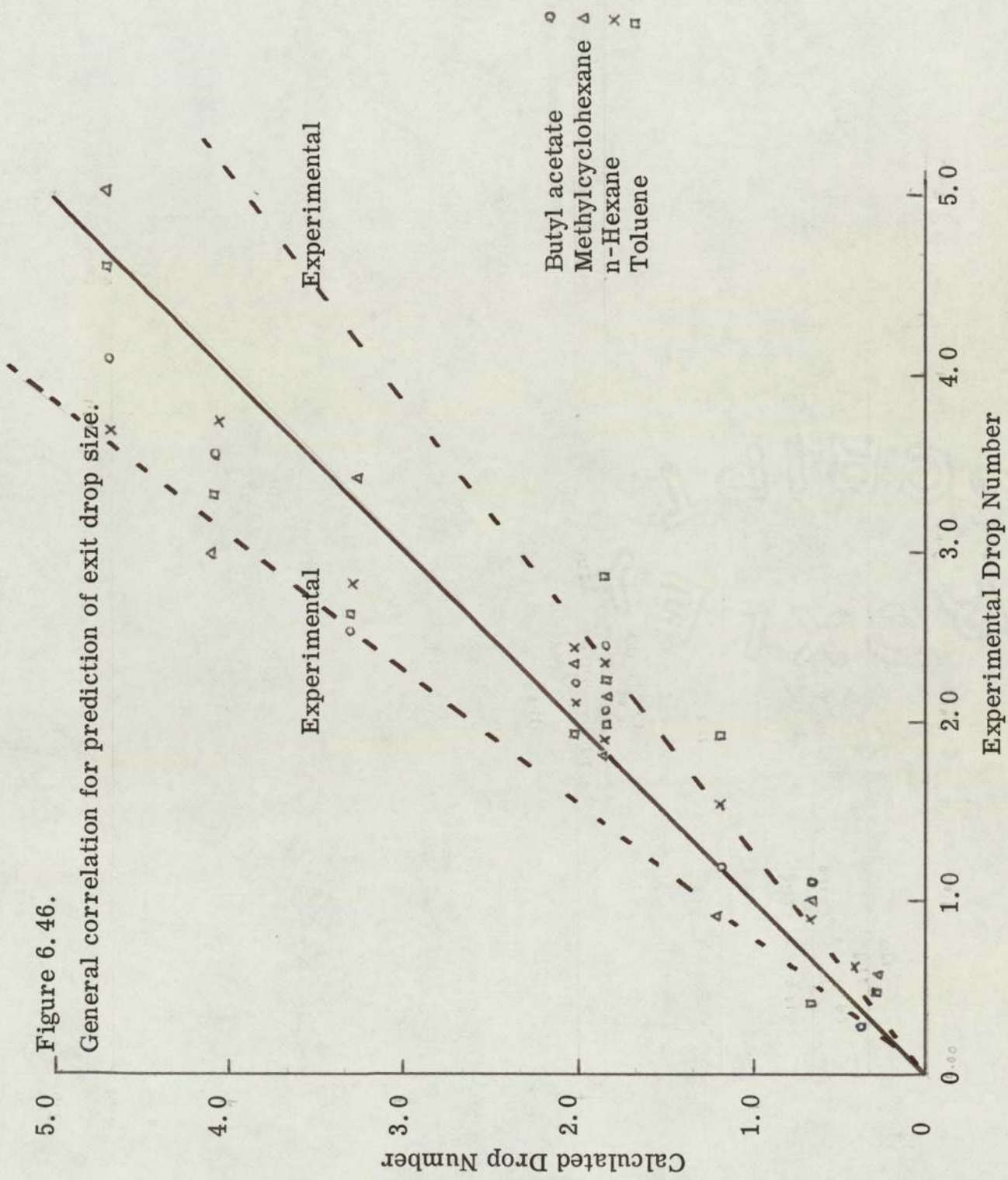
= Junction Number

and K = 0.724; a = 0.273; b = 0.091 and c = 1.220

The accuracy of the correlation was checked by substitution of the experimental values of Bond, Height and Junction numbers in the above expression to give the calculated Drop Number (CDRPNO). This was compared with the experimental value (EDRPNO). The percentage difference between CDRPNO and EDRPNO was also computed (Appendix J). An agreement of  $\pm 20\%$  was found as shown in Figure 6.46 and Appendix J. Inaccuracies were inevitably introduced by interdrop coalescence between entering drops, and between drops prior to detachment from the outlet, and passage of smaller drops. Furthermore, difficulty arose in the substitution of values of

Figure 6.46.

General correlation for prediction of exit drop size.



Experimental

Experimental

- Butyl acetate
- Methylcyclohexane
- n-Hexane
- Toluene

the contact angles i. e.  $\theta$  and  $\beta$ , in the Junction Number. The values of the contact angles vary in the same system with the size of the drop. In any inlet dispersion, a distribution was found (Appendix H) in the drop size, whereas in the Junction Number expression, only one value of drop size was required for contact angle purposes. This difficulty was, however, resolved by calculating the average diameter from the photographs of the dispersions. The contact angle values corresponding to this mean droplet size were used in the correlations. In view of these limitations, the accuracy obtained was considered acceptable.

### 6.2.2. Coalescence mechanisms

#### 6.2.2.a. Inlet mechanisms

The inlet coalescence mechanisms depended on the following factors (Appendix H):

(a)  $N_a$ , the number of drops in the monolayer at the inlet of the coalescer.  $N_a$  was assumed to be the same as the number of holes in the distributor producing the dispersion. The same number of drops was assumed to be present in each subsequent layer of the dispersion. Therefore,  $N_a$  does not include the number of satellite drops, which follow the primary drops as they detach from the distributor.

(b)  $N_c$ , the number of coalescence sites available at the inlet of the coalescer. This number was taken as the number of voids in the coalescer. In the composite coalescer, the number and the geometry of the voids could be controlled and were in fact the same both at the inlet and outlet of the coalescer; therefore,  $N_c$  was readily available.

(c) From above  $N_a - N_c/N_c$  is the ratio of the number of drops which could not have a coalescence site at the voids to the total number of sites available.

(d)  $(d_{vs})_i$ , the Sauter mean diameter of the drops arriving at the coalescer, and  $\% (d_{vs})_i$ , the standard deviation from the Sauter mean diameter due to the distribution in the drop size found at the inlet. This distribution arose because of the satellite drop formation, rupture of drops upon impact, and following interdrop coalescence at the inlet.

(e)  $(d_{vs})_i/d_v$ , the relationship between the size of the drop at the inlet and the void size.

Interdrop coalescence occurred between drops of the same size, i. e. two or more primary drops or two or more satellite drops to produce a single larger drop, or between the drops of unequal sizes. Irrespective of the size of the larger drop thus produced, coalescence of this drop occurred at the void and the coalesced mass of the liquid flowed down the nozzle.

Amongst the drops detaching from the outlet (Figure 6.47.), 5 % were of the same size as the smaller droplets present at the inlet. These could have arisen either due to impact of drops with the solid surface causing breakdown into smaller droplets, or from satellite drops from the distributor plate. Most of the other drops coalesced at the inlet via a chain-type interdrop coalescence process and some interdrop coalescence occurred inside the nozzles. Upto four drops could gather round the void for an interdrop coalescence. Sometimes only two of these coalesced first and passed through the nozzle to be followed by the remaining two as discrete drops. At other times, three or all four drops coalesced together and passed through the nozzle.

The drops first occupied the voids at the inlet of the coalescer. This was followed by a continuous chain of interdrop coalescence, i. e. a drop passing through the void coalesced

with another drop retained at the void etc. When the number of drops arriving was large compared to the sites available for coalescence, some drops coalesced at the junction between the wall of the glass column and the p. t. f. e. surface of the coalescer; a layer of the dispersed phase liquid thus built up only near the wall. As the height of the coalesced mass grew above about two drop diameters, the mass flowed down onto the p. t. f. e. surface and towards the nearest glass void; here it passed down the void after coalescing with the drops residing there.

A graping effect has often been observed at the exit of packings when some of the continuous phase liquid is trapped in during formation of the dispersed phase drop. In this study, this effect was noted at both the inlet and the outlet of the coalescing aid. Although the continuous phase was kept stationary, a local flow of the continuous liquid occurred due to displacement in the channels by the dispersed phase. This continuous phase flow was induced countercurrent to the dispersed phase and its extent depended upon the rate of droplet arrival. It was, however, only observed at selected channels. Grapes of continuous phase liquid were therefore observed forming at the inlet in the medium of the dispersed phase liquid drops and detaching from there. The selected sites became available because of the pressure differential caused by the discontinuity in the drops occupying that channel. Once a site was selected for graping at the inlet, it remained open; the situation could only be altered by increasing the velocity of the dispersed phase liquid or by shutting off and restarting operation. (Figure 6.48 ).

Figure 6.47.

Distribution in drop size at packing exit



### 6.2.2.b. Exit mechanisms

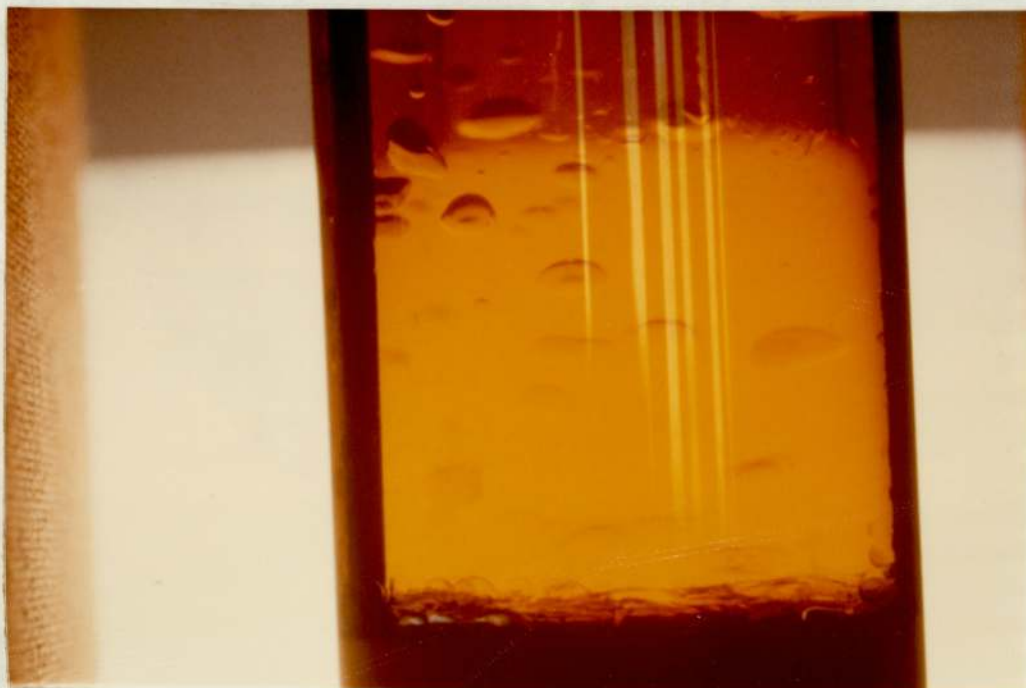
The outlet mechanisms i. e. drop formation at the exit of the coalescer, for a fixed bed height was determined from the following factors (Appendix H):

- (a)  $(d_{VS})_O$ , the Sauter mean diameter of the drops detaching from the voids at the exit of the coalescer;  $\%(d_{VS})_O$  the standard deviation in the Sauter mean diameter due to the distribution in the drop size at the outlet.  $\%(d_{VS})_O$  was lower than at the inlet but arose due to the passage of uncoalesced small satellite or broken drops through the nozzle. However, satellite drops were observed being produced at the outlet as well. When a large drop greater than 0.9 cm. detached from the outlet, more than one satellite drop was formed. Such large drops usually detached following an interdrop coalescence between two adjacent growing drops at voids when the inter-void distance was less than the diameter of the void.
- (b)  $d_V$ , the diameter of the void; larger drops were formed at the larger voids for the range investigated
- (c) The material of the void; larger drops were also formed at the voids wetted by the dispersed phase liquid.

In the junction coalescer used,  $d_V$  was the same both at the inlet and outlet since the voids consisted of straight glass tubes of uniform diameter and these tubes were inserted into the holes drilled in the p. t. f. e. solid plate.

- (d)  $(d_{VS})_O/d_V$  gives a relationship of the diameter of the drop at the exit of the coalescer to the diameter of the void. The fact that values of  $(d_{VS})_O/d_V$  are within 5 % for one solid-solid-liquid-liquid system indicates good control of drop size at the exit.

Figure 6. 48.

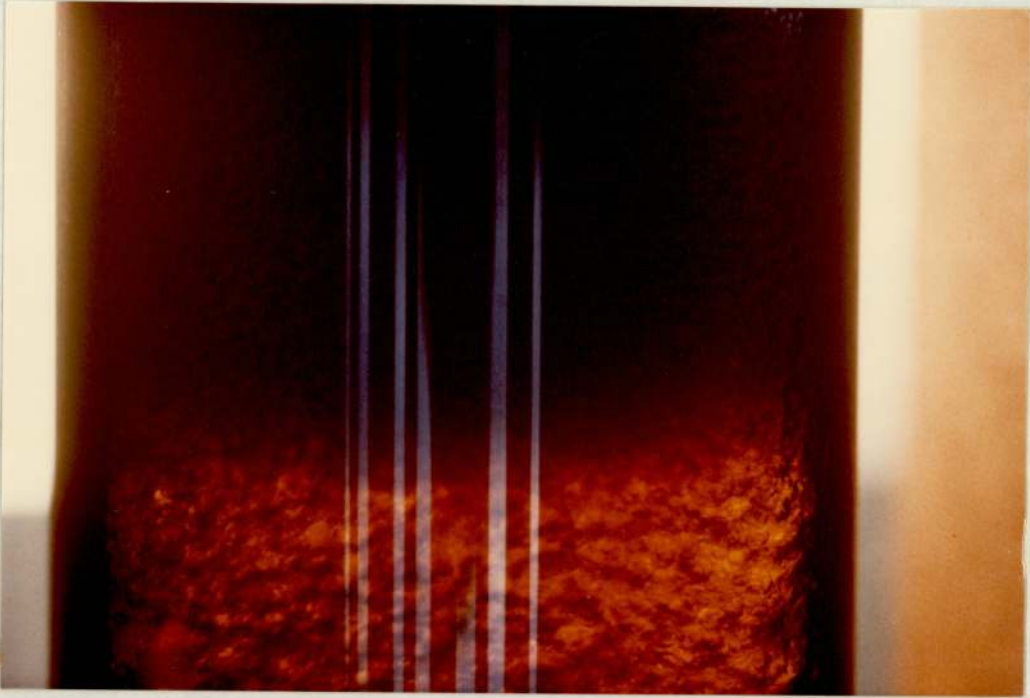
Composite packing surface

(a) Packing surface with dispersed phase flow just shut off.

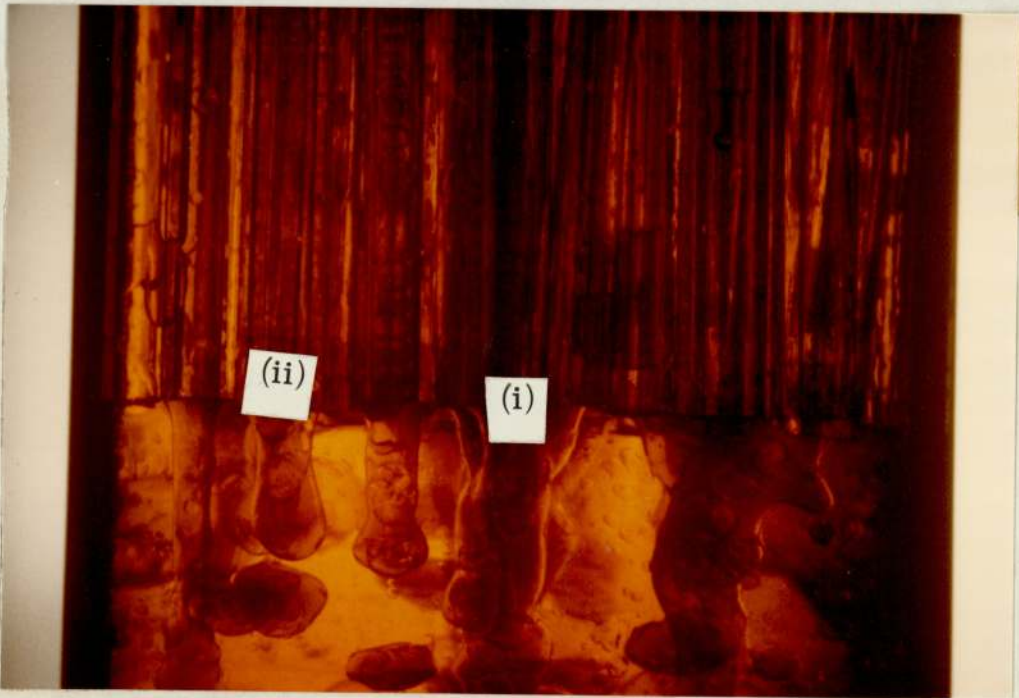


(b) A Close-up view of Figure 6. 48. a. above.

Figure 6. 49.

Coalescence of swarms of drops

(a) Composite packing under full column load.



(b) 'Jetting' and 'graping' phenomena at the exit of the composite packing with the column under full load. (i) jetting (ii) graping

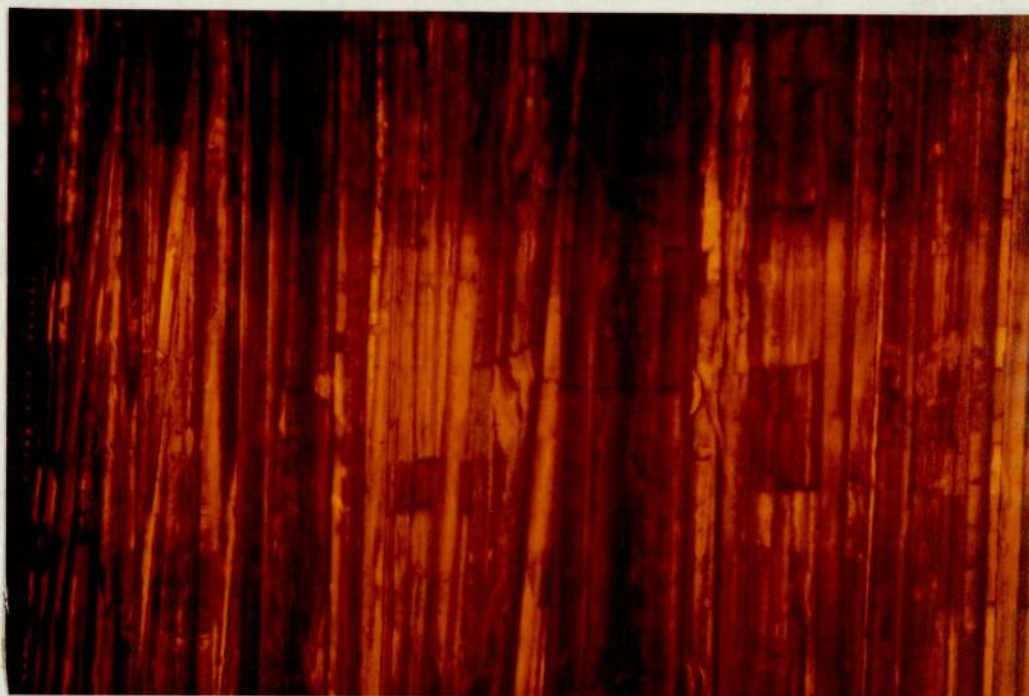
(e)  $(d_{vs})_o / (d_{vs})_i$ , the ratio of the diameter of the drop at the exit to the inlet. Classically, the efficiency of a packing has been determined from this ratio. In this study the value varied from 0.42 to 2.93, and the mean value was around 1.147.

When the column was operated under full load, jets of liquid rather than individual drops resulted from the outlet of the bed (Figure 6.49). However, when the column was instantaneously shut off (Figure 6.48), the packing inlet did not retain any dispersed phase liquid on it since this was immediately cleared through the junction mechanism

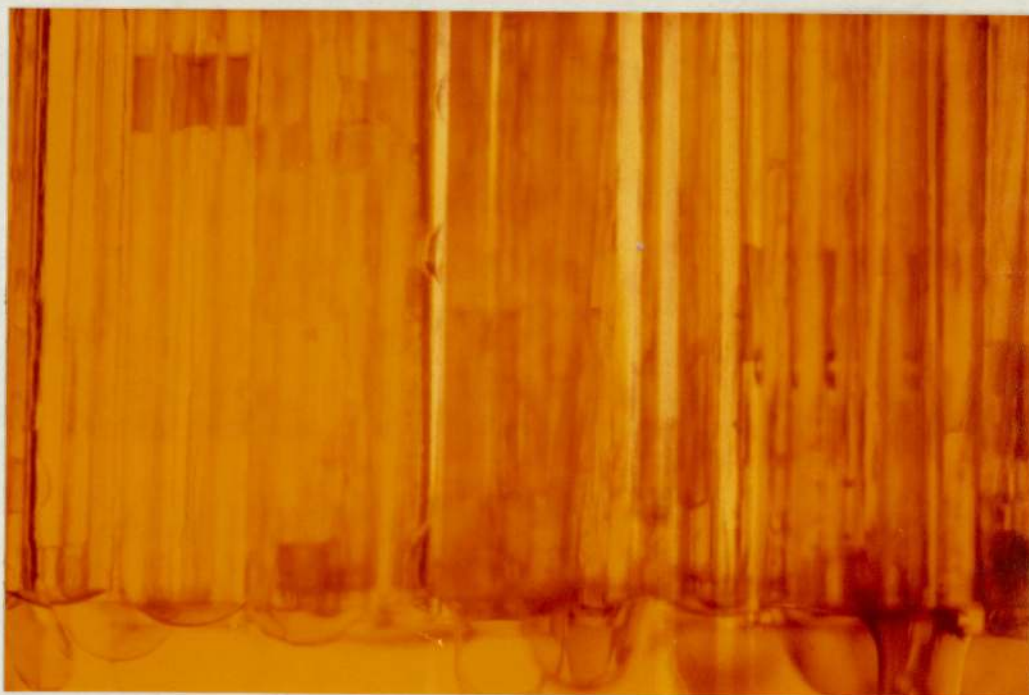
The height of the packing greatly influenced the drop formation at the exit of the bed. In the channels, the liquid of the dispersed phase behaved like a capillary rise (Figure 6.50). When the length of the coalesced mass of dispersed phase liquid in the channel was less than the length of the glass nozzle, the dispersed phase liquid was trapped between slugs of continuous phase liquid on either side. When the length of the dispersed phase liquid was equal to the length of the nozzle, clearly the whole nozzle was filled with a single liquid flowing only in one direction. The graping effect was observed at the exit more often with longer channels. This effect can cause the distribution of drop size to widen at both the inlet and outlet. For example, when graping emerges from the inlet of the dispersed phase, the continuous liquid may promote redispersion.

Hydrodynamics of flow within a packing can greatly affect its performance. The hydrodynamics are complex irrespective of whether one phase is stationary or both the phases are in motion. When the bulk continuous phase is stationary, local flow of this phase still occurs when the flow of the dispersed phase liquid displaces it. Considering a single void through which the dispersed phase liquid tends to flow in one direction and the continuous phase liquid in the other, the relative pressure which the liquids exert

Figure 6.50.

Hydrodynamics in the packed section

(a) Plug flow of dispersed phase liquid through the bed channels.



(b) The drops detach from the wetted nozzle exits via conventional 'drip-point' mechanism.

upon each other determines in which direction both liquids eventually move. The material of the wall of the void therefore plays an important role in enhancing the flow of one liquid over the other. Flow of a liquid would be expected to be higher in a void which is non-wetted by it, but this flow is retarded by the other liquid which wets the walls; therefore, the path of the flowing liquid can be totally blocked by adherence of the other liquid. If the wall of the void contains a junction, no blockage would be anticipated due to either liquid, since the liquids will select their individual channels to flow in opposite directions. Alternatively, in the case of alternating materials, blockage might occur with both liquids. Similarly, in a packed bed, each liquid will select its own channel for flow through the bed, and depending upon the relative flow of the two liquids, both the inlet and exit mechanisms could be effected.

Little attention has been paid in the literature to these hydrodynamics, a phenomena closely related to the coalescence process in the packings. However, the existence of 'preferential channels' is well recognised (15).

To base the efficiency of a packing on one ratio i. e. the diameter of the drop at the outlet of the bed to the diameter at the inlet, may be misleading for the reasons outlined above. The following factors should be considered simultaneously since they all affect the outlet drop size;

- (a) Coalescence at the inlet of the bed
- (b) Hydrodynamics of flow within the packings
- (c) Mechanisms of formation of droplets at the exit of bed.

As pointed out earlier, at a wetted packing, subsequently arriving drops coalesce with the film of the dispersed phase liquid at the packing; this film builds up from coalescence of initial

layer of drops. A packing which is not wetted by the liquid of the dispersed phase acts merely like a mechanical support to hold the drops in close contact for interdrop coalescence to occur. Since the drops move randomly in the packing, some drops can pass through uncoalesced. Therefore, the inlet layer of the packing should consist of composite components of the wetted and non-wetted solid surfaces. Enhanced coalescence can then be obtained, due both to the wetted surface and interdrop coalescence at the junction, and drainage of the coalesced mass of the liquid can occur via the non-wetted component.

Once the coalesced mass of dispersed phase has entered the packing, the function of the packing is to transmit this flow rapidly through without causing any blockage which would result in flooding. Drainage of the liquid will occur without blockage when the intermediate portion of the bed consists of packing which is non-wetted by the dispersed phase liquid. However, as the dispersed phase liquid flows through the non-wetted packings, an increase in velocity, if not controlled, could result in jetting at the outlet of the bed. The easiest way to control this rapid flow at the outlet is by constructing the exit packing layer of a material which is wetted by the dispersed phase liquid. There must be sufficient solid surface area at the packing exit to retain the dispersed phase to an extent that enlarged drops form.

When drops form at the exit layer of a packing without sufficient solid surface area, they may be released early, but an interdrop coalescence may occur between adjacent, forming, drops and result in a wider drop size distribution at the outlet. Only when the above criteria affecting the performance of a packing are satisfied will it be realistic to determine the coalescence

efficiency from the ratio of the diameters of the drops coalescing at the inlet and detaching from the outlet. It is quite unrealistic to estimate this ratio when the inlet drops are coalescing at a film of the dispersed phase liquid at the packing inlet due to the blockage in the packing; this will also result in random drop formation at the exit.

In conclusion, therefore, a composite packing should preferably consist of three storeys, i. e. a junction, a non-wetted and finally a wetted storey. The minimum depth of the intermediate zone depends upon the size relationship of the coalescing drop and the packing channel through which the coalesced liquid flows, and the maximum depth depends upon the pressure head available. For minimum depth, the drop is assumed to form a liquid column of dimensions equivalent to a given packing channel.

## CHAPTER SEVEN

### GENERAL CONCLUSIONS

#### 7.1. Main Conclusions

The main conclusions from this investigation are as follows:

1. The values of liquid-liquid contact angles of dispersed phase liquid drops, in the size range  $2 \times 10^{-3}$  m to  $1.0 \times 10^{-2}$  m

- (a) were less than  $90^{\circ}$  at wetted solid plates
- (b) were greater than  $90^{\circ}$  at non-wetted solid plates.
- (c) varied at non-wetted surfaces because of the density difference between the liquids of continuous and dispersed phase.

2. A solid exhibits a 'wetted' surface with respect to the dispersed phase when the molecular forces of attraction of this phase to the solid surface are greater than those of the continuous phase. A solid has a 'non-wetted' surface when a thin film of continuous phase liquid is adsorbed on it; this prevents the dispersed phase liquid coming into contact with the surface and, therefore, wetting it. In the latter case, the droplet exhibits a contact angle at the adsorbed film and not at the solid surface.

3. With a composite surface, containing a junction between a wetted and a non-wetted component, the dispersed phase liquid droplets 'reside' on the continuous phase liquid film on the non-wetted component, and when they are about two millimeters from the junction line, are redirected from the non-wetted to the wetted component.

4. In an interdrop coalescence process at a junction the flow of the dispersed phase liquid always occurs from the drop at the non-wetted to the drop at the wetted component (Section 6.1.3.d.). No mixing of dispersed phase liquid takes place during interdrop coalescence at a composite surface. Mixing of the liquid of the two drops occurs, after coalescence, through molecular diffusion

(Section 6.1.3) Such junctions enhance coalescence in packings by more than four times.

5. With regard to the behaviour at a packing, the size of the drop that can pass through an aperture is equal to the size of the aperture irrespective of its material of construction but the mechanisms of coalescence depend upon the nature of the material of the packing.

❖ A wetted packing previously soaked in dispersed phase liquid enhances coalescence because the dispersed phase liquid film on the packing surface provides a bridging effect to transmit the coalesced droplets from one side of the packing aperture to the other where they adhere until the gravity or buoyancy force increases due to the addition of subsequently coalescing drops, to enable detachment of the droplets from the exit of the packing.

6. The enhanced coalescence effect, with composite packings, involves redirection, interdrop coalescence and collection of droplets (Section 6.1.3) A model to predict absolute values of solid-liquid interfacial forces in a liquid-solid-liquid-solid system is proposed (Section 6.1.4.a.). A knowledge of these values is necessary to design a composite coalescer.

7. Single drop studies were extended to the coalescence of swarms of drops with a composite coalescer. The coalescence mechanisms in the packed section, and at the packing inlet and outlet depend upon the surface characteristics of the packing and the flow hydrodynamics of the liquids (Section 6.2.). The following correlation is proposed to predict the exit drop size.

$$d_o/d_i = K. (\Delta\rho \cdot d_i^2 \cdot g/\gamma)^a \cdot (d_i/h_b)^b \cdot \left[ \left[ (d_{nd}^2 - d_{wd}^2) \cdot \cos\theta + (d_{wd}^2 - d_v^2) \cdot \cos\alpha \right] / d_i^2 \right]^c$$

Minor conclusions : The following minor conclusions may be drawn.

8. The contact angle does not provide an absolute value of solid-liquid interfacial forces because Equation (6.1), which relates solid-liquids physical properties, has two unknowns in it, and therefore, cannot be solved.
9. The non-wettability of a surface by the dispersed phase liquid increases with a decrease in the density difference between the dispersed and continuous phase liquids.
10. The junction effect requires a certain minimum difference in the surface energies of the components (Section 6.1.3.d.).
11. The rest-times for interdrop coalescence, between a drop at a wetted and a drop at a non-wetted component of a junction, are much less than those for drop-interface or drop-drop coalescence at single solid surfaces.

The rest-time distributions for interdrop coalescence at a junction surface also depend upon the difference between the surface energies of the components of the junction.

12. Irrespective of the material of a packing, drops smaller than the aperture size pass through unhindered. However, a droplet much smaller than the aperture may impinge upon a filament; it then rolls over to its underside from which it may either fall away or adhere depending upon the surface characteristics. Whether a droplet will adhere depends upon the difference between the gravity or buoyancy, and surface forces. In the size range  $2 \times 10^{-3}$  to  $1 \times 10^{-2}$  m droplets up to twice the size of a wetted filament can adhere to it. A larger droplet is retained at the packing when its gravity or buoyancy force is distributed across the voids.
13. With packings previously soaked in dispersed phase liquid, the continuous phase liquid film, trapped between an impinging dispersed phase droplet and a thin film of dispersed phase on the packing ruptures readily, because of the immobility of the non-deformable solid support under the film. This is unlike the situation with a liquid-liquid interface.
14. The contact angle phenomena loses its identity in the dynamic situation in which the packing surface is covered with the coalesced liquid of the drops which are closely packed and move continuously. The characteristics of a solid surface are therefore best determined in a 'static' situation on a macroscopic scale.

## 7.2. Applications to the Design of a Coalescer

It was noted that most of the dispersion droplets from the distributor plate reached and coalesced at the packing inlet, at a certain distance from the column walls. This resulted in blockage of some of the central flow channels in the packing due to a varied pressure differential across the bed. In practice it is preferable for the droplets at the bed inlet to be equally distributed by redirecting them over the packing surface. This can easily be achieved with a convex shaped inlet surface which will enable redirection of the drops towards unoccupied packing surface nearer the column wall (Figure 7.1. ).

During the coalescence of swarms of drops, a number of inlet drops could not perch on coalescing sites at the packing since these were already occupied. This resulted in drops becoming closely packed at the inlet packing surface. In this zone, the coalescence or disappearance of one or more drops produced vibrations and fluctuations throughout the whole zone and hence displacement and movement of the drops and the continuous phase liquid. This enabled the renewal of the continuous phase film between the drops and restricted inter-drop coalescence. For the design of a coalescer, it is therefore desirable for the number of drops in any one monolayer to be limited to the number of coalescing sites.

A convex shaped packing inlet will not serve any purpose if the drops do not utilise each and every site on the coalescer surface. Cavities or indentations in the surface, to restrict the drops as they tend to roll down, will allow most drops to find coalescing sites.

A higher pressure force will be required to cause flow of dispersed phase through any packing wetted by it. This pressure is partly determined by the force with which the liquid is adhering to the packing surface. However, a lower pressure will be sufficient with a packing which has a wetted layer at the inlet and at the outlet, but a non-wetted intermediate zone. In this case, the dispersed phase liquid adheres at either end of the packing but is only supported by the intermediate non-wetted zone. To obtain improved separation efficiency by using a composite packing, the inlet layer should contain junctions, the intermediate zone should consist of non-wetted material, and the exit layer should be either of wetted, non-wetted or junction surfaces depending upon the drop size required.

In a subsidiary experiment coalescence was observed at junctions situated in a pipe parallel to the flow of dispersion. In this experiment, in effect an extension of the classical experiments of Jeffreys et al ( 64 ), a number of p. t. f. e. tubing pieces were inserted, about one centimeter apart, in a glass tube. The dispersed phase droplets in the dispersion coalesced on coming into contact with the wetted surface. Larger droplets were thus built up along the pipe by repeated coalescence. These droplets were dragged along by the flowing dispersion and flowrate was a critical factor. At low flowrates, the coalesced mass blocked the flow line whilst at high flowrates, the droplets in the dispersion could not come into contact with the surface. For the drops to come into contact, a balance is required between the kinetic energy of the drops in the moving dispersion and the gravitational or buoyancy forces for the drops to approach the surface. This criteria was satisfied at intermediate flowrates. A number of junction baffles at right

angles to the flow could assist the drops to achieve contact. This is one simple design for a primary dispersion coalescer arising from this work.

Junction surfaces can be useful in almost every coalescence equipment where droplets coalesce upon a stationary or moving solid surface. The net velocity with which the droplets approach a solid surface should be determined from the rest-times of the drops at such solid surfaces; this is the minimum time to be provided for drop-solid contact for the coalescence to occur. In such cases, it is necessary that the drops approach and strike normally on a wetted surface of the junction rather than on the non-wetted component since the latter only aids the flow of the coalesced mass of the liquid.

The effect of ageing of the surface of a packing is another factor which must be taken into consideration at the design stage. Although no ageing effects were encountered in the present studies, because of the meticulous cleaning techniques used, such effects and deposition of scum can be anticipated in the absence of proper cleaning techniques and from prolonged use of the packing. A standard cleaning technique should be adopted based upon the materials of construction of the packing. The emphasis should be on chemical cleanliness and an appropriate chemical may be used to dissolve any scum deposited and to renew the packing surface.

In the design of a composite mesh, a balance is necessary between the ease of construction and the efficiency and practical performance of the packing. It may be worth sacrificing ease of construction to design a packing which will enhance coalescence, collection and separation of two

immiscible phases. Therefore, the designer should be aware of all possible limitations of various wetted and non-wetted materials as set out in Section 6.1. Not only the proper surface ratio of the components ( 66 ) but the geometry and the size of the voids require attention. Each drop of a dispersion needs a coalescing site and each site should have a symmetrical junction to enhance coalescence and passage. If the junctions are nearer than a drop diameter, then the drops at both the voids will coalesce via interdrop coalescence, and the coalesced mass will adhere to the wetted material across the two voids with non-wetted material between them.

### 7.3. Recommendations for Further Work

1. The mechanisms of contact angle formation have been shown to depend upon the wetting characteristics of the solid surface. Various methods were attempted, including a technique involving Newton's rings, to photograph the adsorbed film of the continuous phase liquid at the non-wetted surface. However, since the film was less than one micron thick, it requires the development of a special optical technique, to photograph it with a higher magnification but without loss of contrast. To achieve this will require:

- a. a specific point light source of single wavelength to generate a beam of light parallel to the solid surface.
- b. synchronisation of the light source with the camera.
- c. magnification of the trapped continuous phase liquid film prior to photography.

2. The wetting characteristics of the natural surfaces of the solids investigated in the present study were not altered by the application to the surface of any wetting agent. Based upon

this criteria, a combination of p. t. f. e. and glass gave an ideal pair of components for a junction surface. However, junction effects can be investigated further when different wetting agents are applied to the same surface to alter its wetting characteristics. Furthermore, the application of such chemicals is likely to facilitate an increase in the span of difference in surface energies between the components of a junction.

A tabulation of surface energies of most solids will eventually be required for design purposes. Therefore, it would be worth examining certain other solid surfaces with respect to both wetting characteristics and junction effect; this will involve determination of the solid-liquid interfacial tensions for which a model is proposed in this work.

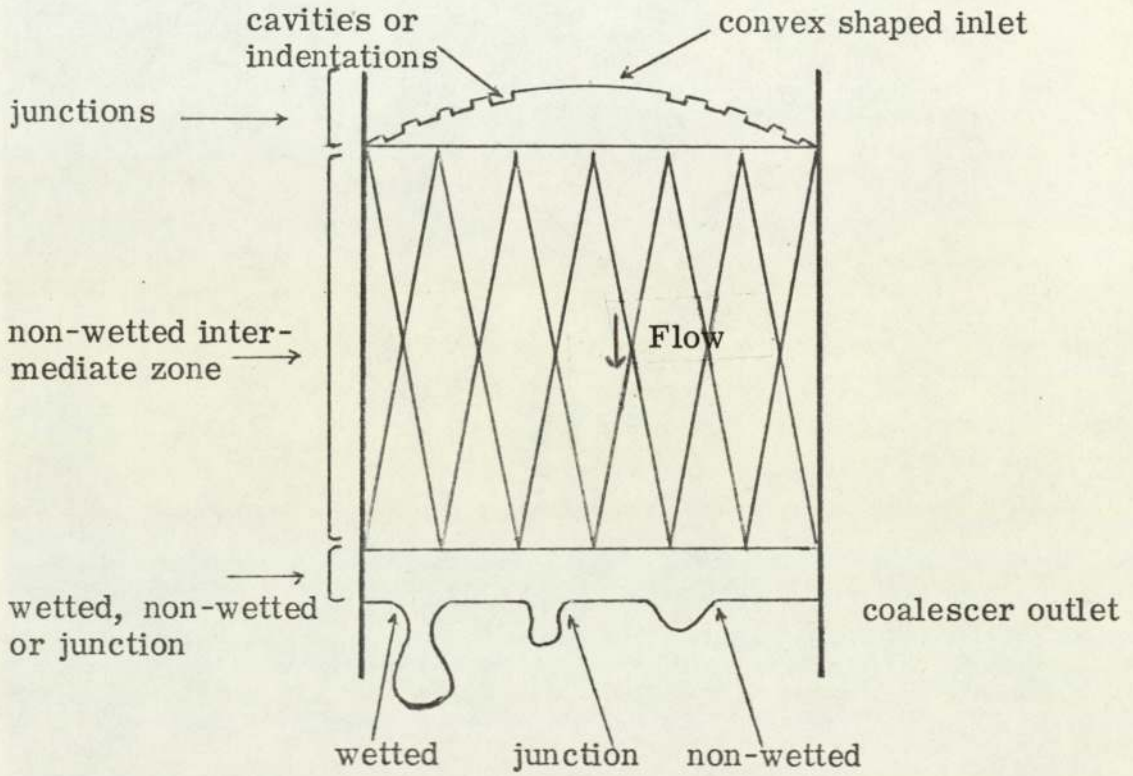
3. The coalescence of liquid dispersions has only been studied with an ideal composite coalescer element. However, such studies could be extended by developing a method of construction of a composite packing so that the arrangements of junctions, geometry of the apertures and the ratio of the surface areas of solid components could conveniently be investigated.

4. The ideal composite coalescer had junctions only at the inlet or outlet of the element. However, further enhancement in coalescence, and improved control over the exit drop size and the hydrodynamics in the packed section could be achieved by a 3-storey composite packing in which the inlet layer will have junctions, the intermediate zone will have only non-wetted material and the exit layer will have either wetted, non-wetted or junction surfaces to give the required drop size as described in Section 7.3.

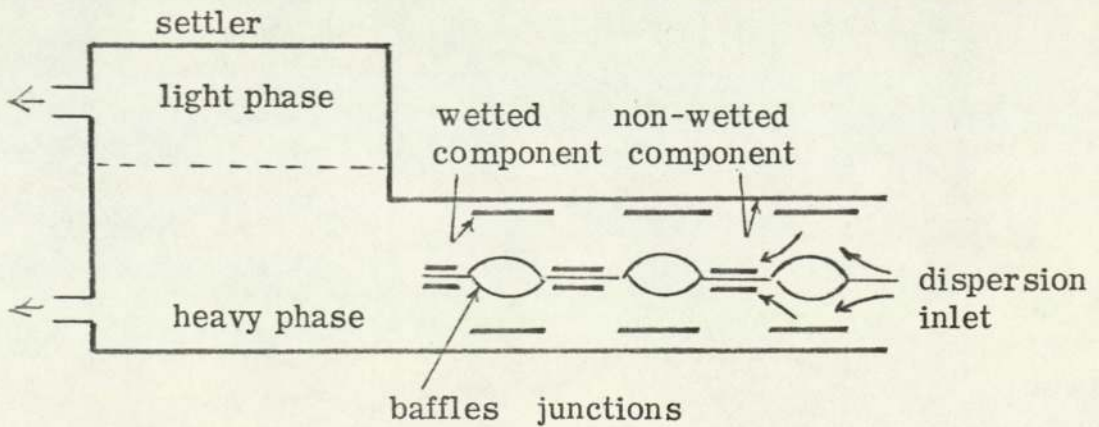
Figure 7.1.

Design of a composite coalescer

## (a) Packed bed



## (b) Baffle arrangement



APPENDIX A

Physical properties of liquid-liquid systems  
at 20°C

Appendix A

LIQUID-LIQUID INTERFACIAL TENSIONS

Organic liquids	Interfacial tension $\times 10^{-3} \text{ Nm}^{-1}$
n-hexane	52.1
methylcyclohexane	41.3
toluene	34.5
n-butyl acetate	13.4
ethyl acetate	8.2

SURFACE TENSIONS

Organic liquid	Surface tension $\times 10^{-3} \text{ Nm}^{-1}$
n-hexane	18.3
methylcyclohexane	27.8
toluene	36.4
n-butyl acetate	57.1
ethyl acetate	28.0
distilled water	71.2

DENSITIES

	$\times 10^3 \text{ Kgm}^{-3}$
n-hexane	0.662
methylcyclohexane	0.771
toluene	0.864
n-butyl acetate	0.890
ethyl acetate	0.898
distilled water	0.998

APPENDIX B

Matching the density of organic liquids with distilled  
water by gradual additions of carbon tetrachloride at 20°C

Appendix BMATCHING OF DENSITY OF ORGANIC LIQUIDS

litre of $\text{CCl}_4$ per litre organic liquid, $\times 10^{-3}$	density difference $\text{Kgm}^{-3} \times 10^3$
<u>ethyl acetate</u>	
0.0	0.101
40.0	0.087
75.0	0.024
117.0	0.006
165.0	0.001
<u>n-butyl acetate</u>	
0.0	0.110
45.0	0.091
100.0	0.013
163.0	0.008
195.0	0.001
<u>toluene</u>	
0.0	0.136
58.0	0.107
115.0	0.083
183.0	0.015
257.0	0.001
<u>methylcyclohexane</u>	
0.0	0.229
83.0	0.178
135.0	0.097
220.0	0.018
315.0	0.001
<u>n-hexane</u>	
0.0	0.338
95.0	0.223
213.0	0.106
305.0	0.075
398.0	0.001

APPENDIX C

Calculation of volume and  
surface area of the drop

Calculation of drop volume,  $V_c$ :

The photographs of the liquid drop at the junction nozzle suggest that the drop shape can be approximated as shown in Figure 6.45a. For the calculation of the volume of the drop, the shape is broken down into three separate parts (Figure 6.45b) and the volume of each of these calculated.

$$V_c = v_1 + v_2 + v_3 \quad (C.1)$$

where  $v_1$  = volume generated by the revolution of the solid hemisphere of radius 'R'. (C.2)

$v_2$  = volume of the cylinder of radius 'C' and height '2.R'. (C.3)

$v_3$  = volume of the hemisphere of radius  $d_v$ .

Calculation of  $v_1$ :

The equation of a semicircle is:

$$(x - C)^2 + y^2 = R^2 \quad (C.4)$$

The volume generated by revolving the solid about the y-axis is given by,

$$v_1 = \int_C^{C+R} 2\pi \cdot x \cdot 2y \, dx \quad (C.5)$$

by substitution for y from Equation C.4

$$v_1 = \int_C^{C+R} 2\pi \cdot x \cdot 2 \int_C^{C+R} \sqrt{R^2 - (x - C)^2} \, dx \quad (C.6)$$

The integral in Equation C.6 can conveniently be solved via a substitution procedure, thus substituting  $(x - C) = R \cdot \cos\theta$ , the integral becomes

$$\begin{aligned} v_1 &= (4\pi \cdot R^2) \int_0^{\pi/2} (R \cdot \sin^2\theta \cdot \cos\theta + C \cdot \sin^2\theta) \, d\theta \\ &= 4\pi \cdot R^2 (R/3 + C \cdot \pi/4) \end{aligned} \quad (C.7)$$

Now the calculated volume,  $V_c$ , of the drop is given by Equation C. 8 after substituting the values of  $v_1$ ,  $v_2$  and  $v_3$ .

$$V_c = 4\pi.R^2(R/3 + C.\pi/4) + 2\pi.R.C^2 + \pi.d_v^3/12 \quad (C. 8)$$

Calculation of liquid-liquid surface area:

The liquid-liquid surface area,  $S$ , is given by

$$S = s_1 + s_2 + s_3 \quad (C. 9)$$

where  $s_1$  = surface area of the liquid-liquid interface around the drop at the junction surface.

$s_1$  = surface area generated by the semicircle of radius 'R'.

$s_2$  = surface area of top of the cylinder of radius 'C' =  $\pi.C^2$  (C. 10)

$s_3$  = surface area of the hemisphere of radius  $d_v$   
=  $\pi.d_v^2/2$  (C. 11)

Calculation of  $s_1$ :

The surface area of revolution about y-axis is given by,

$$s_1 = \int \sqrt{1 + (dy/dx)^2} \quad (C. 12)$$

$$s_1 = 2\pi \int x \cdot ds \quad (C. 13)$$

where  $ds = \sqrt{1 + (dy/dx)^2} dx$  (C. 14)

Equation of a semicircle is

$$(x - C)^2 + y^2 = R^2 \quad (C. 15)$$

which gives  $y = \sqrt{R^2 - x^2 - C^2 + 2.C.x}$  (C. 16)

and  $dy/dx = (-2.x + 2.C)/2.y$  (C. 17)

Therefore  $s_1 = 4\pi \int_C^{C+R} (x.R)/\sqrt{R^2 - (x - C)^2} dx$   
 $= 4\pi.R \int_0^{\pi/2} (R.\cos\theta + C). R d\theta$   
 $= 4\pi.R(R + \pi.C/2)$  (C. 18)

Therefore  $S = 4\pi.R(R + \pi.C/2) + \pi.C^2 + \pi.d_v^2/2$  (C. 19)

## APPENDIX D

Liquid-liquid-solid-solid  
interfacial tension

Table D.1 - Solid liquid interfacial tension

Dispersed phase: Distilled water		Continuous phase: Ethyl acetate		Junction nozzle: Glass-PTFE		
C	R	$V_c$	$D_c$	$d_v$	$D_e/d_v$	$V_e$
$m. \times 10^{-2}$	$m. \times 10^{-2}$	$m. \times 10^{-6}$	$m. \times 10^{-2}$	$m. \times 10^{-2}$		$m^3 \times 10^{-6}$
0.256	0.129	078.924	0.532	0.213	2.499	085.135
0.298	0.151	128.617	0.626	0.261	2.400	139.527
0.386	0.177	218.543	0.747	0.327	2.2856	230.763
0.415	0.215	367.151	0.888	0.392	2.266	395.348
$D_e$	$D_e/d_v$	$2C+R$	$s_1$	$s_2$	$s_3$	S
$m. \times 10^{-2}$		$m. \times 10^{-2}$	$m. \times 10^{-4}$	$m. \times 10^{-4}$	$m^2 \times 10^{-4}$	$m^2 \times 10^{-4}$
0.546	2.562	0.641	0.860	0.205	0.0712	1.137
0.643	2.4664	0.820	1.174	0.278	0.107	1.560
0.761	2.327	1.022	1.679	0.425	0.167	2.272
0.910	2.323	1.199	2.3421	0.541	0.241	3.124

Continued Table D. 1

$\gamma_{dc} \cdot s$ Nm x 10 <sup>-5</sup>	$\alpha_{wda}$ deg.	$\gamma_{da} \cos \alpha_{wda}$ Nm <sup>-1</sup> x 10 <sup>-3</sup>	$\beta_{nca}$ deg.	$\gamma_{ca} \cos \beta_{nca}$ Nm <sup>-1</sup> x 10 <sup>-3</sup>	$\gamma_{dc} \cos(\theta_{wd})_c$ Nm <sup>-1</sup> x 10 <sup>-3</sup>	$(\theta_{wd})_e$ deg.	$\gamma_{dc} \cos \theta_{wd} e$ Nm <sup>-1</sup> x 10 <sup>-3</sup>	$\beta_{wc}$ deg.	$\gamma_{dc} \cos \beta_{wc}$ Nm <sup>-1</sup> x 10 <sup>-3</sup>
09.263	33.5	59.289	126.0	-16.457	9.237	16.0	7.882	147.5	-6.915
12.503	36.0	57.521	128.0	-17.238	9.117	17.5	7.820	149.0	-7.028
18.612	37.5	56.407	129.0	-17.810	9.050	18.5	7.776	149.5	-7.065
25.588	38.5	55.643	130.0	-17.998	8.980	20.5	7.680	151.0	-7.171

$\Delta l \cdot g \cdot d / 2 \gamma_{dc} (\cos \theta_{wd} - \cos \beta_{wc})$ Kg. sec. <sup>-2</sup> N <sup>-1</sup> Nm <sup>-1</sup> x 10 <sup>-2</sup>	$V_e \cdot \Delta l \cdot g$ Kg. m. sec. <sup>-2</sup> x 10 <sup>-5</sup>	$\gamma_{nc}$ Nm <sup>-1</sup> x 10 <sup>-3</sup>	$\gamma_{wd}$ Nm <sup>-1</sup> x 10 <sup>-3</sup>	$\gamma_{wc}$ Nm <sup>-1</sup> x 10 <sup>-3</sup>	$\gamma_{hd}$ Nm <sup>-1</sup> x 10 <sup>-3</sup>	$\gamma_{dc} / (\gamma_{wd} - \gamma_{nc})$ ( $\gamma_{dc} / \gamma_{wc}$ )
3.331	08.516	3.601	11.483	22.475	15.559	1.040
3.923	13.960	3.552	11.373	20.865	13.836	1.048
4.643	23.086	3.517	11.293	18.525	11.463	1.054
5.552	39.558	3.501	11.181	9.936	2.764	1.067

Table D. 2 - Solid-liquid interfacial tension

Dispersed phase: Distilled water		Continuous phase: Ethyl acetate				
Junction nozzle: Glass-PTFE						
C	R	$V_c^3$	$D_c$	$d_v$	$D_c/d_v$	$V_c^3$
$\text{m.} \times 10^{-2}$	$\text{m.} \times 10^{-2}$	$\text{m.} \times 10^{-6}$	$\text{m.} \times 10^{-2}$	$\text{m.} \times 10^{-2}$		$\text{m.} \times 10^{-6}$
0.263	0.134	0.88.726	0.553	0.213	2.599	094.539
0.307	0.162	152.513	0.663	0.261	2.544	162.362
0.374	0.193	264.207	0.796	0.327	2.435	285.126
0.423	0.231	429.431	0.936	0.392	2.387	462.447
$D_e$	$D_e/d_v$	$2C+R$	$s_1$	$s_2$	$s_3$	S
$\text{m.} \times 10^{-2}$		$\text{m.} \times 10^{-2}$	$\text{m.} \times 10^{-4}$	$\text{m.} \times 10^{-4}$	$\text{m.} \times 10^{-4}$	$\text{m.} \times 10^{-4}$
0.565	2.654	0.663	0.921	0.217	0.071	1.209
0.677	2.593	0.775	1.315	0.296	0.107	1.714
0.816	2.497	0.943	1.892	0.439	0.167	2.500
0.959	2.447	1.077	2.599	0.562	0.241	3.402

Continued Table D. 2

$\gamma_{dc}^s$	$\alpha_{wda}$	$\gamma_{da}^{\cos}$	$\beta_{hca}$	$\gamma_{ca}^{\cos}$	$\beta_{hca}$	$\gamma_{dc}^{\cos(\theta_{wdc})}$	$(\theta_{wdc})$	$\gamma_{dc}^{\cos(\theta_{wdc})}$	$\beta_{wca}$	$\gamma_{dc}^{\cos}$	$\beta_{wca}$	$\gamma_{dc}^{\cos}$
$Nm \times 10^{-5}$	deg.	$Nm^{-1} \times 10^{-3}$	deg.	$Nm^{-1} \times 10^{-3}$	deg.	$Nm^{-1} \times 10^{-3}$	deg.	$Nm^{-1} \times 10^{-3}$	deg.	$Nm^{-1} \times 10^{-3}$	deg.	$Nm^{-1} \times 10^{-3}$
16.209	35.5	87.616	129.5	-18.128	129.5	7.891	17.5	12.779	149.0	-11.485	149.0	-11.485
38.356	36.5	57.154	131.5	-18.884	131.5	5.674	18.0	12.743	150.0	-11.604	150.0	-11.604
46.232	37.5	56.407	132.5	-19.254	132.5	5.646	20.5	12.550	152.0	-11.830	152.0	-11.830
54.334	39.0	55.255	133.0	-19.436	133.0	5.574	22.0	12.423	153.5	-11.991	153.5	-11.991

$Mg \cdot d / 2 \gamma_{dc}$	$\gamma_{dc}^{\cos(\theta_{wdc})}$	$V_e \Delta \rho$	$\gamma_{nc}$	$\gamma_{wd}$	$\gamma_{wc}$	$\gamma_{nd}$	$\gamma_{dc} /$	$\gamma_{dc} /$
$Kg \cdot sec \cdot N^{-1} \times 10^{-2}$	$Nm^{-1} \times 10^{-3}$	$Kg \cdot m \cdot sec^{-2} \times 10^{-5}$	$Nm^{-1} \times 10^{-3}$	$Nm^{-1} \times 10^{-3}$	$Nm^{-1} \times 10^{-3}$	$Nm^{-1} \times 10^{-3}$	$(\gamma_{wd}^{-1} \gamma_{nc})$	$(\gamma_{nd}^{-1} \gamma_{wc})$
2.388	24.264	10.708	6.195	18.975	38.350	26.865	1.048	-1.166
2.862	24.347	18.391	6.121	18.864	53.296	41.691	1.051	-1.154
3.450	24.381	32.306	6.068	18.618	47.825	35.994	1.067	-1.132
4.054	24.414	52.397	6.039	18.462	36.443	24.453	1.078	-1.117

Table D.3 - Solid-liquid interfacial tension

Dispersed phase: Distilled water		Continuous phase: Toluene				
Junction nozzle: Glass-PTFE						
C	R	$V_c$	$D_c$	$d_v$	$D_c/d_v$	$Ve$
$m. \times 10^{-2}$	$m \times 10^{-2}$	$m. \times 10^{-6}$	$m. \times 10^{-2}$	$m. \times 10^{-2}$		$m. \times 10^{-6}$
0.271	0.138	096.883	0.570	0.213	2.676	586.0
0.319	0.170	174.402	0.692	0.261	2.261	200.362
0.392	0.207	313.537	0.846	0.327	2.588	355.274
0.441	0.243	496.462	0.982	0.392	2.506	565.519
$D_e$	$D_e/d_v$	$2C+R$	$s_1$	$s_2$	$s_3$	S
$m. \times 10^{-2}$		$m. \times 10^{-2}$	$m. \times 10^{-4}$	$m. \times 10^{-4}$	$m. \times 10^{-4}$	$m. \times 10^{-4}$
0.586	2.751	0.683	0.977	0.230	0.0712	1.279
0.726	2.782	0.809	1.433	0.319	1.107	1.860
0.878	2.687	0.991	0.482	0.482	0.167	2.790
1.0257	2.6166	1.125	2.857	0.610	0.241	3.709

Continued Table D. 3

$\gamma_{dc} S$ Nm x10 <sup>-5</sup>	$\alpha_{wda}$ deg.	$\gamma_{da} \cos \alpha_{wda}$ Nm x10 <sup>-3</sup>	$\beta_{nca}$ deg.	$\gamma_{ca} \cos \beta_{nca}$ Nm x10 <sup>-3</sup>	$\gamma_{dc} \cos(\theta_{wd})^c$ Nm <sup>-1</sup> x10 <sup>-3</sup>	$(\theta_{wd})^e$ deg.	$\gamma_{dc} \cos(\theta_{wd})^e$ Nm <sup>-1</sup> x10 <sup>-3</sup>	$\xi_{wc}$ deg.	$\gamma_{dc} \cos \xi_{wc}$ Nm <sup>-1</sup> x10 <sup>-3</sup>
044.139	36.0	57.521	133.5	-25.056	32.465	19.5	32.512	152.0	-30.466
064.180	37.5	56.407	134.5	-25.513	30.894	20.5	32.312	153.5	-30.874
096.382	38.5	55.643	136.0	-26.183	31.005	21.0	32.205	154.0	-31.005
127.984	39.5	54.862	136.5	-26.403	28.458	21.0	32.205	155.0	-31.267

$\Delta \beta. g. d / 2$ Kg. sec. x 10 <sup>-3</sup>	$\gamma_{dc} (c \cos \theta_{wd} - \cos \xi_{wc})$ Nm <sup>-1</sup> x 10 <sup>-3</sup>	$V e. \Delta \beta. g.$ Kg. m. sec. x 10 <sup>-5</sup>	$\gamma_{nc}^{-1}$ Nm <sup>-3</sup> x 10 <sup>-3</sup>	$\gamma_{wd}^{-1}$ Nm <sup>-3</sup> x 10 <sup>-3</sup>	$\gamma_{wc}^{-1}$ Nm <sup>-3</sup> x 10 <sup>-3</sup>	$\gamma_{nd}^{-1}$ Nm <sup>-1</sup>	$\gamma_{dc} / (\gamma_{wd}^{-1} \gamma_{nc})$	$\gamma_{dc} / (\gamma_{nd}^{-1} \gamma_{wc})$
1.128	62.978	14.119	19.059	51.524	113.186	082.720	1.062	-1.132
1.399	63.186	26.635	18.899	51.212	121.030	090.156	1.067	-1.117
1.693	63.210	47.229	18.710	50.916	132.668	101.663	1.071	-1.112
1.976	63.473	75.178	18.657	50.863	136.913	105.645	1.071	-1.103

Table D.4 - Solid-liquid interfacial tension

Dispersed phase: Distilled water		Continuous phase: Methylcyclohexane						
Junction nozzle: Glass-PTFE		C	R	$V_{C_3}$ m. $\times 10^{-2}$	$D_c$ m. $\times 10^{-2}$	$d_v$ m. $\times 10^{-2}$	$D_c/d_v$	$V_{e_3}$ m. $\times 10^{-6}$
0.283	0.146	113.301	0.600	0.213	2.820	129.627		
0.329	0.181	200.317	0.726	0.261	2.784	224.335		
0.412	0.213	351.481	0.875	0.327	2.673	404.116		
0.473	0.256	586.274	0.383	0.392	2.641	644.829		
Junction nozzle: Glass-PTFE		$D_e$ m. $\times 10^{-2}$	$D_e/d_v$	$2C+R$ m. $\times 10^{-2}$	$s_1$ m. $\times 10^{-4}$	$s_2$ m. $\times 10^{-4}$	$s_3$ m. $\times 10^{-4}$	S m. $\times 10^{-4}$
0.628	2.949	0.712	1.083	0.251	0.071	1.406		
0.754	2.889	0.965	1.587	0.340	0.107	2.034		
0.917	2.805	1.037	2.302	0.537	0.167	3.003		
1.071	2.734	1.202	3.213	0.702	0.241	4.157		

Continued Table D. 4

$\gamma_{dc} \cdot S$	$\alpha_{wda}$	$\gamma_{da} \cos \alpha_{wda}$	$\beta_{nca}$	$\gamma_{ca} \cos \beta_{nca}$	$\gamma_{dc} \cos(\theta_{wd})_c (\theta_{wd})_e$	$\gamma_{dc} \cos(\theta_{wd})_e$	$\beta_{wc}$	$\gamma_{dc} \cos \beta_{wc}$
$Nm \times 10^{-5}$	deg.	$Nm^{-1} \times 10^{-3}$	deg.	$Nm^{-1} \times 10^{-3}$	deg.	$Nm^{-1} \times 10^{-3}$	deg.	$Nm^{-1} \times 10^{-3}$
058.080	36.0	57.521	136.5	-20.165	23.0	38.016	155.0	-37.430
084.009	37.5	56.407	137.5	-20.496	24.0	37.727	155.5	-37.581
124.044	38.5	55.643	138.5	-20.820	24.5	37.578	157.0	-38.016
171.721	39.5	54.862	139.0	-20.980	24.5	37.578	158.0	-38.289

$\Delta \rho \cdot g \cdot d / 2 \gamma_{dc}$	$\gamma_{dc} (\cos \theta_{wd} - \cos \beta_{wc})$	$V_e \Delta f \cdot g$	$\gamma_{nc}$	$\gamma_{wd}$	$\gamma_{wc}$	$\gamma_{nd}$	$\gamma_{dc} / (\gamma_{wd} - \gamma_{nc})$	$\gamma_{dc} / (\gamma_{nd} - \gamma_{wc})$
Kg. sec. $\times 10^{-2}$	$Nm^{-1} \times 10^{-3}$	Kg m. sec. $\times 10^{-5}$	$Nm^{-1} \times 10^{-3}$	$Nm^{-1} \times 10^{-3}$	$Nm^{-1} \times 10^{-3}$	$Nm^{-1} \times 10^{-3}$		
1.708	75.446	29.121	25.834	63.851	131.947	94.517	1.086	-1.103
2.050	75.308	50.400	25.654	63.382	136.621	99.040	1.094	-1.098
2.494	75.595	90.792	25.517	63.095	136.859	98.843	1.099	-1.086
2.915	75.868	144.872	25.470	63.049	131.102	92.812	1.099	-1.078

Table D.5 - Solid-liquid interfacial tension

Distilled Dispersed phase: water		Continuous phase: n-Hexane				
Junction nozzle: Glass-PTFE						
$C$	$R$	$V$	$D_c$	$d_v$	$D_c/d_v$	$V_e$
$m. \times 10^{-2}$	$m. \times 10^{-2}$	$m. \times 10^{-6}$	$m. \times 10^{-2}$	$m. \times 10^{-2}$		$m. \times 10^{-6}$
0.297	0.162	143.127	0.649	0.213	3.051	157.415
0.371	0.201	280.603	0.812	0.261	3.112	314.272
0.512	0.231	454.617	0.954	0.327	2.917	518.246
0.623	0.275	763.248	1.133	0.392	2.891	877.681
$D_e$	$D_e/d_v$	$2C+R$	$s_1$	$s_2$	$s_3$	$S$
$m. \times 10^{-2}$		$m. \times 10^{-2}$	$m. \times 10^{-4}$	$m. \times 10^{-4}$	$m. \times 10^{-4}$	$m^2 \times 10^{-4}$
0.670	3.146	0.756	1.279	0.277	0.0712	1.627
0.849	3.232	0.904	1.979	0.432	0.107	2.519
0.996	3.047	1.255	3.005	0.823	0.167	3.172
1.187	3.029	1.521	4.332	1.219	0.241	4.573

Continued Table D. 5

$\gamma_{dc} S$	$\alpha_{wda}$	$\gamma_{da} \cos \alpha_{wda}$	$\beta_{nca}$	$\gamma_{ca} \cos \beta_{nca}$	$\gamma_{dc} \cos(\theta_{wd})_c$	$(\theta_{wd})_e$	$\gamma_{dc} \cos(\theta_{wd})_e$	$\delta_{wc}$	$\gamma_{dc} \cos \delta_{wc}$
$Nm \times 10^{-5}$	deg.	$Nm^{-1} \times 10^{-3}$	deg.	$Nm^{-1} \times 10^{-3}$	$Nm^{-1} \times 10^{-3}$	deg.	$Nm^{-1} \times 10^{-3}$	deg.	$Nm^{-1} \times 10^{-3}$
084.813	36.5	57.154	140.5	-14.120	41.816	25.5	47.022	157.5	-48.369
131.244	38.0	56.027	143.0	-14.615	41.222	26.0	46.822	158.0	-48.301
165.319	39.0	55.255	144.0	-14.805	40.270	26.0	46.822	158.5	-48.473
238.280	40.0	54.465	145.0	-14.990	40.513	26.5	46.624	159.5	-48.790

$\Delta f. g. d/2 \gamma_{dc}^{-2} N^{-1}$	$\gamma_{dc} (\cos \theta_{wd}^{-1} \cos \delta_{wc})$	$V e. \Delta f. g^{-2}$	$\gamma_{nc}$	$\gamma_{wd}$	$\gamma_{wc}$	$\gamma_{nd}$	$\gamma_{dc} / (\gamma_{wd} - \gamma_{nc})$	$\gamma_{dc} / (\gamma_{nd} - \gamma_{wc})$
$Kg. sec. \times 10^{-2}$	$Nm \times 10^{-3}$	$Kg. m. sec. \times 10^{-5}$	$Nm^{-1} \times 10^{-3}$	$Nm^{-1} \times 10^{-3}$	$Nm^{-1} \times 10^{-3}$	$Nm^{-1} \times 10^{-3}$		
02.135	95.386	052.276	38.104	38.126	168.164	119.799	1.107	-1.077
22.707	95.124	104.369	37.850	84.672	162.556	114.254	1.112	-1.078
03.175	95.296	172.108	37.780	84.602	129.463	080.989	1.112	-1.074
03.785	95.421	291.479	37.640	84.264	83.647	034.850	1.117	-1.067

Table D.6 - Solid-liquid interfacial tension

Dispersed phase: Ethyl acetate		Continuous phase: Distilled water					
Junction nozzle: Glass-PTFE		$R$	$V_c$	$D_c$	$d_v$	$D_c/d_v$	$V_e$
$C$	$m. \times 10^{-2}$	$m. \times 10^{-2}$	$m. \times 10^{-6}$	$m. \times 10^{-2}$	$m. \times 10^{-2}$		$m^3 \times 10^{-6}$
0.210	0.106	0.58.416	0.501	0.157	3.192	064.503	
0.278	0.141	137.834	0.641	0.234	2.739	153.461	
0.327	0.157	208.507	0.735	0.298	2.469	225.137	
0.395	0.205	411.743	0.923	0.359	2.571	456.058	
$D_e$	$D_e/d_v$	$2C+R$	$s_1$	$s_2$	$s_3$	$S$	
$m. \times 10^{-2}$		$m. \times 10^{-2}$	$m. \times 10^{-4}$	$m. \times 10^{-4}$	$m. \times 10^{-4}$	$m^2 \times 10^{-4}$	
0.497	3.171	0.525	0.579	0.138	0.138	0.756	
0.664	2.839	0.696	1.021	0.242	0.086	1.350	
0.754	2.533	0.811	1.325	0.335	0.041	1.702	
0.955	2.66	0.994	2.121	0.490	0.072	2.684	

Continued Table No. D. 6

$\gamma_{dc} S$ $Nm \times 10^{-5}$	$\alpha_{wda}$ deg.	$\gamma_{da} \cos \alpha_{wda}$ $Nm^{-1} \times 10^{-3}$	$\beta_{nca}$ deg.	$\gamma_{ca} \cos \beta_{nca}$ $Nm^{-1} \times 10^{-3}$	$\gamma_{dc} \cos(\theta_{wd})_c$ $Nm^{-1} \times 10^{-3}$	$(\theta_{wd})_e$ deg.	$\gamma_{dc} \cos(\theta_{wd})_e$ $Nm^{-1} \times 10^{-3}$	$\delta_{wc}$ deg.	$\gamma_{dc} \cos \delta_{wc}$ $Nm^{-1} \times 10^{-3}$
06.202	125.0	-16.346	34.5	58.595	42.248	150.0	-7.101	15.5	7.901
11.074	128.0	-17.546	36.0	57.521	39.974	153.0	-7.306	18.0	7.798
13.962	129.5	-18.128	38.0	56.027	37.899	154.5	-7.401	18.5	7.776
22.0096	130.5	-18.509	38.5	55.643	37.134	156.5	-7.519	20.5	7.680

$\Delta f \cdot g \cdot d / 2 \gamma_{dc}$ $Kg. \text{ sec.}^{-2} N^{-1}$ $\times 10^{-2}$	$\gamma_{dc} (\cos \theta_{wd})^{-1}$ $Nm^{-1}$ $\times 10^{-3}$	$V_e \Delta f$ Kg. m. sec. $\times 10^{-5}$	$\gamma_{nc}$ $Nm^{-1}$ $\times 10^{-3}$	$\gamma_{wd}$ $Nm^{-1}$ $\times 10^{-3}$	$\gamma_{wc}$ $Nm^{-1}$ $\times 10^{-3}$	$\gamma_{nd}$ $Nm^{-1}$ $\times 10^{-3}$	$\gamma_{dc} / (\gamma_{wd}^{-1} \gamma_{nc})$	$\gamma_{dc} / (\gamma_{nd}^{-1} \gamma_{wc})$
3.306	15.003	6.969	11.503	4.401	29.045	36.946	-1.154	1.037
4.412	15.104	16.712	11.319	4.013	25.198	32.997	-1.122	1.051
5.010	15.177	24.517	11.090	3.689	20.725	28.501	-1.107	1.054
6.341	15.200	49.665	11.018	3.498	4.404	12.085	-1.090	1.067

Table D7 - Solid-liquid interfacial tension.

Dispersed phase: Ethyl acetate; Continuous phase: distilled water; Junction nozzle: P TFE-glass

C	R	$V_c$	$D_c$	$d_v$	$D_c/d_v$	$V_e$
$m. \times 10^{-2}$	$m. \times 10^{-2}$	$m. \times 10^{-6}$	$m. \times 10^{-2}$	$m. \times 10^{-2}$		$m. \times 10^{-6}$
0.218	0.110	065.461	0.500	0.157	3.186	068.732
0.286	0.150	158.173	0.671	0.234	2.867	176.904
0.335	0.162	225.764	0.755	0.298	2.535	257.255
0.405	0.220	476.916	0.969	0.359	2.713	524.536

$D_e$	$D_e/d_v$	$2C+R$	$s_1$	$s_2$	$s_3$	S
$m. \times 10^{-2}$		$m. \times 10^{-2}$	$m. \times 10^{-4}$	$m. \times 10^{-4}$	$m. \times 10^{-4}$	$m. \times 10^{-4}$
0.508	3.238	0.546	0.149	0.625	0.038	0.813
0.696	2.977	0.722	1.129	0.256	0.086	1.472
0.789	2.648	0.832	1.401	0.352	0.139	1.893
1.005	2.786	1.035	2.366	0.515	0.202	3.084

Continued Table No. D. 7

$\gamma_{dc}$	S	$\alpha_{wda}$	$\gamma_{da} \cos \alpha_{wda}$	$\beta_{nca}$	$\gamma_{ca} \cos \beta_{nca}$	$\gamma_{dc} \cos(\theta_{wd})c$	$(\theta_{wd})e$	$\gamma_{dc} \cos(\theta_{wd})e$	$\delta_{wc}$	$\gamma_{dc} \cos \delta_{wc}$
Nm x 10 <sup>-5</sup>	deg.	Nm <sup>-1</sup> x 10 <sup>-3</sup>	deg.	Nm <sup>-1</sup> x 10 <sup>-3</sup>	Nm <sup>-1</sup> x 10 <sup>-3</sup>	deg.	Nm <sup>-1</sup> x 10 <sup>-3</sup>	deg.	Nm <sup>-1</sup> x 10 <sup>-3</sup>	Nm <sup>-1</sup> x 10 <sup>-3</sup>
10.899	129.0	-17.935	34.5	58.595	46.709	152.5	-11.885	21.0	12.509	
19.731	131.5	-18.884	37.5	56.407	44.214	155.5	-12.193	23.5	12.228	
25.366	132.5	-19.254	38.5	55.643	43.354	156.5	-12.288	24.5	12.193	
41.334	133.0	-19.436	40.0	54.465	41.998	158.5	-12.467	26.5	11.992	

$\Delta \rho$	$\gamma_{dc} (\cos \theta_{wd} - \cos \delta_{wc}) V_e \Delta \rho_g$	$\gamma_{nc}$	$\gamma_{wd}$	$\gamma_{wc}$	$\gamma_{nd}$	$\gamma_{dc} / (\gamma_{nd} - \gamma_{wd})$
Kg. sec. <sup>-2</sup> N <sup>-1</sup>	Nm <sup>-1</sup>	Nm <sup>-1</sup>	Nm <sup>-1</sup>	Nm <sup>-1</sup>	Nm <sup>-1</sup>	( $\gamma_{nd} - \gamma_{wd}$ )
x 10 <sup>-2</sup>	x 10 <sup>-3</sup>	x 10 <sup>-3</sup>	x 10 <sup>-3</sup>	x 10 <sup>-3</sup>	x 10 <sup>-3</sup>	
2.159	24.395	17.975	6.089	47.607	60.117	-1.127
2.958	24.482	17.378	5.185	44.418	56.707	-1.098
3.351	24.482	17.173	4.884	41.101	53.295	-1.090
4.248	24.459	16.849	4.381	27.200	39.192	-1.074

Table D.8 - Solid-liquid interfacial tension

Dispersed phase: Toluene		Continuous phase: Distilled water				
Junction nozzle: Glass-PTFE						
C	R	$V_c$	$D_c$	$d_v$	$D_c/d_v$	$V_e$
$m. \times 10^{-2}$	$m. \times 10^{-2}$	$m. \times 10^{-6}$	$m. \times 10^{-2}$	$m. \times 10^{-2}$		$m. \times 10^{-6}$
0.222	0.113	075.695	0.525	0.157	3.344	078.713
0.297	0.158	192.920	0.717	0.234	3.064	216.905
0.348	0.183	415.932	0.925	0.298	3.107	440.582
0.419	0.231	696.324	1.099	0.359	3.062	779.835
$D_e$	$D_e/d_v$	$2C+R$	$s_1$	$s_2$	$s_3$	$S$
$m. \times 10^{-2}$		$m. \times 10^{-2}$	$m. \times 10^{-4}$	$m. \times 10^{-4}$	$m. \times 10^{-4}$	$m. \times 10^{-4}$
0.532	3.388	0.557	0.657	0.155	0.038	0.850
0.746	3.191	0.753	1.246	0.122	0.086	1.454
0.944	3.167	0.880	1.688	0.381	0.139	2.208
1.141	3.180	1.070	2.587	0.553	0.202	2.825

Continued Table D. 8

$\gamma_{dc}$	$S$	$\alpha_{wda}$	$\gamma_{da} \cos \alpha_{wda}$	$\beta_{nca}$	$\gamma_{ca} \cos \beta_{nca}$	$\gamma_{dc} \cos(\theta_{wd})c$	$(\theta_{wd})e$	$\gamma_{dc} \cos(\theta_{wd})e$	$\gamma_{dc} \cos \xi_{wc}$
$Nm \times 10^{-5}$	deg.	$Nm \times 10^{-3}$	deg.	$Nm \times 10^{-3}$	deg.	$Nm^{-1} \times 10^{-3}$	deg.	$Nm^{-1} \times 10^{-3}$	deg.
29.356	132.5	-24.591	35.0	58.241	155.0	-31.267	22.5	31.873	
50.194	134.5	-25.513	37.5	56.407	157.5	-31.873	25.0	31.267	
76.203	136.0	-26.183	38.5	55.643	159.5	-32.315	27.0	30.739	
97.466	137.0	-26.621	39.0	55.255	161.0	-32.620	28.0	30.461	

$\Delta \rho$	$d/2 \gamma_{dc}$	$\gamma_{dc} (\cos \theta_{wd} - \cos \xi_{wc})$	$V_e \Delta \rho$	$\gamma_{nc}$	$\gamma_{wd}$	$\gamma_{wc}$	$\gamma_{hd}$	$\gamma_{dc}$	$\gamma_{dc}$
$Kg. \text{ sec.} \times 10^{-2}$	$Nm^{-1} \times 10^{-3}$	$Nm^{-1} \times 10^{-3}$	$Kg. \text{ m. sec} \times 10^{-5}$	$Nm^{-1} \times 10^{-3}$	$Nm^{-1} \times 10^{-3}$	$Nm^{-1} \times 10^{-3}$	$Nm^{-1} \times 10^{-3}$	$(\gamma_{wd} - \gamma_{dc})$	$(\gamma_{nc} - \gamma_{wc})$
1.043	63.141	63.141	10.655	29.950	1.317	112.837	144.710	-1.204	1.082
1.465	63.141	63.141	29.501	28.797	3.076	143.598	174.865	-1.341	1.103
1.852	63.054	63.054	59.640	28.227	4.087	109.697	140.437	-1.429	1.122
2.240	63.081	63.081	105.578	27.899	4.720	85.110	115.571	-1.488	1.132

Table D.9 - Solid-liquid interfacial tension

Dispersed phase: Methylcyclohexane		Continuous phase: Distilled water						
Junction nozzle: Glass-PTFE		$C$	$R$	$V_c$	$D_c$	$d_v$	$D_c/d_v$	$V_e$
$m. \times 10^{-2}$	$m. \times 10^{-2}$	$m. \times 10^{-2}$	$m. \times 10^{-2}$	$m. \times 10^{-6}$	$m. \times 10^{-2}$	$m. \times 10^{-2}$		$m. \times 10^{-6}$
0.232	0.119	0.81.748	0.538	0.157	3.831	084.155		
0.306	0.169	210.097	0.737	0.234	3.152	239.412		
0.366	0.188	323.052	0.851	0.298	2.857	361.818		
0.450	0.244	648.226	1.073	0.359	2.990	693.602		
$D_e$	$D_e/d_v$	$2C+R$	$s_1$	$s_2$	$s_3$	$S$		
$m. \times 10^{-2}$		$m. \times 10^{-2}$	$m. \times 10^{-4}$	$m. \times 10^{-4}$	$m. \times 10^{-4}$	$m. \times 10^{-4}$		
0.543	3.464	0.584	0.729	0.169	0.0387	0.937		
0.770	3.293	0.782	1.382	0.295	0.086	1.764		
0.884	2.966	0.920	1.813	0.420	0.139	2.737		
1.098	3.058	1.144	2.916	0.636	0.202	3.755		

Continued Table D. 9

$\gamma_{dc} S$	$\alpha_{wda}$	$\gamma_{da} \cos \alpha_{wda}$	$\beta_{nca}$	$\gamma_{ca} \cos \beta_{nca}$	$\gamma_{dc} \cos (\theta_{wd})_c$	$\overline{(\theta_{wd})_c}$	$dc \cos (\theta_{wd})_c$	$\beta_{wc}$	$\gamma_{dc} \cos \beta_{wc}$
Nm x 10 <sup>-5</sup>	deg	Nm <sup>-1</sup> x 10 <sup>-3</sup>	deg	Nm <sup>-1</sup> x 10 <sup>-3</sup>	Nm <sup>-1</sup> x 10 <sup>-3</sup>	deg.	Nm <sup>-1</sup> x 10 <sup>-3</sup>	deg.	Nm <sup>-1</sup> x 10 <sup>-3</sup>
48 866	135.5	-19.828	35.0	58.241	38.413	159.0	-38.556	24.0	37.729
91.936	137.5	-20.496	37.5	56.407	35.911	161.5	-39.165	27.5	36.633
123.656	138.5	-20.820	38.5	55.643	34.822	163.0	-39.495	28.5	36.295
195.670	139.0	-20.980	40.0	54.465	33.484	164.0	-39.700	29.0	36.121

$\Delta f g d / 2 \gamma_{dc}$	$\gamma_{dc} (\cos \theta_{wd} - \cos \beta_{wc})$	$V_e \Delta \beta_e$	$\gamma_{nc}$	$\gamma_{wd}$	$\gamma_{wc}$	$\gamma_{nd}$	$\gamma_{dc} /$
Kg. sec. x 10 <sup>-2</sup>	Nm <sup>-1</sup> x 10 <sup>-3</sup>	Kg. m. sec. x 10 <sup>-5</sup>	Nm <sup>-1</sup> x 10 <sup>-3</sup>	( $\gamma_{wd} - \gamma_{nc}$ ) ( $\gamma_{nd} - \gamma_{wc}$ )			
2.151	76.286	27.476	9.283	-29.273	109.110	146.840	-1.065 1.094
3.047	75.799	78.134	8.805	-30.360	101.454	138.087	-1.054 1.127
3.496	75.790	118.202	8.591	-30.903	93.333	129.628	-1.045 1.137
4.343	75.821	226.603	8.321	-31.378	57.553	93.674	-1.040 1.143

Table D.10 - Solid-liquid interfacial tension

Dispersed phase: n-Hexane		Continuous phase: Distilled water				
Junction nozzle: Glass-PTFE						
$C$ $m. \times 10^{-2}$	$R$ $m. \times 10^{-2}$	$V_c$ $m. \times 10^{-6}$	$V_e$ $m. \times 10^{-6}$			
		$D_c$ $m. \times 10^{-2}$	$D_c/d_v$			
		$d_v$ $m. \times 10^{-2}$				
		$s_1$ $m. \times 10^{-4}$	$s_2$ $m. \times 10^{-4}$			
		$s_3$ $m. \times 10^{-4}$	$S$ $m. \times 10^{-4}$			
0.243	0.133	108.274	0.591	0.157	3.767	112.424
0.346	0.187	303.256	0.833	0.234	3.562	321.392
0.454	0.204	000.513	0.993	0.298	3.334	565.180
0.592	0.262	1090.614	1.276	0.359	3.556	1221.472
$D_e$ $m. \times 10^{-2}$	$D_e/d_v$	$2C+R$ $m. \times 10^{-2}$	$s_1$ $m. \times 10^{-4}$	$s_2$ $m. \times 10^{-4}$	$s_3$ $m. \times 10^{-4}$	$S$ $m. \times 10^{-4}$
0.599	3.816	0.619	0.861	0.185	0.006	1.053
0.849	3.632	0.879	1.222	0.376	0.014	1.613
1.025	3.442	1.114	2.366	0.650	0.023	3.039
1.325	3.693	1.448	3.932	1.104	0.033	5.070

Continued Table D. 10

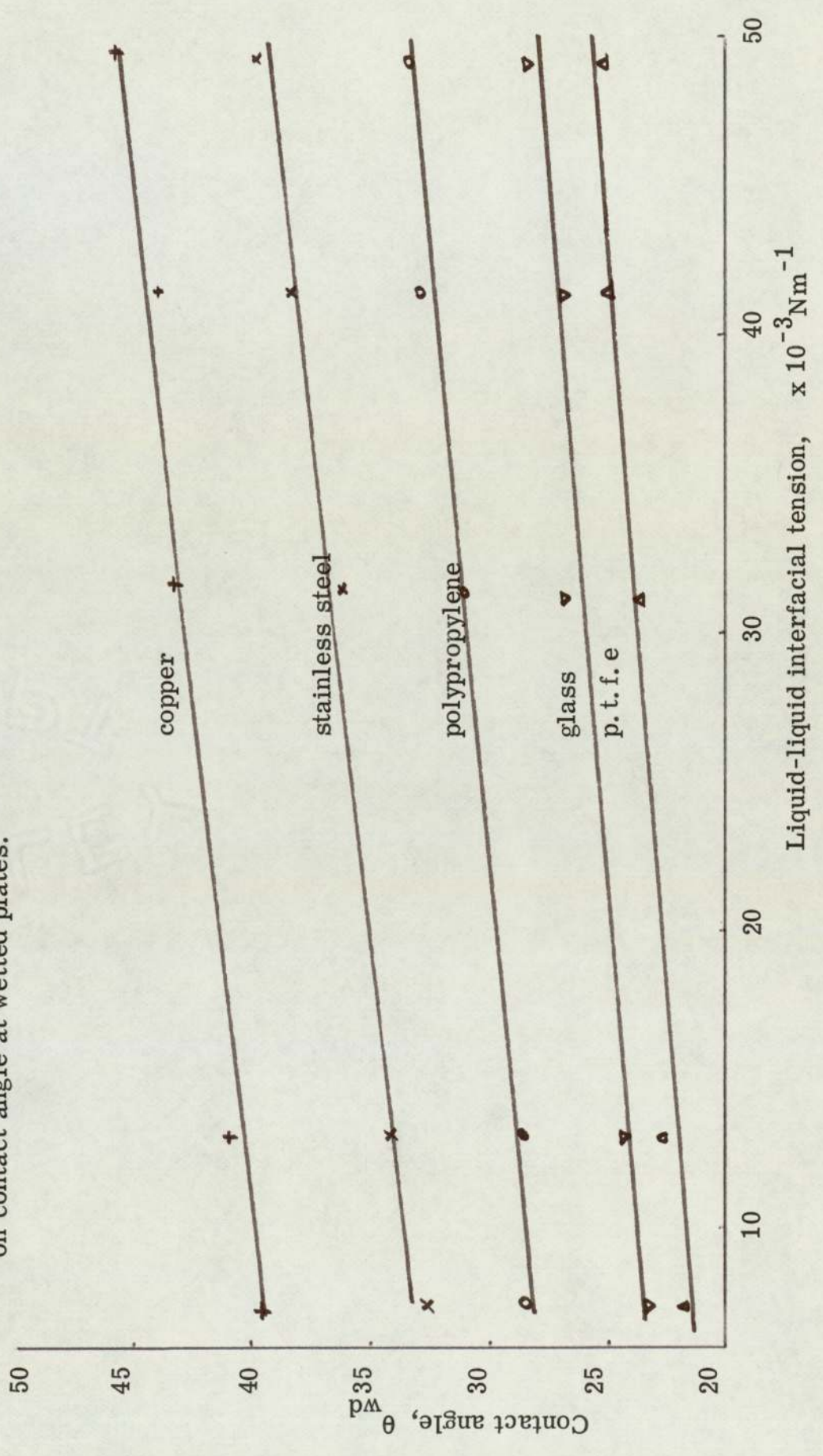
$\gamma_{dc} S$	$\alpha_{wda}$	$\gamma_{da} \cos \alpha_{wda}$	$\beta_{nca}$	$\gamma_{ca} \cos \beta_{nca}$	$\gamma_{dc} \cos(\theta_{wd})c$	$(\theta_{wd})e$	$\gamma_{dc} \cos(\theta_{wd})e$	$\alpha_{wc}$	$\gamma_{dc} \cos \alpha_{wc}$
Nm x 10 <sup>-5</sup>	deg	Nm <sup>-1</sup> x 10 <sup>-3</sup>	deg.	Nm <sup>-1</sup> x 10 <sup>-3</sup>	Nm <sup>-1</sup> x 10 <sup>-3</sup>	deg.	Nm <sup>-1</sup> x 10 <sup>-3</sup>	deg.	Nm <sup>-1</sup> x 10 <sup>-3</sup>
54.861	140.5	-14.120	35.5	57.883	43.762	164.0	-50.081	25.5	47.024
84.050	143.0	-14.615	37.5	56.407	41.792	166.5	-50.660	28.5	45.786
158.352	144.5	-14.898	39.0	55.255	40.356	167.5	-50.865	29.5	45.345
264.181	146.0	-15.171	40.5	54.064	38.893	169.0	-51.142	30.5	44.890
$\Delta \rho g d / 2 \gamma_{dc}$		$\gamma_{dc} (\cos \theta_{wd} - \cos \alpha_{wc})$	$\gamma_{nc}$	$V_e \Delta \rho g$	$\gamma_{wd}$	$\gamma_{wc}$	$\gamma_{nd}$	$\gamma_{dc} /$	$\gamma_{dc} /$
Kg. sec. <sup>-2</sup> N <sup>-1</sup>		Nm <sup>-1</sup>	Kg. m. sec <sup>-2</sup> Nm <sup>-1</sup>	Nm <sup>-1</sup>	Nm <sup>-1</sup>	Nm <sup>-1</sup>	Nm <sup>-1</sup>	( $\gamma_{wd} - \gamma_{nc}$ )	( $\gamma_{nd} - \gamma_{wc}$ )
x 10 <sup>-2</sup>		x 10 <sup>-3</sup>	x 10 <sup>-5</sup>	x 10 <sup>-3</sup>	x 10 <sup>-3</sup>	x 10 <sup>-3</sup>	x 10 <sup>-3</sup>		
1.912		97.106	37.383	37.153	-12.928	153.650	200.675	-1.040	1.107
2.712		96.446	106.862	34.228	-16.431	110.576	156.362	-1.028	1.137
3.271		96.210	187.974	32.296	-18.568	102.156	147.502	-1.024	1.148
4.231		96.033	406.228	30.207	-20.935	89.236	143.134	-1.018	1.160

Appendix E

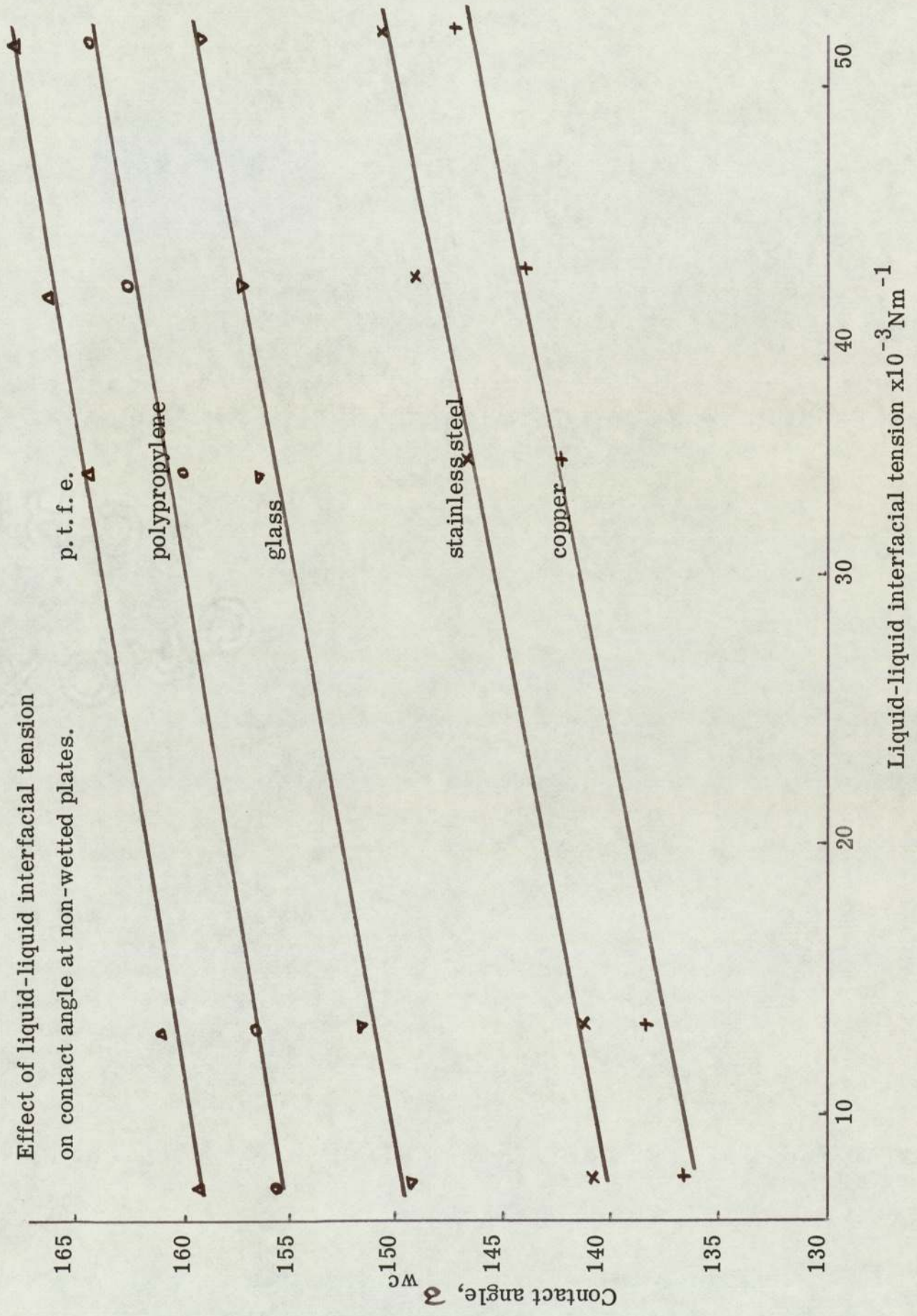
Effect of liquid-liquid interfacial tension on contact angles

---

Effect of liquid-liquid interfacial tension on contact angle at wetted plates.



Effect of liquid-liquid interfacial tension on contact angle at non-wetted plates.



Liquid-liquid interfacial tension  $\times 10^{-3} \text{ Nm}^{-1}$

Contact angle,  $\theta_w^c$

APPENDIX F

The relationship of the contact  
angle of liquid drops to the  
drop size .

Table F.1 - Exponential factor 'f'

The relationship of the contact angle of water drops at low surface energy solid plates to the drop size.

$d_2$ $mx10^{-2}$	$d_1$ $mx10^{-2}$	$\bar{\theta}_2$ degs.	$\theta_1$ degs	Organic liquid	$d_{av}$ $mx10^{-2}$	$\bar{\theta}_{av}$ degs.	$d_{1(av)}$ $mx10^{-2}$	$\bar{\theta}_{1(av)}$ degs	f
1.418	0.518	135.0	121.5	E					
1.418	0.051	154.0	144.5	E	1.366	11.5	0.051	133.0	1.626
1.456	0.072	137.5	125.0	B					
1.456	0.073	156.5	146.5	B	1.383	11.5	0.072	135.5	1.774
2.416	0.129	142.5	122.0	T					
2.416	0.129	161.0	150.0	T	2.287	15.5	0.129	136.2	5.314
2.781	0.207	148.5	136.5	M					
2.781	0.206	165.0	153.5	M	2.735	11.25	0.218	149.2	23.393
2.954	0.218	153.0	141.5	H					
2.954	0.218	168.0	157.0	H	2.735	11.25	0.218	149.2	23.393

Table F.2 - Exponential 'f'

The relationship of the contact angles of organic liquid drops at low surface energy solid plates to the drop size.

$d_2$ $mx10^{-2}$	$d_1$ $mx10^{-2}$	$\theta_2$ degs.	$\theta_1$ degs.	Organic liquid	$d_{av}$ $mx10^{-2}$	$\theta_{av}$ degs.	$d_1(av)$ $mx10^{-2}$	$\theta_1(av)$ degs.	f $mx10^{-2}/deg.$
1.104	0.049	27.0	15.5	E					
1.104	0.048	28.5	18.0	E	1.055	11.0	0.049	16.5	1.049
1.195	0.058	29.0	18.5	B					
1.195	0.059	30.0	19.5	B	0.136	10.5	0.058	19.0	1.138
1.311	0.072	29.0	18.5	T					
1.310	0.072	32.5	22.5	T	1.238	10.25	0.072	20.5	1.235
1.423	0.089	31.5	20.5	M					
1.423	0.089	32.0	22.5	M	1.335	10.5	0.089	23.0	1.444
1.519	0.110	32.0	22.5	H					
1.520	0.110	36.5	25.5	H	1.409	10.25	0.110	10.25	1.631

Table F.3 - Exponential 'f'

The relationship of the contact angle of water drops at high surface energy solid plates to the drop size.

$d_2$	$d_1$	$\theta_2$	$\theta_1$	Organic	$d_{av}$	$\theta_{av}$	$d_{1(av)}$	$\theta_{1(av)}$	f
$mx10^{-2}$	$mx10^{-2}$	degs.	degs.	liquid	$mx10^{-2}$	degs.	$mx10^{-2}$	degs.	$mx10^{-2}/deg.$
0.910	0.051	20.5	14.0	E					
1.419	0.051	33.5	25.0	E					
1.418	0.051	42.0	29.0	E	1.197	9.33	0.051	22.66	1.216
1.456	0.072	23.0	15.5	B					
1.456	0.073	38.5	28.5	B					
1.456	0.072	43.0	31.5	B	1.383	25.16	0.0727	25.16	1.081
2.417	0.129	24.5	18.0	T					
2.416	0.129	44.5	35.0	T					
2.416	0.129	48.0	37.0	T	2.287	9.0	0.129	30.0	4.22
2.781	0.206	28.0	21.5	M					
2.780	0.207	47.5	37.5	M					
2.781	0.206	53.5	39.0	M	2.735	9.33	0.218	36.66	7.869
2.954	0.218	30.5	24.0	H					
2.954	0.219	49.5	40.0	H					
2.953	0.218	58.0	46.0	H	2.735	9.33	0.218	36.66	11.685

Table F.4 - Exponential 'f'

The relationship of the contact angle of organic liquid drops at high surface energy solid plates to the drop size.

$d_2 - d_1$ $mx10^{-2}$	$\delta_2$ degs.	$\delta_1$ degs.	$d_{av} - \delta_{av}$ $mx10^{-2}$ degs.	$d_{1(av)} - \delta_{1(av)}$ $mx10^{-2}$ degs.	$f$ $mx10^{-2}/deg.$
<u>Ethyl Acetate</u>					
1.104	0.490	157.5	146.0		
1.104	0.491	147.0	135.0	1.055	10.66
1.104	0.492	130.0	121.0	0.049	134.16
					1.019
<u>n-Butyl Acetate</u>					
1.195	0.058	159.0	147.5		
1.195	0.058	148.5	139.0	1.136	10.33
1.195	0.058	134.5	125.5	0.585	136.83
					1.244
<u>Toluene</u>					
1.311	0.072	162.5	151.0		
1.311	0.072	153.0	142.0	1.238	10.66
1.310	0.072	137.0	127.0	0.072	140.16
					1.479

Table F.4 - Exponential 'f'

The relationship of the contact angle of organic liquid drops at high surface energy solid plates to the drop size.

$d_2$ $mx10^{-2}$	$d_1$ $mx10^{-2}$	$\theta_2$ degs.	$\theta_1$ degs.	$d_{av}$ $mx10^{-2}$ degs.	$\theta_{av}$ $mx10^{-2}$ degs.	$d_{1(av)}$ $mx10^{-2}$ degs.	$\theta_{1(av)}$ degs.	f $mx10^{-2}/deg.$
<u>Methylcyclohexane</u>								
1.424	0.089	166.0	154.5					
1.424	0.089	155.0	145.0	1.334	10.66	0.089	143.16	1.780
1.423	0.089	141.0	130.0					
<u>n-Hexane</u>								
1.520	0.110	171.0	158.0					
1.159	0.110	158.5	147.5	1.409	11.33	0.110	146.66	2.089
1.520	0.110	144.0	134.5					

## APPENDIX G

The ratios for the passage  
of the maximum drop diameter  
to the aperture diameter

Table G.1

The ratio for the passage of the maximum drop diameter to the void diameter

$d_v$	$S_v$	$d_n$	$S_s$	$S_s/S_v$	Maximum Drop Diameter					$D_d/d_v$					
					H	M	T	B	E	H	M	T	B	E	
Solid surface: glass nozzle															
						Continuous phase: organic liquid					Dispersed phase: distilled water				
0.213	0.035	0.321	0.045	1.269	0.217	0.219	0.219	0.219	0.221	0.223	1.020	1.030	1.032	1.039	1.047
0.261	0.053	0.372	0.055	1.029	0.269	0.270	0.271	0.272	0.274	1.031	1.037	1.039	1.044	1.050	
0.327	0.083	0.440	0.068	0.810	0.328	0.329	0.330	0.331	0.333	1.004	1.007	1.009	1.012	1.018	
0.392	0.120	0.523	0.094	0.780	0.397	0.397	0.398	0.399	0.401	1.010	1.014	1.016	1.016	1.024	
Solid surface: glass nozzle															
						Continuous phase: distilled water					Dispersed phase: organic liquid				
0.213	0.035	0.321	0.045	1.267	0.224	0.217	0.216	0.219	0.220	1.052	1.020	1.018	1.019	1.035	
0.261	0.053	0.372	0.055	1.029	0.263	0.297	0.269	0.270	0.268	1.024	1.140	1.030	1.934	1.030	
0.327	0.083	0.440	0.068	0.810	0.334	0.332	0.331	0.327	0.330	1.021	1.018	1.013	1.000	1.011	
0.392	0.126	0.523	0.094	0.780	0.409	0.402	0.397	0.396	0.398	1.044	1.025	1.013	1.010	1.0163	

Table G.2

The ratio for the passage of the maximum drop diameter to the void diameter

$d_v$	$S_v$	$d_h$	$S_s$	$S_s/S_v$	Maximum drop diameter				$D_d/d_v$					
					H	M	T	B	E	H	M	T	B	E
Solid surface: PTFE nozzle														
Continuous phase: organic liquid														
0.235	0.043	0.435	0.105	2.431	2.431	0.238	0.230	0.234	0.236	1.017	1.013	0.979	0.997	1.005
0.293	0.067	0.593	0.208	3.096	0.296	0.294	0.291	0.295	0.297	1.012	1.006	1.074	1.008	1.013
0.337	0.089	0.737	0.337	3.787	0.340	0.338	0.342	0.339	0.341	1.010	1.004	1.015	1.008	1.012
0.416	0.135	0.916	0.523	3.848	0.418	0.415	0.410	0.411	0.413	1.006	0.999	0.986	0.988	0.994
Dispersed phase: distilled water														
Solid surface: PTFE nozzle														
Continuous phase: distilled water														
0.235	0.043	0.045	0.105	2.431	0.232	0.231	0.235	0.237	0.231	0.989	0.989	1.001	0.009	0.983
0.293	0.067	0.593	0.208	3.098	0.293	0.292	0.290	0.299	0.294	1.003	0.998	0.990	1.021	1.005
0.337	0.089	0.737	0.337	3.787	0.337	0.358	0.339	0.341	0.338	1.001	1.065	1.008	1.012	1.003
0.416	0.135	0.916	0.523	3.848	0.419	0.420	0.412	0.416	0.414	1.009	1.010	0.991	1.000	0.995
Dispersed phase: organic liquid														

Table G. 3

The ratio for the passage of the maximum drop diameter to the equivalent aperture diameter of the mesh

Dimension of aperture $mx10^{-3}$	Thickness of element $mx10^{-3}$	Equivalent mesh diameter $mx10^{-2}$	Material of mesh	Maximum drop diameter						$D_d/d_e$				
				H	M	T	B	E	H		M	T	B	E
Solid surface: Mesh														
Continuous phase: Organic liquid				dispersed phase: distilled water										
3 x 3	1.5	0.338	P	0.321	0.320	0.319	0.321	0.320	0.320	0.949	0.945	0.943	0.948	0.947
2 x 2	1.0	0.225	P	0.210	0.209	0.208	0.210	0.209	0.209	0.933	0.928	0.925	0.931	0.929
2 x 2	1.0	0.225	C	0.211	0.210	0.209	0.207	0.205	0.936	0.932	0.928	0.928	0.911	0.911
1.5 x 1.5	0.75	0.169	S	0.154	0.155	0.153	0.152	0.151	0.914	0.916	0.932	0.903	0.893	0.893
1 x 1	0.5	0.112	N	0.106	0.104	0.101	0.103	0.102	0.944	0.922	0.916	0.914	0.910	0.910
Solid surface: mesh														
Continuous phase: distilled water				dispersed phase: organic liquid										
3 x 3	1.5	0.338	P	0.342	0.338	0.345	0.341	0.329	1.011	1.000	1.021	1.010	0.972	0.972
2 x 2	1.0	0.225	P	0.232	0.227	0.231	0.224	0.230	1.030	1.010	1.025	0.997	1.021	1.021
2 x 2	1.0	0.225	C	0.233	0.231	0.228	0.222	0.227	1.036	1.025	1.013	0.985	1.007	1.007
1.5 x 1.5	0.75	0.169	S	0.172	0.174	0.172	0.165	0.171	1.021	1.030	1.018	0.978	1.015	1.015
1 x 1	0.5	0.112	N	0.114	0.114	0.116	0.114	0.111	1.017	1.017	1.034	1.011	0.992	0.992

APPENDIX H

The inlet and outlet coalescence  
mechanisms of swarms of drops

Table H.1 - Inlet and Outlet Mechanisms

Continuous phase: Ethyl acetate

Dispersed phase: Distilled water

$N_a$	$N_c$	$N_a/N_c$	$(d_{vs})_i$ $mx10^{-2}$	$\%(d_{vs})_i$ $mx10^{-2}$	$(d_{vs})_o$ $mx10^{-2}$	$\%(d_{vs})_o$ $mx10^{-2}$	$d_v$ $mx10^{-2}$	$(d_{vs})_i/d_v$	$(d_{vs})_o/d_v$	$(d_{vs})_o/(d_{vs})_i$
152	97	1.5	0.253	8.3	0.241	8.1	0.213	1.18	1.13	0.95
118	85	1.4	0.485	4.7	0.438	12.5	0.327	1.48	1.34	0.90
111	63	1.8	0.602	10.5	0.697	10.7	0.392	1.53	1.78	1.16
111	97	1.1	0.614	9.1	0.258	14.3	0.213	2.88	1.21	0.42
152	85	1.8	0.247	6.4	0.423	11.6	0.327	0.75	1.29	1.71
118	63	1.9	0.468	8.2	0.681	9.2	0.392	1.19	1.74	1.45
118	97	1.2	0.471	10.8	0.232	13.4	0.213	2.21	1.09	0.49
111	85	1.3	0.616	5.3	0.443	8.5	0.327	1.88	1.35	0.72
152	63	2.4	0.269	7.9	0.674	15.7	0.392	0.69	1.72	2.51

Table H.2 - Inlet and Outlet Mechanisms

Dispersed phase liquid: Distilled water				Continuous phase liquid: n-Butyl acetate						
$N_a$	$N_c$	$N_a/N_c$	$(d_{vs})_i$ $mx10^{-2}$	$\%(d_{vs})_i$ $mx10^{-2}$	$(d_{vs})_o$ $mx10^{-2}$	$\%(d_{vs})_o$ $mx10^{-2}$	$d_v$ $mx10^{-2}$	$(d_{vs})_i/d_v$	$(d_{vs})_o/d_v$	$(d_{vs})_o/d_{vs,i}$
152	97	1.5	0.278	8.7	0.295	10.3	0.213	1.30	1.38	1.06
118	85	1.4	0.521	11.5	0.513	7.8	0.327	1.59	1.57	0.98
111	63	1.8	0.793	7.3	0.781	14.5	0.392	2.02	1.99	0.98
111	97	1.1	0.781	14.5	0.289	9.3	0.213	3.66	1.35	0.37
152	85	1.8	0.265	9.1	0.497	11.6	0.327	0.81	1.52	1.87
118	63	1.9	0.509	7.2	0.767	13.4	0.392	1.29	1.96	1.51
118	97	1.2	0.498	9.6	0.275	15.2	0.213	2.33	1.29	0.55
111	85	1.3	0.813	12.7	0.483	12.5	0.327	3.05	1.48	0.59
152	63	2.4	0.256	8.5	0.752	8.1	0.392	0.65	1.92	2.93

Table H.3 - Inlet and Outlet Mechanisms

Dispersed phase: Distilled water				Continuous phase: Toluene						
$N_a$	$N_c$	$N_a/N_c$	$(d_{vs})_i$ $\text{mx}10^{-2}$	$\%(d_{vs})_i$ $\text{mx}10^{-2}$	$(d_{vs})_o$ $\text{mx}10^{-2}$	$\%(d_{vs})_o$ $\text{mx}10^{-2}$	$d_v$ $\text{mx}10^{-2}$	$(d_{vs})_i/d_v$	$(d_{vs})_o/d_v$	$(d_{vs})_o/(d_{vs})_i$
152	97	1.5	0.312	17.2	0.338	6.9	0.213	1.46	1.59	1.08
118	85	1.4	0.545	11.5	0.597	11.2	0.327	1.65	1.82	1.10
111	63	1.8	0.842	9.7	0.838	8.5	0.392	2.14	2.14	0.99
111	97	1.1	0.829	13.6	0.378	5.7	0.213	3.89	1.77	0.46
152	85	1.8	0.318	15.1	0.556	9.3	0.327	0.97	1.87	1.92
118	63	1.9	0.537	9.5	0.812	7.8	0.392	1.37	2.07	1.51
118	97	1.2	0.518	16.1	0.297	10.2	0.213	2.43	1.39	0.57
111	85	1.3	0.875	8.3	0.589	6.5	0.327	2.67	1.80	0.67
152	63	2.4	0.306	10.7	0.861	9.1	0.392	0.78	2.19	2.81

Table H.4 - Inlet and Outlet Mechanisms

Dispersed phase: Distilled water				Continuous phase: Methylcyclohexane						
$N_a$	$N_c$	$N_a/N_c$	$(d_{vs})_i$ $\text{mx}10^{-2}$	$\%(d_{vs})_i$ $\text{mx}10^{-2}$	$(d_{vs})_o$ $\text{mx}10^{-2}$	$\%(d_{vs})_o$ $\text{mx}10^{-2}$	$d_v$ $\text{mx}10^{-2}$	$(d_{vs})_i/d_v$	$(d_{vs})_o/d_v$	$(d_{vs})_o/(d_{vs})_i$
152	97	1.5	0.341	15.0	0.392	8.5	0.213	1.60	1.84	1.14
118	85	1.4	0.575	13.3	0.628	6.8	0.327	1.75	1.92	1.09
111	63	1.8	0.878	10.5	0.890	11.0	0.392	2.24	2.27	1.02
111	97	1.1	0.912	8.3	0.405	13.4	0.213	4.28	1.90	0.45
152	85	1.8	0.335	11.7	0.612	9.5	0.327	1.02	1.87	1.83
118	63	1.9	0.581	14.5	0.875	7.1	0.392	1.48	2.23	1.51
118	97	1.2	0.561	9.1	0.378	10.6	0.213	2.63	1.77	0.67
111	85	1.3	0.931	12.4	0.640	14.3	0.327	2.84	1.96	0.69
152	63	2.4	0.358	8.6	0.901	12.5	0.392	0.91	2.30	2.52

Table H.5 - Inlet and Outlet Mechanisms

Dispersed phase: Distilled water		Continuous phase: Methylcyclohexane								
$N_a$	$N_c$	$N_a/N_c$	$(d_{vs})_i$ $\text{mx}10^{-2}$	$\%(d_{vs})_i$ $\text{mx}10^{-2}$	$(d_{vs})_o$ $\text{mx}10^{-2}$	$\%(d_{vs})_o$ $\text{mx}10^{-2}$	$d_v$ $\text{mx}10^{-2}$	$(d_{vs})_i/d_v$	$(d_{vs})_o/d_v$	$(d_{vs})_o/(d_{vs})_i$
152	97	1.5	0.341	15.0	0.392	8.5	0.213	1.60	1.84	1.14
118	85	1.4	0.575	13.2	0.628	6.8	0.327	1.75	1.92	1.09
111	63	1.8	0.878	10.5	0.890	11.0	0.392	2.24	2.27	1.02
111	97	1.1	0.912	8.3	0.405	13.4	0.213	4.28	1.90	0.45
152	85	1.8	0.335	11.7	0.612	9.5	0.327	1.02	1.87	1.83
118	63	1.9	0.581	14.5	0.875	7.1	0.392	1.48	2.23	1.51
118	97	1.2	0.561	9.1	0.378	10.6	0.213	2.63	1.77	0.67
111	85	1.3	0.931	12.4	0.640	14.3	0.327	2.84	1.96	0.69
152	63	2.4	0.358	8.6	0.901	12.5	0.392	0.91	2.30	2.52

Table H. 6 - Inlet and Outlet Mechanisms

Dispersed phase: Distilled water				Continuous phase: n-Hexane						
$N_a$	$N_c$	$N_a/N_c$	$(d_{vs})_i$ $mx10^{-2}$	$\%(d_{vs})_i$ $mx10^{-2}$	$(d_{vs})_o$ $mx10^{-2}$	$\%(d_{vs})_o$ $mx10^{-2}$	$d_v$ $mx10^{-2}$	$(d_{vs})_i/d_v$	$(d_{vs})_o/d_v$	$(d_{vs})_o/(d_{vs})_i$
152	97	1.5	0.385	16.6	0.428	7.8	0.213	1.80	2.01	1.13
118	85	1.4	0.626	12.5	0.699	11.3	0.327	1.91	2.14	1.11
111	63	1.8	0.939	9.8	0.942	8.2	0.392	2.39	2.40	1.00
111	97	1.1	0.895	21.5	0.441	10.6	0.213	4.20	2.07	0.49
152	85	1.8	0.401	17.3	0.696	8.5	0.327	1.22	2.13	1.73
118	63	1.9	0.638	19.1	0.923	9.7	0.392	1.62	2.35	1.44
118	97	1.2	0.603	18.6	0.409	10.3	0.213	2.83	1.92	0.67
111	85	1.3	0.915	20.4	0.715	7.6	0.327	2.79	2.18	0.78
152	63	2.4	0.372	14.7	0.961	6.5	0.392	0.94	0.94	2.58

APPENDIX I

Effect of density difference on the contact angles

Solid surface	p. t. f. e.	Polypropylene	Glass	Stainless Steel
Density difference	Contact	angle		
Water-ethyl acetate system				
0.101	146	125	148	137
0.087	156	149	157	155
0.024	167	161	165	163
0.006	173	175	176	176
0.001	180	180	180	180
Water-n-butyl acetate system				
0.110	148	128	153	144
0.091	159	144	162	159
0.013	165	155	170	168
0.008	172	173	178	177
0.001	180	180	180	180
Water-toluene system				
0.136	156	135	155	146
0.107	168	151	163	157
0.083	173	168	171	163
0.015	178	176	177	176
0.001	180	180	180	180
Water-methylcyclohexane system				
0.229	155	138	157	148
0.178	168	159	165	163
0.097	171	163	172	172
0.018	178	177	178	177
0.001	180	180	180	180
Water-n-hexane system				
0.338	157	141	162	152
0.223	161	162	169	161
0.106	169	170	171	170
0.075	175	174	175	174
0.001	180	180	180	180

APPENDIX J

Analysis of factors affecting  
coalescence of swarms of drops  
in a composite packing

## COALESCENCE OF LIQUID DISPERSIONS

Factors affecting coalescence of swarms of drops in a composite coalescer:

The following factors were considered to affect the coalescence of liquid dispersions at a coalescer element constructed with the junction between high and low surface energy materials.

<u>Symbol</u>	<u>Factor</u>	<u>Dimension</u>
$d_o$	diameter of the drop at the exit of the coalescer	L
$d_i$	diameter of the drop at the inlet of the coalescer	L
$\Delta P$	pressure drop across the coalescer	$ML^{-2}$
$\rho_d$	density of dispersed phase	$ML^{-3}$
	density difference between the liquid phases = $(\rho_d - \rho_c)$	$ML^{-3}$
$g$	acceleration due to gravity	$LT^{-2}$
$h_b$	packing height	L
$\gamma$	interfacial tension	$MT^{-2}$
$\mu_d$	viscosity of dispersed phase	$ML^{-1}T^{-1}$
$U_d$	flowrate of dispersed phase	$LT^{-1}$
$S_g$	surface area of wetted solid	$L^2$
$S_t$	surface area of non-wetted solid	$L^2$
$S_v$	surface area of void	$L^2$

A variable, namely the contact angle, must also be included to relate the physical properties of the solid components of the junction to the liquids of the continuous and dispersed phases.  $\cos \theta$  is a quantity which has generally been used to symbolise the wetting characteristics of the solid of the packing. However, it is a dimensionless quantity which may conveniently be combined later with the Junction Group without interfering with the dimensions of this group. For this reason,  $\cos \theta$  is not included in the following process of group formation.

#### Dimension Matrix.

According to Buckingham's theorem, the number of independent dimensionless groups that may be employed to describe the coalescence phenomena known to involve 'n' variables i. e. equal to the number 'n - r'. In the above case, the number of variables are 13, thus making 'n' = 13. A correct procedure for ascertaining the value of 'r' is as follows.

The variables involved in the coalescence phenomena are listed along a horizontal axis, and the basic dimensions, M, L, etc. to be used are listed along a vertical axis, as shown below. Under each variable, a column of numbers is listed representing the powers to which the basic dimension must be raised in the dimensional representation of the particular variable.

	$d_o$	$\Delta P$	$\beta_d$	$g$	$d_i$	$h_b$	$\gamma$	$\mu_d$	$U_d$	$S_g$	$S_t$	$S_v$	$\rho$
M	0	1	1	0	0	0	1	1	0	0	0	0	1
L	1	-2	-3	1	1	1	0	-1	1	2	2	2	-3
T	0	0	0	-2	0	0	-2	-1	0	0	0	0	0

Thus in the above representation, the variable  $\mu_d$  must have the dimensions  $M/LT$  while the variable  $g = L/T^2$ . The array of the numbers so formed is called the dimensional matrix of the phenomena and is represented as

$$\begin{pmatrix} 0 & 1 & 1 & 0 & 0 & 0 & 1 & 1 & 0 & 0 & 0 & 0 & 1 \\ 1 & -2 & -3 & 1 & 1 & 1 & 0 & -1 & 1 & 2 & 2 & 2 & -3 \\ 0 & 0 & 0 & -2 & 0 & 0 & 2 & -1 & -1 & 0 & 0 & 0 & 0 \end{pmatrix}$$

From basic algebra one may take the determinant of a group of numbers forming an arrangement having an equal number of rows and columns. The above array may be squared up by adding 10 rows of zeros. However, the determinant of this matrix is zero. The size of the next smaller square subgroup that has a non-zero determinant is determined. The number of rows of the columns in this determinant then defines the rank of the original matrix. For instance, using first three rows and columns give

$$\begin{vmatrix} 1 & 1 & 1 \\ -1 & 0 & -5 \\ -1 & -2 & 0 \end{vmatrix} = -6 \quad (\text{J.1})$$

Making the rank of the dimensional matrix equal to three. The value of 'r' in Buckingham's theorem is the rank of the dimensional matrix i. e.  $r = 3$ .

In expressing the variables dimensionally, three basic dimensions M, L and T are employed; this gives the value of 'r' equal to three since 'r' has also been regarded as the number of the basic dimensions needed to express the variables dimensionally. The number of dimensionless groups can be calculated by subtracting 'r' from 'n' since both of these numbers have already been determined i. e.  $13 - 3 = 10$

Formation of groups:

Now when the correct number of the dimensionless groups = 10 is determined, the groupings are formed as follows.

Functionally, the exit drop size may be expressed as

$$d_o = f(\Delta P, \rho, \rho_d, g, d_i, h_b, \gamma, \mu_d, U_d, S_g, S_t, S_v) \quad (\text{J.1. a})$$

The right side of Equation J.1. a is replaced by an infinite series,

$$d_o = (K_1 \cdot \Delta P^{a_1} \cdot \rho_d^{b_1} \cdot \Delta \rho^{c_1} \cdot g^{d_1} \cdot d_i^{e_1} \cdot h_b^{f_1} \cdot \gamma^{l_1} \cdot \mu_d^{m_1} \cdot U_d^{n_1} \cdot S_g^{p_1} \cdot S_t^{q_1} \cdot S_v^{u_1}) + K_2 \cdot \Delta P^{a_2} \cdot \rho_d^{b_2} \cdot \Delta \rho^{c_2} \cdot g^{d_2} \cdot d_i^{e_2} \cdot h_b^{f_2} \cdot \gamma^{l_2} \cdot \mu_d^{m_2} \cdot U_d^{n_2} \cdot S_g^{p_2} \cdot S_t^{q_2} \cdot S_v^{u_2} + K_3 \dots \quad (\text{J.2})$$

Where  $K_1, K_2, \dots$  are the dimensionless coefficients and  $a_1, b_1, \dots, a_2, b_2, \dots$  are the exponents required by the series. Since each grouping in Equation J.2 must have the same dimensions by the Law of Dimensional Homogeneity, only the first term of the series needs to be included in the dimensional representation of the above equation. Hence, dropping the subscripts of the exponents and expressing the equation dimensionally,

$$L = [ML^{-2}]^a \cdot [ML^{-3}]^b \cdot [LT^{-2}]^d \cdot [ML^{-3}]^c \cdot [L]^e \cdot [L]^f \cdot [MT^{-2}]^l \cdot [ML^{-1}T^{-1}]^m \cdot [LT^{-1}]^n \cdot [L^2]^p \cdot [L^2]^q \cdot [L^2]^u \quad (\text{J.3})$$

The exponents of the basic dimensions M, L and T on both sides of Equation J.3 respectively can be equated according to the Law of Dimensional Homogeneity to form the following set of simultaneous algebraic equations:

For L  $1 = -2a - 3b - 3c + d + e + f - 1 - m + n + 2p + 2q + 2u$

For M  $0 = a + b + c + 1 + m$

For T  $0 = -2d - m - n$

Since there are 13 quantities which are related by only three simultaneous equations, any ten quantities can be solved in terms of the remaining three.

$$a = -b - c - 1 - m$$

$$n = -2d - m$$

$$e = 1 + b + c - 1 + d - f - 2p - 2q - 2u$$

Substituting the values of the exponents 'a', 'n' and 'e' in Equation J. 2 gives,

$$d_o = K(\Delta P)^{-b-c-1-m} \cdot (\rho_d)^b \cdot (\Delta \rho)^c \cdot (g)^d \cdot (d_i)^{1+b+c-1+d-f-2p-2q-2u} \\ (h_b)^f \cdot (\mu_d)^m \cdot (\gamma)^1 \cdot (U_d)^{-2d-m} \cdot (S_g)^p \cdot (S_t)^q \cdot (S_v)^u \quad (J. 4)$$

Upon grouping these terms with the same exponents together and extending the results to the other members of the series, Equation J. 4 may be expressed as,

$$d_o/d_i = K_1 (\rho_d \cdot d_i / \Delta P)^{b1} \cdot (\Delta \rho \cdot d_i / \Delta P)^{c1} \cdot (g \cdot d_i / U_d^2)^{d1} \cdot (h_b / d_i)^{f1} \\ (\gamma / \Delta \rho d_i)^{11} \cdot (\mu_d / \Delta P U_d)^{m1} \cdot (S_g / d_i^2)^{p1} \cdot (S_t / d_i^2)^{q1} \cdot \\ (S_v / d_i^2)^{u1} + K_2(\dots\dots) + K_3(\dots\dots) + \dots \quad (J. 5)$$

Finally returning to the functional representation of the series,

$$d_o/d_i = K(\rho_d \cdot d_i / \Delta P)^b \cdot (\Delta \rho d_i / \Delta P)^c \cdot (g \cdot d_i / U_d^2)^d \cdot (h_b / d_i)^f \\ (\gamma / \Delta P d_i)^1 \cdot (\mu_d / \Delta P U_d)^m \cdot (S_g / d_i^2)^p \cdot (S_t / d_i^2)^q \cdot (S_v / d_i^2)^u \quad (J. 6)$$

$$\text{or } \bar{\kappa}_o = K \cdot \bar{\kappa}_1 \cdot \bar{\kappa}_2 \cdot \bar{\kappa}_3 \cdot \bar{\kappa}_4 \cdot \bar{\kappa}_5 \cdot \bar{\kappa}_6 \cdot \bar{\kappa}_7 \cdot \bar{\kappa}_8 \cdot \bar{\kappa}_9 \quad (J. 7)$$

where  $d_o/d_i = \pi_0$        $\rho_d \cdot d_i/\Delta P = \pi_1$        $\Delta\rho \cdot d_i/\Delta P = \pi_2$

$g \cdot d_i/U_d^2 = \pi_3$        $h_b/d_i^2 = \pi_4$        $/\Delta P \cdot d_i = \pi_5$

$\mu_d/\Delta\rho \cdot U_d = \pi_6$        $S_g/d_i^2 = \pi_7$        $S_t/d_i^2 = \pi_8$

and  $S_v/d_i^2 = \pi_9$  (J. 8)

**Pie Transformations:**

The term  $\Delta P$ , although difficult to measure, was included because it was considered important in the coalescence process. To eliminate this term and to form more recognisable groups, the standard technique of  $\pi$ -transformation was carried out.

$\pi_6 \cdot \pi_2 \cdot \pi_3 / \pi_1 \cdot \pi_5 = \Delta\rho \cdot d_i^2 \cdot g \cdot \mu_d / U_d^3 \cdot \rho_d \cdot \gamma = \text{Group 1}$

$\pi_6^2 / \pi_1 \cdot \pi_5 = \mu_d^2 / \gamma \cdot U_d^2 \cdot \rho_d = \text{Group 2}$

$\pi_2 \cdot \pi_3 / \pi_1 = d_i \cdot g \cdot \Delta\rho / U_d^2 \cdot \rho_d = \text{Group 3}$

$\pi_1 \cdot \pi_3 / \pi_5 = g \cdot d_i^3 \cdot \Delta\rho / U_d^2 \cdot \gamma = \text{Group 4}$

$1/\pi_4 = d_i/h_b = \text{Group 5}$

$1/\pi_9 = d_i^2/S_v = \text{Group 6}$

$\pi_1 \cdot \pi_2 \cdot \pi_3 / \pi_6 = \Delta\rho \cdot d_i \cdot \rho_d \cdot g / \mu_d^2 = \text{Group 7}$

$\pi_8 = (S_t/d_i^2) \cdot \cos \theta = \text{Group 8}$

$\pi_9 = (S_v/d_i^2) \cdot \cos \theta = \text{Group 9}$

$\pi_0 = d_o/d_i = \text{Group 0}$

(J.9)

It may be noted that the contact angle is now combined with the respective high and low energy groups where  $\theta$  and  $\theta_2$  are the contact angles of the drop at a high and low surface energy solid material respectively.

Rewriting Equation J.7 in terms of the above ten groups,

$$\begin{aligned} (\text{Group } 0) = & K. (\text{Group } 1)^b. (\text{Group } 2)^c. (\text{Group } 3)^d. (\text{Group } 4)^f. \\ & (\text{Group } 5)^l. (\text{Group } 6)^m. (\text{Group } 7)^p. (\text{Group } 8)^q. \\ & (\text{Group } 9)^u \end{aligned} \quad (\text{J. } 10)$$

The ten constants i. e. K, b, c, d, f, l, m, p, q and u in Equation J.10 were evaluated using the Statistical Analysis Mark 2 computer program of the ICL 1900 series. The values of four of these ten constants, i. e. c, d, m and p, were found to be zero, thus eliminating the corresponding four groups from Equation J.10. The groups 1 and 4 were combined to give Bond Number and the remaining three groups were re-named as follows:

Groups 1 and 4	Bond Number
Group 5	Height Number
Group 8	High Surface Energy Number
Group 9	Low Surface Energy Number

Regression analysis was carried out on these four groups with Group 0 as a dependent variable. However, when the experimental values were inserted in Equation J.10 with four groups and five constants, a general correlation of reasonable accuracy could not be obtained. This was probably due to the two groups, i. e. low and high surface energy groups, being taken separately whereas the effect of the junction of these two groups together was being investigated.

### Greco-Latin Squares:

Further experimental studies were carried out and the results were formed into randomised blocks and the latin squares as explained by Davis (28). The twelve parameters involved in the analysis were grouped into the following seven sets of variables:

(a) Physical properties of liquids	A, B, C, D
(b) Flowrates of dispersed phase liquid	1, 2, 3, 4
(c) Bed heights	1, 2, 3, 4
(d) Void diameters	1, 2, 3, 4
(e) Drop diameter at the inlet	1, 2, 3, 4
(f) Surface area of high surface energy solid	1, 2, 3, 4
(g) Surface area of low surface energy solid	1, 2, 3, 4

The formation of the above sets resulted in a 7x4 matrix and in order to form a 4x4 latin square, the groups (d) and (e) were combined to give the ratio void diameter/inlet drop diameter. Similarly, groups (f) and (g) were combined to give the effect of a junction. In this manner, the following 4x4 square matrix was obtained and the experiments were carried out at various flowrates of dispersed phase.

(a) Physical properties of the liquid system	A, B, C, D
(b) bed heights	1, 2, 3, 4
(c) void diameter /inlet drop diameter	1, 2, 3, 4
(d) surface area of junction	1, 2, 3, 4

With the above approach of analysis of the results, the maximum number of variables possible with the existing apparatus could be included thus economising on the number of experiments that would otherwise be needed to investigate each individual parameter. The following is a typical Greco-Latin square formed by arranging the above variables in randomised blocks. The experimental data for the analysis consisted of four such squares which required 64 experimental trials, thus enabling an optimisation of the amount of experimental work.

No. 1	Bed Heights			
	1	2	3	4
1	A	B	C	D
$d_v$	2	B	A	D
	3	C	D	A
$\frac{d_v}{d_i}$	4	D	C	B
				A

A multiple regression analysis was carried out on these randomised blocks and latin squares with three independent dimensionless groups i. e. Bond Number, Height Number and Junction Number. The regression coefficients were evaluated for these independent groups at 99.0 % significant level and with Drop Number as the dependent group.

From the above process of analysis of experimental results of coalescence of swarms of drops in a junction coalescer the following correlation was finally obtained.

$$\text{Drop Number} = K. (\text{Bond Number})^a. (\text{Height Number})^b. (\text{Junction Number})^c \quad (\text{J. 11})$$

where  $K = 0.724$  and

$$a = 0.273 \quad b = 0.091 \quad \text{and} \quad c = 1.220$$

To test the accuracy of the correlation (Equation J. 11 ), the experimental values were substituted on the right hand side of Equation J. 11 and the Drop Number was evaluated by inserting the values of the constants calculated. The value of the calculated Drop Number (CDRPNO) was compared with the values of the experimental Drop Number (EDRPNO). Both these values are shown in this appendix where a percentage difference between these two is also shown. The mean value of this difference was 0.2 which showed the correlation was of a reasonable accuracy.

DELIM NAME IS TEST 1

TA (I) CARLS  
INPUT FILE NAME IS ICL STATFILE  
REEL SEQUENCE NUMBER IS  
FILE GENERATION NUMBER IS  
RETENTION PERIOD IS

312

SERVATION MATRIX M1  
METHODS ARE NOT USED  
NAMES M1

- DIOUT
- DIAIN
- DLDEN
- GRVIT
- VSDIS
- VLDIS
- DNDIS
- INTER
- REDHT
- DVOID
- DPTFE
- DGLAS

NUMBER OF COL NAMES IS 12

TRANSFORMATIONS M1 CHANGE M3

RP0=(DIOUT)/(DIAIN)  
 RP1=(DLDEN\*(DIAIN\*\*2.0)\*GRVIT\*VSDIS)/((VLDIS\*\*3.0)\*DNDIS\*INTER)  
 RP2=(VSDIS\*\*2.0)/(INTER\*(VLDIS\*\*2.0)\*DNDIS)  
 RP3=(DIAIN\*GRVIT\*DLDEN)/((VLDIS\*\*2.0)\*DNDIS)  
 RP4=(GRVIT\*(DIAIN\*\*3.0)\*DLDEN)/((VLDIS\*\*2.0)\*INTER)  
 RP5=(DIAIN)/(REDHT)  
 RP6=(0.605\*DIAIN)/(DVOID)  
 RP7=(DLDEN\*DNDIS\*(DIAIN\*\*3.0)\*GRVIT)/(VSDIS\*\*2.0)  
 RP8=(0.785\*((DPTFE-DGLAS)\*\*2.0))/(DIAIN\*\*2.0)  
 RP9=(0.785\*((DGLAS-DVOID)\*\*2.0))/(DIAIN\*\*2.0)

NUMBER OF TRANSFORMATIONS 0010  
TRANSFORMATIONS M3 TRANS1 M2

RP0=ALOG(GRP0)  
 RP1=ALOG(GRP1)  
 RP2=ALOG(GRP2)  
 RP3=ALOG(GRP3)  
 RP4=ALOG(GRP4)  
 RP5=ALOG(GRP5)  
 RP6=ALOG(GRP6)  
 RP7=ALOG(GRP7)  
 RP8=ALOG(GRP8)  
 RP9=ALOG(GRP9)

NUMBER OF TRANSFORMATIONS 0010

CROSS PRODUCT M2  
 NUMBER OF OBSERVATIONS IN CROSS PRODUCT IS 12  
 COVARIANCE M2  
 CORRELATION M2  
 MEAN VALUES M2 LP

XDS3/25

ICL 1900 STATISTICAL ANALYSIS

17/07/78

CUT OFF PARAMETER

.100000E-5

DEGREE OF FREEDOM 10

99.00 %

INDEPENDENT VARIABLES AT SIGNIFICANT LEVEL 99.00 %

GRP1 GRP2 GRP3 GRP4 GRP5 GRP6 GRP7 GRP8 GRP9

VARIABLE GRP1 JOINED THE REGRESSION SET

VARIABLES IN THE REGRESSION SET

VAR NAME	REGRESSION COEFF	STANDARD ERROR	CONFIDENCE INTERVAL	T STAT	PART CORR	MULTIPLE CORRELATION	E S S
GRP1	0.584020	.291892E 0		1.32	0.38	0.000	.110000E 2

VARIABLES NOT IN THE REGRESSION SET

VAR NAME	T STAT	PART CORR	MULTIPLE CORRELATION	E S S
GRP2	3.39	0.75	0.791	.411932E 1
GRP3	5.05	0.86	0.882	.244361E 1
GRP4	5.89	-0.89	0.908	.193123E 1
GRP5	1.87	-0.53	0.621	.675647E 1
GRP6	6.89	-0.92	0.930	.149371E 1
GRP7	4.66	-0.84	0.866	.274936E 1
GRP8	1.15	0.36	0.508	.816360E 1
GRP9	4.79	0.85	0.872	.263862E 1

E.S.S. .957213E 1

RESIDUAL ERROR .968698E 0

MULT CORR 0.385

INTERCEPT TERM - 0.9973735

XDS3725

ICL 1900 STATISTICAL ANALYSIS

17/01/78

17/07/78

REGRESSION ANALYSIS CORR 92 CUT OFF PARAMETER .100000E-5

DEPENDENT VARIABLE GRP9 DEGREES OF FREEDOM 9

INDEPENDENT VARIABLES AT SIGNIFICANT LEVEL 90.00 %

GRP1 GRP2 GRP3 GRP4 GRP5 GRP6 GRP7 GRP8 GRP9

VARIABLE GRP4 JOINED THE REGRESSION SET

VARIABLES IN THE REGRESSION SET

VAR NAME	REGRESSION COEFF	STANDARD ERROR	CONFIDENCE INTERVAL	T STAT	PART CORR	MULTIPLE CORRELATION	E S S
GRP1	0.1980461	.143220E 0		1.38	0.42	0.887	.234155E 1
GRP4	0.6433754	.143220E 0		5.89	-0.89	0.385	.937213E 1

VARIABLES NOT IN THE REGRESSION SET

VAR NAME	T STAT	PART CORR	MULTIPLE CORRELATION	E S S
GRP2	2.37	-0.64	0.947	.113603E 1
GRP3	2.37	0.64	0.947	.113603E 1
GRP5	0.26	0.09	0.909	.191467E 1
GRP6	1.64	-0.50	0.932	.144497E 1
GRP7	2.37	0.64	0.947	.113603E 1
GRP8	2.37	-0.64	0.947	.113603E 1
GRP9	0.78	-0.27	0.915	.179409E 1

E.S.S. .193123E 1

RESIDUAL ERROR .403230E 0

MULT CORR 0.908

INTERCEPT TERM 4.2494052

REGRESSION ANALYSIS CORR B2 CUT OFF PARAMETER .100000E-5

DEPENDENT VARIABLE GRP0 DEGREES OF FREEDOM 8

INDEPENDENT VARIABLES AT SIGNIFICANT LEVEL 99.00 %

GRP1 GRP2 GRP3 GRP4 GRP5 GRP6 GRP7 GRP8 GRP9 GRP0

VARIABLE GRP3 JOINED THE REGRESSION SET

VARIABLES IN THE REGRESSION SET

VAR NAME	REGRESSION COEFF	STANDARD ERROR	CONFIDENCE INTERVAL	T STAT	PART CORR	MULTIPLE CORRELATION	E S S
GRP1	0.2594678	.117799E 0		2.03	0.58	0.918	.172149E 1
GRP4	1.0709352	.153509E 0		7.03	-0.93	0.508	.816360E 1
GRP8	0.5663843	.154827E 0		2.37	-0.64	0.908	.193123E 1

VARIABLES NOT IN THE REGRESSION SET

VAR NAME	T STAT	PART CORR	MULTIPLE CORRELATION	E S S
GRP2	0.00		0.947	.113603E 1
GRP3	0.00	-0.00	0.947	.113603E 1
GRP5	0.00	-0.00	0.947	.113603E 1
GRP6	0.60	-0.22	0.950	.108013E 1
GRP7	0.00	0.00	0.947	.113603E 1
GRP9	0.60	-0.22	0.950	.108013E 1

E.S.S. .113603E 1

RESIDUAL ERROR .576654E 0

MULT CORR 0.947

INTERCEPT TERM 6.9042064

REGRESSION ANALYSIS      CORR      0.2      CUT OFF PARAMETER      .100000E- 5

DEPENDENT VARIABLE      GRP0      DEGREES OF FREEDOM      7

INDEPENDENT VARIABLES AT SIGNIFICANT LEVEL      99.00 %

GRP1      GRP2      GRP3      GRP4      GRP5      GRP6      GRP7      GRP8      GRP9

VARIABLE GRP5 JOINED THE REGRESSION SET

VARIABLES IN THE REGRESSION SET

VAR NAME	REGRESSION COEFF	STANDARD ERROR	CONFIDENCE INTERVAL	T STAT	PART CORR	MULTIPLE CORRELATION	E S S
GRP1	0.2591678	.137309E 0		1.74	0.55	0.923	.162849E 1
GRP4	1.0799152	.185465E 0		5.82	-0.91	0.630	.663826E 1
GRP5	0.0000000	.177090E 0		0.00	-0.00	0.947	.113603E 1
GRP6	0.3665343	.167268E 0		2.19	-0.64	0.909	.191467E 1

VARIABLES NOT IN THE REGRESSION SET

VAR NAME	T STAT	PART CORR	MULTIPLE CORRELATION	E S S
GRP2	0.00		0.947	.113603E 1
GRP3	0.00	-0.00	0.947	.113603E 1
GRP0	0.56	-0.22	0.950	.108013E 1
GRP7	0.00	0.00	0.947	.113603E 1
GRP9	0.56	-0.22	0.950	.108013E 1

E.S.S.      .113603E 1

RESIDUAL ERROR      .402653E 0

MULT CORR      0.947

INTERCEPT TERM      4.9642044

REGRESSION ANALYSIS CORR 012 CUT OFF PARAMETER .100000E-5

DEPENDENT VARIABLE 6300 DEGREES OF FREEDOM 6

INDEPENDENT VARIABLES AT SIGNIFICANT LEVEL 99.00 %

GRP1 GRP2 GRP3 GRP4 GRP5 GRP6 GRP7 GRP8 GRP9

VARIABLE GRP6 JOINED THE REGRESSION SET

VARIABLES IN THE REGRESSION SET

VAR NAME	REGRESSION COEFF	STANDARD ERROR	CONFIDENCE INTERVAL	T STAT	PART CORR	MULTIPLE CORRELATION	E S S
GRP1	0.4162708	.540175E 0		1.19	0.44	0.937	.133601E 1
GRP4	- 1.4251920	.642693E 0		2.19	-0.67	0.907	.194640E 1
GRP5	- 0.0000000	.186513E 0		0.00	-0.00	0.950	.108013E 1
GRP6	- 0.3513151	.178233E 0		1.97	-0.63	0.916	.177956E 1
GRP9	- 0.4573616	.764902E 0		0.59	-0.22	0.947	.113603E 1

VARIABLES NOT IN THE REGRESSION SET

VAR NAME	T STAT	PART CORR	MULTIPLE CORRELATION	E S S
GRP2	0.00		0.950	.108013E 1
GRP3	0.00	-0.00	0.950	.108013E 1
GRP6	0.00	-0.00	0.950	.108013E 1
GRP7	0.00	0.00	0.950	.108013E 1

E.S.S. .108013E 1

RESIDUAL ERROR .424290E 0

MULT CORR 0.950

INTERCEPT TERM 5.6521165

XDS3/25

ICL 1900 STATISTICAL ANALYSIS

10/02/76

10/05/53

CUT OFF PARAMETER .100000E- 5

DEGREES OF FREEDOM 59

99.00 %

REGRESSION ANALYSIS

DEPENDENT VARIABLE DROPO

INDEPENDENT VARIABLES AT SIGNIFICANT LEVEL

BONDRO HIGHTNO HSEJNO LSEJNO

VARIABLE BONDRO JOINED THE REGRESSION SET

VARIABLES IN THE REGRESSION SET

VAR NAME	REGRESSION COEFF	STANDARD ERROR	CONFIDENCE INTERVAL	T STAT	PART CORR	MULTIPLE CORRELATION	F S S
BONDRO	0.6375055	.711190E- 1		11.78	-0.84	0.000	.600000E 2

VARIABLES NOT IN THE REGRESSION SET

VAR NAME	T STAT	PART CORR	MULTIPLE CORRELATION	F S S
HIGHTNO	0.62	-0.08	0.839	.177876E 2
HSEJNO	4.40	0.50	0.881	.134242E 2
LSEJNO	1.77	0.23	0.847	.169857E 2

F.S.S. .179050E 2

RESIDUAL ERROR .530836E 0

MULT CORR 0.838

INTERCEPT TERM 0.416603E

10/56/54 10/02/76 ICL 1900 STATISTICAL ANALYSIS XDS5/25

REGRESSION ANALYSIS CORR DATS CUT OFF PARAMETER .100000F- 5

DEPENDENT VARIABLE DR0PNO DEGREES OF FREEDOM 58

INDEPENDENT VARIABLES AT SIGNIFICANT LEVEL 99.00 %

RONDNO HGHTR0 HSEJNO LSEJNO

VARIABLE HGHTR0 JOINED THE REGRESSION SET

VARIABLES IN THE REGRESSION SET

VAR NAME	REGRESSION COEFF	STANDARD ERROR	CONFIDENCE INTERVAL	T STAT	PART CORR	MULTIPLE CORRELATION	E S S
RONDNO	0.7724171	.127316E 0		6.07	-0.62	0.718	.290755E 2
HGHTR0	0.0787821	.127316E 0		0.62	-0.08	0.838	.179050E 2

VARIABLES NOT IN THE REGRESSION SET

VAR NAME	T STAT	PART CORR	MULTIPLE CORRELATION	E S S
HSEJNO	4.75	0.53	0.887	.177491E 2
LSEJNO	1.68	0.22	0.847	.169526E 2

F.S.S. .177676E 2

RESIDUAL ERROR .553789E 0

MULT CORR 0.339

INTERCEPT TERM 0.2784249

10/30/54

10/02/76

ICL 1900 STATISTICAL ANALYSIS

XDS3/25

REGRESSION ANALYSIS CORR MATS CUT OFF PARAMETER .100000E-5

DEPENDENT VARIABLE DROPNO DEGREES OF FREEDOM 57

INDEPENDENT VARIABLES AT SIGNIFICANT LEVEL 99.00 %

BONDNO HGTNO HSEJNO LSEJNO

VARIABLE USEJNO JOINED THE REGRESSION SET

VARIABLES IN THE REGRESSION SET

VAR NAME	REGRESSION COEFF	STANDARD ERROR	CONFIDENCE INTERVAL	T STAT	PART CORR	MULTIPLE CORRELATION	F S S
BONDNO	0.4563675	.256421E 0		1.85	-0.24	0.837	.179667E 2
HGTNO	0.0424317	.127242E 0		0.33	-0.04	0.847	.169857E 2
LSEJNO	0.3050152	.229780E 0		1.68	0.22	0.839	.177876E 2

VARIABLES NOT IN THE REGRESSION SET

VAR NAME	T STAT	PART CORR	MULTIPLE CORRELATION	F S S
HSEJNO	5.12	0.56	0.899	.115426E 2

E.S.S. .159526E 2

RESIDUAL ERROR .545357E 0

MULT CORR 0.347

INTERCEPT TERM 0.2480350

XDS4/25

ICL 1900 STATISTICAL ANALYSIS

10/02/76

10/06/55

REGRESSION ANALYSIS CORR DATA CUT OFF PARAMETER .100000E-5

DEPENDENT VARIABLE DRBPNO DEGREES OF FREEDOM 56

INDEPENDENT VARIABLES AT SIGNIFICANT LEVEL 99.00 %

ROHPNO HGHINO ASEJNO LSEJNO

VARIABLE HSEJNO JOINED THE REGRESSION SET

VARIABLES IN THE REGRESSION SET

VARIABLE	REGRESSION COEFF	STANDARD ERROR	CONFIDENCE INTERVAL	T STAT	PART CORR	MULTIPLE CORRELATION	F S S
ROHPNO	0.7952392	.510730E 0		2.56	0.32	0.886	.128929E 2
HGHINO	0.2734754	.122568E 0		2.25	0.29	0.889	.125688E 2
HSEJNO	1.4593624	.284954E 0		5.12	0.56	0.847	.169526E 2
LSEJNO	0.4642976	.101914E 0		2.42	0.51	0.887	.127491E 2

F, S, S. .115426E 2 .

RESIDUAL ERROR .454003E 0

MULT CORR 0.899

INTERCEPT TERM 1.2490222



18/22/06 06/02/78 ICL 1900 STATISTICAL ANALYSIS XDS3/25

REGRESSION ANALYSIS CORR MATS CUT OFF PARAMETER .100000E-5

DEPENDENT VARIABLE DROPNO DEGREES OF FREEDOM 61

INDEPENDENT VARIABLES AT SIGNIFICANT LEVEL 99.00 %

BONDNO HGTNO JNCTNO

VARIABLE BONDNO JOINED THE REGRESSION SET

VARIABLES IN THE REGRESSION SET

VAR NAME	REGRESSION COEFF	STANDARD ERROR	CONFIDENCE INTERVAL	T STAT	PART CORR	MULTIPLE CORRELATION	E S S
BONDNO	0.8442558	.686201E-1		12.30	0.84	0.000	.620000E 2

VARIABLES NOT IN THE REGRESSION SET

VAR NAME	T STAT	PART CORR	MULTIPLE CORRELATION	E S S
HGTNO	0.71	0.09	0.846	.176607E 2
JNCTNO	3.78	0.44	0.876	.143836E 2

E.S.S. .178084E 2

RESIDUAL ERROR .540316E 0

MULT CORR 0.844

INTERCEPT TERM 0.4062891

XDS3/25

ICL 1900 STATISTICAL ANALYSIS

18/22/08 06/02/78

REGRESSION ANALYSIS CORR MATJ CUT OFF PARAMETER .100000E-5

DEPENDENT VARIABLE DROPNO DEGREES OF FREEDOM 60

INDEPENDENT VARIABLES AT SIGNIFICANT LEVEL 99.00 %

BONDNO HGTNO JNCTNO

VARIABLE HGTNO JOINED THE REGRESSION SET

VARIABLES IN THE REGRESSION SET

VAR NAME	REGRESSION COEFF	STANDARD ERROR	CONFIDENCE INTERVAL	T STAT	PARTY CORR	MULTIPLE CORRELATION	E S S
BONDNO	0.7707617	.124542E 0		6.19	=0.62	0.730	.289343E 2
HGTNO	0.0882261	.124542E 0		0.71	=0.09	0.844	.178084E 2

VARIABLES NOT IN THE REGRESSION SET

VAR NAME	T STAT	PARTY CORR	MULTIPLE CORRELATION	E S S
JNCTNO	3.76	0.44	0.878	.142495E 2

E.S.S. .176607E 2

RESIDUAL ERROR .542535E 0

MULT CORR 0.846

INTERCEPT TERM 0.2495855

XDS3/25

ICL 1900 STATISTICAL ANALYSIS

06/02/78

18/22/10

REGRESSION ANALYSIS CORR MATS CUT OFF PARAMETER .100000E- 5

DEPENDENT VARIABLE DROPNO DEGREES OF FREEDOM 59

INDEPENDENT VARIABLES AT SIGNIFICANT LEVEL 99.00 X

RONDNO HGHTNO JNCTNO

VARIABLE JNCTNO JOINED THE REGRESSION SET

VARIABLES IN THE REGRESSION SET

VAR NAME	REGRESSION COEFF	STANDARD ERROR	CONFIDENCE INTERVAL	T STAT	PART CORR	MULTIPLE CORRELATION	E S S
BONDNO	0.2728203	.299725E 0		0.91	0.12	0.876	.144496E 2
HGHTNO	0.0912787	.122509E 0		0.75	0.10	0.876	.143836E 2
JNCTNO	1.2200000	.324626E 0		3.76	0.44	0.846	.176607E 2

E.S.S. .142495E 2

RESIDUAL ERROR .491444E 0

MULT CORR 0.878

INTERCEPT TERM = 0.3233303



OBSERVATION MATRIX MAT5

	R01	R02	R03	R04	R05	R06	R07	R08	R09
CONST	1.000	1.000	1.000	1.000	1.000	1.000	1.000	1.000	1.000
BONDNO	0.594	0.594	0.594	0.594	0.594	0.594	0.594	0.594	0.594
HGHTNO	0.710	0.710	0.710	0.710	0.710	0.710	0.710	0.710	0.710
JNCTNO	23.323	23.323	23.323	23.323	23.323	23.323	23.323	23.323	23.323
NUMBER	9.823	9.823	9.823	9.823	9.823	9.823	9.823	9.823	9.823
CDRPNO	4.677	4.677	4.677	4.677	4.677	4.677	4.677	4.677	4.677
PRCNTA	0.617	-	0.533	0.601	0.281	-	0.036	-	0.617
FDRPNO	2.893	2.757	3.050	2.921	3.650	2.700	4.514	3.150	2.893
CONST1	0.294	0.281	0.310	0.297	0.372	0.275	0.460	0.321	0.294

OBSERVATION MATRIX MAT5

	R10	R11	R12	R13	R14	R15	R16	R17	R18
CONST	1.000	1.000	1.000	1.000	1.000	1.000	1.000	1.000	1.000
RONDNO	0.594	0.916	0.916	0.916	0.916	0.916	1.265	1.265	1.265
HGHTNO	0.710	0.792	0.792	0.792	0.792	0.792	0.890	0.890	0.890
JNCTNO	9.643	5.195	5.195	5.195	5.195	5.195	1.227	1.227	1.227
NUMRER	4.062	3.767	3.767	3.767	3.767	3.767	1.382	1.382	1.382
CDRPNO	1.934	1.794	1.794	1.794	1.794	1.794	0.658	0.658	0.658
PRCNTA	0.475	0.116	-	0.088	0.108	-	0.504	0.333	0.286
FDRPNO	3.686	1.606	1.735	1.648	2.010	1.577	1.327	0.986	0.921
CONST1	0.907	0.426	0.461	0.438	0.533	0.419	0.960	0.713	0.667

AD33723

OBSERVATION MATRIX MATS

	R19	R20	R21	R22	R24	R25	R26	R27	R28
CONST	1.000	1.000	1.000	1.000	1.000	1.000	1.000	1.000	1.000
BONDNO	1.265	1.406	1.406	1.406	1.053	1.406	1.200	1.200	1.200
HGHTNO	0.890	0.906	0.906	0.906	0.863	0.906	0.906	0.906	0.906
JNCTNO	1.227	0.764	0.764	0.764	2.789	0.764	0.764	0.764	0.764
NUMBR	1.382	0.974	0.974	0.974	2.535	0.974	0.831	0.831	0.831
CDRPN0	0.658	0.464	0.464	0.464	1.207	0.464	0.396	0.396	0.396
PRCNTA	0.269	0.679	0.565	0.651	0.338	0.639	0.140	0.059	0.563
FDRPN0	0.900	1.446	1.065	1.329	1.823	1.284	0.347	0.374	0.904
CONST1	0.651	1.485	1.094	1.365	0.719	1.319	0.418	0.450	1.088

1373472 470270 101 1200 PARTIAL CORREL ANALYSIS 4033723

OBSERVATION MATRIX MAT5

	R29	R30	R31	R32	R33	R34	R35	R36	R37
CONST	1.000	1.000	1.000	1.000	1.000	1.000	1.000	1.000	1.000
BONFNO	1.200	1.200	1.200	1.355	1.355	1.355	1.355	1.355	1.355
HGHTNO	1.028	1.028	1.028	1.050	1.050	1.050	1.050	1.050	1.050
JNCTNO	0.764	0.790	0.790	0.458	0.458	0.458	0.458	0.458	0.458
NUMRER	0.943	0.975	0.975	0.652	0.652	0.652	0.652	0.652	0.652
CDRPNO	0.449	0.464	0.464	0.310	0.310	0.310	0.310	0.310	0.310
PRCNTA	0.658	0.622	0.613	0.399	0.732	0.239	0.277	0.571	0.579
EDRPNO	1.315	1.228	1.199	0.516	1.158	0.408	0.429	0.724	0.738
CONST1	1.394	1.259	1.229	0.792	1.775	0.626	0.659	1.110	1.131

OBSERVATION MATRIX MATS

	R38	R39	R40	R41	R42	R43	R44	R45	R46
CONST	1.000	1.000	1.000	1.000	1.000	1.000	1.000	1.000	1.000
BONDNO	1.355	1.355	1.355	1.355	1.609	1.442	1.442	1.442	0.539
HGHTNO	1.050	0.925	0.925	0.925	0.925	0.925	0.868	0.868	0.736
JNCTNO	0.458	0.458	0.458	0.458	0.458	0.443	0.443	0.443	36.138
NUMBR	0.652	0.575	0.575	0.575	0.682	0.591	0.555	0.555	14.347
CDRPNO	0.310	0.274	0.274	0.274	0.325	0.282	0.264	0.264	6.831
PRCNTA	0.492	0.642	0.626	0.684	0.692	0.477	0.528	0.445	0.853
EDRPNO	0.611	0.764	0.751	0.865	1.053	0.539	0.560	0.476	3.686
CONST1	0.936	1.529	1.271	1.505	1.544	0.911	1.009	0.858	0.257

OBSERVATION MATRIX MAT5

	R47	R48	R49	R50	R51	R52	R53	R54	R55
CONST	1.000	1.000	1.000	1.000	1.000	1.000	1.000	1.000	1.000
RONDNO	0.539	0.539	1.149	1.442	1.442	1.580	0.911	0.911	0.911
HGHTNO	0.736	0.736	0.836	0.868	0.837	0.837	0.763	0.763	0.763
JNCTNO	36.138	23.323	0.792	0.286	0.458	0.458	5.372	5.372	5.372
NUMBER	14.347	9.259	0.760	0.358	0.553	0.606	3.736	3.736	3.736
CDRPN0	6.831	4.408	0.362	0.171	0.263	0.289	1.779	1.779	1.779
PRCNTA	0.897	0.004	0.677	0.800	0.447	0.485	0.065	0.121	0.351
FDRPN0	3.600	4.393	1.120	0.854	0.476	0.560	1.903	2.023	2.742
CONST1	0.251	0.474	1.473	2.384	0.861	0.924	0.509	0.541	0.734

OBSERVATION MATRIX MATS

	R56	R57	R58	R59	R60	R61	R62	R63	R64
CONST	1.000	1.000	1.000	1.000	1.000	1.000	1.000	1.000	1.000
BONDNO	0.911	0.911	1.399	1.399	1.399	1.580	0.911	0.591	1.259
HGHTNO	0.763	0.957	1.028	1.028	1.028	0.925	0.844	0.736	0.836
JUNCTNO	5.372	5.372	0.764	0.764	0.493	0.286	3.353	37.366	1.227
NUMBR	3.736	4.687	1.100	1.100	0.710	0.418	2.578	16.253	1.291
CDRPNO	1.779	2.231	0.524	0.524	0.338	0.199	1.227	7.738	0.615
PRCNTA	0.168	0.047	0.639	0.510	0.757	0.817	0.306	-	0.593
EDRPNO	2.139	2.342	1.449	1.068	1.391	1.089	1.768	2.607	1.509
CONST1	0.572	0.500	1.317	0.971	1.960	2.605	0.686	0.160	1.169

PRINT MEANS  
 TOTAL NUMBER OF OBSERVATIONS = 63  
 33 MATS LP



APPENDIX K

Prediction of exit drop size -  
Graeco-Latin square (randomized  
blocks) factorial analysis

Table K.1 - Prediction of Exit Drop Size

Data obtained using Graeco-Latin factorial analysis

Reference	$d_0$ m	$d_i$ m	$\Delta\rho$ $\text{Kgm}^{-3}$	$g$ $\text{ms}^{-2}$	$\mu_d$ $\text{Nsm}^{-2}$	$u_d$ $\text{ms}^{-1}$	$\rho_d$ $\text{Kgm}^{-3}$	$\gamma$ $\text{Nm}^{-1}$	$h_b$ m	$d_v$ m	$d_p$ m	$d_g$ m
1AA1	0.00685	0.00237	121.15	9.81	0.00115	0.0127	998.23	0.0134	0.0085	0.00213	0.00543	0.00321
1AA2	0.00769	0.00279	121.15	9.81	0.00115	0.0116	998.23	0.0134	0.0085	0.00213	0.00543	0.00321
1AA3	0.01040	0.00341	121.15	9.81	0.00115	0.0203	998.23	0.0134	0.0085	0.00213	0.00543	0.00321
1AA4	0.00958	0.00326	121.15	9.81	0.00115	0.0316	998.23	0.0134	0.0085	0.00213	0.00543	0.00321
1AA5	0.00934	0.00256	121.15	9.81	0.00115	0.0149	998.23	0.0134	0.0085	0.00213	0.00543	0.00321
1AA6	0.00710	0.00263	121.15	9.81	0.00115	0.0510	998.23	0.0134	0.0085	0.00213	0.00543	0.00321
1AA7	0.01584	0.00351	121.15	9.81	0.00115	0.0621	998.23	0.0134	0.0085	0.00213	0.00543	0.00321
1A18	0.00428	0.00136	121.15	9.81	0.00115	0.0125	998.23	0.0134	0.0085	0.00213	0.00543	0.00321
1A26	0.00775	0.00268	121.15	9.81	0.00115	0.0598	998.23	0.0134	0.0085	0.00213	0.00543	0.00321
2AA2	0.01382	0.00375	121.15	9.81	0.00115	0.0193	998.23	0.0134	0.0060	0.00261	0.00543	0.00372
2AA3	0.00375	0.00234	121.15	9.81	0.00115	0.0446	998.23	0.0134	0.0060	0.00261	0.00597	0.00372

Continued Table K. 1

Reference	$d_o$ m	$d_i$ m	$\Delta p$ Kgm <sup>-3</sup>	$g$ ms <sup>-2</sup>	$\mu_d$ Nsm <sup>-2</sup>	$U_d$ ms <sup>-1</sup>	$\rho_d$ Kgm <sup>-3</sup>	$\gamma$ Nm <sup>-1</sup>	$h_b$ m	$d_v$ m	$d_p$ m	$d_g$ m
3AA1	0.00813	0.00469	121.15	9.81	0.00115	0.0263	998.23	0.0134	0.0060	0.00261	0.00597	0.00372
3AA3	0.00891	0.00541	121.15	9.81	0.00115	0.0371	998.23	0.0134	0.0060	0.00261	0.00597	0.00372
3AA8	0.00275	0.00137	121.15	9.81	0.00115	0.0635	998.23	0.0134	0.0060	0.00261	0.00597	0.00372
3A18	0.00517	0.00328	121.15	9.81	0.00115	0.0453	998.23	0.0134	0.0060	0.00261	0.00597	0.00372
4AA1	0.00349	0.00263	121.15	9.81	0.00115	0.0276	998.23	0.0134	0.0060	0.00261	0.00597	0.00372
4AA3	0.00426	0.00469	121.15	9.81	0.00115	0.0472	998.23	0.0134	0.0060	0.00261	0.00597	0.00372
4A26	0.00486	0.00528	121.15	9.81	0.00115	0.0643	998.23	0.0134	0.0060	0.00261	0.00597	0.00372
4A29	0.00288	0.00321	121.15	9.81	0.00115	0.0166	998.23	0.0134	0.0060	0.00261	0.00597	0.00372
5AA3	0.00180	0.00125	121.15	9.81	0.00115	0.0384	998.23	0.0134	0.0060	0.00261	0.00597	0.00372
5AA5	0.00481	0.00452	121.15	9.81	0.00115	0.0143	998.23	0.0134	0.0060	0.00261	0.00597	0.00372
5A10	0.00502	0.00378	121.15	9.81	0.00115	0.0523	998.23	0.0134	0.0060	0.00261	0.00597	0.00372
5A14	0.00399	0.00351	121.15	9.81	0.00115	0.0175	998.23	0.0134	0.0060	0.00261	0.00597	0.00372

Continued Table K. 1

Reference	$d_o$	$d_i$	$\Delta p$	g	$\mu_d$	$U_d$	$\rho_d$	$\gamma$	$h_b$	$d_v$	$d_p$	$d_g$
9AA3	0. 0158	0. 0215	136. 15	9. 81	0. 00115	0. 0132	998. 23	0. 0345	0. 0035	0. 00327	0. 00658	0. 00440
9AA4	0. 0347	0. 0568	136. 15	9. 81	0. 00115	0. 0236	998. 23	0. 0345	0. 0035	0. 00327	0. 00658	0. 00440
9AA5	0. 0329	0. 0431	136. 15	9. 81	0. 00115	0. 0434	998. 23	0. 0345	0. 0035	0. 00327	0. 00658	0. 00440
9AA6	0. 0237	0. 0325	136. 15	9. 81	0. 00115	0. 0393	998. 23	0. 0345	0. 0035	0. 00327	0. 00658	0. 00440
9AA8	0. 0426	0. 0493	136. 15	9. 81	0. 00115	0. 0557	998. 23	0. 0345	0. 0035	0. 00327	0. 00658	0. 00440
9AB3	0. 0551	0. 0524	229. 15	9. 81	0. 00115	0. 0141	998. 23	0. 0412	0. 0035	0. 00327	0. 00658	0. 00440
9A34	0. 0330	0. 0613	229. 15	9. 81	0. 00115	0. 0215	998. 23	0. 0412	0. 0035	0. 00327	0. 00658	0. 00440
9A35	0. 0325	0. 0582	229. 15	9. 81	0. 00115	0. 0562	998. 23	0. 0412	0. 0035	0. 00327	0. 00658	0. 00523
0A10	0. 0323	0. 0679	229. 15	9. 81	0. 00115	0. 0184	998. 23	0. 0412	0. 00250	0. 00392	0. 00658	0. 00523
0A12	0. 2598	0. 0705	229. 15	9. 81	0. 00115	0. 0485	998. 23	0. 0412	0. 00250	0. 00392	0. 00658	0. 00523
0A24	0. 1555	0. 0432	229. 15	9. 81	0. 00115	0. 0679	998. 23	0. 0412	0. 00250	0. 00392	0. 00747	0. 00523

Continued Table K. 1

Reference	d <sub>0</sub> m	d <sub>i</sub> m	$\Delta\rho$ Kgm <sup>-3</sup>	$g$ ms <sup>-2</sup>	$\mu_d$ Nsm <sup>-2</sup>	$U_d$ ms <sup>-1</sup>	$\rho_d$ Kgm <sup>-3</sup>	$\gamma$ Nm <sup>-1</sup>	h <sub>b</sub> m	d <sub>v</sub> m	d <sub>p</sub> m	d <sub>g</sub> m
0A26	0.2420	0.0557	229.15	9.81	0.00115	0.0353	998.23	0.0412	0.00225	0.00392	0.00747	0.00523
0A27	0.0648	0.0579	229.15	9.81	0.00115	0.0134	998.23	0.0412	0.00225	0.00392	0.00747	0.00523
1A20	0.0547	0.0641	229.15	9.81	0.00115	0.0573	998.23	0.0412	0.00225	0.00392	0.00747	0.00523
<del>2A21</del>	0.0341	0.0718	229.15	9.81	0.00115	0.0158	998.23	0.0412	0.00225	0.00392	0.00747	0.00523
2A18	0.0057	0.0103	342.15	9.81	0.00115	0.0658	998.23	0.0521	0.00225	0.00392	0.00747	0.00523
1A22	0.1273	0.0669	342.15	9.81	0.00115	0.0284	998.23	0.0521	0.00225	0.00392	0.00747	0.00523
1A19	0.1474	0.0729	342.15	9.81	0.00115	0.0177	998.23	0.0521	0.00225	0.00392	0.00747	0.00523
1A21	0.1571	0.0573	342.15	9.81	0.00115	0.0328	998.23	0.0521	0.00225	0.00392	0.00747	0.00523
1A19	0.1084	0.0507	342.15	9.81	0.00115	0.0586	998.23	0.0521	0.00225	0.00392	0.00747	0.00523
2AA4	0.1623	0.0693	342.15	9.81	0.00115	0.0152	998.23	0.0521	0.00225	0.00392	0.00747	0.00523
2A17	0.1089	0.0752	342.15	9.81	0.00115	0.0224	998.23	0.0521	0.00225	0.00392	0.00747	0.00523
3AA2	0.0788	0.0738	342.15	9.81	0.00115	0.0427	998.23	0.0521	0.00225	0.00392	0.00747	0.00523
4AA3	0.0218	0.0157	342.15	9.81	0.00115	0.0693	998.23	0.0521	0.00600	0.00261	0.00597	0.00372
6A14	0.0476	0.0438	342.15	9.81	0.00115	0.0167	998.23	0.0521	0.00600	0.00261	0.00597	0.00372
7AA0	0.1005	0.0569	342.15	9.81	0.00115	0.0194	998.23	0.0521	0.00225	0.00392	0.00747	0.00523
0A22	0.1223	0.0597	342.15	9.81	0.00115	0.0292	998.23	0.0521	0.00225	0.00392	0.00747	0.00523

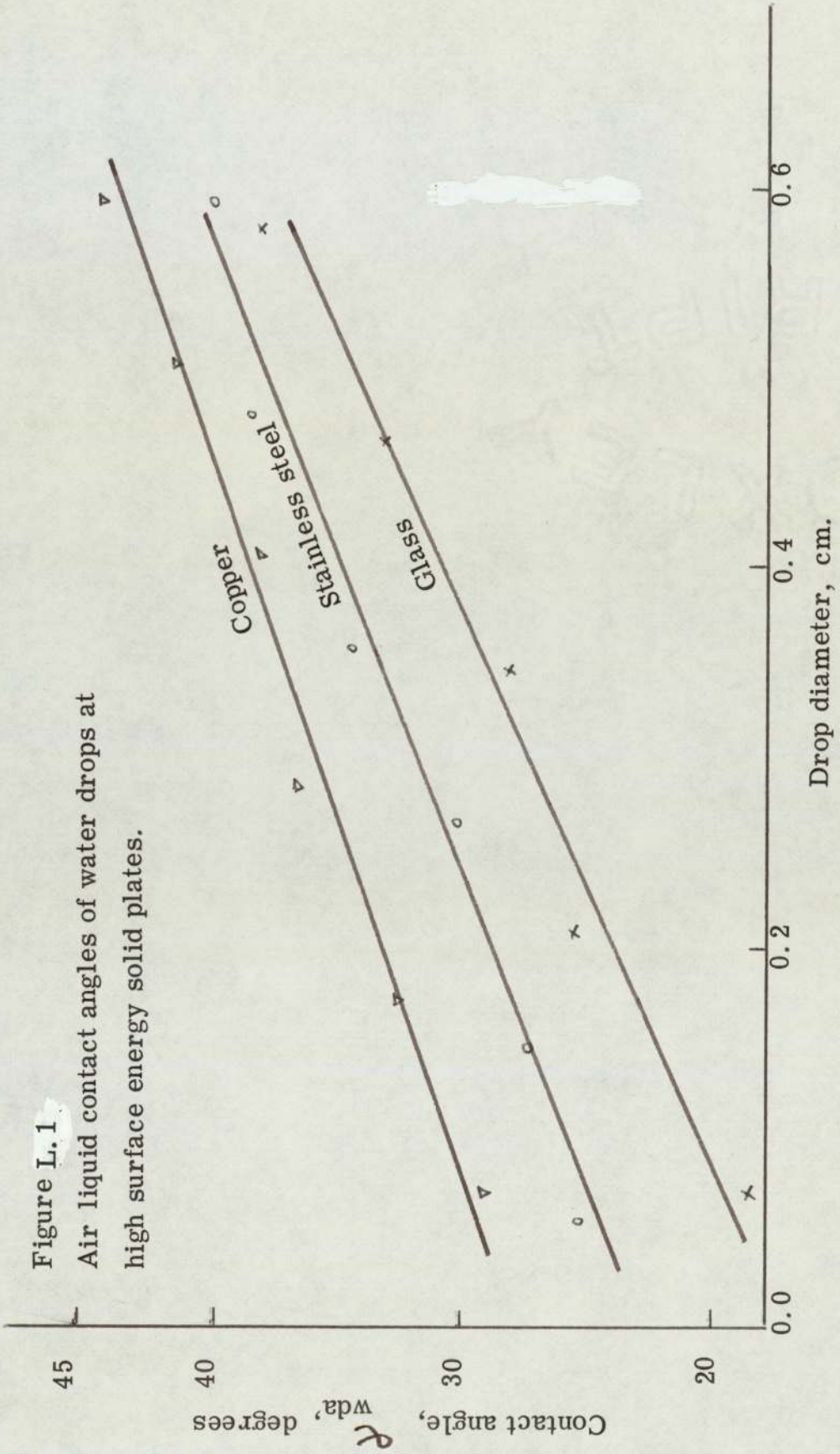
Continued Table K. 1

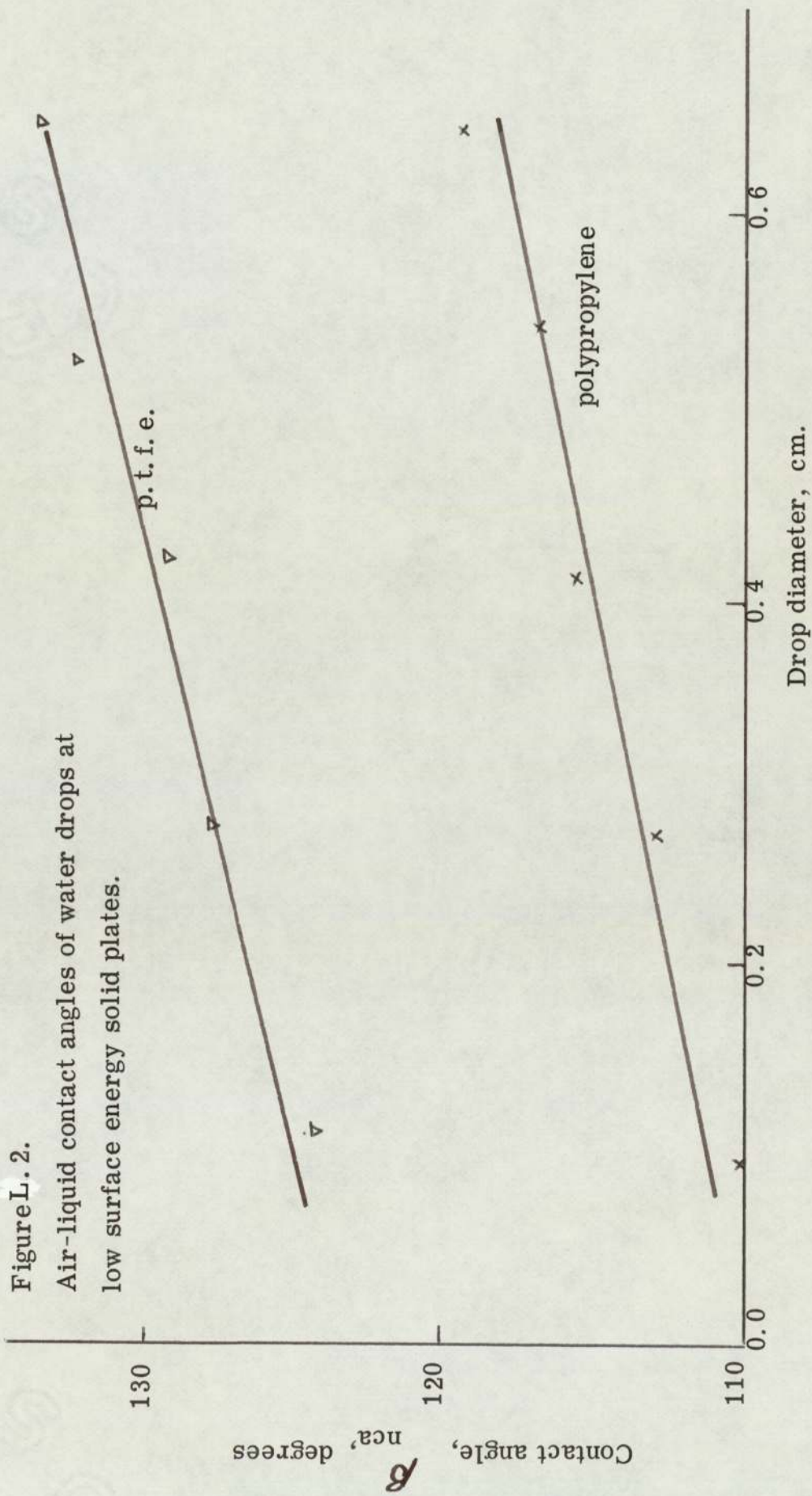
Reference	$d_o$ m	$d_i$ m	$\Delta\rho$ $\text{Kgm}^{-3}$	$\rho_d$ $\text{ms}^{-2}$	$\mathcal{A}_d$ $\text{Nsm}^{-2}$	$U_d$ $\text{ms}^{-1}$	$\rho_d$ $\text{Kgm}^{-3}$	$\gamma$ $\text{Nm}^{-1}$	$h_b$ m	$d_v$ m	$d_p$ m	$d_g$ m
5A28	0.00787	0.00432	121.15	9.81	0.00115	0.0275	998.23	0.0134	0.0060	0.00261	0.00597	0.00372
3A19	0.00650	0.00507	121.15	9.81	0.00115	0.0337	998.23	0.0134	0.0060	0.00261	0.00597	0.00372
4AA2	0.00594	0.00463	136.15	9.81	0.00115	0.0498	998.23	0.0345	0.0060	0.00261	0.00597	0.00372
4AA6	0.00053	0.00142	136.15	9.81	0.00115	0.0621	998.23	0.0345	0.0060	0.00261	0.00597	0.00372
4AA8	0.00289	0.00325	136.15	9.81	0.00115	0.0545	998.23	0.0345	0.0060	0.00261	0.00597	0.00372
4A12	0.0609	0.00451	136.15	9.81	0.00115	0.0345	998.23	0.0345	0.0060	0.00261	0.00597	0.00372
4A21	0.00752	0.00613	136.15	9.81	0.00115	0.0245	998.23	0.0345	0.0035	0.00327	0.00658	0.00372
4A29	0.00703	0.00587	136.15	9.81	0.00115	0.0183	998.23	0.0345	0.0035	0.00327	0.00658	0.00440
6AA2	0.00327	0.00635	136.15	9.81	0.00115	0.0652	998.23	0.0345	0.0035	0.00327	0.00658	0.00440
6AA4	0.00167	0.00145	136.15	9.81	0.00115	0.0461	998.23	0.0345	0.0035	0.00327	0.00658	0.00440
6A11	0.00154	0.00379	136.15	9.81	0.00115	0.0531	998.23	0.0345	0.0035	0.00327	0.00658	0.00440
7AA1	0.00245	0.00573	136.15	9.81	0.00115	0.0364	998.23	0.0345	0.0035	0.00327	0.00658	0.00440
7AA2	0.00443	0.00613	136.15	9.81	0.00115	0.0668	998.23	0.0345	0.0035	0.00327	0.00658	0.00440

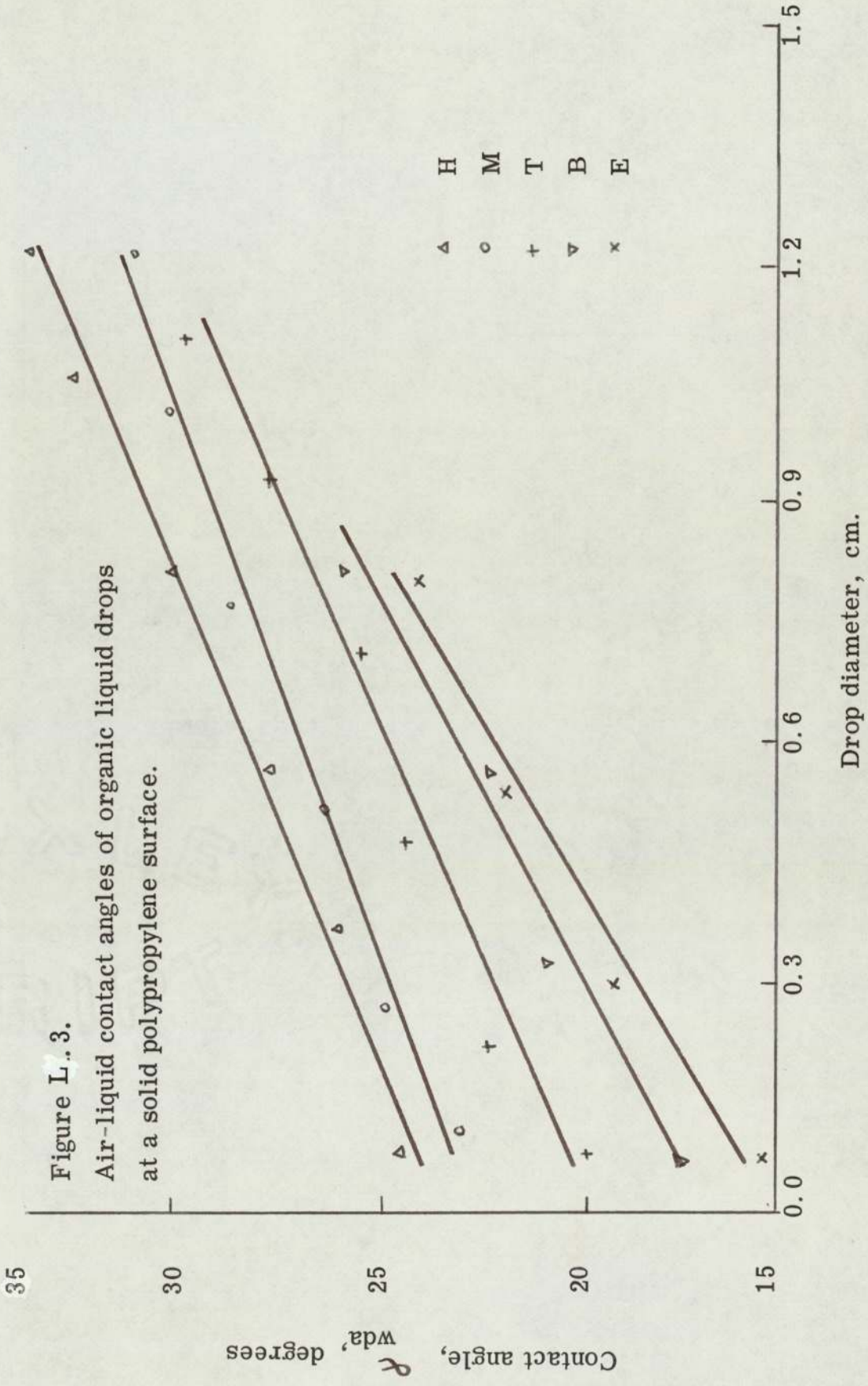
APPENDIX L

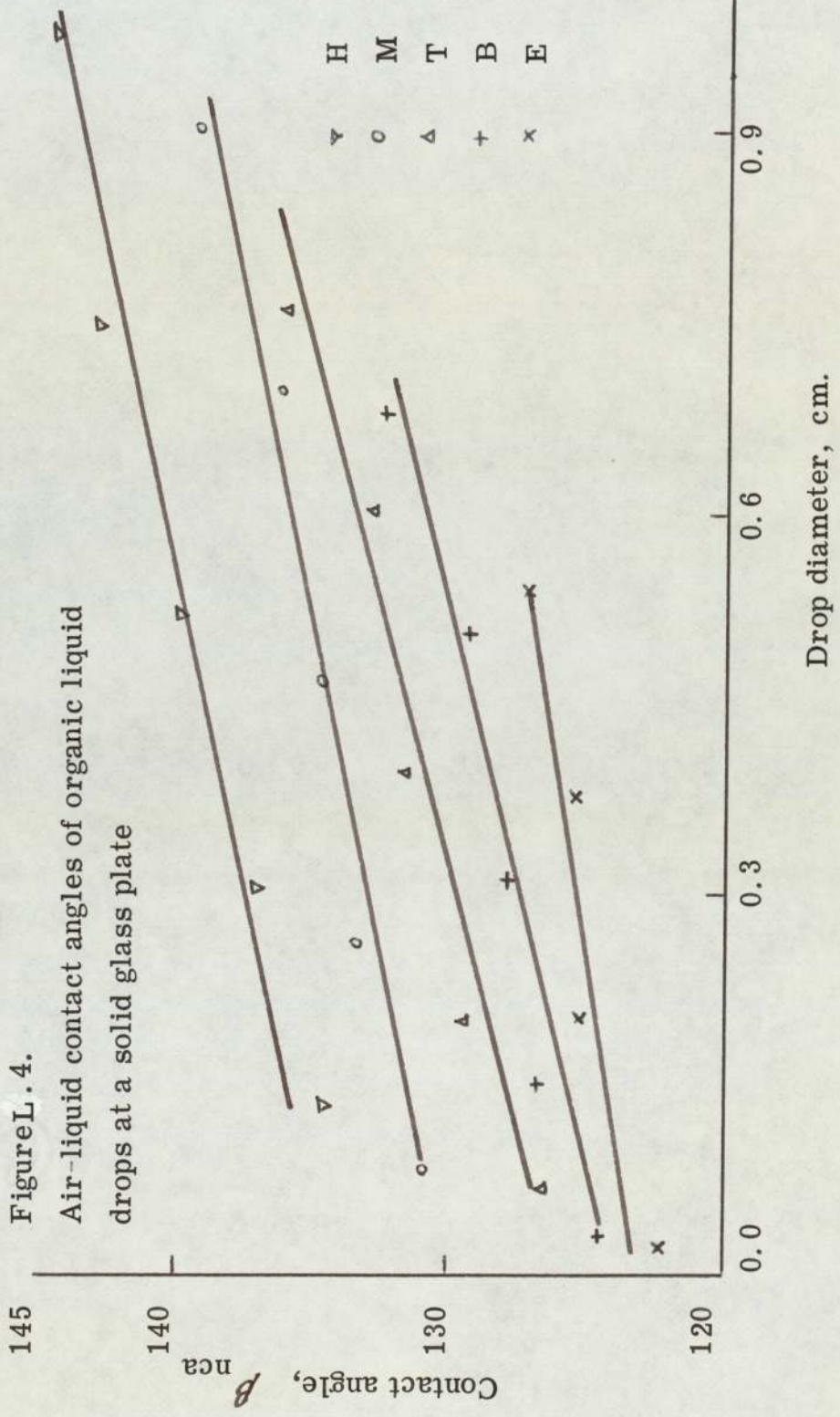
Air-liquid contact angles

Figure L. 1  
Air liquid contact angles of water drops at  
high surface energy solid plates.









145

140

$\beta_{nca}$

Contact angle,

130

120

0.0

0.3

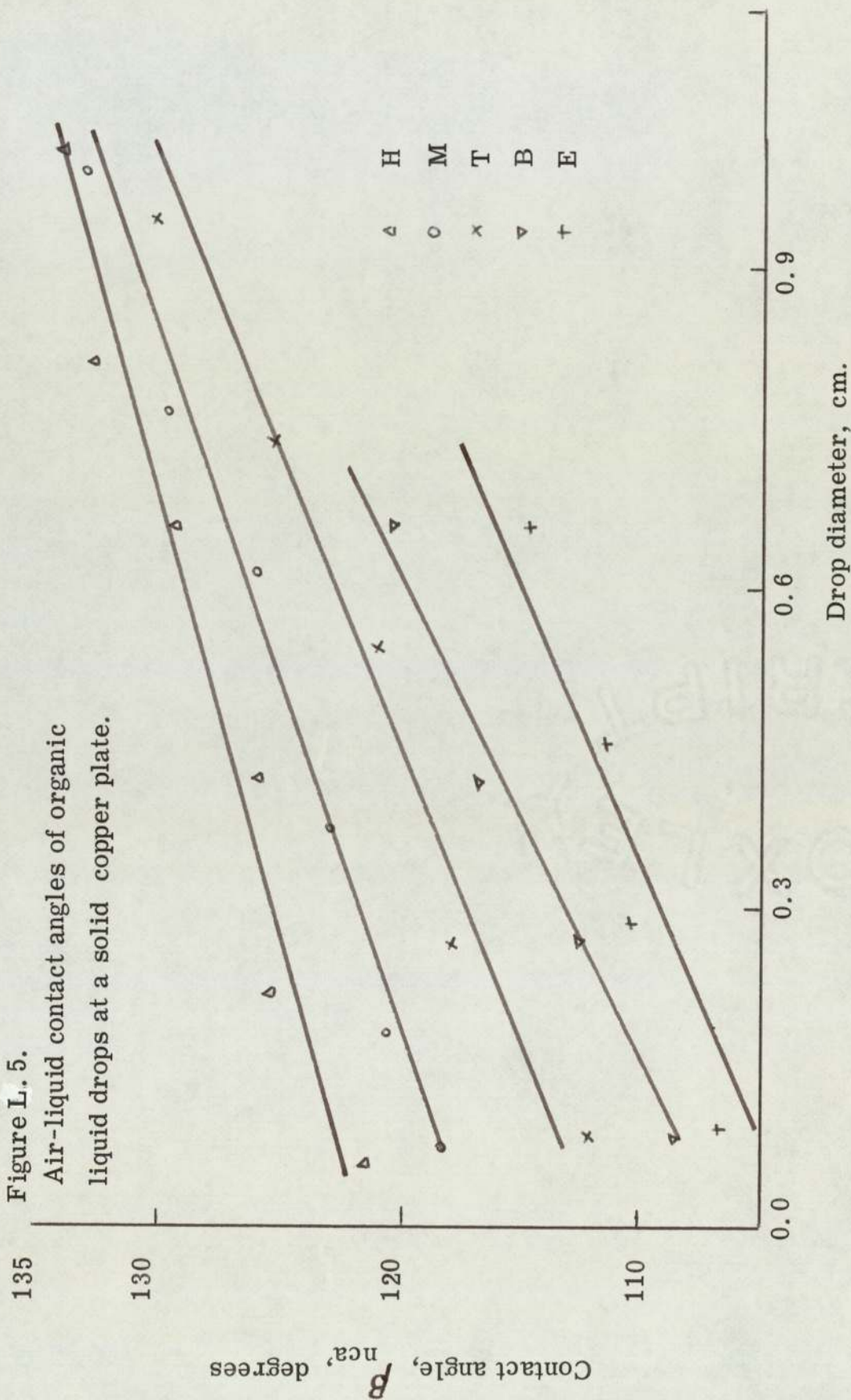
0.6

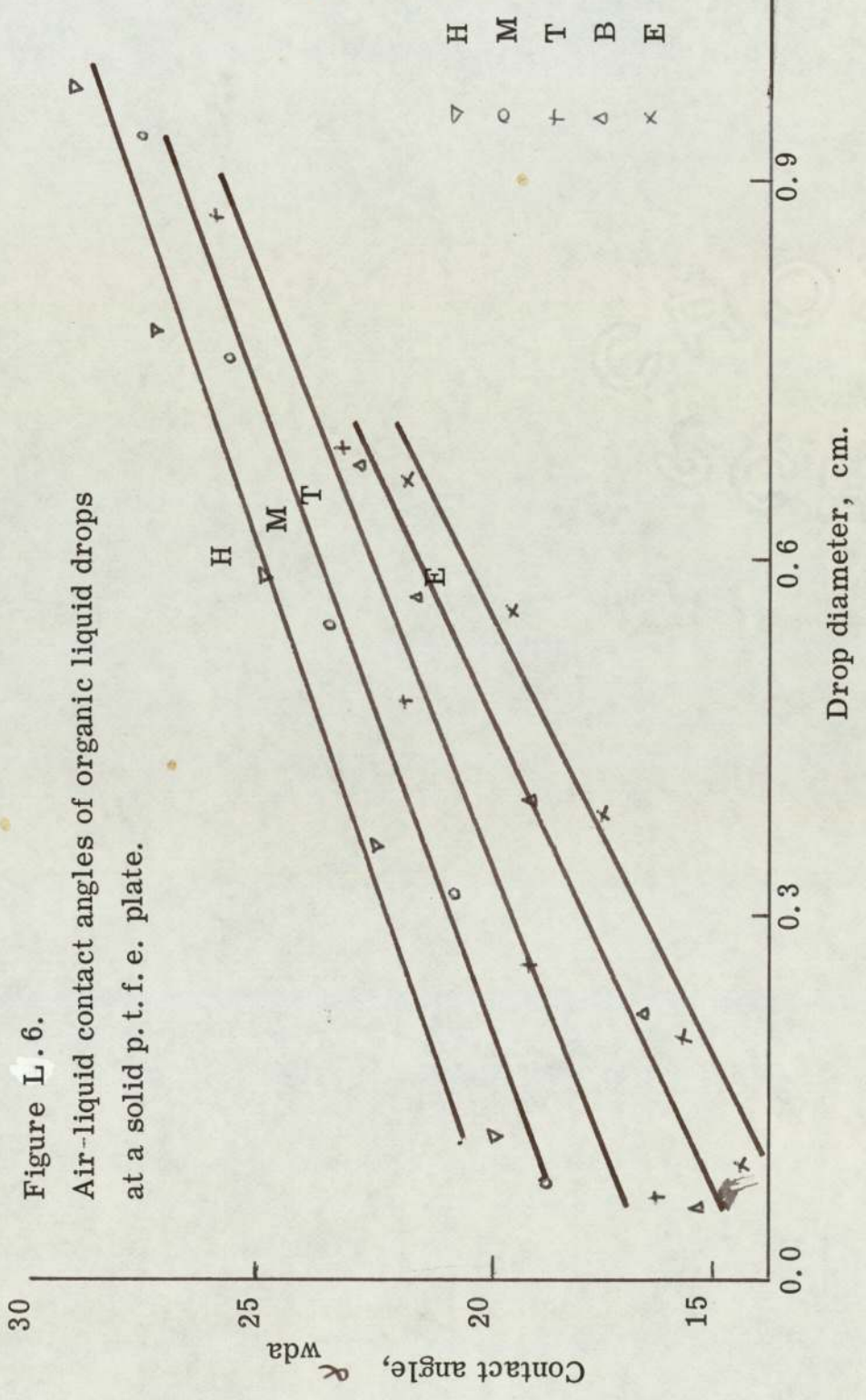
0.9

Drop diameter, cm.

H	M	T	B	E
▽	○	△	+	x

Figure L. 5.  
Air-liquid contact angles of organic  
liquid drops at a solid copper plate.





## NOMENCLATURE

Symbols have the following meaning except where specifically indicated in the text.

a	=	Constant
b	=	Constant
B	=	n-Butyl acetate
C	=	Copper
C	=	Drop dimension
c	=	Constant
$D_c$	=	Calculated diameter of the drop (m)
$D_d$	=	Maximum drop diameter ( $m \times 10^{-2}$ )
$d_e$	=	Equivalent mesh diameter ( $m \times 10^{-2}$ )
$D_e$	=	Experimental value of drop diameter (m)
$d_i$	=	Diameter of inlet droplet (m)
$d_n$	=	Outside diameter of nozzle ( $m \times 10^{-2}$ )
$d_o$	=	Diameter of the exit droplet (m)
$d_v$	=	Diameter of the void (m)
$(d_{vs})_i$	=	Sauter mean diameter of the inlet dispersion droplet (m)
$\%(d_{vs})_i$	=	Percentage of total drops in the inlet dispersion not of diameter equal to $(d_{vs})_i$
$(d_{vs})_o$	=	Sauter mean diameter of the exit dispersion droplet (m)
$\%(d_{vs})_o$	=	Percentage of total drops in the exit dispersion not of diameter equal to $(d_{vs})_o$
$d_1$	=	The maximum drop diameter (m)
$d_2$	=	The minimum drop diameter (m)

$d_{av}$	=	Average of $d_2 - d_1$ (m)
$d_{1(av)}$	=	Average value of $d_1$ (m)
E	=	Ethyl acetate
$F_b$	=	Buoyancy forces (N)
$F_g$	=	Gravitational forces (N)
$F_i$	=	Liquid-liquid interface surface forces (N)
$F_r$	=	Resultant force (N)
$F_s$	=	Surface forces (N)
f	=	Exponential factor ( $m \cdot \text{deg}^{-1}$ )
g	=	Acceleration due to gravity ( $9.81 \text{ ms}^{-2}$ )
H	=	n-Hephane
$h_b$	=	Bed height (m)
K	=	Constant
M	=	Methyl cyclohexane
N	=	Nylon
N	=	Number of pairs of drops coalescing in time 't'
$N_a$	=	Number of drops arriving at the packing inlet in any one mono layer from the distributor plate.
$N_c$	=	Number of coalescing sites available at the packing inlet.
$N_o$	=	Total number of pairs of drops.

$\Delta\rho$	=	Density difference between continuous and dispersed phase liquids ( $\text{Kgm}^{-3}$ )
P	=	Polypropylene
S	=	Stainless steel
$S_g$	=	Surface area of wetted solid components of junction coalescer ( $\text{m}^2$ )
$S_s$	=	Surface area of the solid ( $\text{m}^2 \times 10^{-4}$ )
$S_t$	=	Surface area of non-wetted solid component of junction coalescer
$S_v$	=	Surface area of the void of the junction coalescer (m)
$s_1$	=	Surface area generated by the semi circle of radius 'R' ( $\text{m}^2$ )
$s_2$	=	Surface area of top of the cylinder ( $\text{m}^2$ )
$s_3$	=	Surface area of hemisphere of radius $d_v$ ( $\text{m}^2$ )
T	=	Toluene
t	=	Rest-time (s) $\bar{t}$ = average rest-time
$U_d$	=	Velocity of dispersed phase ( $\text{ms}^{-1}$ )
$V_c$	=	Calculated volume ( $\text{m}^3$ )
$V_e$	=	Experimental value of drop volume ( $\text{m}^3$ )
$v_1$	=	Volume generated by the revolution of solid hemisphere of radius 'R' ( $\text{m}^3$ )
$v_2$	=	Volume of the cylinder of radius 'C' and height '2R', ( $\text{m}^3$ )
$v_3$	=	Volume of hemisphere of radius 'dv' ( $\text{m}^3$ )

GREEK LETTERS

$\gamma_{ca}$	=	Surface tension of continuous phase liquid ( $\text{Nm}^{-1}$ )
$\gamma_{da}$	=	Surface tension of dispersed phase liquid ( $\text{Nm}^{-1}$ )
$\gamma_{dc}$	=	Interfacial tension between dispersed and continuous phase liquids ( $\text{Nm}^{-1}$ )
$\gamma_{nc}$	=	Interfacial tension between the non-wetting continuous phase liquid and the solid surface in the presence of wetting dispersed phase liquid ( $\text{Nm}^{-1}$ )
$\gamma_{nd}$	=	Interfacial tension between the non-wetting dispersed phase liquid and the solid surface in the presence of wetted continuous phase liquid ( $\text{Nm}^{-1}$ )
$\gamma_{wc}$	=	Interfacial tension between the wetting continuous phase liquid and solid surface in the presence of non-wetting dispersed phase liquid ( $\text{Nm}^{-1}$ )
$\gamma_{wd}$	=	Interfacial tension between the wetting dispersed phase liquid and the solid surface in the presence of non-wetting continuous phase liquid ( $\text{Nm}^{-1}$ )
$\gamma_{lv}$	=	Vapour-liquid interfacial tension ( $\text{Nm}^{-1}$ )
$\gamma_{sv}$	=	Solid-vapour interfacial tension ( $\text{Nm}^{-1}$ )
$\gamma_{sl}$	=	Solid-liquid interfacial tension ( $\text{Nm}^{-1}$ )
$\gamma_{32}$	=	Interfacial tension between states 3 and 2 ( $\text{Nm}^{-1}$ )
$\gamma_{31}$	=	Interfacial tension between states 3 and 1 ( $\text{Nm}^{-1}$ )
$\gamma_{12}$	=	Interfacial tension between states 1 and 2 ( $\text{Nm}^{-1}$ )

- $\theta_1$  = Contact angle  $\theta_{wc}$  of drop diameter  $d_1$  (degrees)  
 $\theta_2$  = Contact angle  $\theta_{wc}$  of drop diameter  $d_2$  (degrees)  
 $(\theta_1)_{av}$  = Average value of  $\theta_1$  (degrees)  
 $\theta_{wc}$  = Liquid-liquid contact angle of continuous phase liquid drop at a solid surface immersed in the dispersed phase liquid, solid surface being non-wetted by continuous phase liquid (degrees)  
 $\theta_{wd}$  = Liquid-liquid contact angle of dispersed phase liquid drop at a solid surface immersed in continuous phase liquid, solid surface being wetted by dispersed phase (degrees)  
 $(\theta_{wd})_c$  = Calculated value of  $\theta_{wd}$  (degrees)  
 $(\theta_{wd})_e$  = Experimental value of  $\theta_{wd}$  (degrees)  
 $\Delta P$  = Pressure drop across the bed (N)  
 $\rho_d$  = Density of dispersed phase ( $\text{Kgm}^{-3}$ )  
 $\mu_d$  = Viscosity of dispersed phase ( $\text{ms}^{-1}$ )  
 $\pi$  = Dimensionless group

## REFERENCES

1. Adams, N.K. Dis. of Far. Soc. 3, 5, 1948.
2. Adams, N.K. and Elliott, G. E. P. J. Chem. Soc. 2206, 1962.
3. Al-Hemiri, A. A. R. Ph. D. Thesis, Aston University, 1973.
4. Ali, F. A. Ph. D Thesis, University of Manchester, 1971.
5. Allak, A. M. A. Ph. D. Thesis, University of Aston in Birmingham, 1973.
6. Allan, R. S. and Mason, S. G. Trans, Faraday Society, 1961, 57, 2027.
7. Allan, R. S. and Mason, S. G. J. Colloid Sci. 17, 383, 1962.
8. Arnold, D. R. Ph. D. Thesis, Aston University, 1973.
9. Bartell, F. E. and Shephard, J. W. J. Phys. Chem. 57, 455, 1953.
10. Bartell, F. E. and Shephard, J. W. J. Phys. Chem. 57, 211, 1953.
11. Bashforth, F. and Adams, J. "An Attempt to Test the theories of Capillary Action", Cambridge University Press, England 1883.
12. Binkerman, J. J. Proc. 2nd Int. Cong. Surf. Actvty, Butterworths, 1957.
13. Blanding, F. H. and Elgin, J. C. A. I. Chem. E. J. 33, 305, 1942.
14. Borgin, K. Norsk Skogind 13, 429, 1959.
15. Bowden, F. P. Semain d'etute sur la theme forces moleculaires, 285, pontificae Academia Scientiorum Scripto 31.
16. Breckenfield, R. R. and Wilke, C. R. Chem. Eng. Prog. 46, 187, 1950.
17. Brown, A. H. and Hanson, C. Trans. Far. Soc. 61, 1754, 1965.
18. Brown, A. H. and Hanson, C. Brit. Chem. Eng. Vol. 11 No. 7, 695, 1966.
19. Brown, A. H. and Hanson, C. I. Chem. E. Syp. Series 26 (1967: Inst. Chem. Engrs. London).

20. Buff, F. P. "Handbuch der physik" Vol 10, Springer-verlog, Berlin, 1958.
21. Burrill, K. A. and Woods, D. R. J. Colloid Inter Sci. Vol. 42, 1, 1973
22. Burtis, T. A. and Kirkbride, C. G. Trans. A. I. Ch. E. 42, 413, 1946.
23. Cavers, S. D. and Evanchyna, J. E. Canadian J. Chem. Eng. 35, 113, 1957.
24. Charles, G. E. and Mason, S. G., J. Colloid Sci. 15, 105, 1960.
25. Chin, H. L., M. Chem. E. Thesis, University of New York 1956.
26. Cockbain, E. G. and McRoberts, T. S., J. Colloid Sci. 8, 440, 1953.
27. Crawford, J. W. and Wilke, C. R., Chem. Eng. Prog. 47, 423, 1951.
28. Davies, O. L. "Design & Analysis of Industrial Experiments", Oliver & Boyd London 1967.
29. Davies, J. T. and Rideal, E. K. "Interfacial Phenomena", Academic Press, N. Y. 1961.
30. Davies, J. T., Richie, J. M. and Southwood, D. C., Trans. Inst. Chem. Engrs. 38, p 331, 1960.
31. Derjaguin, B. V. and Kusakov, M., Acta Physicochim 1939, 10, 25.
32. Douglas, E. and Elliott, I. G. Trans. Inst. Mar. Eng. 74, 164, 1962.
33. Edge, R. M. and Greaves, M., I. Chem. E. Symp. Ser. No. 26 (1967: Inst. of Chem. Engrs.), London.
34. Elliott, G. E. P. and Riddiford, A. C. "Recent Progress in Surface Science", Vol. 2, 1964.
35. Elton, G. A. H. and Picknett, R. G. "Proceedings of the Second International Congress of Surface Activity", Butterworths, 1957.
36. Farley, R. and Valentine, F. H. H., Joint Meeting A. I. Chem. E. and I. Chem. Eng. Symp. London, 1965.

37. Fowkes, F. M. and Harkins, W. D. "The State of Monolayers at the Interface Solid-Aqueous Solution", J. Am. Chem. Soc. 62, 3372, 1940.
38. Fox, H. W. and Zissman, W. A., J. Colloid. Sci. 5, 514, 1950.
39. Gayler, R. and Pratt, H. R. C., Trans. Inst. Chem. Engrs. 31, 69, 1953.
40. Gayler, R. and Pratt, H. R. C., Trans. Inst. Chem. Eng. 35, 273, 1957.
41. Gibbs, J. W. "Collected Works", Vol. 1, Yale University Press, Newhaven, 1928.
42. Gillispie, T. and Rideal, E. K., Trans. Far. Soc. 52, 173, 1956.
43. Goodrich, F. C., Surf. & Colloid. Sci., Wiley, Interscience, 1969.
44. Gregg, S. J. J. Chem. Phys. 16, 549, 1948.
45. Groothius, R. and Zuiderweg, F. J. Chem. Eng. Sci. 12, 288, 1960.
46. Hair, M. L. "Clean Surfaces", M. Dekka Incor. N. Y. 1970.
47. Hanson, C., Brit. Chem. Eng. 34, 10, 1965.
48. Hanson, C. and Kaye, D. A., Brit. Pat. App. 44707/63.
49. Hare, E. F. and Zissman, W. A., J. Phys. Chem. 59, 335, 1955.
50. Harkins, W. D. "The Physical Chemistry of Surface Films", N. Y. Reinhold Publication Corporation, 1952.
51. Harkins, W. D. and Brown, F. E., J. Am. Chem. Soc. 41, 499, 1919.
52. Harkins, W. D. and Feldman, A., J. Am. Chem. Soc. 44, 2665, 1922.
53. Hartland, S. Informal Res. Meeting on Sol. Extn. Bradford 1965.
54. Hartland, S., Trans. Inst. Chem. Engrs. Vol. 45, T97, 1967.
55. Hartland, S., J. Colloid. Sci. 26, 383, 1968.
56. Hartland, S., I. Chem. E. Symp. Ser. 26 (1967: Inst. Chem. Engrs. London.)

57. Hayworth, C. B. and Treybal, R. E., *Ind. Eng. Chem.* 42, 1174, 1950.
58. Hayes, et. al., *Chem. Eng. Prog.* 45, 235, 1949.
59. Hawksley, J. L. Ph.D. Thesis, University of Birmingham 1972.
60. Hitit, H. A. Ph.D. Thesis, University of Aston in Birmingham, 1972.
61. Hoffing, E. H. and Lockhart, F. J., *Chem. Eng. Prog.* 50, 94, 1962.
62. Honeykemp, J. R. and Burkart, L. E., *Ind. Engng. Chem. Process Des. Dev.* 1, 177, 1962.
63. Jeffreys, G. V. and Davies, G. A., "Recent Advances in Liquid-Liquid Extraction", Ed. C. Hanson, Pergamon Press, 1971.
64. Jeffreys, G. V., Davies, G. A. and Ali, F. A., *J. Chem. Eng.* Vol. 48, p 328, 1970.
65. Jeffreys, G. V. and Davies, G. A., *Filtration and Separation*, 6, 349, 1969.
66. Jeffreys, G. V., Davies, G. A. and Price-Bailey, D. "A New Packing for Gas-Liquid & Liquid-Liquid Separation Processes", Knitmesh Ltd. 1971.
66. Jeffreys, G. V., Davies, G. A. and Pitt, K., *A. I. Chem. E. J.* 16, 5, 1971.
67. Jeffreys, G. V., Davies, G. A. and Smith, D. V., ISEC, Hague, 1971.
68. Jeffreys, G. V. and Hawksley, J. L., *J. App. Chem.* p 329, 1962 August.
69. Jeffreys, G. V. and Hawksley, J. L., *A. I. Chem. E. J.* Vol. 11, No. 3, 1965.
70. Jeffreys, G. V. and Lawson, G. B., *Trans. Inst. Chem. Engrs.* Vol. 43, 1965.

71. Johnson, R. E., J. Phys. Chem. 63, 1655, 1959.
72. I. M. I. Inst. for Res. and Dev., Israel, U. S. Pat. 3, 489, 526.
73. Katalinic, M., Nature, 127, 627, 1931.
74. Katalinic, M., Nature, 136, 916, 1935.
75. Komasaawa, I. and Otake, T., J. Chem. Eng. Vol. 13, No. 2, 1970.
76. Kowoski, K., J. Colloid. Sci. 17, 167, 1962.
77. Lang, S. B., Ph.D. Thesis, University of California, 1962.
78. Lang, S. B. and Wilke, C. R., Ind. Eng. Chem. Fund. 10, No. 3, 329, 1971.
79. Langdon, W. M. et. al. Petrol. Chem. Eng. 34, Nov. 1963.
80. Lawson, G. B. Ph.D. Thesis, University of Manchester 1967.
81. Lester, G. R., J. Colloid. Sci. 16, 315, 1961.
82. Lewis, S. B., Jones, I. and Pratt, H. R. C., Trans. Inst. Chem. Engrs. 29, 136, 1951.
83. Linton, M. and Sutherland, K. L., J. Colloid Sci. 11, 391, 1956.
84. Lindblad, N. R. J. Colloid. Sci. 19, 729, 1964.
85. L. M. T. S. Lurgi Gassellschaft, Frankfurt am Main.
86. Lowes, L. and Tanner, M. C., Brit. Patent 909485 (1962).
87. Mackay, G. D. M. and Mason, S. G., Can. J. Chem. Eng. 41, 203, 1963.
88. Mackay, G. D. M. and Mason, S. G., J. Coll. Sci. 18, 674, 1963.
89. Mackay, G. D. M. and Mason, S. G., Can. J. Chem. Eng. 41, 202, 1963.
90. Mahajan, L. D., Phil. Mag. 10, 383, 1930.
91. Mahajan, L. D., Kolloid-Z. 65, 20, 1933.
92. Marek, J. and Misek, T., Soc of Chem. Ind. Conference on Sol. Extraction, Ed. C. Hanson, Pergamon Press 1971.
93. Meissner, H. R. and Chertow, B., Ind. Eng. Chem. 38, 856, 1946.

94. Misek, T., Coll. Czech. Chem. Comm. 28, p 426, 1963.
95. Morrello, V.S. and Beckman, R. B., Ind. Engng. Chem. International Edition 42, p 1078, 1950.
96. Morrow, N.R., Ind. Engng. Chem. 62, 32, 1970.
97. Mumford, C.J., Brit. Chem. Eng. 13, 7, 1968.
98. Mumford, C.J., Ph. D. Thesis, University of Aston in Birmingham, 1970.
99. Mumford, C.J. and Jeffreys, G. V., Chisa Congress, Marianska Lanze, September 1969.
100. Mumford, C.J. and Thomas, R. J., ISEC, Hague, Paper No. 50, 1971.
101. Mumford, C.J. and Thomas, R. J., Processing Engineering, December 1972, p 52.
102. Najmi, A. I., M. Sc. Thesis, University of Strathclyde, Glasgow, 1976.
103. Newman, A. W., Proc. 4th Int Cong Surf Activity, Brussels, 1964.
104. Nielsen, L. E., Rev. Sci. Instr. 22, 690, 1951.
105. Nielsen, L. E., Wall, R. and Adams, G., J. Coll. Sci. 13, 441, 1958.
106. Null, H. R. and Johnson, F., AIChemEJ 4, 273, 1958.
107. Padday, J. F., Proc. 2nd Int. Cong. Surface Activity, Vol. 3, London, Butterworth, 1957.
108. Picknett, R. G., Ph. D. Thesis, University of London 1957.
109. Perut, M., Petrale Ann Comb Liquides 27(5), 763, 1972.
110. Pettica, B. A. and Pettica, T. J. P., Proc. of 2nd International Congress on Surface Activity, Butterworths, 1957.
111. Phillips, M. C. and Riddiford, A. C., Wetting Science Monograph No. 25, Soc. of Chem. Eng. 1967.
112. Piper, H., Ph. D. Thesis, University of Manchester 1969.
113. Photography applied to flow visualisation, Kodak Data Sheet 1N-1 Issue A.

114. Princen, H. M. and Mason, S. G., J. Coll. Sci. 18, 178, 1963.
115. Princen, H. M. and Mason, S. G., J. Coll. Sci. 29, 156, 1965.
116. Prokhorov, P., Diss. Far. Soc. 18, 41, 1954.
117. Ramshaw, C. and Thornton, R. D., Inst. Chem. Engrs. Symp. Series No. 26, 73, 1967.
118. Rao, E. V. L., Kumar, R. and Kuloor, N. R., Chem. Eng. Sci. 21, 867, 1966.
119. Ridgeway, K. and Tarbuck, K. J., Brit. Chem. Eng. 12, 384, 1967.
120. Robinson, J. and Hartland, S., ISEC Paper No. 56, 1971.
121. Rosenfeld, J. and Wasan, D. T., Can. J. Chem. Eng. 52, Feb 1974.
122. Rushton, E. and Davies, G. A., ISEC, Lyons, 1974.
123. Ryon, A. D., Daley, F. L. and Lowrie, R. S., Chem. Eng. Prog. 55, 70, 1959.
124. Sareen, S. S., Rose, P. M. and Gudeson, R. C., A. I. Chem. E. J. 12, 1045, 1966.
125. Scheele, G. F. and Lang, D. E., Chem. Eng. Sci. 26, 1867, 1971.
126. Scheele, G. F. and Meister, B. J., AIChE E. J. 14, 9, 1968.
127. Scheibel, E. G., Chem. Eng. Prog. 44, 681, 1948.
128. Schniedegger, A. E. "The Physics of Flow through Porous Media", Macmillan, New York, 1957.
129. Schwartz, A. M., Ind. Engng. Chem. 61, No. 1, 10, 1967.
130. Shafrin, E. G. and Zissman, W. A., J. Phys. Chem. 64, 519, 1960.
131. Shaloub, N. G., Ph. D. Thesis, University of Aston in Birmingham, 1975.
132. Shorony, D. F., Ph. D. Thesis, I. I. T. 1969.
133. Slater, M. A., M. Sc. Thesis, University of Aston, 1968.
134. Smith, D. V., Ph. D. Thesis, University of Manchester, 1969.
135. Smith, D. V. and Davies, G. A., Can. J. Chem. Eng. 48, 628, 1970.
136. Smith, G. J., Ph. D. Thesis, University of Southampton, 1969.
137. Spielman, L. A., Ph. D. Thesis, University of California, 1968.

138. Spielman, L. A. and Goren, S. L. , Ind. Eng. Chem. Fund. 11, 63, 1972.
139. Temperely, H. N. D. , Proc. Camb. Phys. Soc. 48, 683, 1952.
140. Topliss, J. A. , 1st Chem. Eng. Dept. Res. Symp. May 1970.
141. Treybal, R. E. "Liquid Extraction", 2nd ed. McGraw-Hill, N. Y. 1963.
142. Voyutski, S. S. , Kalyanova, K. A. and Panick, R. , Dokl. Akad. Nauk. SSSR, 91, 1155, 1953, CA49, 12053, 1955.
143. Wark, I. W. and Cox, A. B. , Nature 136, 182, 1935.
144. Watanabe, T. and Kusui, M. , Bull. Chem. Soc. Japan 31, 236, 1958.
145. Waterman, L. G. , Chem. Eng. Prog. 61, No. 10, 51, 1965.
146. Waterman, L. G. , "Electrical Coalescers", Theory & Practice, Paper presented to AIChE, San Francisco, May 1965.
147. Wenzel, R. N. , J. Phys. Chem. 53, 1466, 1949.
148. Wilkinson, D. , Mumford, C. J. and Jeffrey, G. V. A. I. Chem. E. J. Vol. 21, No. 5, 910, 1975.
149. Yarnold, G. D. and Mason, B. J. , Proc. Phys. Soc. B62, 125, 1949.
150. Zissman, W. A. , Record of Chem. Prog. 26, 1, 13, 1964.